Evaluating the Potential of CO_2 Foam and CO_2 Polymer Enhanced Foam for Heavy Oil Recovery in Fractured Reservoirs: Pore-Scale and Core-Scale Studies

by

Ali Telmadarreie

A thesis submitted in partial fulfillment of the requirements for the degree of

Doctor of Philosophy

in

Petroleum Engineering

Department of Civil and Environmental Engineering

University of Alberta

Abstract

Besides oil-sand reserves that should be recovered by thermal recovery methods, there are significant reserves of conventional light to heavy crude oil in the Western Canadian Sedimentary Basin (WCSB) that can be also recovered by non-thermal processes. Several carbonate reservoirs have undergone tertiary solvent/gas recovery and some of them finished with low recovery and converted to second or even third EOR process. This is almost the same for the sandstone reservoirs where the chemical flooding is the main non-thermal EOR method. Polymer loss, injectivity reduction, and inadequate sweep efficiency are the main concerns during chemical flooding. Foam and especially Polymer Enhanced Foam (PEF) can control the mobility ratio and improve the sweep efficiency in heavy oil reservoirs over chemical and gas flooding. CO_2 foam (especially in reservoirs with lighter oil) and CO_2 PEF (for those heavier oils) can be a good environmentally friendly choice for improving Canadian heavy oil recovery much further. The challenge is to understand how the combination of surfactant, gas, and polymer allows us to better access the untouched parts of the reservoir and increase the sweep efficiency.

As of yet, there is no complete and rigorous understanding of the mechanisms during heavy oil recovery by foam, especially PEF performance in fractured porous media; therefore, this study aims to investigate direct visual observations of foam/PEF transport and heavy oil displacement phenomena in porous media. The focus of this thesis is conducting experiments to study the behavior and performance of CO_2 foam/PEF for heavy oil recovery. Pore-scale analysis with the help of micromodel study and core-scale analysis by sand-pack and rock sample were performed throughout this thesis to achieve the goals.

In the pore-scale analysis, a new application of CO_2 foam/PEF in combination with current heavy oil recovery methods was introduced and studied. CO_2 foam/PEF was used after surfactant

injection in oil-wet fractured porous media and their performance was visualized with the help of a fractured micromodel. In addition, for those reservoirs where the hydrocarbon solvent injection is used as a heavy oil recovery method, this study showed that how foam/PEF could improve the solvent injection performance by increasing the heavy oil recovery and decreasing the asphaltene deposition and formation damage. Moreover, the dynamic behavior of asphaltene deposition was discussed and visualized in this thesis to show that how foam/PEF can decrease the formation damage.

The core-scale performance of CO_2 foam/PEF for heavy oil recovery was studied in a one-dimensional sand-pack after water flooding. Moreover, CO_2 foam/PEF performance was analyzed in actual rock samples (sandstone and carbonate rocks) and effect of heterogeneity was also considered by applying artificial fracture in the rock samples. In these experiments, the injection pressure profile, oil recovery, and CO_2 gas production were monitored and recorded to analyze and compare the performance of CO_2 foam and CO_2 PEF for both heavy oil recovery and CO_2 sequestration.

The results of this thesis improve our understanding of the heavy oil recovery process with the help of CO_2 foam/PEF injection. Besides enhancing oil production, application of CO_2 foam/PEF may reduce the amount of injected chemical into the reservoir, providing economic and environmental advantages.

Dedicated with love to my wife, parents, and sister for their dedicated partnership for success in my life

Acknowledgements

I would like to express my special appreciation and thanks to my supervisor Dr. Japan Trivedi for giving me the opportunity to carry out my doctoral research. I am thankful to him for all the research experience and applicable knowledge I have gained over these years in his research group and for granting me freedom to explore my ideas.

I would like to acknowledge the financial support provided by Carbon Management Canada (CMC), Alberta Innovates–Technology Futures, Natural Sciences and Engineering Research Council of Canada (NSERC), and the University of Alberta. Department of civil and environmental engineering and Faculty of Graduate Studies and Research (FGSR) at the University of Alberta are also greatly appreciated for their support through scholarships during my PhD research.

I am grateful to Dr. Ergun Kuru for his invaluable advice and feedback on my research. I am also thankful to the University of Alberta technical support staffs especially Todd Kinnee for his technical help and support.

I would like to thank my colleagues and friends who helped me with their comments and discussions especially Dr. Siavash Nejadi.

Finally, I would like to express my sincerest gratitude to my wife and family for their unconditional love and support throughout my studies.

Table of Content

Abstract ii

Acknowledgements v

Chapter 1: Introduction and Literature Review 1

1.1 Introduction 1

1.2 Fundamentals of Foam in Porous Media 7

1.2.1 Foam Generation and Propagation in Porous Media 8

1.2.2 Foam Stability 11

1.2.2.1 Foam Stability in the Presence of Crude Oil 14

1.3 Potential of Foam and PEF for Heavy Oil Recovery: Literature Reviews 18

1.3.1 Application of Foam in Thermal Oil Recovery 22

1.3.2 Nanoparticles Enhanced Foam for EOR 24

1.4 Statement of the Problem 25

1.5 Objectives 27

1.6 Thesis Structure 28

Chapter 2: Post-Surfactant CO_2 Foam/Polymer Enhanced Foam Flooding for Heavy Oil Recovery: Pore-Scale Visualization in Fractured Micromodel 30

2.2 Materials and Methods 32

2.2.1 Materials 32

2.2.2 Methods 33

2.2.2.1 Foam Bulk (Static) Experiments 33

2.2.2.2 Micromodel Experiments 34

2.3 Results 36

2.3.1 Foam/PEF Static Stability 36

2.3.2 Waterflooding 39

2.3.3 Surfactant Injection 39

2.3.4 CO_2 Foam and CO_2 PEF Flooding 41

2.4 Discussion 43

2.4.1 Surfactant Flooding 43

2.4.2 Applying Foam to Improve Surfactant Flooding in Fractured Carbonate Reservoirs 49

2.5 Summary 54

Chapter 3: Dynamic Behavior of Asphaltene Precipitation and Distribution Pattern in Fractured Carbonate Reservoirs during Hydrocarbon Solvent Injection: Pore-Scale Observations 55

3.1 Introduction 55

3.2 Materials and Methods 58
3.2.1 Materials 58
3.2.2 Asphaltene Content Measurement of the Crude Oil 58
3.2.3 Micromodel Experiment 59
3.3 Results 60
3.3.1 Asphaltene Static Study 60
3.3.2 SEM Analysis 62
3.3.3 Asphaltene in Porous Media 65
3.4 Discussions 67
3.4.1 Asphaltene Deposition and Formation Damage 67
3.4.2 Asphaltene Distribution Pattern in Heterogeneous Fractured Porous Media 69
3.4.3 Different Shapes of Asphaltene Deposition in the Fracture and Matrix 72
3.5 Summary 81
Chapter 4: Improving Hydrocarbon Solvent Injection for Heavy Oil Recovery: Applying CO_2 Foam/Polymer Enhanced Foam and Hydrocarbon Solvent Based Foam' 84
Part 1: Pore-Scale Mechanisms of Post-Solvent CO_2 Foam/Polymer Enhanced Foam Flooding 84
4.1 Introduction 84
4.2 Material and Methods 87
4.2.1 Material 87
4.2.2 Foam Bulk (Static) Experiments 89
4.2.3 Micromodel Experiments 89
4.3 Results and Discussions 93
4.3.1 Static Analysis of CO_2 Foam and CO_2 PEF in the Presence of Heavy Oil 93
4.3.2 Effect of Wettability on Heavy Oil Recovery During Waterflooding 96
4.3.3 Hydrocarbon Solvent Flooding 98
4.3.4 Performance of CO_2 Gas, Foam, and PEF Flooding After Solvent Injection 102
Part 2: Pore-Scale Mechanisms of Foam Generated with the Hydrocarbon Solvent: Solvent Based Foam (SBF) 116
4.4 Introduction 116
4.5 Material and Methods 117
4.6 Results 119
4.6.1 Static Performance of Solvent Based Foam 119
4.6.2 Dynamic Performance of Solvent Based Foam: Micromodel Study 124
4.7 Discussions 127
4.8 Summary 133

Chapter 5: CO_2 Foam and Polymer Enhanced Foam for Heavy Oil Recovery: Bulk and Porous Media (Sand-pack) Studies 136

5.1 Introduction 136

5.2 Materials and Methods 138
5.2.1 Materials 138
5.2.2 Foam Bulk (Static) Experiments 139
5.2.3 Foam Dynamic Experiments 141

5.3 Results and Discussions 143
5.3.1 Static Performance of Foam and PEF in the Absence of Heavy Oil 143
5.3.2 Static Performance of Foam and PEF in the Presence of Heavy Oil 146
5.3.3 More Insight into Impact of Oil on the Foam Stability 154
5.3.4 Dynamic Performance of Foam and PEF in the Absence of Heavy Oil 159
5.3.5 Dynamic Performance of Foam and PEF in the Presence of Heavy Oil 162

5.4 Summary 170

Chapter 6: CO_2 Foam and Polymer Enhanced Foam for Heavy Oil Recovery and CO_2 Sequestration: Homogenous and Fractured Core Samples 172

6.1 Introduction 172

6.2 Experimental 174
6.2.1 Fluid Properties 174
6.2.2 Rock Samples 174
6.2.3 Foam Generation 175
6.2.4 Experimental Procedure 176

6.3 Results 179
6.3.1 Homogenous Sandstone Core 179
6.3.1.1 Waterflood 179
6.3.1.2 CO_2 foam/PEF flood 180
6.3.2 Fractured Cores: Sandstone and Carbonate 183
6.3.2.1 Waterflood 183
6.3.2.2 CO_2 foam/PEF flood 184

6.4 Discussions 184
6.4.1 Enhanced Heavy Oil Recovery 185
6.4.2 CO_2 Sequestration 190

6.5 Summary 193

Chapter 7: CO_2 Microbubbles – A Potential Fluid for Enhanced Heavy Oil Recovery: Bulk and Porous Media Studies 195

7.1 Introduction 195

7.2 Materials and Experimental Procedures 201

7.2.1 Materials 201
7.2.2 CO_2 microbubbles Generation and Preparation 202
7.2.3 PVT Analysis 203
7.2.4 Microbubble Size Analysis 204
7.2.5 Rheological Study 205
7.2.6 Porous Media Experiments 205
7.2.7 Fractured Micromodel Experiments 206
7.3 Results and Discussion 207
7.3.1 CO_2 Microbubbles at Elevated Pressure and Temperature (PVT Test) 207
7.3.2 Microbubble Size Analysis of CO_2 Microbubbles 209
7.3.3 CO_2 Microbubbles Stability 209
7.3.4 CO_2 Microbubbles after PVT Tests 212
7.3.5 Rheological Study of CO_2 Microbubbles 216
7.3.6 Rheology of CO_2 Aphrons before and after PVT Tests 217
7.3.7 Potential Use of CO_2 Microbubbles for EOR 220
7.4 Summary 226
Chapter 8: Conclusions and Recommendations 228
8.1 Conclusions and Contributions 228
8.1.1 CO_2 Foam and CO_2 PEF for Improving Chemical EOR Methods 228
8.1.1.1 Static Analysis of Foam/PEF 228
8.1.1.2 Pore-scale 228
8.1.1.3 Core-scale 229
8.1.2 CO_2 Foam/PEF to Improve EOR by Hydrocarbon Solvent Injection 230
8.2 Contributions 230
8.3 Possible Applications 231
8.4 Recommendations for Future Work 231
References 233

List of Tables

Table 1.1: Screening parameters for chemical floods in Alberta (sandstone reservoirs) (Galas et al., 2012). 4
Table 2.1: Experimental parameters (CO_2 foams were injected as a tertiary recovery process). . 36

Table 3.1: Density and viscosity of the hydrocarbon solvents used in this study. 58
Table 3.2: Elemental analysis of asphaltene sample by EDX (element with weight percentage lower than 0.5 wt% cannot be detected by the SEM-EDX system used in this study). 63

Table 4.1: Viscosity values of foaming solution measured at different shear rates (at 22 °C)..... 88
Table 4.2: Experimental parameters including injection flow rate. CO_2 foam and PEF were injected after solvent flooding. 92
Table 4.3: Spreading and entering coefficients of oil for studied surfactant solutions based on surface tension and interfacial tension measurements..... 109

Table 5.1: Summary of dynamic experiments performed on visual sand-pack: with and without the presence of heavy oil. 142
Table 5.2: IFT value (at 25 °C), entering, and spreading coefficients of studied surfactants in the presence of oils. 157

Table 6.1: Summary of core properties and injection parameters. 178

List of Figures

Figure 1.1: Selection of EOR techniques by oil viscosity at reservoir condition 3
Figure 1.2: Schematic of snap-off mechanism showing (a) gas penetrates to the pore structure and a new bubble is formed (b) (Ransohoff and Radke, 1988). 9
Figure 1.3: Schematic of lamella division mechanism showing a lamella is approaching the branch point from (a) and divided gas bubbles formed (b) (Ransohoff and Radke, 1988). 9
Figure 1.4: Schematic of leave-behind mechanism showing gas invasion (a) and lamella formation (b) (Ransohoff and Radke, 1988). 9
Figure 1.5: Schematic of a foam system. 12
Figure 1.6: Schematic representation of a disjoining pressure versus film thickness. 13
Figure 1.7: A moving lamella undergoes stretching or squeezing with a different pore size..... 14
Figure 1.8: Schematic of the antifoaming mechanism of oil: (a) oil drop in a foam film, (b) oil entry at the film surface, (c) spreading of oil drop at air/water interface, and (d) bridging of oil drop within the foam film. 16

Figure 2.1: Schematic of the fractured micromodel set-up for foam injection. 36
Figure 2.2: Normalized foam height versus time; (a) in the absence and (b) in the presence of heavy oil. 38
Figure 2.3: Foamability and foam stability (half-life) values for studied foaming solutions; (a) in the absence and (b) in the presence of heavy oil. 38
Figure 2.4: Micromodel image at the end of waterflood; water could partially sweep the fracture without any impact on matrix oil. 39
Figure 2.5: Images of micromodel at the end of surfactant flooding; (a) anionic DDBS, (b) nonionic N85, and (c) cationic CTAB; representing surfactant imbibition into the matrix; arrows represent surfactant imbibition process. 41
Figure 2.6: Images of micromodel at the end of CO_2 foam/PEF flooding; (a) DDBS foam, (b) N85 foam, (c) CTAB foam, and (d) DDBS PEF. 43
Figure 2.7: Oil recovery profiles at the end of the water, surfactant, and foam/PEF injections... 45
Figure 2.8: Time-lapse images of micromodel during two days of CTAB surfactant injection representing imbibition process; (a) initial, (b) after 12 hours, (c) after 24 hours, and (d) after 48 hours of surfactant injection. 45
Figure 2.9: Microscopic image of micromodel at the end of DDBS surfactant flooding; oil recovered by IFT reduction and emulsification without any significant surfactant imbibition into the matrix. 46
Figure 2.10: A microscopic image of micromodel at the end of N85 surfactant flooding; oil recovered by IFT reduction and emulsification with minor surfactant imbibition into the matrix. 48
Figure 2.11: A microscopic image of micromodel at the end of CTAB surfactant flooding; surfactant could imbibe into the matrix and increase the oil recovery by counter-current imbibition. 48

Figure 2.12: Schematics of wettability alteration mechanisms by surfactant; (a) N85 Surfactant containing EO group, and (b) Cationic CTAB surfactant at an initial stage before wettability change. 49
Figure 2.13: A schematic of wettability alteration and contact angle reduction during surfactant flooding ($\theta_1 > \theta_2 > \theta_3$)..... 50
Figure 2.14: Removing trapped oil in narrow throat of the matrix by foam bubbles. Arrows show the direction of movement (time increases from T_1 to T_4)..... 52
Figure 2.15: Blocking opening area in the matrix by a network of bubbles improving sweep efficiency; (a) camera and (b) microscopic images. Arrows show the direction of liquid movement between foam bubbles and grain. 53

Figure 3.1: Schematic setup of measuring the asphaltene content of the heavy oil using different solvents..... 59
Figure 3.2: Image of the fractured-heterogeneous micromodel showing pore structure. Note: black area shows the porous zone saturated with heavy oil and the white area shows the grain. 60
Figure 3.3: Percentage and images of asphaltene precipitated with different types of solvent in the static condition. 62
Figure 3.4: SEM images of precipitated asphaltene with C5, C7, and C12 hydrocarbon solvent at two different magnifications. 64
Figure 3.5: Images of the micromodel at the end of the heavy oil recovery by solvent injection; (a) C_5, (b) C_7, and (c) C_{12}. The red line represents 1000 microns. 65
Figure 3.6: Images of micromodel showing different time-stage of solvent injection (C5) in the porous media resulting formation damage; (a) early stage of solvent injection representing the diffusion and dilution of oil, (b) second stage showing asphaltene precipitation began at matrix-fracture interface, (c) late stage of solvent flood where there was a severe asphaltene deposition resulting formation damage and pore blocking. 66
Figure 3.7: Deposited asphaltene profile in porous media when injecting different types of solvent. The vertical axis represents the percentage of pore volume covered by the deposited asphaltene. 68
Figure 3.8: Pressure profile during solvent injection (C5) for extra-heavy oil recovery in the fractured micromodel. 69
Figure 3.9: Distribution of asphaltene in porous media precipitated at the end of solvent injection in the fractured porous media, (a) C5 asphaltene, (b) C7 asphaltene, and C12 asphaltene. 70
Figure 3.10: Ultimate heavy oil recovery values when using different solvents in the fractured porous media. 72
Figure 3.11: Images of micromodel during solvent injection at early time stages showing in four frames what happens when hydrocarbon solvent is injected in a fractured porous media. Solvent injection time increases from the images (a) to (d)..... 74

Figure 3.12: Micromodel images showing different shapes of asphaltene precipitated in the fracture and matrix-fracture interface at late time-stage of solvent injection. (a) the increase in the asphaltene deposition at the matrix-fracture interface, (b) creation of rope deposits parallel to the flow direction, (c) combination of lump and rope deposits within the fracture, (d) asphaltene lumps-perpendicular to the flow direction- blocking the fracture path. 76
Figure 3.13: Micromodel image showing the asphaltene deposition pattern in the pore throat. Asphaltene deposited in the narrow pores perpendicular to the solvent flow direction. .. 77
Figure 3.14: Schematic of asphaltene deposition mechanism in the narrow pore throat of the matrix. Parts (a) to (d) shows the time lapse of the deposition mechanism. 78
Figure 3.15: Microscopic images of the micromodel at the end of solvent injection showing different asphaltene deposition pattern in the matrix. (a) parallel rope deposition, (b) asphaltene clusters in the bigger pores of the matrix, (c) asphaltene deposition perpendicular to the flow direction blocking the pore throat. 80
Figure 3.16: Micromodel image showing different patterns of asphaltene deposition in the matrix. Red arrows show the deposition parallel to the flow direction (viscous dominant region) while yellow arrows show the perpendicular depositions (diffusion dominant flow). 81

Figure 4.1: Image of the fractured micromodel (1 mm fracture width) and its frame. The black area shows the void space saturated with heavy oil. 92
Figure 4.2: Oil droplet on the glass surface immersed in water representing wettability alteration (a) WW glass and (b) OW glass. 93
Figure 4.3: Foamability and half-life values of CTAB and DDBS foams and DDBS-PEF in the absence and presence of heavy oil. The numbers represent foam quality (gas percentage). 94
Figure 4.4: Liquid drainage and bubble coarsening phenomena during the static stability of DDBS foam and PEF in the presence of heavy oil (images were taken at 5X magnification). ... 95
Figure 4.5: Oil recovery during water injection in the WW and OW micromodels over time 96
Figure 4.6: Micromodel images (1X magnification) during water flooding in the WW and OW micromodels. (a) OW micromodel after 2 hours, (b) WW micromodel after 2 hours, (c) OW micromodel after 21 hours, and (d) WW micromodel after 21 hours. 97
Figure 4.7: Solvent injection in the heavy oil saturated micromodel. (a) Initial stage (2X magnification), (b) during sweeping of the fracture (2X magnification), arrows show the early stage of asphaltene precipitation, and (c) Asphaltene precipitation, agglomeration, and clustering at the later stage (4X magnification). 101
Figure 4.8: Severe formation damage due to asphaltene precipitation after 5 hours of solvent injection. 101
Figure 4.9: CO_2 gas after solvent injection (a) at the end of the solvent flood and (b) during CO_2 gas injection. The highlighted area represents the diluted matrix oil swept by CO_2 injection. 103

Figure 4.10: Pressure profile of foam generated with CTAB and DDBS surfactants during heavy oil recovery in micromodel after solvent injection; fluctuation in pressure profile representing local instability (collapse) of foam bubbles. 104
Figure 4.11: Images of the micromodel during CO_2 foam injection; images in (a) and (b) were taken after 10 minutes and 1 hour of foam flooding, respectively (same frame, 2X magnification), representing fluid diversion into the matrix by blocking the fracture path (arrows representing direction of fluid diversion), and (c) a later stage of foam flooding (3.5X magnification), demonstrating the emulsification (arrow) and fluid diversion phenomena 105
Figure 4.12: Micromodel image (3.5X magnification) representing the ablation/emulsification process at the late stage of foam flooding. Bubble "A" is trying to invade the matrix opening area, while bubble "B" is already in the matrix pore body, helping the ablation process. The arrow represents the flow direction of detached oil from the glass surface. Bubble "C" represents the late ablation process where most of the oil moved from the glass surface around the bubble, leaving a very thin layer of oil on the grain surface. 106
Figure 4.13: Stability of foam and PEF lamella in the dynamic condition in the presence of heavy oil. Foam lamella collapsed more frequent than that of PEF. The arrow shows the collapse of the foam lamella, leaving oil droplets behind. Images (a1) to (a4) and (b1) to (b4) were captured with one second interval at the late stage of foam and PEF flooding, respectively. 111
Figure 4.14: Images (4X magnification) taken after two hours of (a) DDBS foam, (b) CTAB foam, and (c) DDBS PEF flooding comparing the efficiency of various foaming solutions for the removal of the oil layer around the grain. PEF swept the matrix oil more efficiently and even removed the oil in a dead-end pore (circled area). 112
Figure 4.15: Tertiary CO_2 foam and PEF recovery factors (RF) after 3 hours of solvent injection. 114
Figure 4.16: Performance of CO_2 gas, foam, and PEF heavy oil sweep efficiency after solvent flooding. Images correspond to the end of (a) 3-hour solvent flooding, (b) 5-hour solvent flooding (c) CO_2 flooding, (d) DDBS foam flooding, (e) DDBS PEF flooding, and (f) CTAB foam flooding after 3 hours of solvent injection. 115
Figure 4.17: A schematic of the dynamic experiment: (a) experimental setup, (b) micromodel, black area shows the porous zone (fracture width is 1000 microns, (c) foam generator. MFC: Mass Flow Controller. 119
Figure 4.18: Foam height versus time (foam decay profile) of studied solvent based foams generated with (a) FluorN™ 1740G and (b) Dow Corning 1250 surfactants. 121
Figure 4.19: Changes in initial foam height (a) and surface tension (b) versus surfactant concentration for studied surfactants. 122
Figure 4.20: Visual observation of SBF bubbles generated with 1740G surfactant at two concentrations; (a) 3 wt% and (b) 1 wt%. 124

Figure 4.21: Images of oil saturated micromodel (a) and micromodel at the end of water flooding (b). Note: fracture width is about 1000 microns. 125
Figure 4.22: Images of solvent flooding after initial water flooding (a) 1 hour, and (b) 3 hours. 126
Figure 4.23: Images of SBF flooding after initial water flooding at (a) 1 hour, and (b) 3 hours. 126
Figure 4.24: Heavy oil recovery profile during solvent and solvent based foam (SBF) injections (residual oil recovery after water flooding). 127
Figure 4.25: (a) early stage (1 hour) of solvent flooding: arrows represent slight solvent diffusion around the fracture, (b) next stage (2 hours) of solvent flooding; arrows show the direction of solvent diffusion further into the matrix, and (c) late stage (3 hours) of solvent flooding representing asphaltene precipitation and clustering resulting in formation damage. Dotted rectangle shows the precipitation of asphaltene as a parallel ribbon on the grain surface. 130
Figure 4.26: (a) early stage (1 hour) of SBF flooding: low stability of foam bubbles, (b) next stage (2 hours) of solvent flooding; arrows show the direction of solvent diffusion further into the matrix, and (c) late stage (3 hours) of SBF flooding. 131
Figure 4.27: Late stage (when the most of the oil swept from the matrix areas around the fracture) of SBF flooding showing invasion of bubbles into the opening area in the matrix and increasing sweep efficiency. 132

Figure 5.1: A schematic set-up for foam static analysis. 140
Figure 5.2: Schematic of CO_2 foam/PEF flooding system. 141
Figure 5.3: (a) Foam decay profiles and (b) foamability and half-life values for studied surfactants: anionic DDBS and AOS, nonionic N85 and cationic CTAB. Polymer increased foam stability while decreases the foamability of surfactants. 144
Figure 5.4: (a) PEF decay profile, and (b) liquid drainage profiles of the studied foams and PEFs. 144
Figure 5.5: Surface tension values for the different foaming solutions; the numbers in x-axis represent quality (or gas percentage) of corresponding foam/PEF. 146
Figure 5.6: Effect of heavy oil and mineral oil on (a) foamability and (b) foam stability of studied foams, (c) foamability and (d) foam stability of studied PEFs. 147
Figure 5.7: Foam decay profile for N85 (nonionic) and DDBS (anionic) surfactants; considering the effect of (a) heavy and (b) mineral oil; images correspond to DDBS foam (5X magnification). 150
Figure 5.8: Air diffusion from the small bubbles toward the larger ones leads to the disappearance of the small bubbles and to the gradual accumulation of oil drops in the nodes and the Plateau borders during stage II (DDBS foam with heavy oil). Images (b) were captured seconds after images (a). 151
Figure 5.9: Oil droplets overcome the electrostatic interactions and break a foam lamella during stage III; DDBS foam with heavy oil (2X magnification). 151

Figure 5.10: PEF decay profile in the presence of heavy oil; (a) DDBS (anionic) surfactant and (b) N85 (nonionic) surfactant; images correspond to DDBS-PEF (5X magnification). 153
Figure 5.11: Images of foam generated with DDBS surfactant and heavy oil after 3 minutes (a) and one hour (b); oil saturation increased within the lamella over time (foam top, 2X magnification). 157
Figure 5.12: Flocculation and coalescence of oil droplets within the foam lamella resulting the generation of oil lenses that eventually destabilize the foam (5X magnification). 158
Figure 5.13: Microscopic image of foam-oil systems showing oil emulsion within the lamella (10 X magnification); (a) heavy oil + N85 foam, (b) mineral oil + N85 foam, ... 158
Figure 5.14: Typical profile of pressure during SAG injection in water-saturated porous media. Red and white colors show the existence of liquid and foam, respectively. 161
Figure 5.15: Foam, PEF, and SP pressure/apparent viscosity profiles during flow through water-saturated sand-pack. 161
Figure 5.16: (a) Foamability and (b) foam stability of N85 foaming solution in a dynamic condition; PEF showed lower foamability, but higher stability (less channeling) than that of foam. 162
Figure 5.17: Pressure profiles and apparent viscosity during foam and PEF flow through heavy oil saturated sand-pack. 164
Figure 5.18: Pressure, oil saturation, and oil-cut profiles during heavy oil recovery by foam/PEF; (a) DDBS-PEF, (b) N85-PEF, (c) DDBS-foam and (d) N85-foam. Dotted lines show the oil saturation in which strong foam/PEF begins to propagate. 166
Figure 5.19: Total heavy oil recovery profiles during water and foam/PEF flooding with different foaming solutions. The images show the typical of foam/PEF flooding effluent samples after the water flood; Type #1: oil-in-water emulsion, Type #2: water-in-oil emulsion and free gas, and Type #3: water-in-oil emulsion and foam. 168
Figure 5.20: Heavy oil recovery and pressure profiles during DDBS-PEF flooding: alternate and co-injection modes. Highlighted areas represent the effect of PEF propagation rate (arrows) on oil production profile. 169

Figure 6.1: Images of core samples (Sandstone and carbonate) used in this study. 175
Figure 6.2: Schematic of foam generator used for pre-generated foam/PEF injection. 176
Figure 6.3: (a) Schematic of core flood system used in this study, (b) image of the injection port, and (c) rubber sleeves with three pressure taps for pressure measurement along the core length. 178
Figure 6.4: Pressure profile and water cut during water flooding in a homogeneous core sample. 180
Figure 6.5: Differential pressure profile and oil recovery during injection of Foam(a) and PEF (b) for heavy oil recovery in homogeneous sandstone core. Part#1 and part#2 are 2 inches and 4 inches away from the inlet section, respectively. 182
Figure 6.6: Pressure profile and water cut during water flooding in a fractured core sample. 183

Figure 6.7: Overall pressure drop and oil cut profiles during CO_2 foam and CO_2 PEF injection in fractured sandstone and carbonate core samples. 184
Figure 6.8: Effect of heterogeneity (fracture) on pressure and oil recovery profiles during waterflood. 186
Figure 6.9: Effect of heterogeneity (fracture) on pressure and oil recovery profiles during CO_2 foam flooding process. 187
Figure 6.10: Effect of polymer addition (PEF) on pressure and oil recovery profiles during CO_2 foam flooding in the homogeneous core sample. 188
Figure 6.11: Effect of polymer addition (PEF) on pressure and oil recovery profiles during CO_2 foam flooding in the fractured core sample. 189
Figure 6.12: Ultimate oil recovery values for all experiments during waterflood, foam/PEF injection, and extended waterflood (EWF). 190
Figure 6.13: Cumulative CO_2 gas injection and production profiles during (a) CO_2 foam injection in the homogeneous core, (b) CO_2 PEF injection in the homogeneous core, (c) CO_2 foam injection in the fractured core, and (d) CO_2 PEF injection in the fractured core. 191
Figure 6.14: Amount of CO_2 gas (% of PV) remained inside the porous media at the end of CO_2 foam/PEF injection and extended waterflood process. 192

Figure 7.1: (a) Schematic and (b) microscopic images of CO_2 microbubbles and foam, representing their shape and structure (Sebba, 1987). 200
Figure 7.2: Schematic of experimental procedures for CO_2 microbubbles study. 202
Figure 7.3: Schematic of PVT experimental setup. 204
Figure 7.4: Schematic of fractured micromodel (1 mm fracture width) and its frame. The black area shows void space saturated with heavy oil. 207
Figure 7.5: Pressure versus normalized volume of CO_2 microbubbles at constant temperatures; (a) 24 hours and (b) 48 hours PVT tests. 209
Figure 7.6: Size distributions of CO_2 microbubbles with time. 211
Figure 7.7: CO_2 microbubbles during exposure to the air at room condition. 211
Figure 7.8: (a) Distribution of CO_2 microbubbles size and (b) D50 of CO_2 microbubbles diameter; initially, preserved and after 24 hours PVT tests. 213
Figure 7.9: CO_2 microbubbles size distribution after 48 hours PV tests: (a) 25°C and (b) 50°C, and (c) D50 of CO_2 microbubbles diameter; initially, preserved and after PVT tests. 214
Figure 7.10: Microscopic images of CO_2 microbubbles; (a) Initial, (b) after PVT 25°C, 24 hrs, (c) after PVT 25°C, 48 hrs, (d) after PVT 50°C, 24hrs, (e) after PVT 50°C 48 hrs and (f) after PVT 75°C 24 hrs. 215
Figure 7.11: (a) Viscosity profile versus shear rate, (b) storage (G') and loss (G") modules versus angular frequency for initial CO_2 microbubbles and the base fluid, and (c) G′ and G″ versus frequency and G* versus stress for initial CO_2 microbubbles. 217
Figure 7.12: Rheological comparison of CO_2 microbubbles after HP-HT PVT tests; viscosity profiles (a) and moduli profiles (b) after 24-hr PVT tests. 218

Figure 7.13: Rheological comparison of CO_2 microbubbles after 24-hr and 48-hr PVT tests; (a) viscometry and (b) moduli profiles at 25 °C, (c) viscometry and (d) moduli profiles at 50 °C. 219
Figure 7.14: (a) Injection pressure and oil recovery for CO_2 microbubbles and base fluid during flow through 1D sand-pack experiment, and (b) CO_2 microbubbles effluent samples. . 223
Figure 7.15: Images of the fractured micromodel during microbubble and base fluid flooding for heavy oil recovery (arrow representing flow direction, from left to right); after (a) 10 min, (b) 30 min, (c) 14 h, and (d) 24 h of flooding. 225
Figure 7.16: Heavy oil recovery by CO_2 microbubbles; (a) and (b) images were taken during the early stage (15 and 20 min, respectively); representing fluid invasion into the matrix and emulsification of oil, (b) and (c) images show the later stage of flooding (60 and 65 min, respectively); arrows representing flow direction of emulsified oil from matrix toward the fracture. 226

Chapter 1: Introduction and Literature Review

1.1 Introduction

An oil recovery process from a petroleum reservoir can be divided into three classes: primary, secondary, and Enhanced Oil Recovery (EOR). Solution gas drive, gas cap drive, natural water drive, and gravity drainage are some of the primary oil recovery processes (Green and Willhite, 1998). Secondary recovery can refer to the gas or water injection for pressure maintenance, but nowadays it mostly refers to water flooding. Most of the oil initially present in an oil reservoir is left after primary and secondary recovery. Therefore, EOR methods have to be applied to increase the oil recovery. EOR (or tertiary recovery), usually involves the injection of fluids such as surfactant solutions, polymers, CO_2, foams, hydrocarbon gasses, steam, etc. EOR methods can be classified into at least three categories: chemical recovery, solvent recovery, and thermal recovery. Chemicals used in EOR include polymers, surfactants, and alkalis. They all are mixed with water and, occasionally, other chemicals before injection. Broadly speaking, targets for chemical recovery are crudes in the range between the heavy oils recovered by thermal processes and light oils recovered by miscible gas injection. Adding high molecular weight polymers increases the viscosity of water which can greatly improve waterflood volumetric sweep efficiency. Surfactants injection help lower the interfacial tension that often prevents oil droplets from moving through a reservoir. It also helps change the wettability of the rock surface or cause spontaneous emulsification. The caustic or alkali flooding process relies on a chemical reaction between the caustic and organic acids in the crude oil to produce in-situ surfactants that lower interfacial tension between water and oil. Miscible flooding uses a solvent that mixes fully with residual oil to overcome capillary forces and increase oil mobility. Solvent injection involves the injection of

CO_2, CH_4, N_2 and other agents to dissolve and mobilize hydrocarbon components of the crude oil. A major problem with miscible EOR is the adverse mobility ratio caused by the low viscosity of the typical injecting gas compared to oil. Thermal recovery usually involves the injection of steam to reduce the viscosity of the heavy viscous oil and increase oil mobility. Steam-assisted gravity drainage (SAGD), cyclic steam stimulation (CSS) and steam flooding are the main thermal EOR methods.

Each EOR process is suited to a particular type of reservoir. Because unexpected or unknown reservoir characteristics cause most EOR failures, EOR begins with the thorough geologic study. Taber and coworkers (1983, 1997) performed screening study for different EOR methods based on various criteria such as oil viscosity, permeability, and reservoir depth. A schematic of the EOR screening is shown in Figure 1.1. However, this screening can be different in Canadian reservoirs deposited in western Canadian sedimentary basin (WCSB). The "Sproule Associates Limited" studied the potential of EOR in Alberta, Canada (2012). They discussed the screening criteria for EOR including reviewing the principal EOR methods and summarizing the findings for each method considering the technical issues and the availability of data. They mainly focused on non-thermal recovery methods in Alberta. For example, in contrast to Taber and coworkers screening criteria, polymer flooding was successfully performed at Wabiskaw reservoir of Brintnell Field Horsetail where the oil viscosity in some areas was more than 80,000 cp at reservoir condition. Table 1.1 shows the screening parameters for the chemical flooding in Alberta. This Table was prepared based on 1396 and 935 oil pools for Alkali-Surfactant-Polymer (ASP) and polymer floods, respectively. According to this Table, polymer flooding has been applied in wide range of oil viscosity from 20 cp to about 10,000 cp.

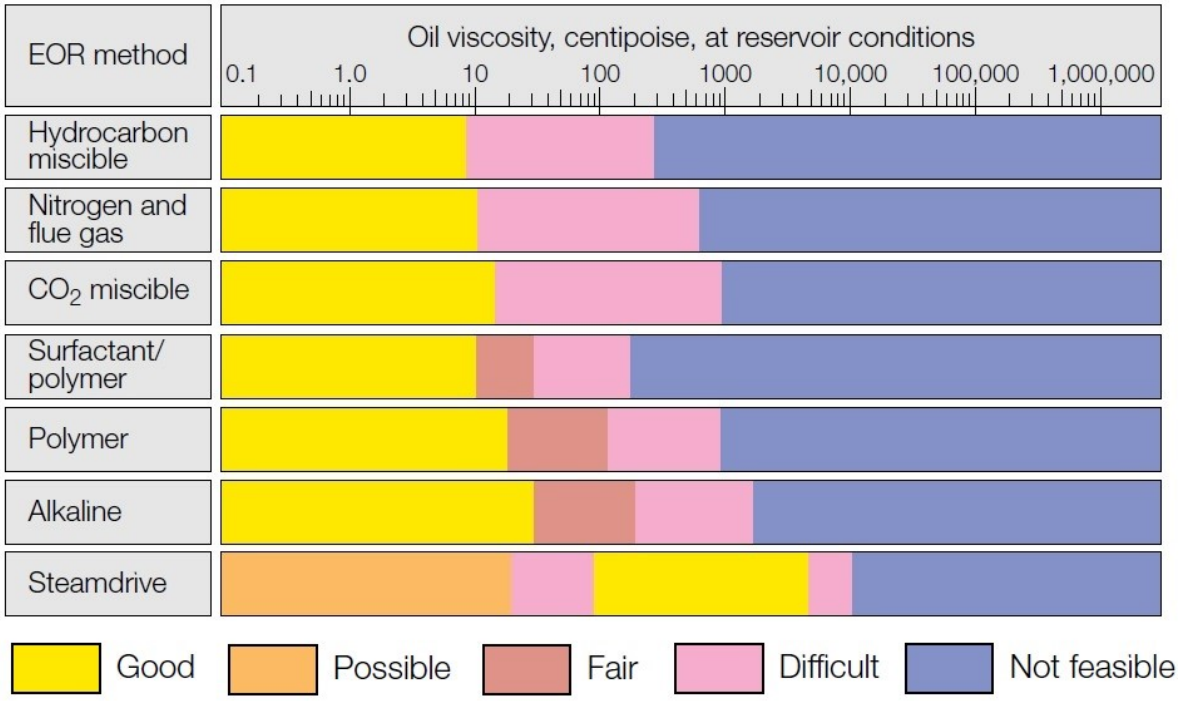

Figure 1.1: Selection of EOR techniques by oil viscosity at reservoir condition (Taber, J.J. and Martin F.D., 1983).

There are significant reserves of heavy oil in WCSB than can be also recovered by non-thermal methods. Per Table 1.1, Alkali-Polymer (AP), ASP, and polymer flooding are the main chemical EOR method for sandstone reservoirs in this area. In addition, the main non-thermal EOR methods used in Alberta carbonate reservoirs include: water flood (mostly as a secondary recovery process), solvent flood (mostly as the first EOR process), Hydrocarbon miscible injection, chase gas (e.g. Pembina field, Nisku formation), CO_2 and acid gas injection (e.g. Judy Creek field, Beaverhill Lake formation), and chemical (e.g. Edgerton field, "Woodbend A" formation). The Edgerton Woodbend A pool is a heavy oil carbonate reservoir that has undergone a chemical EOR process unlike other carbonate reservoirs in Alberta. The polymer flood recovery factor was only 3 % (Galas et al., 2012). Following are the short review of EOR processes introducing their potential and challenges.

Table 1.1: Screening parameters for chemical floods in Alberta (sandstone reservoirs) (Galas et al., 2012).

EOR Type	Property	Unit	Minimum	Maximum
Alkali-Polymer Flooding	Average Pay	m	3	25
	Average Porosity	fraction	0.24	0.35
	Average Permeability	md	350	5000
	Water Saturation	fraction	0.1	0.3
	Initial Pressure	kPa	1000	15000
	Oil Density	kg/m^3	900	960
	Oil Viscosity	cp	1	500
Alkali-Surfactant-Polymer Flooding	Average Pay	m	1	25
	Average Porosity	fraction	0.16	0.35
	Average Permeability	md	500	5000
	Water Saturation	fraction	0.1	0.39
	Initial Pressure	kPa	1000	14000
	Oil Density	kg/m^3	850	975
	Oil Viscosity	cp	3	1100
Polymer Flooding	Average Pay	m	1	25
	Average Porosity	fraction	0.15	0.35
	Average Permeability	md	300	5000
	Water Saturation	fraction	0.1	0.4
	Initial Pressure	kPa	1000	15000
	Oil Density	kg/m^3	875	1075
	Oil Viscosity	cp	20	10000

Solvent Flooding: The key to solvent floods is achieving miscibility between the solvent and the reservoir oil. In a miscible flood, the reservoir oil becomes increasingly solvent rich, so the residual

oil phase has a lower oil component. The solvent also increases the reservoir pressure, swells the oil phase and reduces the oil viscosity-all of which aid in increasing the oil recovery. However, a major difficulty with most solvent floods is early solvent breakthrough due to the unfavorable mobility ratio of any gas flood. This leads to the solvent being recycled through the reservoir. The most common method of mitigating early solvent breakthrough is to inject water and gas in alternating slugs, which is called water-alternating-gas (WAG) flooding. In addition, the cost for a solvent flood should be considered which comprises the cost of the solvent itself, injection facilities, processing facilities and the cost of transportation of the solvent to the EOR site.

Chemical Flooding: The key to chemical floods is to improve the mobility ratio of a waterflood and to reduce the residual oil saturation. Polymer flooding can also improve the vertical conformance of a waterflood. There are several different types of chemical floods including polymer, alkali, alkali-polymer, surfactant, alkali-surfactant-polymer (ASP) flooding. In polymer floods, a polymer, most commonly a polyacrylamide, is added to the injection water to increase its viscosity. This increase in viscosity improves the mobility ratio of the flood. Since the mobility ratio is of most concern in more viscous oil reservoirs, polymer flooding is most often applied to medium and heavy oil pools. In surfactant flood, a surfactant is added to the injected water to reduce the interfacial tension between the oil and the water. The reduction of the interfacial tension, if great enough, can reduce the residual oil saturation, thereby increasing the oil displacement efficiency and the oil recovery factor. Like polymer, surfactants tend to adsorb onto the reservoir rock. In order to adequately flood the reservoir, the concentration of the surfactant must be quite high. Surfactants are relatively expensive, so the cost of a surfactant flood is high. Alkalis such as sodium hydroxide and sodium carbonate are used instead of surfactants due to their lower costs. The alkali can react with acids in the oil to create in-situ surfactants, which then act in the same

way as surfactants injected directly. However, it is usually difficult to sufficiently lower the interfacial tension with alkalis to significantly reduce the residual oil saturation. Both surfactants and alkalis are often used together with polymers for better mobility control. Combining alkali, surfactant, and polymer together (ASP flood) has the added advantage of a synergy between the alkali and the surfactant, significantly reducing the adsorption of the surfactant and bringing the residual oil saturation to very low levels.

Thermal Recovery: The principle of thermal recovery is simple: increasing the oil's temperature dramatically reduces its viscosity, improving the mobility. Cyclic steam stimulation, SAGD, and steam flooding are some of the main thermal oil recovery methods. Foam has also the potential to improve the thermal heavy oil recovery process. Hirasaki (1989) reviewed the steam-foam process for improving the sweep efficiency of the steam drive and steam-soak processes. The concept of using foam for mobility control in petroleum recovery was first suggested by Bond and Holbrook (1958). Steam-foam can control the mobility, improve vertical sweep, maintain injection profile, reduce steam production, and increase oil recovery. However, evaporation and condensation, foam bubbles coalescence at a limiting capillary pressure and coalescence from the action of an oil phase reduce the effectiveness of foam enhanced steam process.

Usually, many advantages of these recovery methods, especially non-thermal methods, are contrasted by their low recovery factor in heavy oil reservoirs. The inadequate sweep efficiency can be due to the adverse mobility ratio resulting from high viscosity oil, heterogeneous nature of reservoir (i.e. natural fractures in carbonate formations), and injectivity problems. In thermal methods, high rate of steam production and inadequate sweep efficiency are some of the main challenges. Foam and polymer enhanced foam (PEF) injection has gained interest in conventional oil recovery in recent times. However, the oil recovery process by foam, especially PEF, is less

understood in both sandstone and carbonate heavy oil reservoirs. The challenge is to understand how the combination of surfactant, gas, and polymer allows us to better access the unswept zones and efficiently improve the sweep efficiency.

1.2 Fundamentals of Foam in Porous Media

Foam in porous media is defined as a dispersion of gas in a liquid such that the liquid phase is connected and at least some part of the gas phase is made discontinuous by thin liquid films called lamellae (Hirasaki, 1989). Foams can be separated into bulk foam and foam in porous media. Bulk foam is foam in a container much larger than the individual bubbles (Rossen, 1996). Rheologically, the bulk foam can be treated as a homogeneous phase (Calvert, 1989). Bulk foams are applied in the oil industry for drilling, fracturing and cementing. Foamability and foam stability (foam half-life) are two main parameters for foam bulk analysis. Foamability is the ability of a foaming solution to generated foam which is equivalent to the gas content of foam (usually more than 70%), representing foam quality. Bulk foam stability is determined by the time required for the foam to be reduced by half. The time required for draining half of the initial liquid from the foam structure can be also considered as a foam half-life.

In porous media, foam is useful in EOR as a mobility control agent because its resistance to flow is usually significantly higher than that of either phase that makes up the foam. The reduced mobility is due to the reduction of gas relative permeability, and rise in apparent viscosity. Foam texture or bubble size determines how much foam reduces gas mobility in porous media. Foam texture, however, is a complicated function of gas and water flow rates, pore geometry, the presence of oil, surfactant concentration, surfactant formulation, etc. Foams with a large reduction in gas mobility are referred to as strong foams and those with small reduction as weak foams or coarse foams.

1.2.1 Foam Generation and Propagation in Porous Media

Foam generation is caused by lamella creation in the porous medium. Lamella destruction refers to lamellae breaking in the porous medium. There are three mechanisms of lamella creation: leave-behind, lamella division, and snap-off.

As illustrated in Figure 1.2, snap-off occurs when gas invades a pore throat and therefore, liquid accumulates in the throat, resulting in the bridging and blocking the throat. This mechanism puts some of the gas into discontinuous form. It can occur repeatedly at the same location, so snap-off can affect a relatively large portion of the flow field. It is widely believed to be a predominant mechanism for foam-generation (Ransohoff and Radke, 1988). The snap-off mechanism influences the flow properties of the gas phase by creating lamellae and therefore, enhancing the discontinuity of the gas phase. The generated gas bubbles may reside at some point in the porous media, thereby blocking gas pathways to reduce gas permeability.

Lamella division occurs when a lamella (pre-generated foam) approaches a branch point so that the lamella is divided into two or more lamellae, as shown in Figure 1.3. This mechanism is similar to the snap-off mechanism in that a separate bubble is formed, and it also occurs numerous times at one site.

Foam lamella can be also generated by the leave-behind mechanism in porous media. Leave-behind begins as two gas menisci invade adjacent liquid-filled pore bodies from different directions (Figure 1.4). Often, two gas fronts approach the same liquid-filled pore space from different directions. When this happens, the liquid in the pore space is squeezed into a lamella by the two fronts. If sufficient surfactant is present in the liquid phase, this lamella may be stable; if not, it ruptures. It is important to realize that this mechanism does not require the two gas fronts to converge simultaneously on the site; they can arrive at different times and squeeze down the

lamella as the local capillary pressure increases. The leave-behind mechanism generates relatively weak foams and it is only important at low velocities (Ransohoff and Radke, 1988).

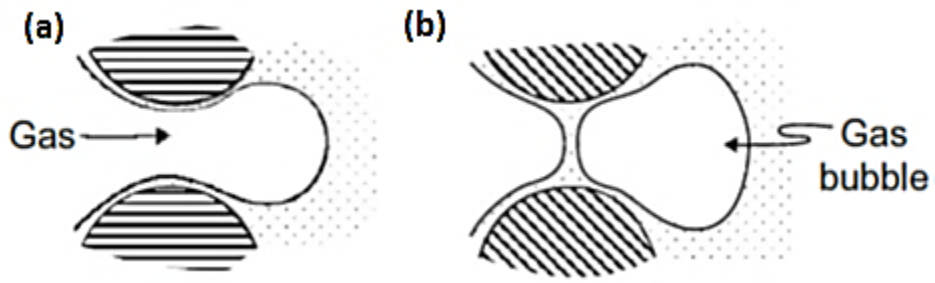

Figure 1.2: Schematic of snap-off mechanism showing (a) gas penetrates to the pore structure and a new bubble is formed (b) (Ransohoff and Radke, 1988).

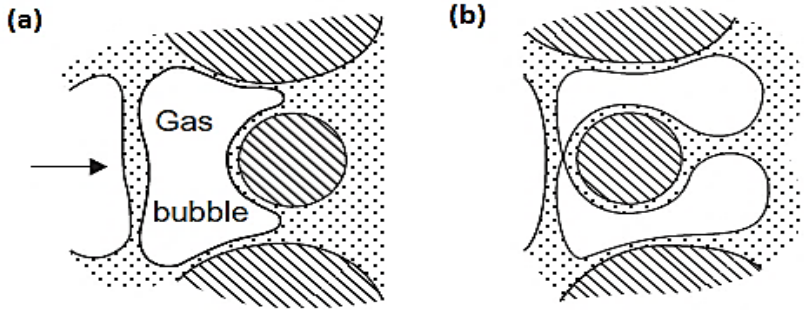

Figure 1.3: Schematic of lamella division mechanism showing a lamella is approaching the branch point from (a) and divided gas bubbles formed (b) (Ransohoff and Radke, 1988).

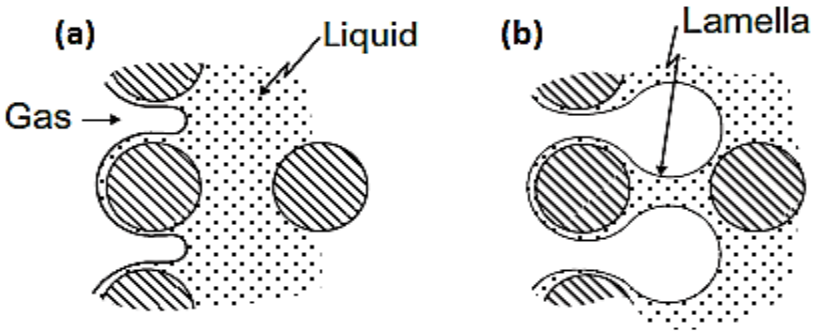

Figure 1.4: Schematic of leave-behind mechanism showing gas invasion (a) and lamella formation (b) (Ransohoff and Radke, 1988).

The requirement of a substantial minimum pressure gradient for foam generation in homogeneous porous media could limit the applications of foam in EOR. Friedmann et al. (1991) reported that foam generation depends on the injection rate and foam quality (gas volume fraction) based on

their experiments in Berea sandstones of permeability roughly 1 Darcy with one surfactant formulation and nitrogen. Baghdikian and Handy (1991) observed a slow increase in pressure gradient while injecting liquid and gas at steady, low velocities until, after many hours or even days, there was a sudden jump in pressure gradient: i.e., "foam generation". This delay is called the "incubation effect." The "incubation effect" illustrates a certain amount of ambiguity of specifying a minimum gas velocity or pressure gradient for foam generation. Ransohoff and Radke (1988) reported a minimum gas velocity for foam generation during drainage in bead packs initially 100% saturated with surfactant solution. Tanzil (2001) concluded that there exists a critical capillary number for foam generation in their gas-only injection experiments, indirectly indicating that there is a minimum gas velocity for foam generation in homogeneous porous media. Gauglitz et al. (2002) observed an unstable foam state between stable "strong" and "coarse" foam states in their fixed-pressure-gradient experiments and showed that the minimum pressure gradient for foam generation is inversely proportional to permeability in sand packs. It should be mentioned that although foam formation and decay are governed by different mechanisms, the final distance foams can travel must be dictated by the surfactant retention. The surfactant availability is a necessary condition for foam generation and propagation. Foam generation and decay is a dynamic process in which foam bubbles are continually be generated and decayed.

In heterogeneous reservoirs, the occurrence of snap-off in flow across a boundary from low permeability to high permeability has been investigated in several studies. Ransohoff and Radke (1988) found that snap-off was observed at all tested velocities at the boundary from low permeability to high-permeability regions of a bead pack undergoing drainage. Rossen (1999) employed a pore-network model to study snap-off at a sharp permeability increase. Snap-off requires a permeability contrast between the high and low permeability media of at least a factor

of four, with higher permeability contrasts required at higher gas fractional flow. Tanzil et al. (2001) created a bead pack with a sharp boundary from low permeability to high permeability and found foam generation at the permeability transition as gas went through the pack initially saturated with surfactant at low foam qualities.

1.2.2 Foam Stability

Chambers and Radke (1991) stated two basic mechanisms of foam coalescence: capillary suction and gas diffusion. Coalescence due to the capillary suction is the primary mechanism for lamellae breakage. As shown in Figure 1.5, the gas/liquid interfaces at the Plateau borders are curved (smaller radii), while the interfaces are flat along the thin-film regions, (larger radii). Because the capillary pressure is inversely related to the radii of an interface (according to the Young-Laplace equation), there is a pressure difference between these two regions. This pressure difference forces the liquid to flow toward the Plateau borders and results in thinning of the films.

The foam lamella is not thermodynamically stable. The existence and destruction of lamellae are governed by disjoining pressure (π) (Figure 1.6), which is combined effect of attractive and repulsive forces within lamella as described by Miller and Neogi (1985). In the absence of surface active agents, the attractive van del Waals force are dominant, resulting in negative disjoining pressure and immediate collapse of the thin film. The lamella is stabilized by surfactant adsorption at the gas/liquid interface. The electrical double-layer caused by surfactant adsorption is responsible for the excess repulsive forces that stabilize the thin film. The stabilizing effect depends on several factors such as the surfactant structure, surfactant concentration and the ionic content of solution (Kovscek and Radke, 1994). A liquid film thins down until it breaks if the disjoining pressure, the term for the stabilizing effect of surfactant (Schramm, 1994), is not

sufficient to stabilize the film. The breaking of films at the "critical disjoining pressure" is the origin of foam collapse at the "limiting capillary pressure.

The liquid film between two gas bubbles undergoes a thinning process, which will eventually cause the foam to rupture. Gravity always tends to force the liquid to flow down through a well-connected network of liquid films. In bulk foam, as the liquid film is being drained, the shape of a gas bubble will be more close to a polyhedron rather than a perfect sphere, and the liquid lamella in between is relatively planar. As shown in Figure 1.5, at the borders, the gas-liquid interface is quite curved, generating low pressure. The interface along the flat lamella is quite flat, so higher pressure resides there. The pressure gradient forces flow towards the borders causing film thinning. Besides pressure gradient as a driving force of film thinning, van der Waals attractive forces also cause film thinning. However, some other factors counteract the film thinning process. These include surface elasticity, surface viscosity, steric interactions, and repulsive force of electric double layer.

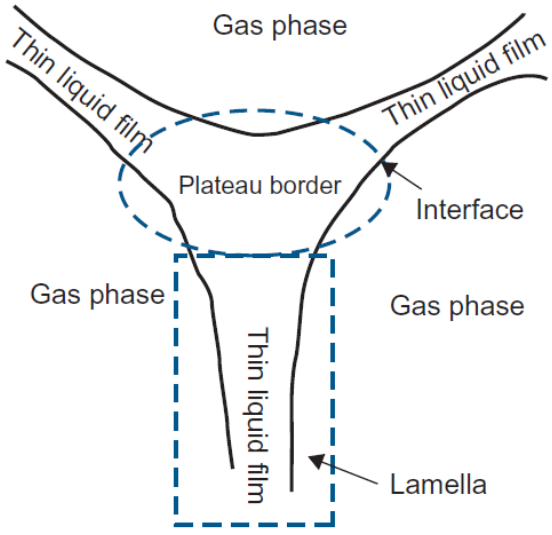

Figure 1.5: Schematic of a foam system.

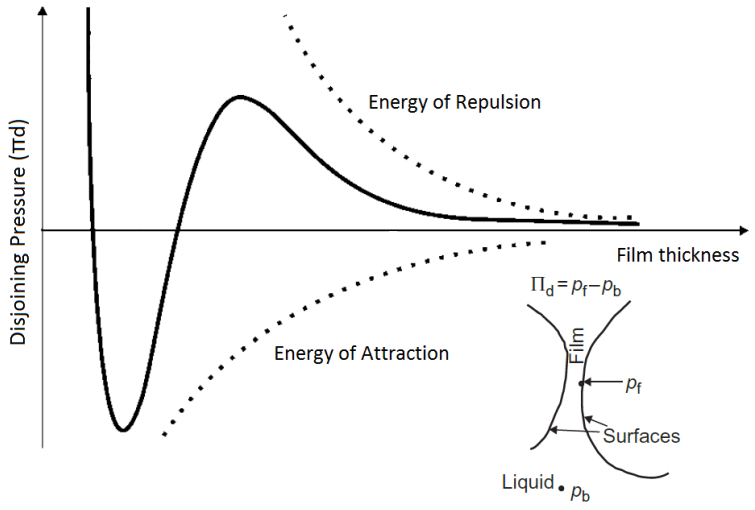

Figure 1.6: Schematic representation of a disjoining pressure versus film thickness.

In porous media, foam coalescence by gas diffusion takes place only when two lamellae happen to reach the same pore throat (Kovscek and Radke, 1994). Therefore, gas diffusion is relatively unimportant for foam in porous media. The curvature of foam in porous media is governed by the pore dimension and lamellae location in the pore space, nor by bubble size. In the case of a moving lamella, its thickness oscillates due to the geometry of the porous media as it translates from a pore body to a pore throat to another pore body. As shown in Figure 1.7, a moving lamella undergoes stretching or squeezing. When it is being stretched, if the film thickness falls below critical film thickness (hcr), the lamella will break (Singh et al., 1997). Therefore, a moving thin film could rupture at a limiting capillary pressure (Pc*) which is less than the maximum disjoining pressure (π_{max}). In other words, moving lamellae are even less stable than static ones.

The thickness of moving lamella depends on the influx of liquid into the lamella from its surrounding. If rapid enough, the influx would restore the film thickness before it reaches the critical value. The Marangoni effect helps the restoration process. Marangoni effect is defined as the mass transfer along an interface between two fluids due to surface tension gradient. Lamella stretching reduces the local surfactant concentration and increases the local surface tension. The

increased surface tension works against the thinning. Together with disjoining pressure, the Marangoni effect is restoring force in a lamella.

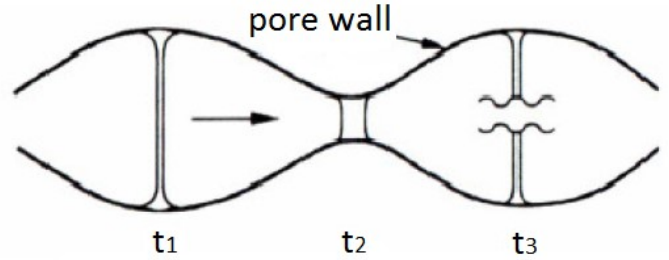

Figure 1.7: A moving lamella undergoes stretching or squeezing with a different pore size (Kovscek and Radke, 1994).

1.2.2.1 Foam Stability in the Presence of Crude Oil

Crude oils often destabilize foam and it is widely believed that light crude oils are more effective in foam destabilization. However, the amount of destabilization depends on the compositions of surfactant, oil, and aqueous-phase. As the oil drop approaches the gas/water interface, it must first overcome electrostatic or steric interactions in the aqueous pseudoemulsion film to destabilize a foam lamella (Nikolov et al. 1986; Manlowe and Radke 1990). Then, the oil can destabilize the lamella by spreading along the gas/water interface (Lau and O'Brien, 1988), by bridging (Garrett, 1993), or by some combination of both. The mechanisms have been extensively investigated (Garrett, 1993; Aveyard, 1994; Zhang et al., 2003; Schramm, 2005). Garrett explained three coefficients, namely entry coefficient (E), spreading coefficient (S), and bridging coefficient (B), which are important in interpreting the mechanisms of oil destabilizing foam. Lamella number (L) can be also used for foam-oil stability studies (Schramm and Novosad, 1990). These coefficients are defined as follows:

$E = \sigma_{wg} + \sigma_{wo} - \sigma_{og}$

$S = \sigma_{wg} - \sigma_{wo} - \sigma_{og}$

$B = \sigma^2_{wg} + \sigma^2_{wo} - \sigma^2_{og}$

$L = 0.15\ (\sigma_{wg}) / (\sigma_{ow})$

Where σ_{wg}, σ_{og}, and σ_{ow} are surface tension of foaming solution, the surface tension of oil, and interfacial tension of water/oil interface, respectively.

To destabilize a foam lamella, an oil drop must first enter the air/water surface, i.e. $E>0$. In order to enter the interface, the oil drops have to overcome the repulsive forces caused by the pseudoemulsion films separating these drops from the interface (Nikolov *et al.*, 1986; Manlowe and Radke, 1990; Basheva, *et al*., 2000). Once an oil drop enters, it may spread at the air/water interface i.e. $S\geq 0$, leading to foam lamella rupture. When $S\leq 0$ an oil drop forms a lens on one side of the air/water interface and as the foam film thins may reach the other side, thus forming a bridge. If $B>0$, the bridge is unstable and the film breaks. A schematic of these processes is shown in Figure 1.8.

In the case of foams contacting oil in a porous medium the oil may not be emulsified, or may not have such small drop sizes. The process of an oil phase emulsifying into foam lamellae has been described from a balance of forces in terms of a lamella number, L (Schramm and Novosad, 1990). Based on these theories, oils can be defined to give unstable foam, moderately stable foam or they are defined to show little interaction on foam. From experiments in a micro-visual cell, Schramm and Novosad (1990, 1992) have defined three types of foams, A, B, and C. Type A foams believed to show the best stability in the presence of oil, by having both negative entering and spreading coefficients. The lamella number is less than 1, so these foams are believed to show little interactions with crude oil. Type B foams have lamella number of $1<L<7$, and show a negative spreading coefficient and a positive entering coefficient. These foams are defined to have the moderate stability to oil. Type C foams defined to give an unstable foam. Both spreading and

entering coefficient are positive for these foams and lamella number is greater than 7. By understanding these mechanisms, surfactants that can stabilize foam in presence of oil can be designed.

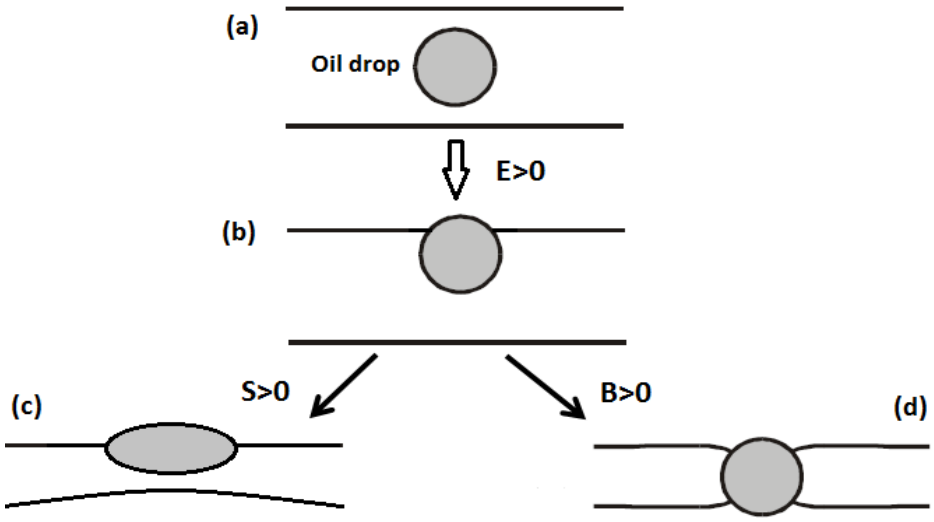

Figure 1.8: Schematic of the antifoaming mechanism of oil: (a) oil drop in a foam film, (b) oil entry at the film surface, (c) spreading of oil drop at air/water interface, and (d) bridging of oil drop within the foam film.

There are several studies on the static and dynamic performance of foam-oil systems (Vikingsad et al., 2005; Andrianov et al., 2012; Scharamm and Novosad, 1992; Koczo et al., 1992; Farajzadeh *et al*., 2010; Simjoo *et al*., 2013). These studies are mainly focused on performing foam stability experiments (bulk tests) in the presence of different types of oils and measuring the foam half-life. Some of these researchers also measured the spreading, entering, and, birding coefficients in the foam-oil system and tried to explain the behavior of the foam-oil system. However, the relation between spreading phenomena and foam stability has been inconclusive for general applications. For instance, Andrianov et al. (2012) concluded that there exists a strong correlation between spreading and entering coefficients, and foam stability while Vikingsad et al. (2005) did not find any direct correlation between spreading coefficient and foam stability. Andrianov, et al. (2012)

studied bulk foam stability in presence of oil. They measured the spreading (S), entering (E), bridging (B), and lamella number (L) for AOS foam in presence of three Alkanes. The result of spreading and entering coefficients was found to be comparable with the foam stability. However, lamella number could not predict the foam/oil stability behavior.

Scharamm and Novosad (1992) classified the foams based on their interaction with oils (Types A, B, and C). This classification was done based on values of E, S, and L. They couldn't find any correlation between E and S values and foam stability. However, they classified the foam/oil system with the help of lamella number.

Tamura et al. (1999) studied the bursting behavior of pseudoemulsion film with the different type of antifoams. They also mentioned that the antifoaming efficiently of antifoams is strongly depends on the stability of the pseudoemulsion film.

Koczo et al. (1992) studied both E and S coefficient as well as pseudoemulsion film. Per their study, although the E and S coefficient are positive (so spreading of the oil drops is thermodynamically favorable), the microscopic observation showed that pseudoemulsion film is very stable and oil drop cannot enter the air/water surface during the first hour. They concluded that the effect of oil on foam stability and its mechanism depends on whether the oil is solubilized or emulsified and whether the pseudoemulsion film is stable or not.

Manlowe and Radke (1990) investigated the foam/oil interaction through direct observation in the micromodel. They showed that the stability of pseudoemulsion film controls the foam stability, regardless of subsequent spreading characteristics of the oil. They visualized the foam/oil interaction in the micromodel and found that for all studied surfactants, the "pseudoemulsion film destabilization" mechanism (film thinning and eventually breakage) observed as the source of foam breakage by residual oil.

Koczo et al. (1992) studied the effect of emulsion on foam stability. They study on solubilized oil as well as emulsified oil systems showed that later one may result in stability of foam system while first one (solubilized oil) will decrease foam stability. They found that the presence of emulsified oil increases the foam stability if the pseudoemulsion film is stable because the oil drops collect in the PBs of the aging foam and this packed emulsion inhibits the liquid drainage through the PB network due to the increased hydrodynamic resistance.

1.3 Potential of Foam and PEF for Heavy Oil Recovery: Literature Reviews

Foam has several applications in petroleum industry including gas coning blocking foam (Heuer and Jacocks, 1968), foams for well stimulation (Chou, 1991), foam as a fracturing fluid, and foam EOR (i.e. CO_2 foam, foam injection in gas miscible flooding, and steam foam). Here the application of foam for EOR is discussed.

Since the 1960s, there have been several field trials of surfactant injection with gas into the subsurface to generated foam (Patzek, 1996). Foam has shown its potential for improving reservoir sweep efficiency over gas injection in EOR projects (Hirasaki 1989; Smith 1988). The effective viscosity of foam is much higher than that of gas, so it can reduce viscous fingering and gravity override caused by injecting gas, supercritical CO_2 or steam (Yan et al., 2006). Besides improving sweep efficiency in gas flooding, foam/PEF can be used for mobility control in chemical EOR where the foam is considered an alternative to polymer mobility control in micellar flooding (Lake, 1989). Due to adverse mobility in heavy oil reservoirs, water flood process usually ends with low recovery factor. Therefore, alternative methods are required to increase the heavy oil recovery. Chemical flooding (e.g. polymer flood) can be used to decrease the mobility ratio and increase the sweep efficiency. However, the presence of water channels after water flooding and heterogeneity of reservoirs can decrease the performance of chemical methods in heavy oil recovery. On the

other hand, foam and PEF have the potential to increase the sweep efficiency in heterogeneous reservoirs by generating strong foam/PEF in the high permeable area. Zhang et al. (2000) reported laboratory and field studies of foam in Daqing oilfield in China, where the foam was successfully applied in a heterogeneous porous media and compared with the performance of chemical flooding. In addition, Tang et al. (2014) presented a new high-temperature resistant nitrogen foam system that gives a low oil/water interfacial tension and improves the sweep efficiency after Surfactant-Polymer (SP) flood in Shuanghe oil field.

There are several challenges for widespread application of foam in porous media such as in situ generation and propagation of foam. Although the principal mechanisms for foam generation have been identified, the precise condition when the strong foam can be generated in the reservoir remained unknown. In a homogeneous porous medium, with steady co-injection of gas and liquid, a minimum pressure gradient is required to create foam (Ransohoff and Radke, 1988; Rossen and Gauglitz, 1990; Tanzil et al., 2002; Gauglitz et al., 2002). One of the proposed ways to enhance foam generation is using small, alternating slugs of liquid and gas (SAG injection) (Rossen and Gauglitz, 1990). SAG injection has several advantages over co-injection of gas and surfactant as it reduces the contact between water and gas in the surface facilities (Mattews, 1989; Heller, 1994) and besides improving injectivity, it can possibly improve foam generation in the near-well-bore region (Rossen and Gauglitz, 1990).

Hoefner et al. (1995) studied the CO_2 foam field trials to determine the effectiveness of foam in reducing CO_2 channeling, to evaluate the economic potential of the process, and to develop application criteria and procedures. Applying foam resulted in a significant reduction in gas production and indications of increased oil production.

Romero et al. (2002) studied the performance of PEF in micromodel. They found that in micromodel scale, the capillary pressure and coalescence do not govern PEF flow in porous media, as it does for conventional foams.

Jian et al. (2014) studied the stability of polymer and surfactant mixture enhanced foams in the presence of oil under static and dynamic conditions. They found that the introduction of the polymer into the foam formula could significantly increase foam stability. The stability of liquid films in PEF can be significantly improved, resulting in stronger oil-resistance ability.

Carbonate Reservoirs: With rising concerns about the depletion of conventional oil reservoirs, more attention is directed to heavy oil reservoirs as potential energy resources. The difficulties and costs of heavy oil production urge further research to find new methods to overcome these difficulties and/or reduce the cost of production. The challenge becomes more complicated when it deals with fractured and carbonates reservoirs. The main target in this type of reservoir is the oil in the tight matrix, but fracture network controls the flow due to its high permeability. Recovery of the matrix heavy oil, while the injected fluid flows in fractures, is a challenge and yet, no systematic technique has been proposed for this type of reservoir.

There are significant reserves of conventional light to heavy oil in the Western Canadian Sedimentary Basin (WCSB) which is in the carbonate formation. However, due to the presence of a fracture network and oil wet matrix (Chillenger and Yen, 1983; Roehl and Choquette, 1985), oil recovery from naturally fractured carbonate reservoirs has always been a challenging task. Fracture networks diminish the effectiveness of water or chemical flooding, and the oil-wet matrix limits the capillary imbibition process, which is an important recovery mechanism in the fractured reservoirs. They exhibit very limited recovery during primary and secondary production because most of the injected fluids preferentially go through fracture openings, leaving behind a significant

amount of oil in the matrix. Therefore, designing a process to recover the matrix oil at an economic rate often turns out to be a real challenge for such reservoirs (Bourbiaux, 2009).

Solvent, gas, water, water alternating gas, and chemical injections have been considered as the main non-thermal methods to recover oil from highly fractured oil-wet carbonate reservoirs (Manrique et al., 2006; Gupta and Mohanty, 2008). Chemical EOR research in carbonate reservoirs has been focused on using surfactants to change the wettability and enhance water imbibition into the matrix, thus driving oil out of the matrix. Different type of surfactants has been used to alter the wettability of originally oil wet carbonate rocks. Austad and collaborators (Austad and Milter, 1997; Standnes and Austad, 2000a, 2000b) have shown that cationic surfactants can recover oil by spontaneous counter-current imbibition due to wettability alteration. The wettability alteration mechanism is supposed to occur by an ion-pair formation by the positively charged cationic surfactant and the negatively charged carboxylates in oil. Although they are effective in altering wettability for oil-wet rocks, cationic surfactants are too expensive for the field treatment. In addition, Stoll et al. (2008) reported that spontaneous imbibition of surfactants, as wettability modification agents could not provide an economically interesting opportunity unless external forces enable forced imbibition of this surfactant. Foam/PEF can provide this external pressure for successful application of chemical EOR in fractured carbonate reservoirs.

Khalil and Asghari (2006), in a series of static and dynamic experiments, studied the effect of reservoir pressure, temperature, and other factors on the effectiveness of the CO_2 foam technique for reducing foam mobility in carbonate rock. Liu et al. (2006) also studied the foam mobility and surfactant adsorption in a carbonate core. Zuta and Fjelde (2008, 2010) studied the performance of CO_2 foam in fractured carbonate reservoirs. They found that co-injecting CO_2 gas and aqueous foaming agent solution had slightly higher oil recovery than CO_2 injection. Aarra et al. (2011)

studied the foam properties for applications in carbonate material. They investigated the foams potential to reduce the mobility of gas and water and found that the generated foams showed good ability to reduce gas and water production at low-pressure gradients.

1.3.1 Application of Foam in Thermal Oil Recovery

Steam foam EOR has been studied extensively to improve sweep efficiency and to reduce steam channeling and override during steam flooding in shallow heavy oil reservoirs. The steam foam process consists of adding a surfactant, with and without the addition of a non-condensable gas, to the injected steam (Hirasaki, 1989; Isaak, 1994). Based on the findings of theory, laboratory studies, and field performance, steam foams are normally more effective in the presence of a non-condensable gas. Steam foams have been used in both continuous and cyclic steam injection (Hirasaki, 1989).

Steam drives that are not stabilized by gravity can have poor vertical sweep efficiency as a result of (1) gravity overlay in the thick sand with vertical communication and/or (2) channeling in a layered formation with poor vertical communication (Hirasaki, 1989). The reduced mobility of steam foam increases the pressure gradient in the swept region and diverts the steam to the unheated interval. Surfactants reduce the steam mobility by stabilizing the liquid lamellae that change the steam to a discontinuous phase. The propagation of surfactant is retarded by adsorption. In the case of ion exchange of divalent ions from the clays, the surfactant is also retarded by precipitation and/or partitioning into the oil. The rate of propagation of foam is also determined by the mechanisms that generate and destroy foam as explained earlier in this chapter. Condensation and evaporation are also considered as one of the foam destruction mechanisms at high temperatures. Adding a small amount of non-condensable gas can retard the evaporation and condensation processes (Hirasaki, 1989).

In a reservoir (or a sand unit of a multizone reservoir) with nonzero vertical permeability and not enough dip and/or horizontal permeability, injected steam will override the reservoir and will result in a poor vertical sweep (Hirasaki, 1989). Such reservoirs have a good potential for the application of foam in the steam-flooding process. An example of such a case is the steam-drive in the Mecca Pilot of the Kern River field, where steam breakthrough occurred early and oil production declined (Dilgren et al., 1980; Patzek and Koinis, 1988).

A thief zone in a steam drive or steam soak is much more severe than in a waterflood. Once the thief zone is swept the high mobility of steam than that of the viscous oil and water causes the thief zone to be a "short circuit" for the subsequently injected steam (Hirasaki, 1989). The foam will improve the injection profile by reducing the contrast between the resistance in the swept thief zone and that in the oil-saturated (unswept) zones. The increase in the injection pressure indicates a reduction of the steam mobility, demonstrating the effectiveness of a steam foam process. The increase in injection pressure corresponds to the increase in the pressure differential for the zones that previously were not taking steam i.e. unswept zone which is beneficial to improvement in the injection profile. Patzek and Koinis (1988) have shown how the injection pressures, along with the saturated steam temperatures in observation wells, can be used to find the in-situ mobility within the reservoir.

Several researchers investigated the potential of foam for improving the thermal oil recovery. The first steam-foam process was patented on 1968 (Needham, 1968) describing a process to block high-permeability layer so that steam may be diverted into the less permeable layer. Dilgren et al. (1982) studied both experimental and field test potential of steam/non-condensable gas foams for mobility control in heavy oil recovery. Reduced steam foam mobility in the field (Mecca) was evidenced by an increase in flowing bottom-hole pressures for the injectors. An increased rate of

oil production was also observed. Hamida et al. (1990) showed that under the experimental conditions at elevating temperature the alpha olefin sulfonate (AOS) generated the strongest and most long-lived foams of all the studied surfactants. They also observed a significant steam relative permeability reduction in the presence of surfactants (steam foam). Cuenca et al. (2014) optimized the formulation required to generate stable steam foams up to temperatures of 200 °C. Lau (2012) performed an experimental work on alkaline steam foam flooding. In steam drive process, he observed that alkaline steam foam has the benefit of increasing foam propagation rate, improving mobility control, improving steam use, and reducing the steam oil ratio.

1.3.2 Nanoparticles Enhanced Foam for EOR

As mentioned earlier, foam is a potential solution to the technical challenges associated with gas-injection processes (Kovscek et al. 1994; Rossen et al. 2010; Haugen et al. 2012). It can significantly reduce gas mobility by increasing the apparent viscosity of gas and trapping a significant amount of gas inside the porous media (Bernard and Jacobs 1965; Hirasaki and Lawson 1985). Conventionally, surfactants are used to stabilize foam lamellae and the continuous regeneration of lamellae is essential for foam transport in the porous media (Rossen 1996; Roostapour and Kam 2013). One of the key factors for the cost associated with surfactant-stabilized foam is the quantity of surfactant required for long-distance propagation of foam from the wellbore (Kibodeaux and Rossen 1997). Several factors limit further the economic viability of surfactant usage in subsurface applications including surface adsorption, surfactant loss caused by partitioning into crude oil, and surfactant degradation under harsh reservoir conditions (Grigg and Mikhalin 2007; Chen et al. 2012). The use of nanoparticles can help mitigate these issues. Due to its potential to withstand harsh conditions of temperature and salinity in reservoirs, Nanoparticle-stabilized foam/emulsion recently has been of interest in the petroleum industry. Moreover,

economical bulk production of nanoparticles can be obtained from low-cost raw materials such as fly ash and silica (Paul et al. 2007).

It has been reported recently that aqueous foams stabilized by Nano and microparticles alone are much more stable than surfactant or polymer-stabilized foams (Alargova et al., 2004; Binks and Horozov, 2005; Gonzenbach et al., 2006; Fujii et al., 2006): the latter typically collapse after a maximum of a few tens of hours. Cervantes Martinez et al. (2008) showed that it is possible to produce large amounts of foam stabilized only by solid particles, that have controlled bubble size and that can last for months. The enhanced stability arises from a combination of the adsorption of coated particles around bubbles preventing coalescence and disproportionation as well as the reduction in the extent of drainage between bubbles due to the increased aqueous phase viscosity of a flocculated dispersion. Singh and Mohanty (2015a) studied foam stabilization by in-situ surface-hydrophobization of hydrophilic nanoparticles. In their study, surface-modified nanoparticles (SMNPs) were obtained by partial hydrophobization of alumina-coated silica nanoparticles with a surface modifier. Foams were then stabilized by these SMNPs, in the absence of surfactants, which tended to adsorb at the air/water interface in both bulk and porous media. Espinosa et al. (2010) investigated supercritical CO_2-in-water foam generation in bead packs using hydrophilic silica nanoparticles coated with poly (ethylene glycol). The generated foam using nanoparticles had 2-18 times more resistance to flow than the same fluid without nanoparticles.

1.4 Statement of the Problem

Enhanced oil recovery (EOR) from heavy oil reservoirs is challenging. The higher viscosity of oil in such reservoirs, add more challenges and severe the difficulties during any EOR method i.e. high mobility ratio, inadequate sweep, reservoir heterogeneity. Besides thermal recovery methods,

non-thermal recovery methods (i.e. solvent, gas, water, and chemical injections) have been used for heavy oil recovery.

- Water and gas injections are usually selected as a first recovery method from heavy oil reservoirs due to their relatively low cost. Although these methods can be effective in light oil reservoirs without any severe heterogeneity/fracture, they suffer from several disadvantages in heavy oil reservoirs (i.e. high mobility ratio, inadequate sweep efficiency and early water/gas breakthrough).
- Chemical methods are most common non-thermal EOR process for heavy oil recovery after water flooding. The main issue with the chemical method for heavy oil reservoirs is low injectivity and inadequate sweep efficiency, especially in heterogeneous reservoirs. Injectivity problem and inadequate sweep efficiency (due to the heterogeneity) are some of the main problems in polymer flooding. Surfactant injection in fractured reservoirs also suffers from several drawbacks such as slow rate of imbibition which reduce the rate of oil recovery from the matrix area where the most of the oil is located.
- Hydrocarbon solvent injection is also one of the heavy oil recovery methods. The solvent injection will reduce the viscosity of heavy oil and make the oil to flow easier. However, besides slow rate of diffusion, asphaltene precipitation and deposition is another main challenge during solvent injection in heavy oil reservoirs. Precipitation and deposition of asphaltene in reservoir rock can cause formation damage and reduce the fluid mobility, resulting in significant loss of the hydrocarbon production.

A comprehensive study for the recovery of heavy oil from fractured reservoirs by means of CO_2 foam/PEF is needed to be investigated from the laboratory to field scale. This work is intended to create a base frame for such study and open new insight to discover the paths and parameters for

further developments. Foam and PEF have the potential to be a displacing fluid in different types of reservoirs. They can be combined with other EOR methods to improve the performance and efficiency of current heavy oil recovery process. The high viscosity of the oil and high heterogeneity of heavy oil reservoirs can result in inadequate sweep efficiency of conventional non-thermal methods. Shallow heavy oil reservoirs in Western Canadian Sedimentary Basin (WCSB), which can be also recovered by non-thermal processes, can be the potential target for foam/PEF EOR application.

1.5 Objectives

This research aims to investigate the potential of CO_2 foam and CO_2 PEF for heavy oil recovery to improve the performance of conventional EOR methods for heavy oil reservoirs. The focus of this research is conducting experiments which would help in understanding mechanisms and in the design of foam/PEF EOR processes in various challenges exist at the reservoir conditions such as heterogeneity, effects of crude oil, wettability, asphaltene deposition, etc. A major attraction of foam is the possibility of diverting flow from high-permeability to low-permeability layers. It can also provide better control of the injected fluids as stronger foams can spontaneously block the flow channels in high-permeability media. Therefore, the main objective of this research is evaluating the potential of foam/PEF for heavy oil recovery by combining foam/PEF EOR with current EOR method to overcome the disadvantage of current heavy oil recovery methods and improve the efficiency of heavy oil recovery. Extensive pore-scale and core-scale studies are performed in this research to achieve this goal. To evaluate the potential of foam and PEF for heavy oil recovery, followings are the main objectives of this research:

- Examine the static performance of foam (generated with a different type of surfactants) and effect of polymer addition on foam stability in the presence and absence of heavy crude oil.
- Study the dynamic of foam flow (pore-scale mechanisms of CO_2 foam and CO_2 PEF) to improved conventional surfactant flooding in fractured carbonate reservoirs.
- Analyze the pore scale performance of hydrocarbon solvent injection for heavy oil recovery and improve its performance in fractured reservoirs with the help of foam and PEF.
- Studying the dynamic behavior of foam/PEF flow (core-scale) in the presence of waterflood residual oil and providing the mechanisms by which foam recovers tertiary oil and the criteria for generation and propagation of a stable foam/PEF.

1.6 Thesis Structure

The organization of this dissertation is as follows:

Chapter 1 includes the general introduction, literature review, and objectives of the thesis.

The CO_2 foam and CO_2 PEF are studied in a fractured micromodel after surfactant flooding in Chapter 2. The mechanisms involved in the heavy oil recovery be foam and surfactant in the fractured reservoir are investigated in this chapter with the help of pore-scale visualization.

Chapter 3 investigates one of the main problems during the hydrocarbon solvent injection which is asphaltene deposition and formation damage. Therefore, the dynamic behavior of asphaltene precipitation and distribution pattern in fractured porous media is investigated in this chapter.

Chapter 4 discuss the potential of CO_2 foam and CO_2 PEF to improve the performance of conventional solvent injection discussed in Chapter 3. At the first part of this chapter performance of CO_2 foam/PEF are visualized in a fractured micromodel after solvent injection. The second part

evaluates the potential of solvent based foam (SBF) as an EOR method to improve the hydrocarbon solvent injection process for heavy oil recovery.

Chapter 5 studies the performance of CO_2 foam/PEF in bulk and porous media. Effect of polymer addition and heavy crude oil is investigated in both bulk and porous media (homogenous sand-pack) in this chapter.

Chapter 6 presents the experimental results of CO_2 foam/PEF in homogenous and fractured core samples during heavy oil recovery. CO_2 foam/PEF are used as a tertiary EOR process after water flood to improve the heavy oil recovery. Moreover, the potential of CO_2 sequestration by CO_2 foam/PEF are also presented in this chapter.

The potential of CO_2 microbubbles for EOR application is studied in Chapter 7. Results of microscopic study, PVT, rheology and porous media experiments are presented in this chapter.

Chapter 8 provides the conclusions and recommendations of this study and suggestions for further work.

Chapter 2: Post-Surfactant CO_2 Foam/Polymer Enhanced Foam Flooding for Heavy Oil Recovery: Pore-Scale Visualization in Fractured Micromodel[1]

2.1 Introduction

A significant amount of the world's oil reserve is in carbonate formations; however, due to the presence of fracture networks and oil wet matrix (Chillenger and Yen, 1983; Roehl and Choquette, 1985), oil recovery from naturally fractured carbonate reservoirs has always been a challenging task. After the primary production period, waterflooding is often performed to increase the recovery efficiency. In fractured reservoirs, oil recovery from waterflooding relies on the spontaneous imbibition of water to expel oil from the matrix into the fracture system. The spontaneous imbibition process is most efficient in strongly water-wet rock where the capillary driving force is strong. In oil- or mixed-wet fractured carbonate reservoirs, however, the capillary driving force for the spontaneous imbibition process is weak, and therefore the water flooding oil recoveries are low. The recovery efficiency in fractured oil- or mixed-wet carbonate reservoirs can be improved by dissolving low concentrations of surfactants in the injected water to alter the wettability of the reservoir rock to a more water-wet state. This wettability alteration accelerates the spontaneous imbibition of water into matrix blocks, thus driving oil out of the matrix. The fracture networks diminish the effectiveness of water or chemical flooding in the fractured reservoirs. Recovery is limited in primary and secondary production because most of the injected fluids preferentially go through fracture openings, leaving behind a significant amount of oil in the

[1] A version of this chapter has been published:
Telmadarreie and Trivedi, 2016. Transport in Porous Media, doi:10.1007/s11242-016-0721-z.

matrix. Therefore, designing a process to recover the matrix oil at an economic rate often turns out to be a real challenge for such reservoirs (Bourbiaux, 2009).

Many researchers proposed surfactants as wettability altering agents for oil-wet fractured reservoirs (Austad and Miller, 1997; Standnes and Austad, 2000a, 2000b; Seethepalli et al. 2004; Hirasaki and zhang, 2004). The nature of positively charged carbonate surface makes cationic surfactants the most attractive candidates for oil recovery. Cationic surfactants, although effective in altering wettability for oil-wet rocks, are too expensive to be implemented in a field treatment. Spontaneous imbibition or buoyancy displacement of oil by the surfactant is main recovery mechanism in fractured carbonate reservoirs. However, for the surfactant to imbibe and change the wettability of the matrix and subsequently recover oil, it must first diffuse into the matrix porous media. Due to the presence of fractures, poor volumetric sweep efficiency is the main problem in the fractured carbonate reservoirs that limits the amount of the surfactant that meets the oil-wet matrix. According to Stoll et al. (2008), external forces are necessary to enable forced imbibition of surfactant. Otherwise, the spontaneous imbibition of surfactant as a wettability modification agent could not provide an economically interesting opportunity.

A major attraction of foam is the possibility of diverting flow from high-permeability to low-permeability layers. It can also provide better control of the injected fluids as stronger foams can spontaneously block the flow channels in high-permeability media (Hirasaki, 1989; Zhou and Rossen, 1995). For example, in a work performed by Conn et al. (2014) in a 2D model heterogeneous porous media, they showed that foam effectively displaced trapped oil in the low-permeability region by bubble resistances in the fracture and high-permeability zones. Foam and Polymer Enhanced Foam (PEF) can improve sweep efficiency, especially in heterogeneous reservoirs, over gas and chemical injections. Since the effective viscosity of foam is much higher

than that of gas, it can reduce viscous fingering and gravity override caused by injecting gas, supercritical CO_2 or steam (Yan et al., 2006). Besides improving sweep efficiency in gas flooding, foam and PEF can be used for mobility control in chemical EOR, an alternative to a polymer or micellar flooding (Lake, 1989). In addition, the main issue with the chemical method for carbonate reservoirs is the slow rate of the wettability alteration and surfactant imbibition processes. Therefore, forced imbibition has to be applied. Foam and PEF could offer this external force by providing a high injection pressure gradient that will force the surfactant solution, and eventually foam bubbles into the oil-wet matrix, resulting in further improvement of oil recovery in carbonate formations.

Porous media micromodels have been used to better understand multiphase fluid transport at the pore-level scale (Lee et al., 2015; Song and Kovscek. 2015; Conn et al., 2014; de Haas et al., 2013; Gunda et al., 2011). Micromodel systems allow real-time, in situ observation of relevant fluid transport in porous media. This chapter aimed to visualize the performance of CO_2 foam/PEF in a fractured micromodel during heavy oil recovery. CO_2 foam/PEF were injected as a tertiary EOR method after surfactant flooding. The performance of water flood, surfactant injection, and CO_2 foam/PEF were compared and visualized in the micromodel during the oil recovery process.

2.2 Materials and Methods

2.2.1 Materials

Surfactants are the major chemical constituent in foams. They are classified according to the nature of the charged group present on the surfactant head. Their main function is to lower the surface tension. Three different types of surfactants (anionic, cationic, and nonionic) and a polymer were selected for this research.

Surfactants: Sodium dodecyl benzene sulfonate (Na-DDBS, provided by ACROS) was used as an anionic surfactant. It is a major component of laundry detergent with the formula $C_{12}H_{25}C_6H_4SO_3Na$ (Mw=348.5 g/mol). Cetyltrimethylammonium bromide (CTAB) (Sigma–Aldrich, 99 % purity) was also used as a cationic foaming agent ($C_{19}H_{42}BrN$, Mw=364.5 g/mol). Foam also generated with a nonionic surfactant (Surfonic N85, Huntsman Corporation). It is Nonylphenol-ethoxylated nonionic surfactant with a chemical formula of $C_{15}H_{23}$ $(OCH_2CH_2)_n$ OH (n = number of ethylene oxide units ≈ 8-9).

Polymer: Polymers are used to enhance the stability of the foam by increasing viscosity. The polyacrylamide polymer FLOPAAM 3330S (supplied by SNF SAS) in dry powder form was used in the preparation of polymer solutions. Polyacrylamide polymers are one of the most general polymer types used in the enhanced oil recovery process. FLOPAAM 3330S is anionic and water-soluble with a degree of hydrolysis of 25-30 % and average molecular weight of 8×10^6.

2.2.2 Methods

Foam/PEF static tests were performed to observe the stability of foam generated with different foaming solutions in the presence and absence of crude oil. During dynamic experiments, water followed by surfactant was injected in heavy oil saturated micromodel. Surfactant flood was performed at a low flow rate over a long period of time to monitor the spontaneous imbibition process. Thereafter, CO_2 foam/PEF was injected to improve heavy oil recovery and visualize the performance of foam bubbles.

2.2.2.1 Foam Bulk (Static) Experiments

CO_2 Foam/PEF generation: For the preparation of the foaming solution, a surfactant and polymer (for CO_2 PEF generation) were mixed in water. The concentrations of the surfactant and polymer

were 0.29 wt % and 0.15 wt %, respectively. For foam/PEF analysis in the presence of oil, 5 cc of oil was added to the foaming solution before high-speed mixing. Detailed procedure is explained later in Chapter 5.

Static Stability: In each experiment, both the height of the liquid and the height of the foam column were measured as a function of time. The time required to drain half of the liquid from the foam was measured as a foam half-life value, representing foam stability. Moreover, the initial foam height value was also measured as the foamability of foaming solutions, defined as the ability of a solution to generate the foam. All the experiments were performed at ambient condition. The range of uncertainty in the foam height measurements was ±0.2 cm. It should be mentioned that each experiment was repeated at least once to assure the reproducibility of results.

2.2.2.2 Micromodel Experiments

The micromodel was designed to represent its highly fractured carbonate analog through a high permeability contrast. Flow visualization experiments were performed using a specially designed micromodel (made from Borosilicate glass) with high permeability contrast between the matrix and fracture to imitate the highly-fractured carbonate formation. The micromodel was placed in a holder consisting of the inlet and outlet ports, which communicate with the micromodel at the drilled holes. An in-line foam generator was designed before the micromodel inlet. It consists of porous screens with a mesh size of 80 (Figure 2.1).

To change the wettability of the micromodel, which was originally water wet (WW), a siliconizing fluid (SurfaSil^{TM}, the chemical composition is primarily dichloro-octamethyl-tetrasiloxane) was used to coat the glass surface. SurfaSil^{TM} works by reacting directly with polar groups (silanols) on the glass surface. The detailed procedure for the wettability alteration of the micromodel is explained in Chapter 4.

For each experiment, heavy crude oil (viscosity of ~ 6000 cp at 22 ºC) was used to saturate the micromodel. An image of the heavy oil saturated micromodel (1 cm × 7 cm with fracture thickness of 1 mm) is shown in Figure 2.1. After oil saturation (aged for 24 hours), the micromodel was flooded with water for 200 minutes. Thereafter, the surfactant solution was injected for about two days, followed by 200 minutes of CO_2 foam/PEF injection. Three different types of surfactants (anionic, nonionic and cationic) were used during surfactant flood to observe further oil recovery, especially by imbibition process. The surfactant solution was injected into the micromodel at a very low flow rate (0.0016 cc/min) to ensure enough surfactant concentration for imbibition process over a period of two days. A syringe pump (ISCO Model 500D) was used for liquid injection. A gas mass flow controller (MFC) (provided by Hoskin Scientific Ltd) was used for the accurate injection of CO_2 gas at a constant volumetric flow rate. The pressure was also measured and recorded by a pressure transducer (OMEGADYNE Model PX409) connected to a computer. A high-quality digital camera was used for imaging the flooding processes, and then the captured images/movies were processed using MATLAB to assess the oil recovery performance. For image analysis, all images were converted to black and white scale before analysis. A constant cut off value (for color conversion) was defined for all images for consistency of results. Reduction in back color (representing oil saturation) over time was calculated and recorded as the oil recovery factor. At the end of each test, micromodel was analyzed under the microscope (Leica DM 6000M microscope) for further analysis of residual saturations in the pores and overall recovery mechanism

The detailed information of each experiment is represented in Table 2.1. The CO_2 foam and CO_2 PEF quality were kept constant at 92 %. Foam quality is defined as the ratio of gas volume to total volume of foam. Imbibition process was monitored during surfactant injection by visualizing and

then calculating matrix oil recovery. During foam/PEF flooding, micromodel was studied in detail with higher magnification microscope. Observing the behavior of foam/PEF bubbles and mechanisms involved in matrix oil recovery were the key objectives during foam/PEF flooding experiments.

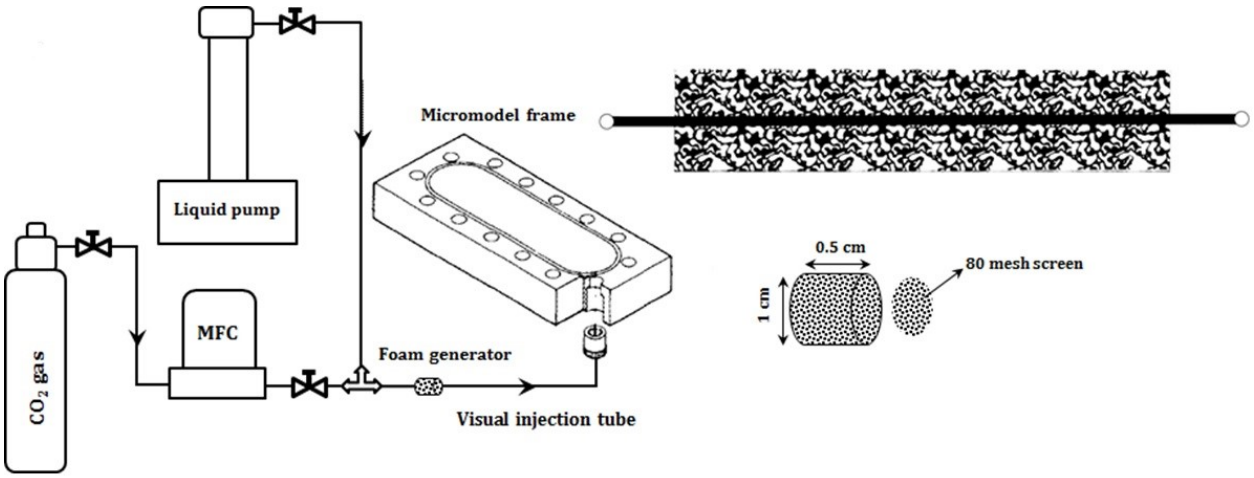

Figure 2.1: Schematic of the fractured micromodel set-up for foam injection.

Table 2.1: Experimental parameters (CO_2 foams were injected as a tertiary recovery process).

Experiment	Foaming solution	Injected fluid flow rate (cc/min)			
		Water	Surfactant	CO_2 gas	Foam/PEF solution
#1	DDBS	0.0016	0.0016	0.1	0.0083
#2	N85	0.0016	0.0016	0.1	0.0083
#3	CTAB	0.0016	0.0016	0.1	0.0083
#4	DDBS+Flopaam	0.0016	NA	0.1	0.0083

2.3 Results

2.3.1 Foam/PEF Static Stability

The change of normalized foam height versus time for the studied surfactants is shown in Figure 2.2. The effect of crude oil on foam decay profile is shown in this Figure (2.2b). The addition of

heavy oil reduces the foam stability. This effect is more pronounced in the case of foam generated with a nonionic surfactant (N85). Furthermore, foamability and stability (half-life) of foams and PEF are shown in Figure 2.3. The foam decay profiles of the studied ionic surfactants (DDBS and CTAB) are similar; however, DDBS shows better stability (half-life) than that of CTAB. The good foamability of anionic surfactants has been reported in several references (Flick, 1993; Urban, 2003; Rosen and Kunjappu, 2012). Nonionic surfactants generally produce less foam and much less stable foam than ionic surfactants in aqueous media. These effects are probably due to the larger surface area per molecule and the absence of highly charged surface films in these foams. In both ionic and nonionic surfactants, the static stabilization is achieved by repulsive forces between the surfactant monolayers. For ionic surfactants, the repulsive force is electrostatic and caused by the charged groups at the interfaces, whereas for nonionic surfactants, static stabilization is achieved by a steric repulsion, which is due to the overlap of the surfactant chains. Based on many researchers' observations, anionic and cationic surfactant generate more stable (last longer) foam films than those of nonionic surfactants. This is explained by the DLVO theory, which deals with the mutual repulsion of the electric double layer (Israelachvili, 1991; Schramm and Wassmuth, 1994). Therefore, the ionic surfactants (DDBS, and CTAB) generated more foam volume with relatively higher stability compared to that of nonionic N85 surfactant. Both foamability (initial foam height) and foam stability (half-life) of ionic surfactants are higher than the nonionic surfactant as shown in Figure 2.3a.

DDBS surfactant was selected for studying the effect of polymer addition (PEF study). The major advantage of polymer addition in foaming solution is viscosity enhancement. Increasing viscosity of foaming solution may reduce the liquid drainage rate within the foam lamella. Polymer increases the viscosity of liquid solution within the foam lamella, reduces the rate of liquid drainage, and consequently increases the stability of the foam. According to Figure 2.3b, the addition of polymer in DDBS solution has a significant effect on the stability of foam such that the heavy oil has no significant effect on DDBS-PEF stability.

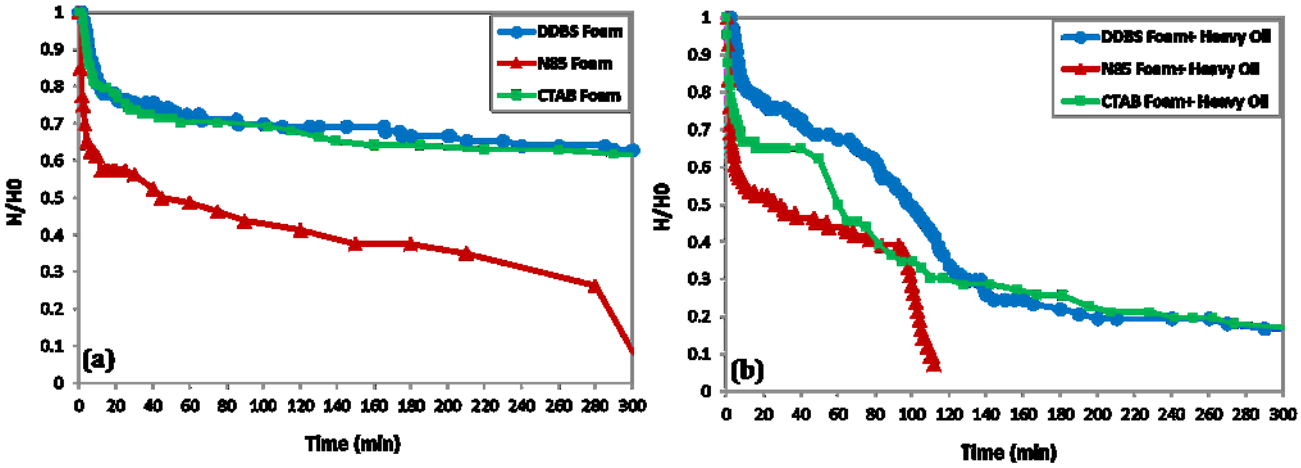

Figure 2.2: Normalized foam height versus time; (a) in the absence and (b) in the presence of heavy oil.

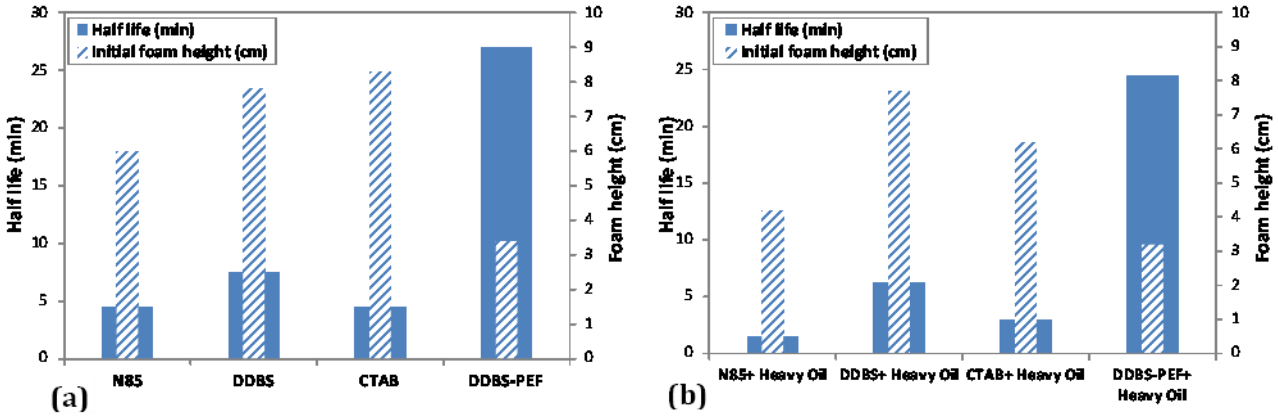

Figure 2.3: Foamability and foam stability (half-life) values for studied foaming solutions; (a) in the absence and (b) in the presence of heavy oil.

2.3.2 Waterflooding

Waterflooding is the most common method for recovering oil from reservoirs. Water displaces oil from the pore spaces, but the efficiency of such displacement depends on many factors, including oil viscosity and reservoir characteristics including wettability and heterogeneity. In fractured carbonate formation, especially those containing heavy oil, both wettability, and heterogeneity significantly diminish the performance of waterflooding. Water was injected for 200 minutes to imitate the residual oil saturation condition. For all the experiments, the primary waterflood recovery factor was around 18±1 %. An image of water flooded micromodel is shown in Figure 2.4. Water could only sweep the oil from the fracture without any effect on matrix oil.

Figure 2.4: Micromodel image at the end of waterflood; water could partially sweep the fracture without any impact on matrix oil.

2.3.3 Surfactant Injection

At typical carbonate reservoir conditions, rock surfaces have a positive charge. The negatively charged carboxylic acid anions in oil are attracted to positively charged carbonate surfaces, thus generating oil-wet surfaces. Waterflooding can be ineffective in recovery from carbonate reservoirs because the capillary pressure curve is predominantly negative, therefore surfactant/polymer flooding is considered to be a more viable option (Seethepalli et al., 2004). It is worth mentioning that the carbonate minerals in the rock play a role in the effectiveness of the surfactant flooding. Several mechanisms are responsible for adsorption of surfactants (ionic and nonionic) into the rock surface (Rosen, 1978) such as electrostatic attraction/repulsion, ion-

exchange, chemisorption, chain–chain interactions, hydrogen bonding, and hydrophobic bonding. The nature of the surfactants, minerals, and solution conditions as well as the composition of reservoir rocks play an important role in determining the interactions between the reservoir minerals and externally added reagents (surfactants and/or polymers) and their effect on surface charge and wettability. Since our experiments are done on glass etched porous media, these mechanisms don't play a role in our studies.

Figure 2.5 shows the images of the micromodel at the end of surfactant flooding. Anionic DDBS surfactant does not significantly improve the oil recovery after the waterflood (Figure 2.5a and Figure 2.7) and there is no imbibition. The oil recovery is mainly from the regions around the matrix-fracture interface with almost no effect on matrix oil. On the other hand, the nonionic surfactant (N85) can slightly imbibe into the matrix area only near the fracture zone and increases the oil recovery further (Figure 2.5b and Figure 2.7). Based on Figure 2.5c and Figure 2.7, the cationic CTAB surfactant significantly imbibes into the matrix and decreases the residual oil saturation much further. CTAB surfactant imbibes into the matrix and moves the oil toward the matrix by counter-current imbibition process. The presence of oil within the fracture and existence of swept zone in the matrix support the occurrence of imbibition process as shown in Figure 2.5c. Due to low flow rate, and thus a weak pressure gradient, the main mechanism in charge of further oil recovery (after waterflood) is imbibition of surfactant into the matrix. It should be mentioned that the oil recovery mechanism by reduction of IFT is also present to the lesser extent, especially in the case of anionic surfactant without any significant imbibition. The IFT values for the DDBS, CTAB and N85 surfactant with studied oil are 0.35 mN/m, 0.28 mN/m, and 0.55 nN/m, respectively. Surfactant reduces the IFT between oil and water result in moving some residual oil near the matrix-fracture interface where the surfactant solution is in contact with oil.

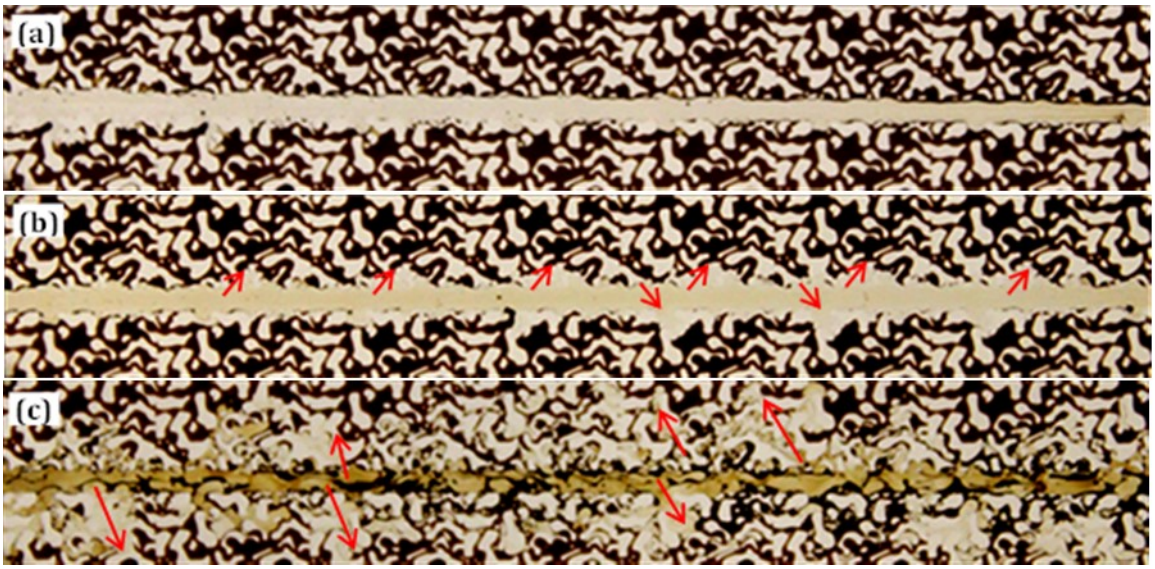

Figure 2.5: Images of micromodel at the end of surfactant flooding; (a) anionic DDBS, (b) nonionic N85, and (c) cationic CTAB; representing surfactant imbibition into the matrix; arrows represent surfactant imbibition process.

2.3.4 CO_2 Foam and CO_2 PEF Flooding

The main issue with surfactant injection into naturally fractured carbonate reservoirs is the low penetration of surfactant into the matrix. Even a wettability altering agent such as cationic CTAB surfactant cannot produce the heavy oil from the matrix in acceptable rate. Therefore, some external force is required to improve matrix oil recovery. Beside wettability alteration, high-pressure gradients between fracture and matrix result in viscous force promoting the oil displacement from the matrix. Foam and PEF can effectively provide this pressure gradient. Foam/PEF bubbles can decrease the mobility and result in a resistance to flow within the fracture diverting the fluid toward the matrix. It should be mentioned that fracture will be still preferential flow path for the injected liquid; however, when they are in the fracture path, foam/PEF bubbles create a resistance to flow compared to the case without foam bubbles. This resistance will give the injected fluid enough time to move toward the matrix and increase the sweep efficiency.

After two days of surfactant flooding, CO_2 foam generated with the same type of surfactant was injected for a period of 200 minutes to improve the matrix oil recovery. The results are presented in Figure 2.6. For effective oil recovery, the stable foam should be generated in the fracture path (or swept parts of the reservoir). Therefore, the ability of the surfactant to generate stable foam has a good accordance with its performance during oil recovery. Foam generated with anionic DDBS surfactant recovers the matrix oil 20% and 4 % higher than that of N85 and CTAB foams, respectively. This observation is comparable to the foam static results in Figure 2.3. DDBS has higher static stability than both CTAB and N85 foams in the presence of heavy oil. Despite having higher oil recovery during N85 surfactant flooding, the N85 foam cannot block the fracture path effectively, only recovering 6 % of initial oil saturation (Figure 2.7).

In addition, as seen in Figure 2.6d, DDBS PEF was also injected into the water flooded micromodel to compare its oil recovery performance with that of foam. It should be mentioned that DDBS PEF was injected after waterflooding without any surfactant flooding as DDBS surfactant injection shows no significant oil recovery over a period of two days. PEF significantly improves the matrix residual oil recovery (70%) compared to that of DDBS foam flooding (26%). This performance is in accordance with the observations from the static stability results where PEF is much more stable than that of foam and crude oil has almost no significant effect on its stability.

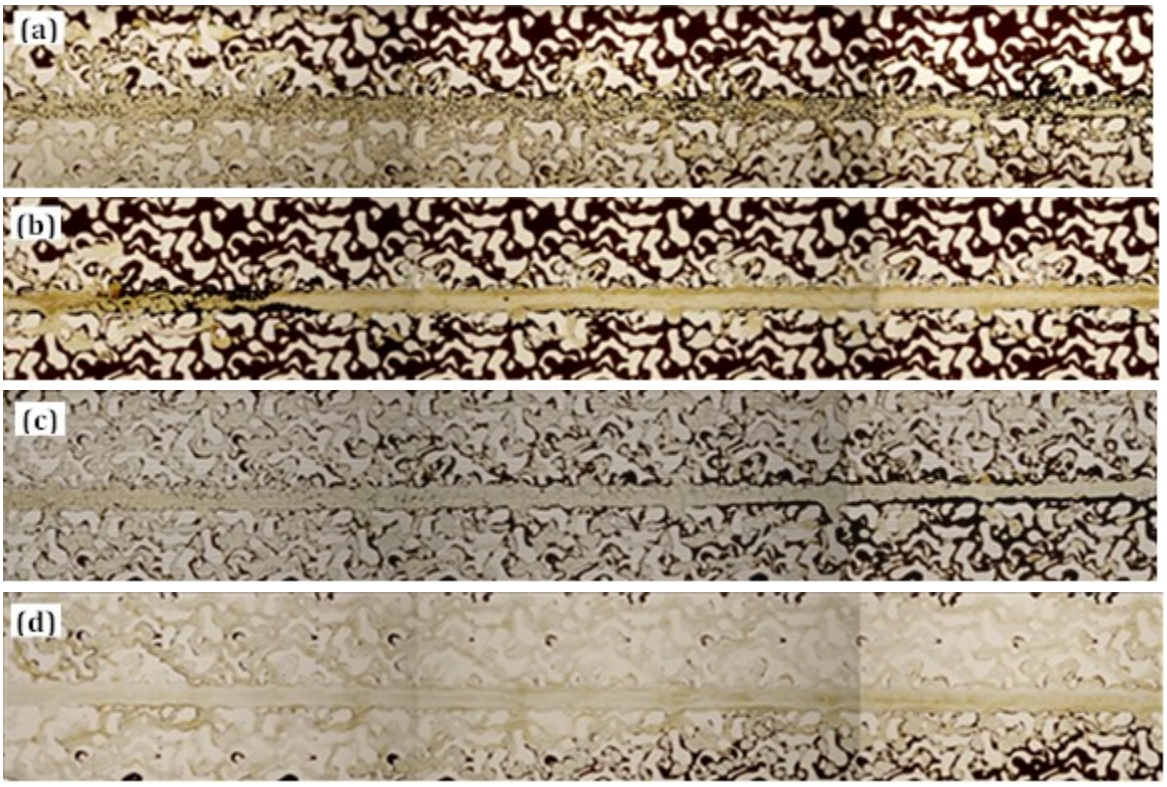

Figure 2.6: Images of micromodel at the end of CO_2 foam/PEF flooding; (a) DDBS foam, (b) N85 foam, (c) CTAB foam, and (d) DDBS PEF.

2.4 Discussion

2.4.1 Surfactant Flooding

Chemical treatment for wettability alteration is one of the techniques to recover oil from naturally fractured carbonate reservoirs. The surfactant molecules diffuse/flow from fractures into the matrix and change wettability and IFT. The reduction in IFT decreases the entry capillary pressure. The key to recovering oil is the wettability alteration to preferentially water-wet or intermediate-wet conditions.

Austad and collaborators (Austad and Milter, 1997; Standnes and Austad, 2000a, 2000b) have shown that cationic surfactants can recover oil by spontaneous counter-current imbibition due to wettability alteration. The mechanism of wettability alteration is supposed to take place by an ion-

pair formation by the cationic surfactant and the negatively charged carboxylates in oil. Ethoxylated sulfonate surfactants with high Ethylene oxide (EO) numbers can also displace oil spontaneously in a slow process (Gupta and Mohanty, 2008). In addition, Gupta and Mohanty (2010) observed the wettability alteration by Nonylphenol Ethoxylate nonionic surfactant in oil-wet calcite plate.

Cationic CTAB, anionic DDBS and nonionic N85 (Nonylphenol Ethoxylate) were used for surfactant flooding experiments. Figure 2.7 shows the oil recovery factor for each experiment. According to Figure 2.5 and Figure 2.7, the ability of studied surfactants to imbibe into the matrix is in order of CTAB >> N85 > DDBS, while their ability of matrix oil recovery during foam flooding after surfactant flooding (Figure 2.6 and Figure 2.7) is in order of DDBS > CTAB > N85. CTAB surfactant solution has the highest amount of imbibition and therefore oil recovery, while DDBS surfactant solution has no significant effect on wettability alteration or oil recovery after waterflooding. Figure 2.8 shows the detailed time-lapse images of CTAB surfactant solution imbibition into the matrix over the period of two days. Due to nature of the charge in carboxylates in oil, in contrast to cationic CTAB surfactant, the negatively charged anionic surfactants are not effective in changing wettability (due to electrostatic repulsion), unless they have Ethylene oxide (EO) group in their structure which is not the case for DDBS surfactant. Therefore, as expected from surfactant structure, the only mechanism for further oil recovery by DDBS surfactant is IFT reduction, which is fairly ineffective in fractured heavy oil saturated model. Figure 2.9 represents the microscopic images of micromodel after two days of DDBS surfactant flooding. Without any major imbibition, IFT reduction and emulsification are the main mechanisms of oil recovery during DDBS surfactant flooding.

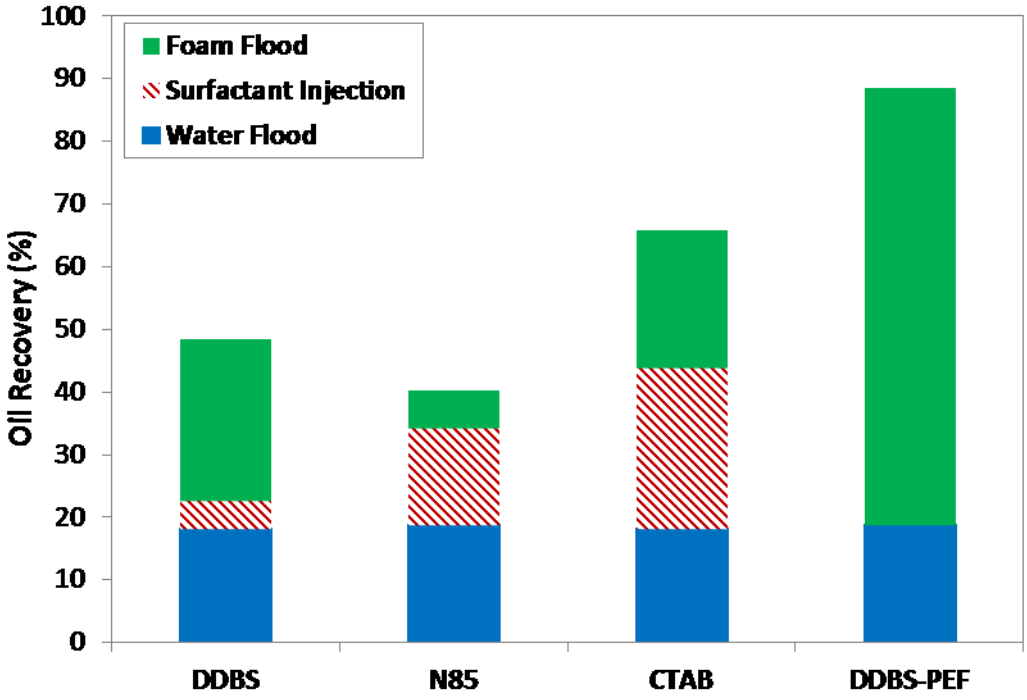

Figure 2.7: Oil recovery profiles at the end of the water, surfactant, and foam/PEF injections.

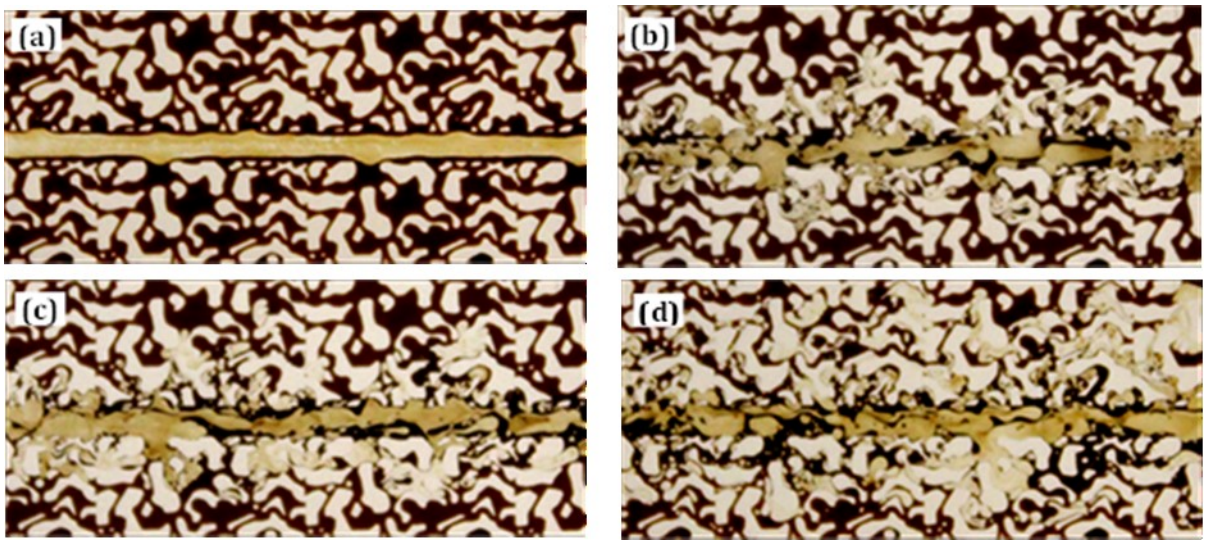

Figure 2.8: Time-lapse images of micromodel during two days of CTAB surfactant injection representing imbibition process; (a) initial, (b) after 12 hours, (c) after 24 hours, and (d) after 48 hours of surfactant injection.

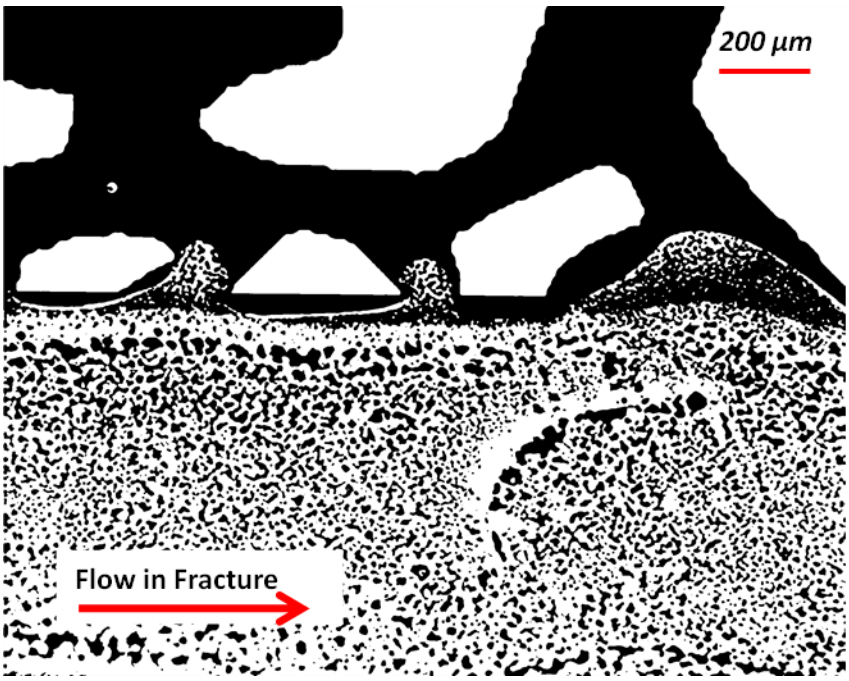

Figure 2.9: Microscopic image of micromodel at the end of DDBS surfactant flooding; oil recovered by IFT reduction and emulsification without any significant surfactant imbibition into the matrix.

The nonionic N85 surfactant can diffuse into the matrix much better than DDBS surfactant and recover more oil (Figure 2.5(b) and Figure 2.7). Figure 2.10 and Figure 2.11 represent the microscopic images of micromodel at the end of the N85 and CTAB surfactant flooding, respectively. The slight diffusion of N85 surfactant into the matrix can be seen in Figure 2.10. Although the imbibition is not significant, it is still higher than DDBS surfactant. Therefore, N85 can slightly change the wettability toward the water-wet condition. This can be explained by the presence of Ethylene oxide group in N85 surfactant structure. The EO-surfactant is supposed to adsorb with the hydrophobic part onto the hydrophobic surface of micromodel (Standnes and Austad, 2000b). The water-soluble head group of the surfactant (the EO-groups) may decrease the contact angle below 90° by forming a small water zone between the coated surface and the oil. A schematic of this process is shown in Figure 2.12(a). However, this mechanism must not be

regarded as a permanent wettability alteration. In fact, it will probably be fully reversible due to the weak hydrophobic bonds between the surfactant and the hydrophobic surface (Standnes and Austad, 2000b).

For cationic CTAB surfactant, surfactant imbibition into the matrix was much higher than other studied surfactants. The cationic surfactant imbibed into the matrix and increased the heavy oil recovery by wettability alteration as seen in Figure 2.11. The mechanism of wettability alteration is due to an ion-pair formation by the cationic surfactant and the negatively charged carboxylates in oil. A schematic of this process is shown in Figure 2.12(b). The cationic monomers will interact with adsorbed anionic materials from the crude oil by electrostatic forces. The adsorbed material at the interface between oil, water, and grain will be desorbed by forming an ion-pair between the cationic surfactant and the negatively charged adsorbed carboxylic groups. In addition to electrostatic interactions, the ion-pair is stabilized by hydrophobic interactions (Standnes and Austad, 2000b). Some of the desorbed material may also be dissolved in the micelles. In this way, the water will penetrate the pore system, and oil will be expelled from the matrix through connected pores with high oil saturation in a so-called counter-current flow mode. Thus, once the adsorbed organic material has been released from the surface, the surface becomes more water-wet and the imbibition of water is in fact governed by capillary forces.

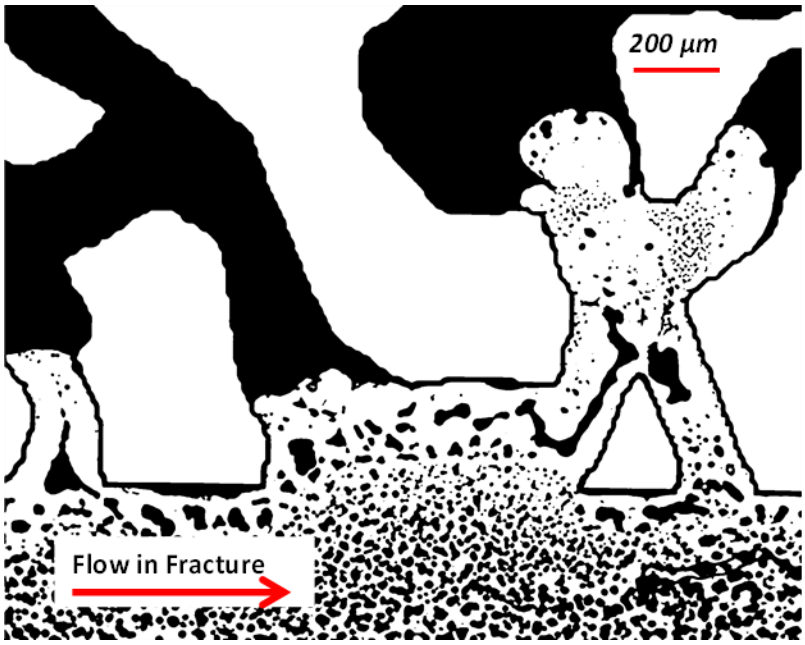

Figure 2.10: A microscopic image of micromodel at the end of N85 surfactant flooding; oil recovered by IFT reduction and emulsification with minor surfactant imbibition into the matrix.

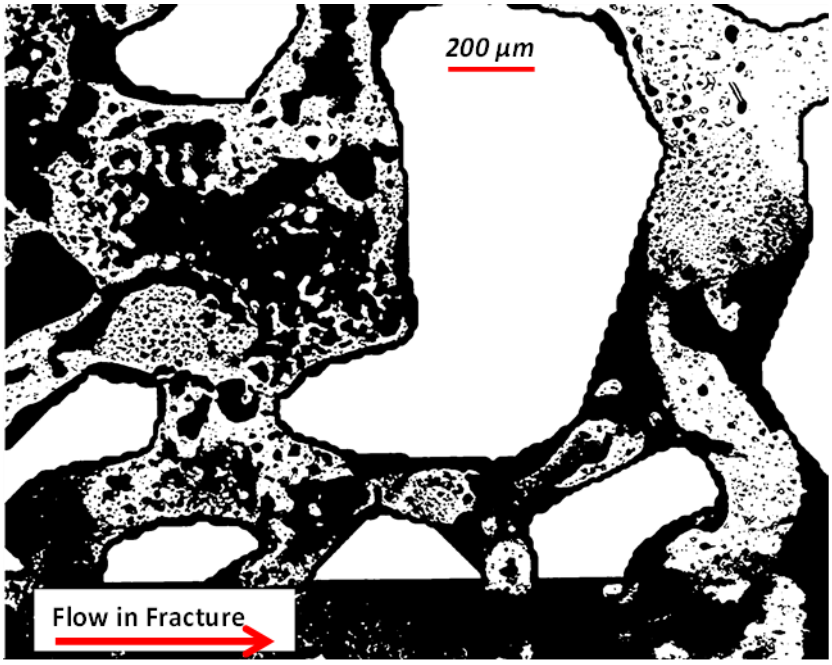

Figure 2.11: A microscopic image of micromodel at the end of CTAB surfactant flooding; surfactant could imbibe into the matrix and increase the oil recovery by counter-current imbibition.

The primary displacement mechanism during cationic surfactant flooding is countercurrent movement as seen in Figure 2.8 and Figure 2.11. Surfactant imbibes into the matrix pores and oil is moved into the fracture by countercurrent flow. Countercurrent movement is believed to be a function of not only capillary forces but also the Marangoni effect that describes spontaneous interfacial flows induced by water-oil interfacial tension (IFT) gradient (Pratt, 1991; Austad and Milter, 1997; Lyford, 1998). It is believed that the Marangoni effect created a hydrodynamic shear stress at the oil-water interface that provided additional force to mobilize the displaced oil phase in the direction opposite to the imbibed aqueous phase. As also mentioned before, the cationic surfactant improved oil recovery by altering rock wettability (Austad et al., 1998; Standnes and Austad, 2000b) that maximized counter-current movement.

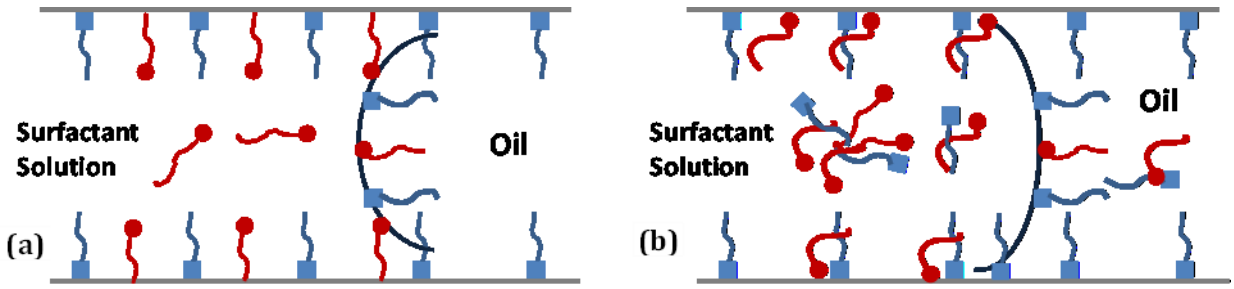

Figure 2.12: Schematics of wettability alteration mechanisms by surfactant; (a) N85 Surfactant containing EO group, and (b) Cationic CTAB surfactant at an initial stage before wettability change. Circles and cubes show the surfactant and oil molecules, respectively.

2.4.2 Applying Foam to Improve Surfactant Flooding in Fractured Carbonate Reservoirs

Wettability and matrix block size are two major factors in fluid transfer between fractures and matrix (Kiani et al., 2001). For an oil-wet fractured carbonate reservoir, injected water can flow in fractures easily and much faster than in the matrix. Gravity drainage can produce oil if the matrix block is thick enough to overcome the negative water-oil capillary pressure. The surfactant injection in an oil-wet fractured reservoir might not be effective because of the following reasons

(Kiani et al., 2001): 1) Pressure gradient may be too small to displace oil from the matrix in fractured formations, and 2) High permeable fractures could act like thief zones. In these cases, using mobility control agents like foam might be considered. Foam and Polymer Enhanced Foam (PEF) can improve sweep efficiency, especially in heterogeneous reservoirs, over gas and chemical injections.

The spontaneous invasion of aqueous surfactant solution into an initially oil-wet porous media is a slow process. At early times, the rate of surfactant penetration is controlled by the dynamics of transfer of surfactant from the meniscus to the solid surface through the three-phase contact line, whereas at late times the rate of penetration is controlled by the rate of diffusion of surfactant in the bulk (Hammond and Unsal, 2009). A schematic of probable mechanism of surfactant adsorption and wettability alteration is shown in Figure 2.13. At the meniscus, surfactant molecules are adsorbed onto the solid surface through the three-phase contact line. This transfer from the bulk solution to solid surface results in a decrease in the bulk surfactant concentration near the meniscus and causes a concentration gradient that supports the moving meniscus (Figure 2.13; T_1 and T_2). Adsorption of surfactant on the solid surface causes the wettability to alter, and so, the pore becomes more water wet (Figure 2.13; T_3).

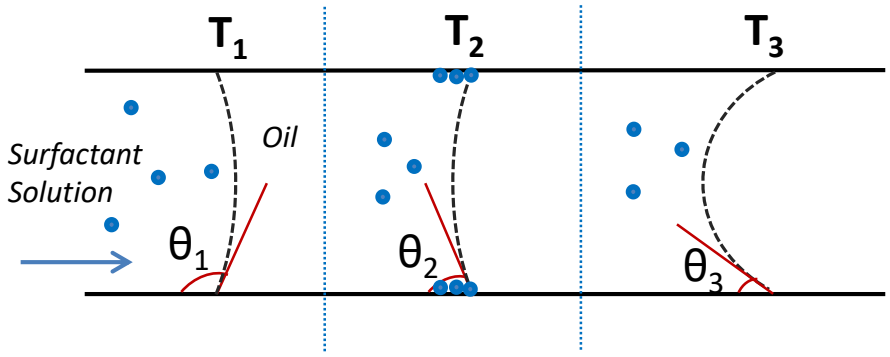

Figure 2.13: A schematic of wettability alteration and contact angle reduction during surfactant flooding ($\theta_1 > \theta_2 > \theta_3$).

Displacement of the oil phase from a porous medium under an externally applied pressure difference is known as forced imbibition/drainage. Forced imbibition is potentially much faster than the spontaneous case, at least when the applied pressure is large enough to overcome the capillary pressure threshold for entrance into the oil-wet pores. However, when the applied pressure is less than the threshold pressure for entry, the meniscus can only penetrate if surfactant changes the contact angle. Diffusion and adsorption of surfactant molecules are very slow processes. Applied differential pressure does not make these two processes faster; it only speeds up the meniscus (Hammond and Unsal, 2009).

At applied pressures, larger than the threshold for entry into the oil-wet capillary, provided by foam injection, the speed meniscus advancement is controlled by the balance between viscous forces and applied pressure, which leads to the comparatively rapid motion. Therefore, there is little time for any surfactant on the meniscus to transfer to the solid surface, and as a result, the concentration on the solid surface remains small, and so, there is little change in wettability.

The performance of a foaming solution depends on its ability to generate strong foam rather than its wettability alteration potential. This is the reason for higher oil recovery factor of DDBS foam flooding compared to that of the N85 and CTAB foams as seen in Figure 2.6 and Figure 2.7. Figure 2.3 shows that DDBS foam relatively has more stability than other studied surfactants in the presence of oil.

Once strong foam generates in the fracture, there will be a resistance to flow due to the presence of foam bubbles in the fracture. Thereafter, forced imbibition pushes the surfactant solution, and eventually the foam bubbles, into the matrix. Beside forced imbibition, visualization through this study showed that there are other mechanisms involved in further matrix oil recovery. Foam bubbles can increase the viscous force in narrow zones of the matrix and push the oil bulbs trapped

in those zones. This process is shown in Figure 2.14. Foam bubbles increase the local pressure in the narrow capillary zone and recover the trapped oil. Furthermore, blocking opening area in the matrix by the network of bubbles can further increase the oil recovery from the matrix. When they reach a larger opening area, bubbles release their energy (based on the Laplace formula) and block those areas. As a result, the liquid is pushed to move in a narrow zone between the bubble and grain surface, where most of the oil is located. Thereafter, the foaming solutions sweep the oil by emulsification in the area around the grain. Figure 2.15 presents the camera and microscopic images of this process. The residual oil at the end of foam/PEF flooding is mainly left as a thin oil layer around the oil wet grain surface. The more effective foaming solution results in the thinner oil layer at the end of flooding.

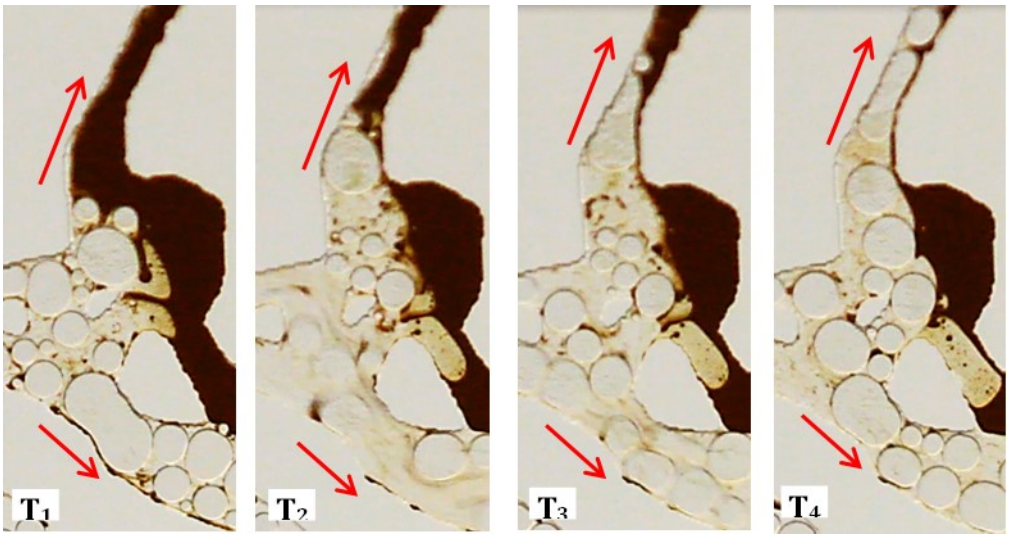

Figure 2.14: Removing trapped oil in narrow throat of the matrix by foam bubbles. Arrows show the direction of movement (time increases from T_1 to T_4).

The mechanism involved in PEF flooding is similar to that of foam. However, the effectiveness of PEF in heavy oil sweep efficiency is much higher than that of foam (Figures 2.6 and 2.7). PEF can provide higher differential pressure, resulting in better matrix oil recovery. Also, due to the presence of polymer, bubbles are more stable comparing to that of conventional foam increasing

the sweep efficiency further. It is worth mentioning that, foam/PEF flooding tends to increase the injection pressure to improve sweep efficiency. Therefore, it will be more effective when used as a tertiary recovery process, when a swept path has been created in the reservoir and there won't be any injectivity problem.

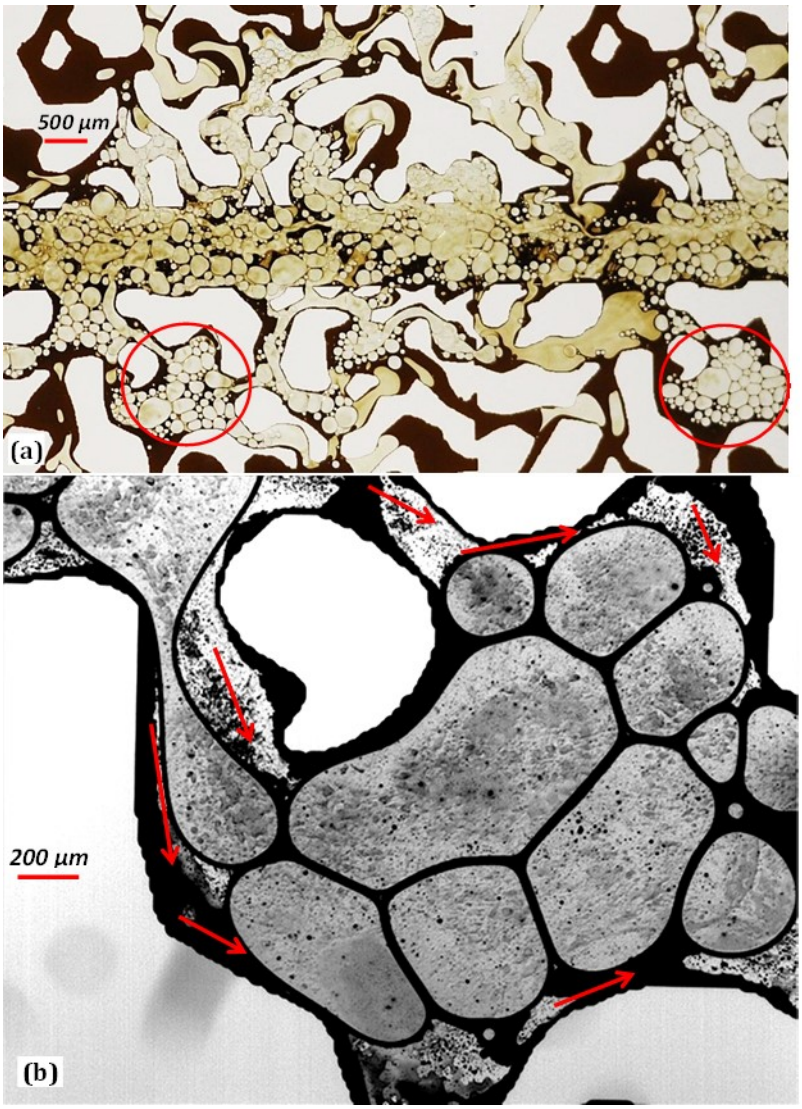

Figure 2.15: Blocking opening area in the matrix by a network of bubbles improving sweep efficiency; (a) camera and (b) microscopic images. Arrows show the direction of liquid movement between foam bubbles and grain.

2.5 Summary

This chapter investigated the pore-scale phenomena during surfactant and CO_2 foam/PEF flooding for heavy oil recovery in fractured oil-wet porous media. After surfactant flooding, the CO_2 foam was injected as a tertiary EOR process. Followings are the summary of this chapter:

- Among studied surfactants, cationic CTAB can imbibe into the oil wet matrix and increased the matrix oil recovery. The oil recovery factor at the end of anionic DDBS, nonionic N85, and cationic CTAB surfactant flooding were 4.4 %, 15.6 %, and 25.8 %, respectively.
- The combined injection of surfactant and foam/PEF resulted in a higher injection pressure gradient due to the high flow resistance resulting from the presence of foam bubbles. This increased pressure produced an additional force to drive surfactant into the matrix or low-permeability areas.
- The performance of each foaming solution in oil-wet fractured porous media depends on its ability to generate stable foam rather than its wettability alteration potential.
- Per the results of this chapter, there is a good agreement between the static performance of each foaming solution and its dynamic efficiency during heavy oil recovery; stable foam/PEF in the static test have more chance to be stable in the dynamic condition.
- Foam flooding can significantly increase the heavy oil recovery from oil wet matrix. Besides increasing the viscous force in narrow zones of the matrix, foam bubbles can block opening area in the matrix and increase sweep efficiency in the matrix.
- The effectiveness of PEF in heavy oil sweep efficiency was much higher than that of conventional foams. Due to the presence of polymer, PEF bubbles were more stable than that of foam in the presence of heavy oil and therefore increased the sweep efficiency.

Chapter 3: Dynamic Behavior of Asphaltene Precipitation and Distribution Pattern in Fractured Carbonate Reservoirs during Hydrocarbon Solvent Injection: Pore-Scale Observations[2]

3.1 Introduction

In heavy oil reservoirs, asphaltene precipitation and deposition is one of the main challenges during oil recovery, especially in the solvent injection process. Asphaltene deposition within reservoir rocks and production facilities is one of the major technical obstacles in hydrocarbon productivity (Sheu and Mullins, 1995).

The most common used definition of asphaltenes is based on their solubility. They are insoluble in alkanes (i.e. n-pentane, n-hexane, n-heptane) but soluble in aromatics (i.e., benzene, toluene, and xylene). Several factors are responsible for amount and composition of asphaltene such as; the nature of crude oil, pressure, temperature, type of solvent (e.g. number of carbons), contact time, and solvent/crude ratio (Speight et al., 1984; Andersen and Birdi, 1990). For example, Ferworn et al. (1993), Hammami et al. (2000), and Speight (1999) observed that asphaltene flocculation increases with decreases in the carbon number of the solvent. Besides, Moreno and Babadagli (2013) noted that when the carbon number of the solvent increases from C3 to C15, the heavy-oil production would also increase due to the asphaltene solubility effect.

Eskin et al. (2016) published a critical review of formation damage induced by asphaltene deposition. They present several field case studies as well as laboratory works which deal with asphaltene deposition and formation damage problem. According to this review, no systematic laboratory research has been conducted to investigate mechanisms of asphaltene impairment in

[2] A version of this chapter has been published:
Telmadarreie and Trivedi, 2017. SPE paper 184970 presented at the SPE Heavy Oil Conference, Calgary, Alberta.

porous media. There was also no field case study for which systematic laboratory research had been performed to determine primary causes of formation damage and to develop a technique for formation damage prevention in that area. Several studies observed asphaltene deposition in core scale while using hydrocarbon solvent for heavy oil recovery (Leyva-Gomez and Babadagli, 2016; Kelli Rankin, 2013; Zekri and Shedid, 2004). Such studies cannot directly observe the mechanisms involved in asphaltene deposition. However, Arciniegas and Babadagli (2014) observed the asphaltene deposition on glass beads under the microscope after solvent injection. They also measured the thickness of asphaltene on the glass beads surface which was deposited by different types of solvent.

Micromodel studies can be used for direct observation of phenomena happening at pore scale in a dynamic condition. There are relatively limited numbers of micromodel study on asphaltene deposition observation, especially in a fractured porous media containing heavy oil. For example, Danesh et al. (1988) investigated the precipitation of asphaltene during miscible gas injection. They used heterogeneous glass micromodel to visualization the asphaltene precipitation and deposition process. Dehghan et al. (2010) also used a heterogeneous glass micromodel to visualize the heavy oil recovery by water alternating solvent (WAS) injection. They observed that although the precipitated asphaltene may initially result in the better spread of solvent in the media, during the time the solvent propagation would be prevented by asphaltene plugging effect. Farzaneh et al. (2010) conducted a series of hydrocarbon solvent injection experiments in a fractured five-spot glass micromodel. They observed that the oil recovery decreased with increase in the fractures' spacing, discontinuity, overlap, and distribution. They also observed that most of the asphaltene was precipitated on walls of the fracture. Pathak et al. (2012) used a high permeability glass bead micromodel for heavy oil recovery with hot solvent injection. They found that the asphaltene

flocculation is greater for lighter paraffinic solvents as compared with heavier paraffinic solvents. They also found that the asphaltene flocculation (and deposition) mostly occurs at the interface of pure solvent and heavy oil, where the concentration gradient of the solvent is highest. Asphaltene deposition reduced as the solvent continues to diffuse into the oil zone. Most recently, Doryani et al. (2016) investigate the process of asphaltene precipitation and deposition in a uniformly patterned glass micromodel. Based on their results, the destabilization of dissolved asphaltene occurred along with the formation of a cloud-like, semi-solid phase due to the diffusion of solvent (n-heptane) molecules indicating the onset of asphaltene precipitation.

Precipitation and deposition of asphaltene in reservoir rock can cause formation damage and reduce the fluid mobility, resulting in significant loss of the hydrocarbon production. Hydrocarbon solvent injection, as a non-thermal heavy oil recovery method, suffers from asphaltene deposition problem. A detailed study on asphaltene deposition behavior in porous media improves the understanding of asphaltene-induced formation damage and provides the possible solutions for preventing and/or controlling formation damage. This chapter aimed to open new insight on asphaltene deposition mechanisms in fractured reservoirs. Asphaltene precipitation, deposition, distribution in porous media and formation damage (pore blocking) were observed by a uniquely designed fractured micromodel representing the fractured reservoirs. The deposition behavior of asphaltene was studied with three different types of solvent during extra-heavy oil recovery. The observations through this study improve our understanding of the situations that asphaltene deposition may result in blocking the flow path and increase the formation damage and thus help us to control this problem.

3.2 Materials and Methods

3.2.1 Materials

Normal pentane (nC5), normal heptane (nC7), and Dodecane (nC12) (provided by Fisher Scientific) were used as the hydrocarbon solvent for extra-heavy oil recovery (dead oil viscosity = 30,000 cp at 22 °C and dead oil density = 0.933 g/cm³). Table 3.1 lists some of the main properties of applied solvents.

Table 3.1: Density and viscosity of the hydrocarbon solvents used in this study.

Solvent name	Chemical formula	Density (g/cm³)	Viscosity (at 20 °C)
Pentane (C_5)	C_5H_{12}	0.626	0.25 cp
Heptane (C_7)	C_7H_{16}	0.689	0.4 cp
Dodecane (C_{12})	$C_{12}H_{26}$	0.749	1.34 cp

3.2.2 Asphaltene Content Measurement of the Crude Oil

Asphaltene content of crude oil was measured using all three solvents following the ASTM (D2007-80) method. It should be mentioned that the objective was to compare the amount of asphaltene precipitation by each solvent. In this method, a certain amount of oil (10 ml in this case) was measured and 40-times that volume of solvent was added to the glass flask. The solution was stirred and let to equilibrate for two days. After aging for two days, a funnel filter assembly was used to separating asphaltene particles from the solution. A clean filter paper (0.22 μ) was weighted before separating the asphaltene. The filter paper was put inside a funnel cup connected to the glass flask. The vacuum pump was connected to the side arm of the filtration flask to begin filtration. A schematic of this process is shown in Figure 3.1. After passing the whole solution from the filter paper, it was dried and weighted to measure the asphaltene content of the crude oil. The weight of precipitated asphaltene was monitored over time to make sure that it is completely dry i.e. when the weight change was less than 0.001 grams over the period of 12 hours. This process

was repeated for all three solvents. The precipitated asphaltenes were also studied under SEM-EDX for further analysis.

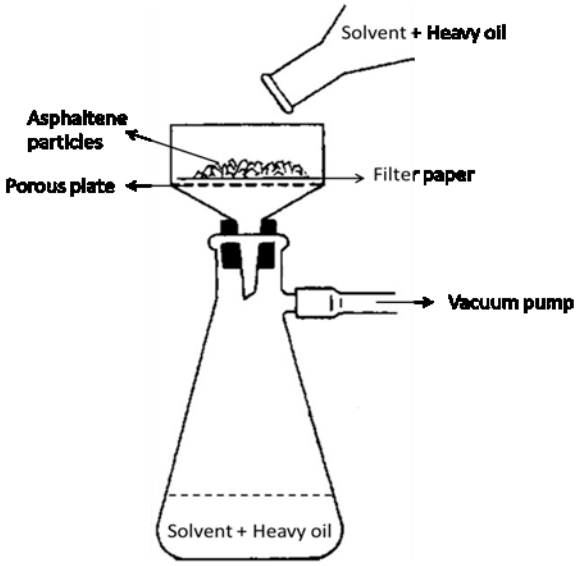

Figure 3.1: Schematic setup of measuring the asphaltene content of the heavy oil using different solvents.

3.2.3 Micromodel Experiment

A special fractured-heterogeneous micromodel (1×7 cm with fracture thickness of 1000 microns) was designed to imitate the fractured carbonate reservoirs as shown in Figure 3.2. The ranges of pore sizes and the fracture dimension are shown in this image. The wettability of the micromodel was also altered to oil wet (OW) conditions with the help of a siliconizing fluid. After initial water and oil saturation, hydrocarbon solvents were injected into the micromodel. The phenomena happening during the solvent injection were monitored by capturing images and video with the help of a high-quality camera. At the end of each test, micromodel was analyzed under the microscope (Leica DM 6000M microscope) for further analysis. Image analysis was performed to calculate the amount of deposited asphaltene in the micromodel. Each image processed with a similar color threshold to have the same condition for the measurement. After that, the images

were analyzed with the MATLAB software for measuring the percentage of deposited asphaltene as well as ultimate oil recovery. It should be mentioned that all the experiments were performed at ambient condition.

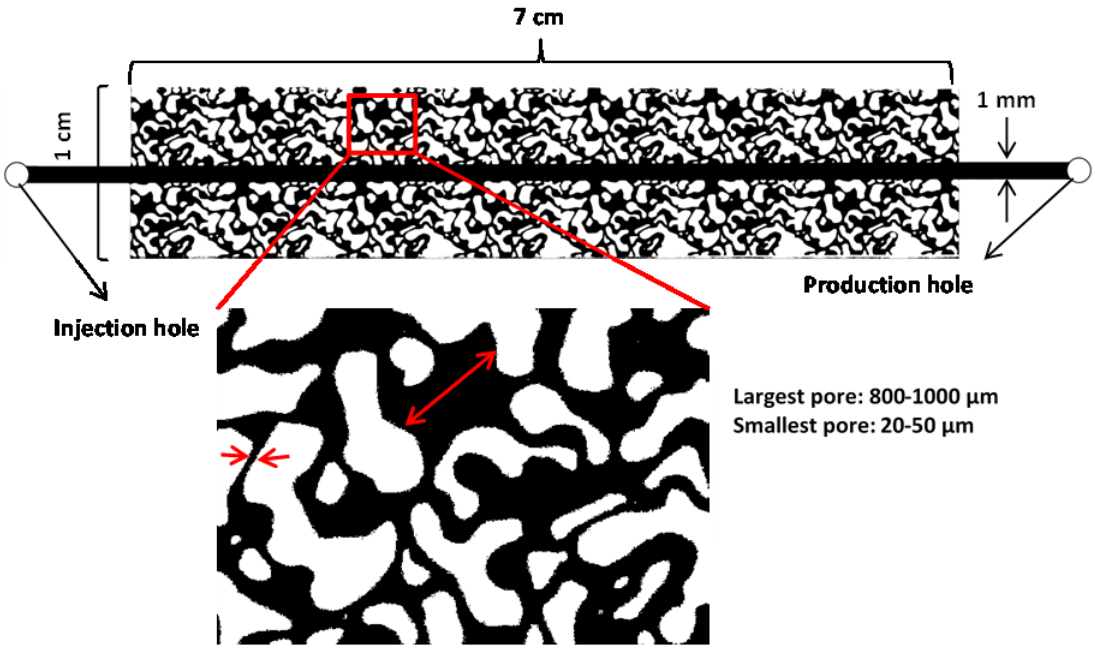

Figure 3.2: Image of the fractured-heterogeneous micromodel showing pore structure. Note: black area shows the porous zone saturated with heavy oil and the white area shows the grain.

3.3 Results

3.3.1 Asphaltene Static Study

In this study, normal pentane, heptane, and dodecane were used for hydrocarbon solvent injection for extra-heavy oil recovery. After fluid saturation (water and oil) in micromodel, hydrocarbon solvent was injected to observe the pore-scale phenomena during solvent injection for heavy oil recovery. The injection rate was selected to be small enough to have relatively stable injection profile (0.08 cc/min). However, heterogeneity of the model will result in various flow behaviors. This will influence the asphaltene deposition and formation damage which will be discussed later

in this chapter. Before visual observation of solvent heavy oil recovery in the micromodel, the amount of asphaltene precipitated with each solvent was measured in the static condition. The amount of precipitated asphaltene from the studied heavy oil has an indirect relationship with the number of carbons in the solvent (Figure 3.3). Higher carbon number solvent precipitated less asphaltene from the heavy oil. This result was also observed in the previous studies (Mitchell and Speight, 1973; Fuhr et al., 1991; Ferworn et al., 1993; Hammami et al., 2000; Speight, 1999; Moreno and Babadagli, 2013). Besides, Corbett and Petrossi (1978) have found that the amount of asphaltene precipitated is almost constant from n-heptane to the higher carbon number. The type of solvent also influences the properties of the precipitated asphaltenes. Asphaltenes precipitated by n-heptane are heavier and more polar. On the other hand, asphaltenes are less polar, and the molecular weight is lower when using n-pentane (Andersen, 1990).

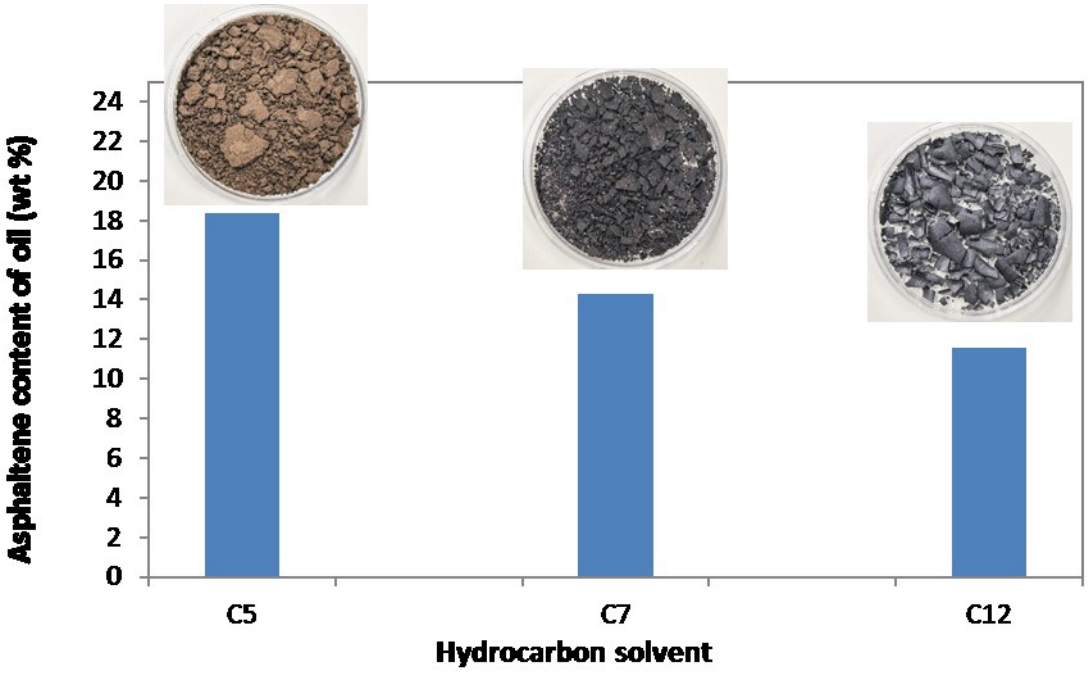

Figure 3.3: Percentage and images of asphaltene precipitated with different types of solvent in the static condition.

3.3.2 SEM Analysis

According to Speight et al. (1984), the aromaticity (hydrogen/carbon atomic ratio) and molecular weight of asphaltene depend on the precipitating solvent. They showed that the H/C ratio decreases with increase in carbon number of the solvent. They also observed that the amounts and natures of asphaltenes precipitated with n-heptane or heavier alkanes are very similar. The elemental analysis of precipitated asphaltenes in this study (Table 3.2) showed that all three samples are similar; however, there are some minor changes in sulfur and oxygen contest as the carbon number of solvent increases. The S and O content decreased and increased respectively with increasing carbon number of the solvent. Furthermore, a relatively significant amount of Nitrogen was detected in asphaltene precipitated by C12 solvent compared to other solvents.

Precipitated asphaltenes were also studied under the SEM as shown in Figure 3.4. The objective of SEM analysis was to find out any difference in morphology and the structure of the precipitated

asphaltene. Samples were studied at different magnifications, and two magnifications from each sample are presented in Figure 3.4. Although there is no significant difference in the appearance of the asphaltene samples, in particular between asphaltene precipitated by C7 and C12 solvents, the C5 asphaltene showed a small difference in the structure. The C5 asphaltene was smaller and more irregular and amorphous in shape while the other two samples were larger and had a more distinct structure which can be seen at the higher magnification.

Table 3.2: Elemental analysis of asphaltene sample by EDX (element with weight percentage lower than 0.5 wt% cannot be detected by the SEM-EDX system used in this study).

Asphaltene sample	C (wt %)	S (wt %)	O (wt%)	N (wt%)
Pentane (C_5)	88.2	6.6	5.2	NA
Heptane (C_7)	88.9	3.9	7.2	NA
Dodecane (C_{12})	85.1	3.5	7.8	3.6

Per Wang et al. (2015), collisions among small particles or collisions between small and coarse particles are more frequent and efficient than that of coarse particles leading to much easier agglomeration of smaller particles. As seen in Figure 3.4, the size of asphaltene particle increases with the carbon number of the solvent. The smaller size of C5 asphaltene (Figure 3.4a and 3.4b) can create clusters of asphaltene more easily than that of C7 and C12 asphaltenes. Therefore, C5 asphaltene has a high potential of creating clusters and agglomeration in porous media which can be detrimental for formation damage.

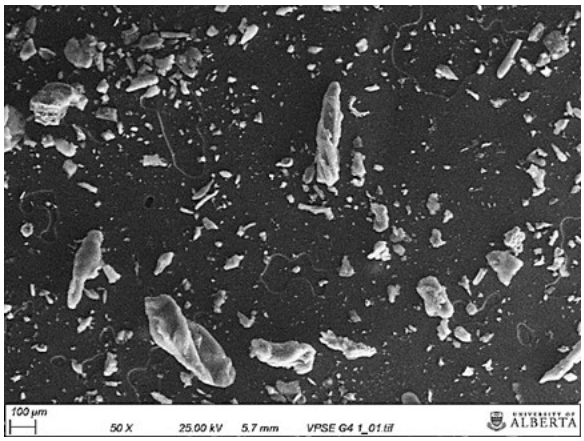

(a) C5 Asphaltene (100 microns)

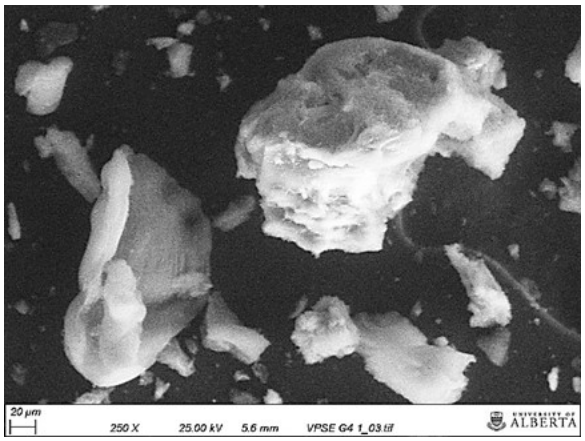

(b) C5 Asphaltene (20 microns)

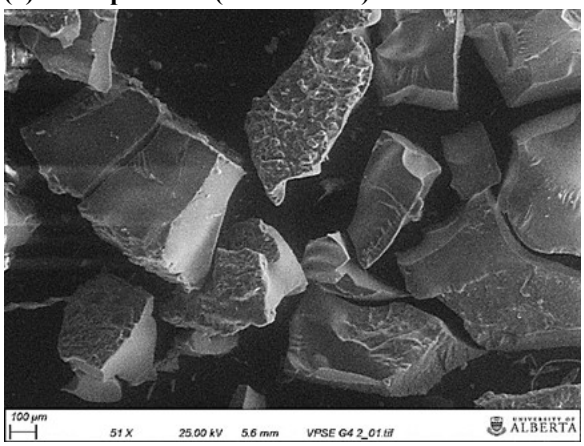

(c) C7 Asphaltene (100 microns)

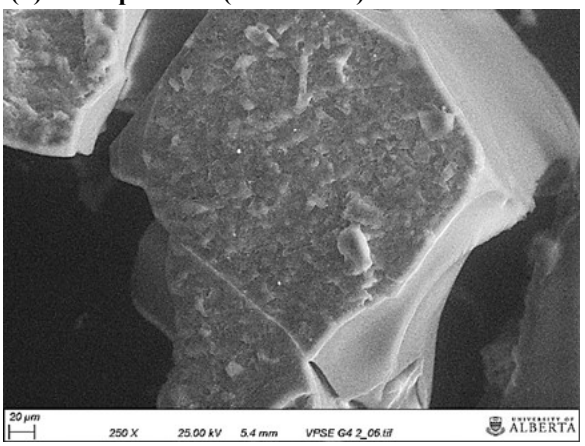

(d) C7 Asphaltene (20 microns)

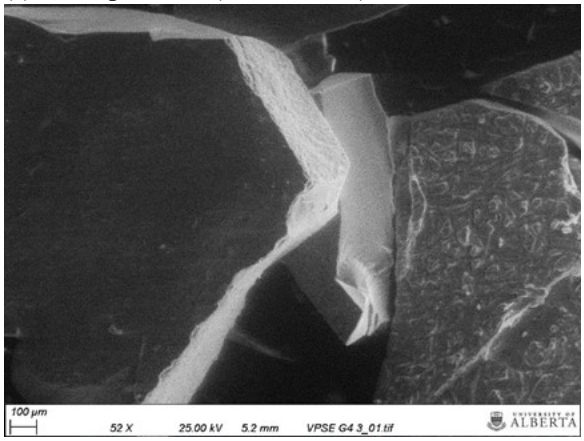

(e) C12 Asphaltene (100 microns)

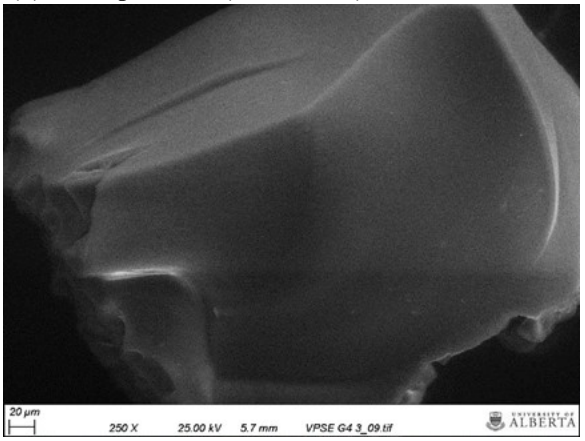

(f) C12 Asphaltene (20 microns)

Figure 3.4: SEM images of precipitated asphaltene with C5, C7, and C12 hydrocarbon solvent at two different magnifications.

3.3.3 Asphaltene in Porous Media

Figure 3.5 shows the pictures of heavy oil saturated micromodel at the end of solvent injection (C5, C7, and C12). At initial look, there might be no significant different in micromodel at the end of the solvent flood. However, the detailed look can reveal some differences. Like bulk study, the amount of asphaltene precipitation reduced with increasing carbon number of solvent. Also, formation damage resulting from the asphaltene deposition was more severe in the case of C5 than other studied solvents. Furthermore, the amount of deposition is relatively higher near the outlet of micromodel, especially inside the fracture since the precipitated asphaltene moves along the flow path (which is mainly the fracture) toward the micromodel outlet and clump together.

Figure 3.5: Images of the micromodel at the end of the heavy oil recovery by solvent injection; (a) C_5, (b) C_7, and (c) C_{12}. The red line represents 1000 microns.

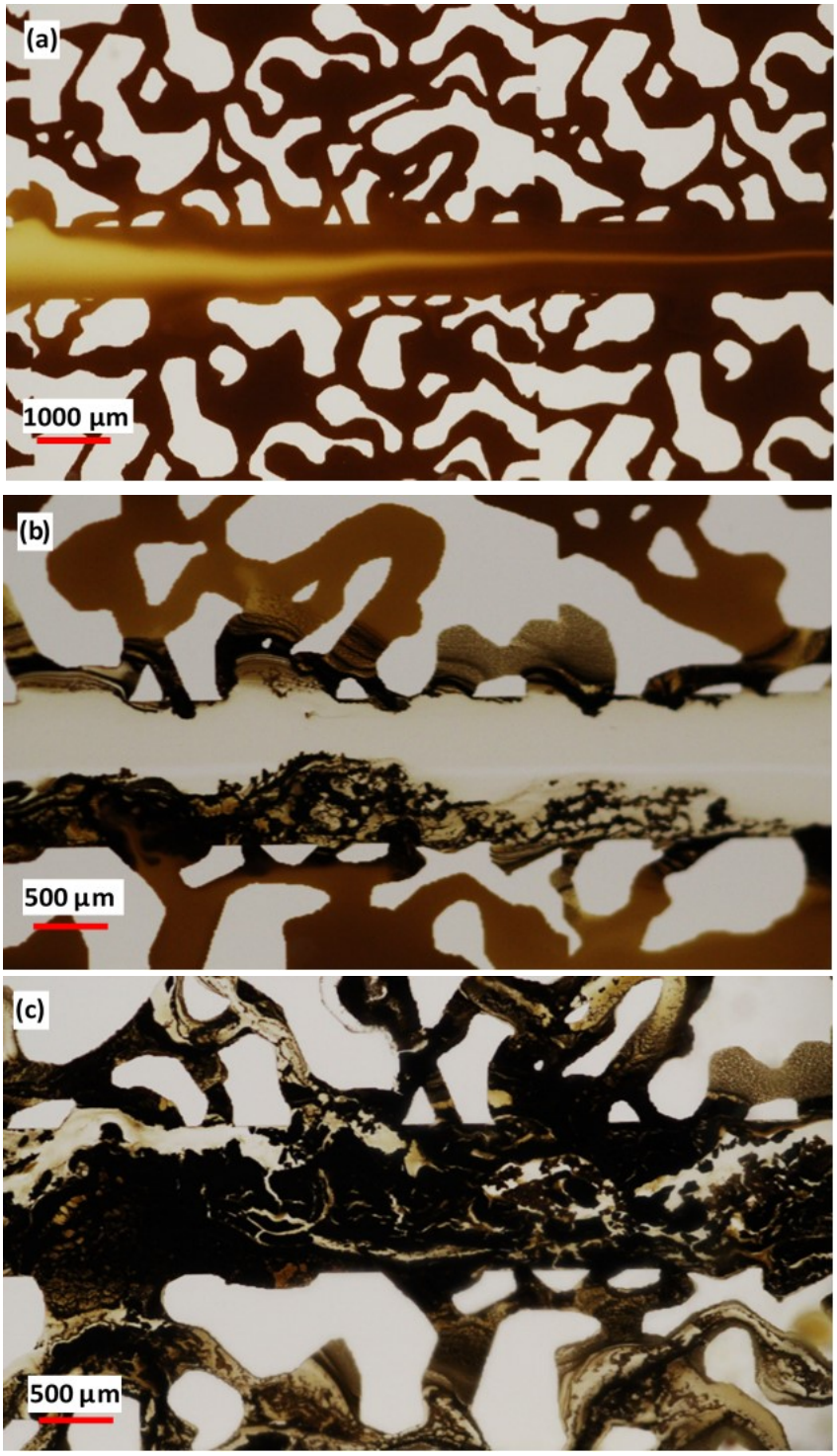

Figure 3.6: Images of micromodel showing different time-stage of solvent injection (C5) in the porous media resulting formation damage; (a) early stage of solvent injection representing the diffusion and dilution of oil, (b) second stage showing asphaltene precipitation began at matrix-fracture interface, (c) late stage of solvent flood where there was a severe asphaltene deposition resulting formation damage and pore blocking.

Different stages are involved in solvent injection into a heterogeneous porous media as observed in this study. First, the solvent will select the easiest path to move (i.e. fracture) and start to diffuse at the solvent-oil interface. It will leave behind the diluted oil. Although solvent molecules diffuse into the heavy oil at an early stage, the dissolved asphaltene will not become unstable to precipitate (Figure 3.6a). There is a threshold for dispersed solvent that would cause asphaltene molecules to flocculate and form asphaltene precipitates (Doryani et al., 2016). As solvent injection continues, asphaltene precipitation will intensify and create different layers or clusters of asphaltene precipitate (Figure 3.6b). This cluster may have adhered together to form multi-layer (or bigger) asphaltene deposits. At the late stage of solvent injection, the severe asphaltene deposition may also block the fracture which is the main flow path in a fractured-heterogeneous porous media. This phenomenon can be seen in Figure 3.6c.

3.4 Discussions

3.4.1 Asphaltene Deposition and Formation Damage

Before going into detail about the visual observation of asphaltene deposition, let's see how different types of hydrocarbon affect the amount and rate of asphaltene deposition. Figure 3.7 shows the cumulative amount of deposited asphaltene in micromodel while using different solvent. Like bulk study (Figure 3.3) the C5 resulted in more asphaltene precipitation than other studied solvents. Increasing carbon number of solvent decreases the amount of deposited asphaltene in porous media. Moreover, the rate of deposition is higher in lower carbon number as can be inferred from the Figure 3.7. The C5 solvent deposited asphalted much faster, which can be due to the higher diffusion rate of this solvent compared to that of C7 and C12.

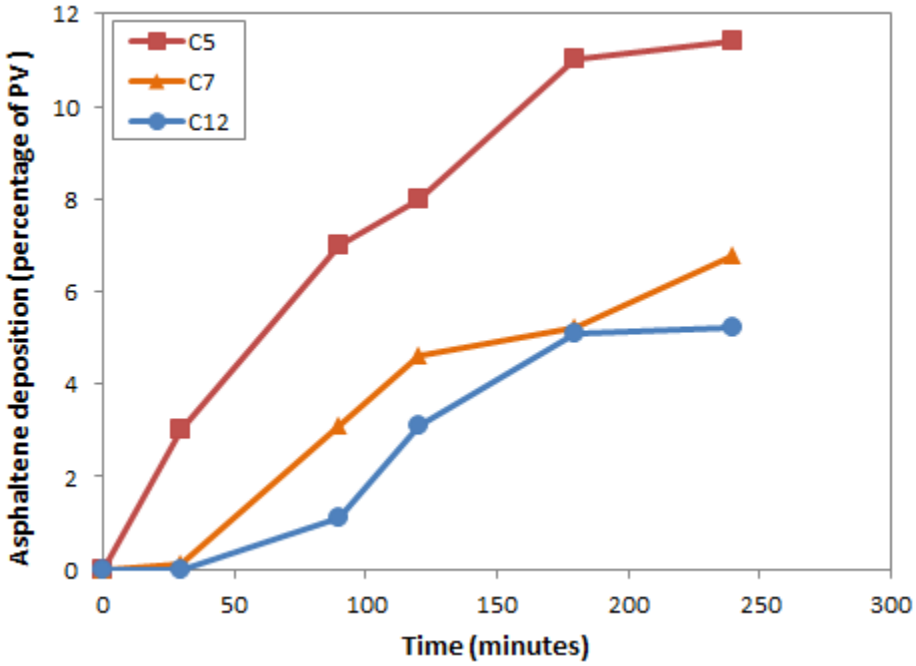

Figure 3.7: Deposited asphaltene profile in porous media when injecting different types of solvent. The vertical axis represents the percentage of pore volume covered by the deposited asphaltene.

An excessive amount of asphaltene deposition may result in a severe formation damage and sometimes block the flow path as seen in Figure 3.6c. Therefore, the injected solvent cannot further diffuse deep into the matrix (due severe to asphaltene deposition) and eventually causes injectivity problem. In this study, C5 injection resulted in the high amount of asphaltene deposition in porous media (11.4 % per Figure 3.7) and it could block the main flow path, the fracture (as seen in Figure 3.6c). The pressure profiles of C5 injection shown in Figure 3.8 can also explain the formation damage caused by severe asphaltene deposition. At early time-stage of solvent injection, solvent mainly diffuses into the oil within the fracture path (while diffusing into the matrix as well) and recovered most of the oil in this area (up to 80 minutes in Figure 3.8). After that, the solvent is occupied the whole fracture, and due to the concentration gradient between the solvent and matrix's oil, the solvent diffused into the matrix, dilute the oil by precipitation and deposition of

asphaltene. Continuing solvent injection resulted in more asphaltene deposition in the matrix and especially fracture-matrix interface (where the highest concentration gradient is) that eventually cause the formation damage and reduce the injectivity. This can be seen in Figure 3.7 from time 90 minutes to 280 minutes where the injection pressure increased until the time that was no injection at all (after about 280 minutes).

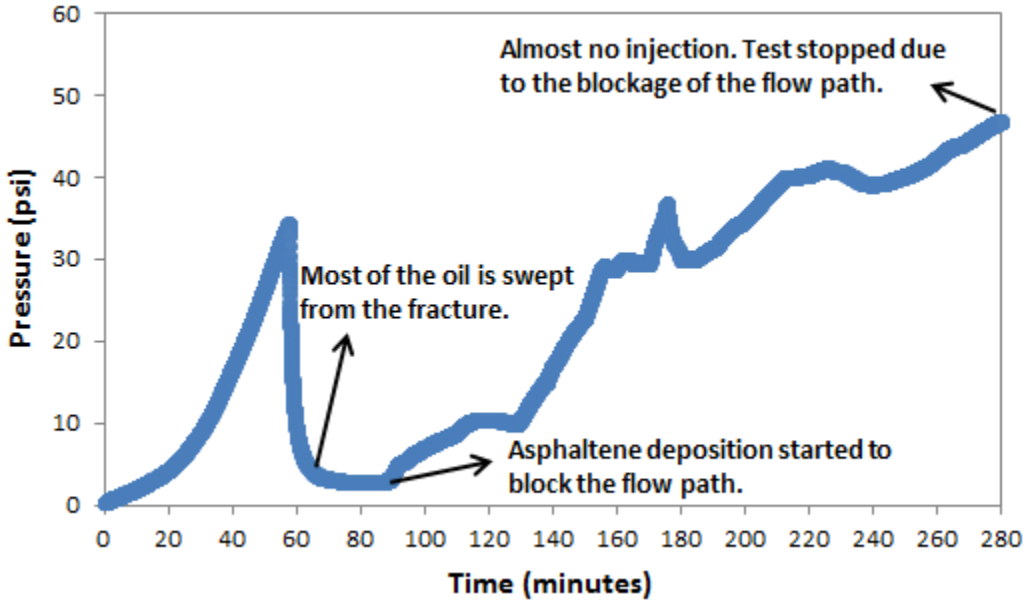

Figure 3.8: Pressure profile during solvent injection (C5) for extra-heavy oil recovery in the fractured micromodel.

3.4.2 Asphaltene Distribution Pattern in Heterogeneous Fractured Porous Media

Image analysis was performed to study the distribution of asphaltene deposition in the fractured micromodel. By changing the color threshold of images taken at the end of the solvent flood, the dark zones representing the asphaltene deposition can be distinguished. The distribution pattern of asphaltene deposition at the end of C5, C7, and C12 injection are shown in Figure 3.9a, Figure 3.9b, and Figure 3.9c, respectively. A detailed look at these images revealed interesting facts about

asphaltene deposition using different solvents in a fractured heterogeneous porous media as follow:

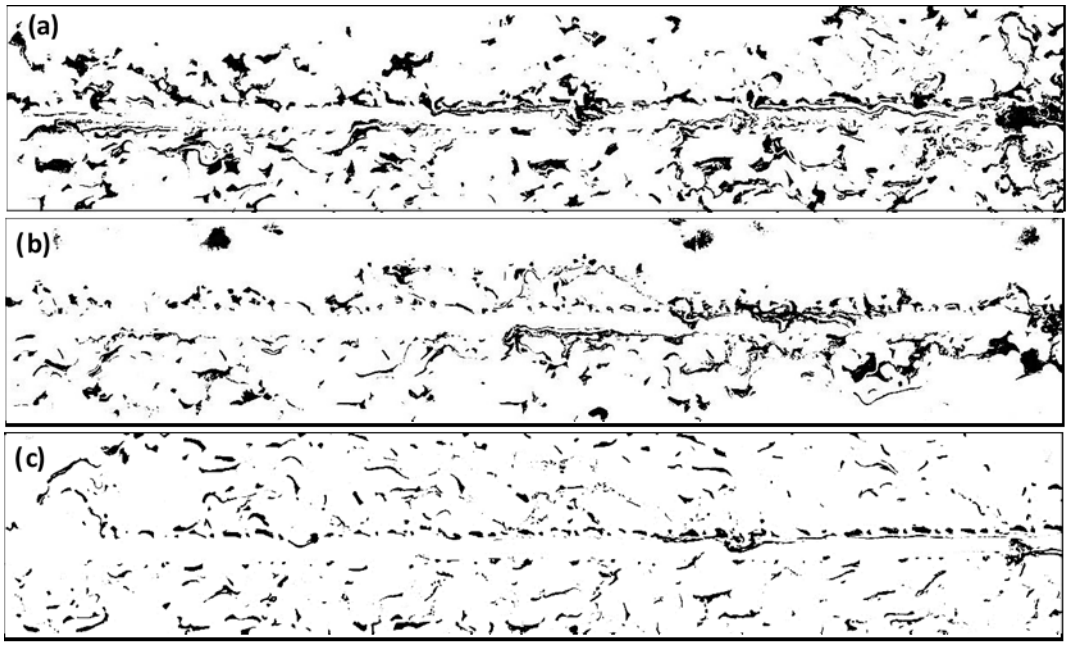

Figure 3.9: Distribution of asphaltene in porous media precipitated at the end of solvent injection in the fractured porous media, (a) C5 asphaltene, (b) C7 asphaltene, and C12 asphaltene.

- The profile of asphaltene deposition after C5 injection is presented in Figure 3.9a. The amount of asphaltene deposition (dark color area) after C5 injection is more than that of both C7 and C12, showing that asphaltene deposition is higher when using lower carbon number solvent. This is also quantitatively measured in Figure 3.7.
- A significant amount of asphaltene was deposited along the matrix-fracture interface (highest in C5 and lowest in C12). This can be due to the sharp solvent concentration gradient at the fracture-matrix interface, enhancing the asphaltene precipitation and deposition. Also, more mixing will happen in the flow path (i.e. fracture) which reinforce the asphaltene precipitation. The latter is also the reason for asphaltene deposition in bigger

pores of the matrix, especially during C5 injection. This phenomenon is less seen in the case of C12 injection due to the lower asphaltene precipitation.

- At lower carbon number solvent (C5) where the asphaltene precipitation is severe, the deposition could also block the fracture path which is primary flow path for fluid in this type of porous media. This can also be inferred from Figure 3.6c and Figure 3.8. It is worth mentioning that SEM analysis results suggest that C5 asphaltene can clump together and make bigger deposits more easily compare to the asphaltene precipitated by C7 and C12. Therefore, besides the amount of precipitated asphaltene (which is highest in C5) its ability to make bigger clusters is also a reason for more formation damage compared to other studied solvents.
- Another interesting observation is the distribution pattern of asphaltene deposition in C12 which relatively different from that of C7 and C5. In C12 injection, there can be seen more asphaltene in matrix area than that of other studied solvents. This is because of less asphaltene deposition at the matrix-fracture interface which could not prevent the solvent from further diffusion into the matrix. In the case of lower carbon number solvents, more asphaltene deposition at matrix-fracture interface blocked the diffusion path of the solvent into the matrix especially those areas far from the fracture. Therefore, in C12 injection, asphaltene precipitation is less than that of C7 and C5 solvents, which is the main reason for wider distribution of asphaltene in porous media.

It is worth mentioning that the oil recovery and sweep efficiency depends on the balance between diffusion (higher is preferred; C5 > C7 > C12) and asphaltene deposition (lower is preferable; C5 > C7 > C12). Therefore, although less asphaltene precipitation did not prevent the C12 solvent diffusion into the untouched parts, less diffusion rate of this solvent results in less significant

improvement of the oil recovery compared to that of other studied solvents. The ultimate heavy oil recovery of each solvent calculated by image analysis is shown in Figure 3.10 where C5, C7, and C12 could recover the 47.8 %, 35.9 %, and 33.4 % of initial oil, respectively.

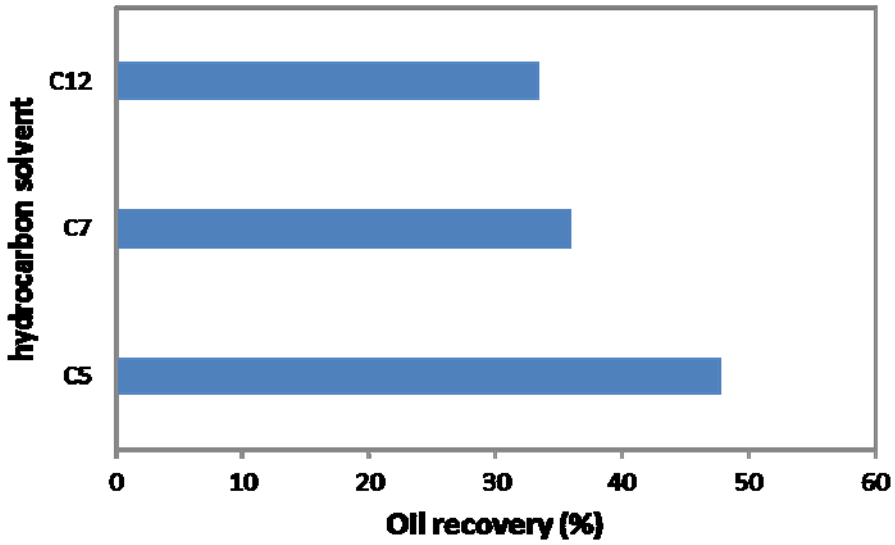

Figure 3.10: Ultimate heavy oil recovery values when using different solvents in the fractured porous media.

3.4.3 Different Shapes of Asphaltene Deposition in the Fracture and Matrix

The objective of this section is to study the mechanisms of asphaltene precipitation and deposition in the fractured micromodel including both fracture and matrix areas. The primary goal is to observe how asphaltene deposition will result in formation damage in a fractured-heterogeneous porous media.

As seen before, asphaltene deposition could block the pore throat in the matrix as well as the fracture which is the main flow path. Observation through this study revealed that different stages and mechanism are involved in blocking fracture path and pore throat by asphaltene deposition.

Figure 3.11 shows the time-lapse image of micromodel at an early stage of solvent flooding in heavy oil saturated micromodel. The solvent plume when contacting with extra-heavy oil in the fracture is not homogenous as seen in Figure 3.11a. In another word, the solvent will not diffuse into the oil as a piston-like displacement. The solvent concentration is highest in the center of the plume and decreases toward the edge as shown in the image. As injection continues, the high solvent concentration zone at the center of the area will expand and cover the width of the fracture as seen in Figure 3.11b and Figure 3.11c. It should be mentioned that the solvent diffuses into the matrix area from the edge of the plume. Later, on those areas where the whole width of the fracture covered by the solvent, asphaltene begins to precipitate at the fracture-matrix interface where the concentration gradient of the solvent is highest. Further solvent injection increases the solvent diffusion into the matrix and enhances the asphaltene precipitation and deposition. Precipitated asphaltene particles flocculate together and create a bigger asphaltene deposition as seen in Figure 3.11d. These high asphaltene depositions which are mainly located at the matrix-fracture interface will restrain further diffusion of solvent into the matrix and may block the fracture path.

At this stage, the asphaltene precipitation/deposition starts to block the pore throat and may also block the fracture path eventually. Let's first consider the steps and mechanisms involved in asphaltene deposition in the fracture. As mentioned earlier, solvent plume moves in a relatively wide fracture with a concentration gradient inside the plume. The solvent diffuses from the edge of the plume into the oil. In time, as seen in Figure 3.11, asphaltene will precipitate mainly at the fracture-matrix interface. The early stage of solvent flood and asphaltene precipitation and deposition have been shown in Figure 3.11. Figure 3.12 shows the late stage of asphaltene deposition in the fracture area. At this juncture, solvent had already swept the fracture and diffused into the matrix, and asphaltene precipitation increased at the fracture-matrix interface. Asphaltene

was precipitated at the interface in two main shapes as observed in this study. First, in the shape of ropes parallel to the flow direction in the fracture and the asphaltene lump resulting from flocculation of smaller asphaltene at certain locations.

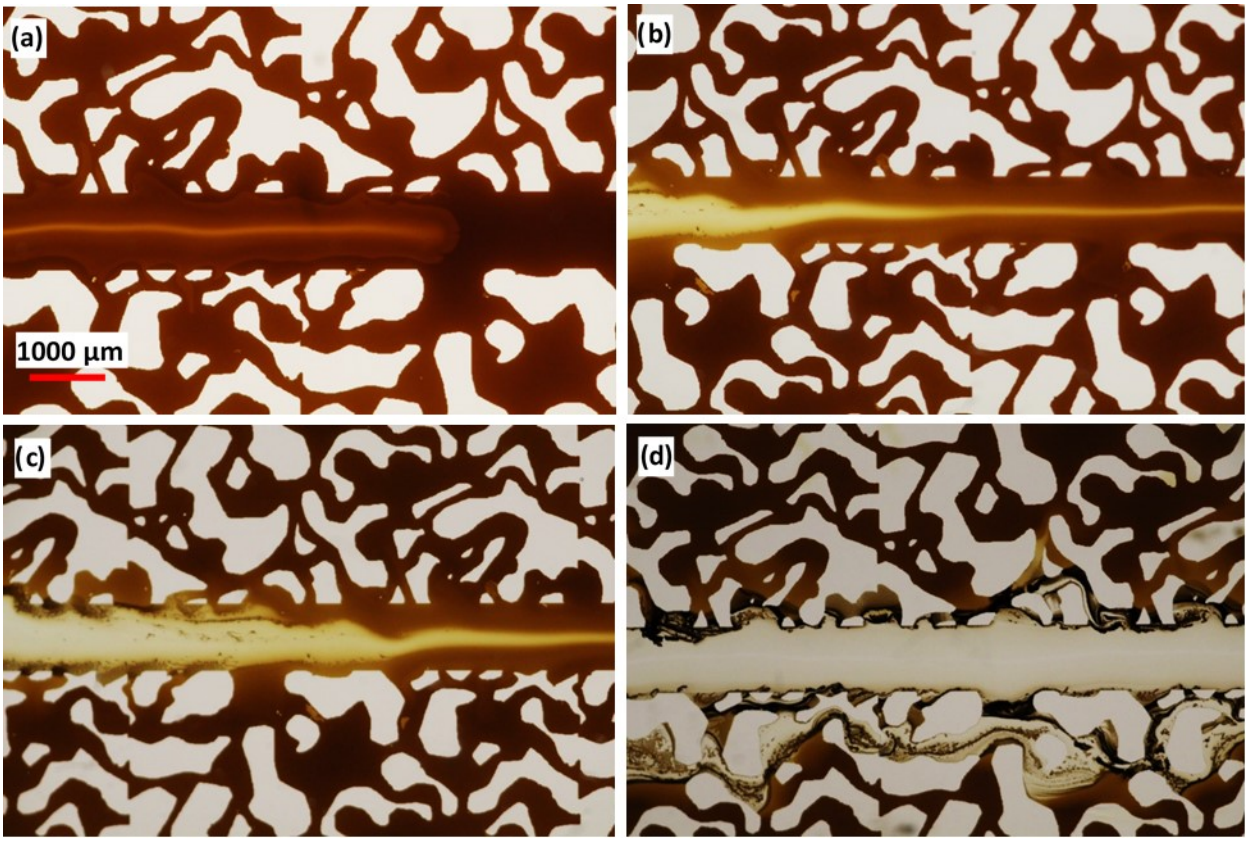

Figure 3.11: Images of micromodel during solvent injection at early time stages showing in four frames what happens when hydrocarbon solvent is injected in a fractured porous media. Solvent injection time increases from the images (a) to (d).

Asphaltene was deposited in the shape of ropes parallel to the flow direction (i.e. Figure 3.12b and Figure 3.12c) as the solvent and diluted oil moved in the fracture along the matrix-fracture interface. Asphaltene particles mainly attached to the grain at the matrix-fracture interface and create series of ropes parallel to the flow direction. Furthermore, as seen in Figure 3.12c and Figure 3.12d, there is some wider opening area of the matrix which is connected to the fracture. These

areas are susceptible to create the asphaltene lumps by further injection of solvent. At this wide opening area, more oil is in contact with the solvent in the fracture and deposition and precipitation of asphaltene will be more dominant than other regions. The asphaltene particles deposited in these areas flocculate together. Besides, precipitated asphaltenes moving in the fracture trap and attach to these lumps and make it bigger. This trend continuous and eventually the combination of parallel rope (parallel to the direction of flow) and lumps (perpendicular to the direction of flow) can block the wide fracture path as seen in Figure 3.12c. It is worth mentioning that the asphaltene lumps grow and sometimes can block the flow path without the help of any other type of asphaltene deposition (i.e. parallel rope). The observations through this study revealed that the precipitated asphaltene in the flow path tends to stick to these lumps and make them bigger. This phenomenon can be seen in Figure 3.12d.

Now let's consider the asphaltene precipitation/deposition and the potential blockage of flow in the pore structure of the matrix. Figure 3.13 represents the formation and deposition of asphaltene in pore throat. A detailed look as shown in the magnified section of this image shows the series of asphaltene rope which is deposited at pore throat. Also, usually, these ropes are thicker at the entrance of the pore than at the other side which is further downstream considering the flow direction. A schematic of steps involving in pore blocking by asphaltene is shown in Figure 3.14.

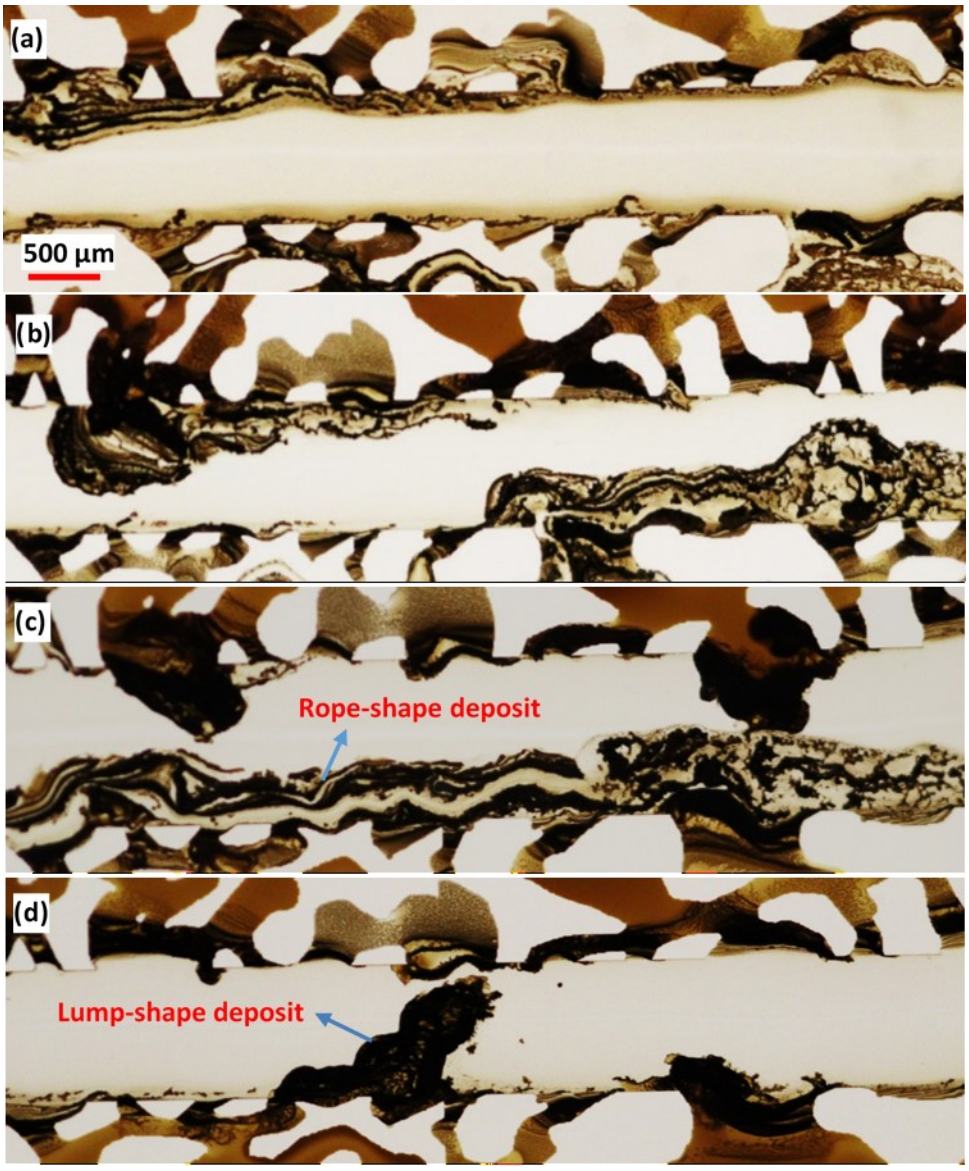

Figure 3.12: Micromodel images showing different shapes of asphaltene precipitated in the fracture and matrix-fracture interface at late time-stage of solvent injection. (a) the increase in the asphaltene deposition at the matrix-fracture interface, (b) creation of rope deposits parallel to the flow direction, (c) combination of lump and rope deposits within the fracture, (d) asphaltene lumps-perpendicular to the flow direction-blocking the fracture path.

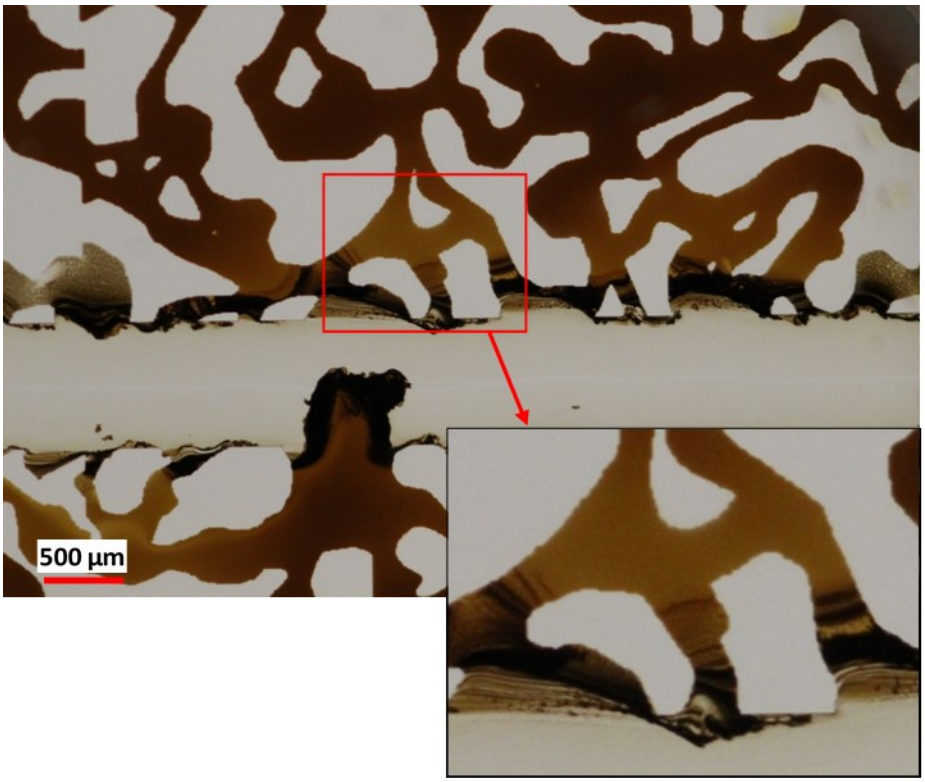

Figure 3.13: Micromodel image showing the asphaltene deposition pattern in the pore throat. Asphaltene deposited in the narrow pores perpendicular to the solvent flow direction.

Initially, asphaltene starts to precipitate at the solvent-heavy oil interface due to the concentration gradient (Figure 3.14a). As pore throat is narrow, the precipitated asphaltene usually creates a rope perpendicular to the direction of flow along the solvent-heavy oil interface. This is not always the case especially in the fracture where the width is much bigger compared to that of pore throat. As solvent diffuses into the heavy oil, the asphaltene continues to precipitate at the initial interface as well as new interface created by the solvent moving further inside the heavy oil saturated zone. The amount of deposition at the initial interface is highest and decreases in new interfaces as the solvent moves. This is due to lower concentration of the solvent at solvent-heavy oil interface in the newer interface than that of the older one. Eventually, these interfaces can combine and reach together and may partially or permanently block the diffusion path of the solvent toward the other

parts of the matrix. It is worth mentioning that this deposition pattern was observed mainly in those areas of the matrix where the solvent diffuses slowly (viscous flow was not dominant) in the heavy oil saturated zone and the pore throat was narrow.

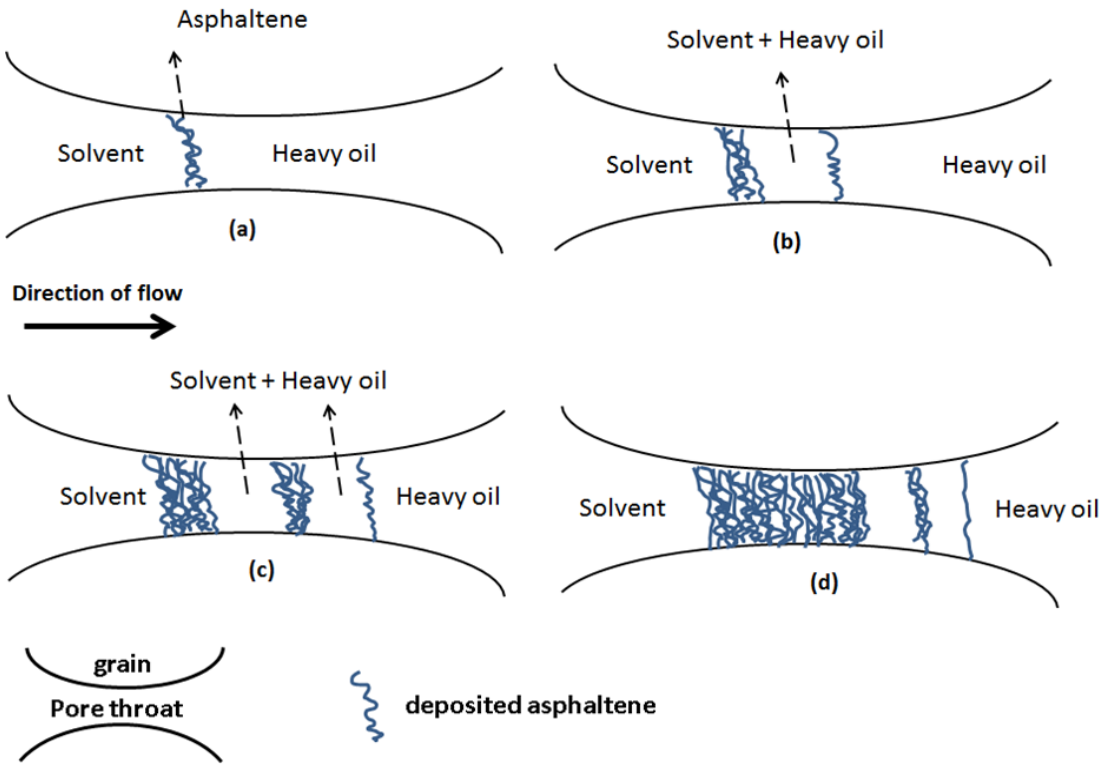

Figure 3.14: Schematic of asphaltene deposition mechanism in the narrow pore throat of the matrix. Parts (a) to (d) shows the time lapse of the deposition mechanism.

Microscopic observation of micromodel at the end of solvent flooding revealed that asphaltene can also precipitate in the form of parallel rope at those areas of the matrix where the flow rate is faster (like the fracture condition) which is shown in Figure 3.15a. These areas usually contain diluted oil without any obstacle like narrow pore or severe curve for fluid movement. Also, they are mainly near the fracture rather than deep into the matrix where the flow is not fast. The reason for higher flow in these areas is due to the partially blocking of the fracture causing the injected solvent create

its way toward the easiest path in the matrix near the fracture. Thus, it will create precipitation pattern similar to that of the fracture zone. This is shown in Figure 3.16 by red arrows. The asphaltene deposition pattern in open area of the matrix is also different. Due to movement of fluid from narrow channels in the matrix to opening pore in the matrix (as seen in Figure 3.15b) the solvent entered to this area will mix with diluted oil rather than one-direction flow as observed in a narrow zone of the matrix and the fracture path. The mixing will create an asphaltene deposition pattern containing asphaltene clusters generated with smaller deposited particles. Figure 3.15c also shows the microscopic image of asphaltene deposition in narrow pore throat which is blocked the flow path based on the mechanism explained in Figure 3.14.

Figure 3.16 summarize the different deposition patterns of asphaltene in the heterogeneous matrix. As explained earlier, asphaltene can deposit in the heterogeneous matrix in two main shapes; parallel to the flow direction (red arrows in Figure 3.16) and perpendicular to the flow direction showing by yellow arrows in Figure 3.16. Partial blockage of fracture by asphaltene deposition resulted in injected fluid find its way into the matrix near the fracture where the oil is diluted. In these zones, fluid will move faster than normal in the matrix and create a rope shape asphaltene deposition. However, still in those areas of the matrix where the flow is slower, the deposition is perpendicular to the flow direction as explained in Figure 3.14.

It worth mentioning that the parallel pattern of deposition is not usually blocked the pore but may narrow the flow path in the matrix. The only mechanisms observed for asphaltene deposition in the matrix that can significantly impede the solvent flow and diffusion is the deposition perpendicular to the flow direction.

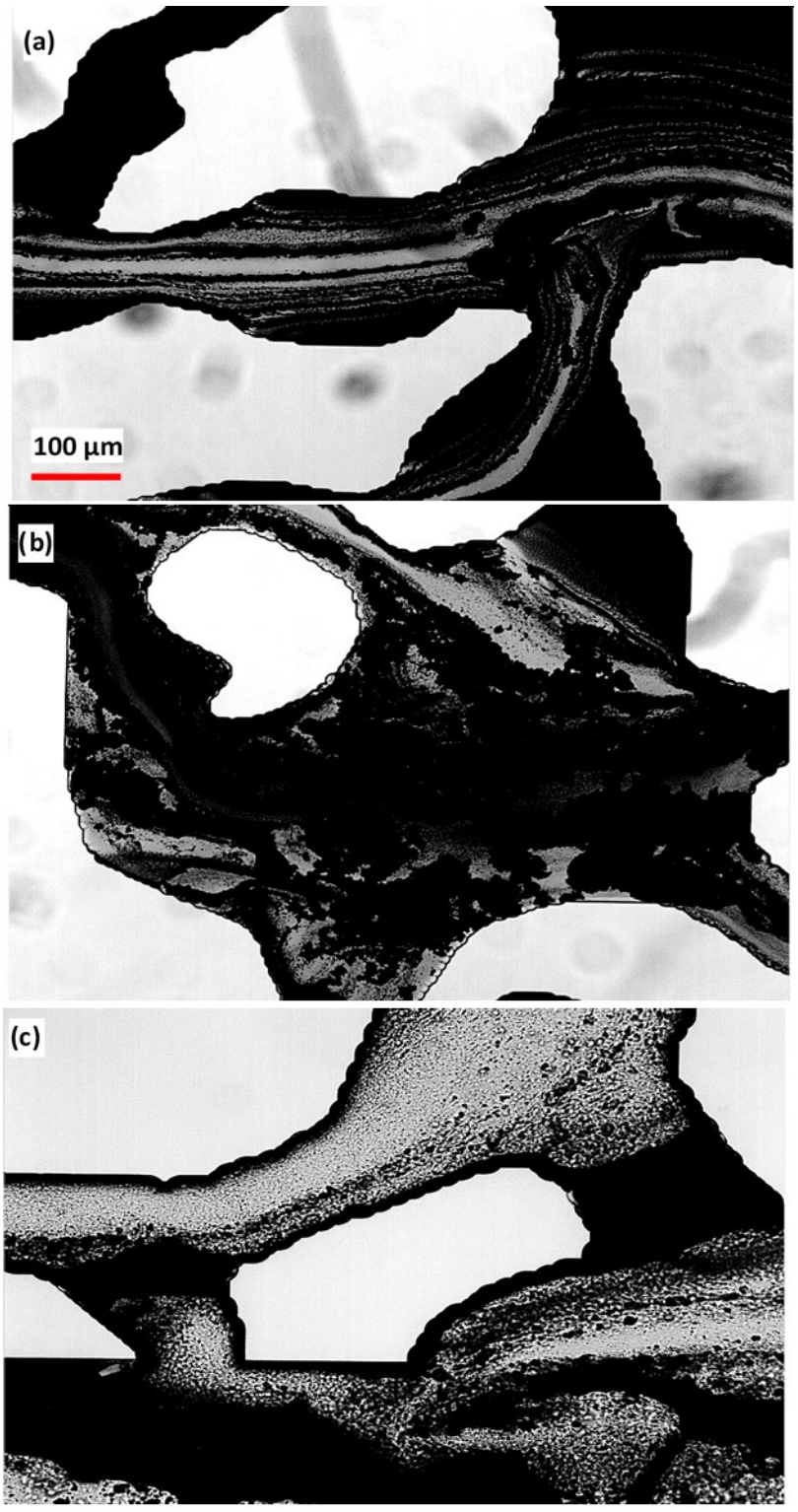

Figure 3.15: Microscopic images of the micromodel at the end of solvent injection showing different asphaltene deposition pattern in the matrix. (a) parallel rope deposition, (b) asphaltene clusters in the bigger pores of the matrix, (c) asphaltene deposition perpendicular to the flow direction blocking the pore throat.

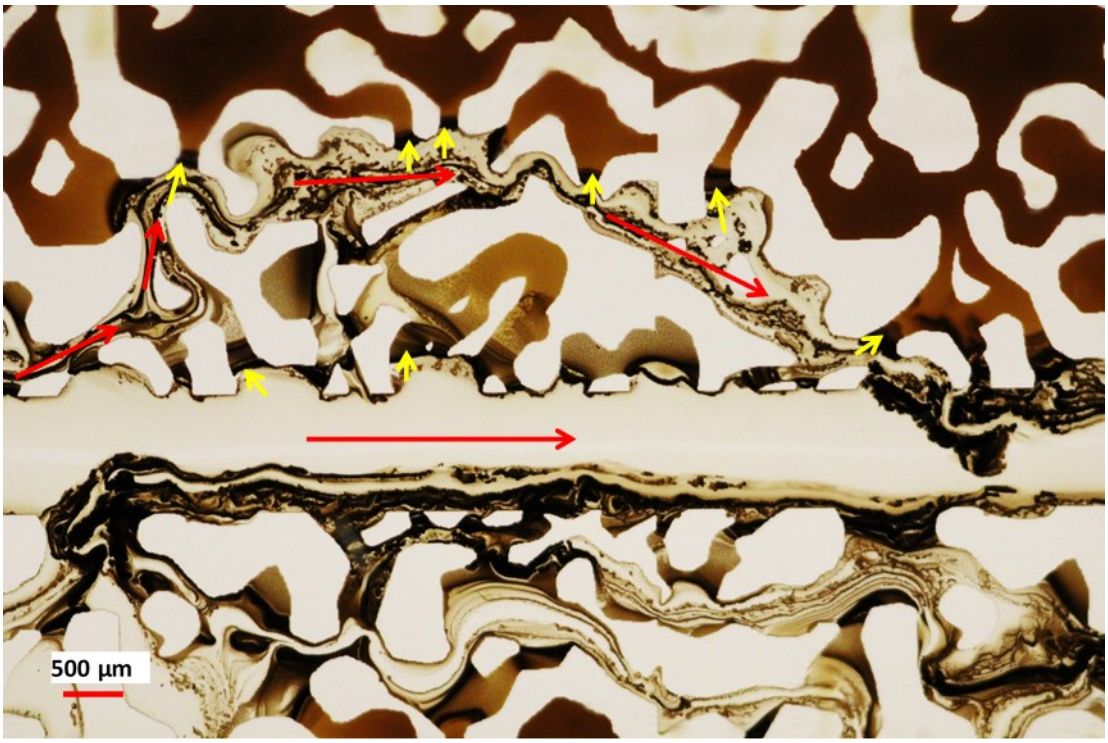

Figure 3.16: Micromodel image showing different patterns of asphaltene deposition in the matrix. Red arrows show the deposition parallel to the flow direction (viscous dominant region) while yellow arrows show the perpendicular depositions (diffusion dominant flow).

3.5 Summary

The focus of this chapter was to visualize the asphaltene deposition during solvent flooding in a heterogeneous porous media. Observations through this study revealed different mechanisms and shapes for deposited asphaltene. Knowing this information can help us to optimize the solvent EOR method that deals with asphaltene precipitation issue. Following are the summary of this chapter:

- Static analysis of precipitated asphaltene showed that with increasing the carbon number of the solvent, the amount of precipitated asphaltene would decrease. Also, the SEM study revealed that the asphaltene particles precipitated by C5 are much smaller than that of C7

and C12 solvents having a higher potential of agglomeration and clustering which may result in formation damage and pore blocking in porous media.

- During solvent injection, especially C5 and C7, asphaltene mainly deposited at the fracture-matrix interface where there is a high concentration of the solvent. Also, the amount of asphaltene deposition decreased when using a solvent with higher carbon number.
- In the fracture, asphaltene is mainly deposited in rope-shape patterns parallel to the flow direction. Also, in the area where the matrix's oil has more contact area with the solvent in the fracture, the chance of lump-shape deposition of asphaltene is high. The combination of these two structures may result in blocking the fracture path and severe formation damage.
- Asphaltene mainly deposits in two shapes in the heterogeneous matrix; Parallel deposition and perpendicular deposition related to flow direction. The parallel deposition mainly occurs in the area where the solvent flows relatively faster, and the viscous force is more dominant whereas the perpendicular deposition is a stepwise deposition of asphaltene taking place mainly on narrow pore throat of the matrix. The flow rate is relatively slow, and diffusion of solvent is the primary mechanisms of displacement.
- Deposition of asphaltene parallel to the flow direction (both in matrix and fracture) cannot solely block the flow path without the presence of any other shape of deposition i.e. lumps or perpendicular deposition. On the other hand, perpendicular deposition may block the pore throat and prevent further diffusion of solvent deep into the matrix.
- The size of the pore throat and rate of solvent movement are two of the main reasons for asphaltene to block a path or not. The relatively higher rate of solvent movement where the flow is viscous dominant will not result in pore blockage by asphaltene precipitation (either

small pores or the larger one). However, when the rate is low, the asphaltene precipitation in smaller pore throat can block the solvent diffusion path. The asphaltene precipitation pattern can explain this at different pore size and dominant flow mechanisms (i.e. viscous flow or diffusion flow).

- It is a well-established fact that the amount of asphaltene deposition is the same from C7 and higher carbon number solvent; however, this study showed that the distribution pattern of deposition is not necessary the same in a fractured porous media. The distribution pattern and shape of asphaltene deposition are the important factors on formation damage and pore blocking in heterogeneous porous media.

Chapter 4: Improving Hydrocarbon Solvent Injection for Heavy Oil Recovery: Applying CO_2 Foam/Polymer Enhanced Foam and Hydrocarbon Solvent Based Foam[3,4]

The performance of hydrocarbon solvent injection for heavy oil recovery from fractured carbonate reservoir was visualized and analyzed in Chapter 3. Here the objective is to improve the performance of pure solvent injection in terms of both increasing the heavy oil recovery and decreasing the asphaltene deposition. Therefore, CO_2 foam/PEF was combined with the solvent injection in two different methods 1) post-solvent CO_2 Foam/PEF flooding and 2) solvent based foam injection. So, this chapter contains two different parts which analyze and visualize these methods.

Part 1: Pore-Scale Mechanisms of Post-Solvent CO_2 Foam/Polymer Enhanced Foam Flooding

4.1 Introduction

Because of the presence of a fracture network and oil-wet matrix (Chilingar and Yen 1983; Roehl and Choquette 1985), oil recovery from naturally fractured carbonate reservoirs has always been a challenging task. Fracture networks diminish the effectiveness of waterflooding or chemical flooding, and the oil-wet matrix limits the capillary-imbibition process, which is an important recovery mechanism in the fractured reservoirs. The heterogeneity of carbonate reservoirs is caused by the large permeability difference between the matrix and fractures. The wettability of

A version of this chapter has been published:
[3] Telmadarreie and Trivedi, 2016. SPEJ, http://dx.doi.org/10.2118/174510-PA
[4] Telmadarreie and Trivedi, 2016. SPE paper 179658 presented at the SPE Improved Oil Recovery Conference, Tulsa, Oklahoma.

carbonate reservoirs often ranges from intermediate-wet to oil-wet (OW) (Treiber et al. 1972; Chilingar and Yen 1983). They exhibit very limited recovery during primary and secondary production because most of the injected fluids preferentially go through fracture openings, leaving behind a significant amount of oil in the matrix. Therefore, designing a process to recover the matrix oil at an economic rate often turns out to be a real challenge for such reservoirs (Bourbiaux 2009).

Solvent, gas (especially CO_2), water, WAG, and chemical injections have been considered as the main nonthermal methods to recover oil from highly fractured oil-wet carbonate reservoirs (Manrique et al. 2006; Gupta and Mohanty 2008). Chemical enhanced-oil-recovery (EOR) research in carbonate reservoirs has been focused on the use of surfactants to change the wettability and enhance water imbibition into the matrix, thus driving oil out of the matrix. Different types of surfactants, including cationic (Austad and Milter 1997; Standnes and Austad 2000a, b), anionic (Hirasaki and Zhang 2004; Seethepalli et al. 2004; Adibhatla and Mohanty 2006; Gupta and Mohanty 2007, 2008), and nonionic (Xie et al. 2005; Gupta and Mohanty 2007) have been used to alter the wettability of originally oil-wet carbonate rocks. Austad and Milter (1997) and Standnes and Austad (2000a, b) have shown that cationic surfactants can recover oil by spontaneous countercurrent imbibition caused by wettability alteration. The mechanism of wettability alteration is supposed to take place by an ion-pair formation by the cationic surfactant and the negatively charged carboxylates in oil. Cationic surfactants, although effective in altering wettability for oil-wet rocks, are too expensive to be implemented in a field treatment. In addition, Stoll et al. (2008) reported spontaneous imbibition of surfactants, because wettability-modification agents could not provide an economically interesting opportunity unless external forces enable forced imbibition of this surfactant.

Gupta and Mohanty (2008) worked with several anionic surfactants for carbonate-wettability alteration. Most anionic surfactants are not able to desorb anionic organic carboxylates from the crude oil in an irreversible way. However, ethoxylated sulfonate surfactants with high ethylene oxide (EO) numbers can displace oil spontaneously in a slow process. Standnes and Austad (2000b) showed that other anionic surfactants (without the EO group) did not imbibe any significant amount of water into the OW chalk, confirming that the EO groups play an important role regarding the imbibition mechanism. Therefore, the main role of anionic surfactants is to reduce the interfacial tension (IFT) between oil and brine. Once the IFT is reduced, the gravity drive can be enhanced and oil droplets can move upward from the matrix (Standnes and Austad 2000b). However, gravity drainage is not thought to be a significant recovery mechanism in naturally fractured reservoirs, except possibly in thick formations with high matrix permeability and low matrix capillary pressure (Reis 1990). Therefore, forced imbibition is required for better results. Moreover, Zhang et al. (2009) have shown that anionic surfactants enhanced natural imbibition mainly by emulsification and solubilization. Their results showed that the formation of microemulsion strongly promotes water imbibition. The rate was highest for Winsor Type II microemulsion and lowest for Winsor Type I.

The main nonthermal EOR methods used in Alberta carbonate reservoirs include waterflood (mostly as a secondary recovery process), solvent flood (mostly as the first EOR process), hydrocarbon miscible injection, chase gas (such as in the Pembina field, Nisku formation), CO_2 and acid-gas injection (such as in the Judy Creek field, Beaverhill Lake formation), and chemical injection (such as in the Edgerton field, Woodbend A formation). The Edgerton Woodbend A pool is a heavy-oil-carbonate reservoir that has undergone a chemical EOR process unlike other carbonate reservoirs in Alberta. The polymer flood recovery factor was only 3% (Galas et al.

2012). Because of the fractured nature of carbonate formations, many advantages of these production methods are usually contrasted by their low recovery factor. Alternative processes are therefore needed to increase oil sweep efficiency from carbonate reservoirs. A major attraction of foam is the possibility of diverting flow from high to low permeability layers. It can also provide better control of the injected fluids because stronger foams can spontaneously block the flow channels in high-permeability media (Hirasaki 1989; Zhou and Rossen 1995). In addition, the main problem of the chemical method is the slow rate of the wettability alteration and surfactant imbibition processes. Therefore, forced imbibition should be applied. Foam and PEF could offer this external force by providing a high injection pressure gradient that will force the surfactant solution, and eventually foam bubbles, into the oil-wet matrix, resulting in further improvement of oil recovery in carbonate formations. The objective of this part is to see how CO_2 foam/PEF can improve the conventional heavy oil recovery by solvent injection in fractured carbonate formations.

4.2 Material and Methods

4.2.1 Material

Surfactants are the major chemical constituent in foams. They are classified according to the nature of the charged group present on the surfactant head. Their main function is to lower the surface tension. An anionic surfactant and polymer were selected for CO_2-foam and CO_2-PEF generation in this research. In all tests (bulk and porous media), foam solution was generated with tap water (Ca^{2+}= 34, Mg^{2+}= 10 ppm, and Na^{+}= 35 ppm) without any addition of salt.

Surfactants: Sodium dodecylbenzene-sulfonate was used as an anionic surfactant. Sodium dodecylbenzene sulfonate (Na-DDBS, provided by ACROS) is a colorless salt with useful properties as a surfactant. It is a major component of laundry detergent with the formula

$C_{12}H_{25}C_6H_4SO_3Na$ (Mw=348.5 g/mol, CMC = 0.065 wt%). Cetyltrimethylammonium bromide (CTAB) (Sigma–Aldrich, 99% purity) was also used as a cationic foaming agent ($C_{19}H_{42}BrN$, Mw=364.5 g/mol, CMC = 0.036 wt%). The viscosities of foaming solutions are shown in Table 4.1.

Polymer: Polymers are used to enhance the stability of the foam by increasing the viscosity of the liquid portion of the foam. The polyacrylamide polymer FLOPAAM 3330S (supplied by SNF SAS) in dry powder form was used in the preparation of polymer solutions. FLOPAAM 3330S is anionic and water soluble with a degree of hydrolysis of 25–30% and average molecular weight of 8×10^6. Polyacrylamide polymers are one of the most general polymer types used in the EOR process.

Hydrocarbon: Normal pentane (provided by Fisher Scientific) was applied as a hydrocarbon solvent for heavy oil recovery. For oil saturation, heavy crude oil (dead oil viscosity ~ 30,000 cp at 22 ˚C and dead oil density ~ 933 kg/m^3) (provided by Husky Energy) was used.

Table 4.1: Viscosity values of foaming solution measured at different shear rates (at 22 °C).

Foaming Solution	Concentrations (wt. %)		Viscosity (cp)			
	Surfactant	Polymer	1 *1/s*	10 *1/s*	20 *1/s*	30 *1/s*
CTAB	0.29	NA	2.2	1.8	1.4	1.3
DDBS	0.29	NA	2.8	2	1.6	1.5
DDBS-PEF	0.29	0.15	237	73	55	43

4.2.2 Foam Bulk (Static) Experiments

CO_2 Foam/PEF Generation: For the preparation of the foaming solution, a surfactant and polymer (for CO_2 PEF generation) were mixed in water. The concentrations of the surfactant and polymer were 0.29 wt% and 0.15 wt%, respectively. The concentration range of the surfactants used is greater than their CMC. The surfactant is dispersed in the water or polymer solution (for CO_2 PEF generation) by magnetic stirring (400 rpm for 20 minutes) to prevent the foam generation. Thereafter, foam/PEF was generated by use of a Polytron DT6100 digital homogenizer (provided by Kinematica). The solution (100 cm^3) was put into a glass cylinder (1000 cm^3) and mixed at high speed for 2 minutes. The shearing speed and shearing time were kept constant for uniformity of the foam created throughout the experiments. For foam/PEF analysis in the presence of oil, 5 cc of oil was added to the foaming solution before high-speed mixing.

Static Stability: The glass cylinder was closed with a plastic seal after foam generation. In each experiment, the height of the foam column above the liquid phase as well as the height of the liquid was measured as a function of time. The time required to drain half of the liquid from the foam was measured as a foam half-life value, representing foam stability. Moreover, the initial foam height value was also measured as the foamability of foaming solutions, which is the ability of a solution to generate the foam. The experiments were performed at ambient conditions. The range of uncertainty in the foam height measurements was ± 0.2 cm. In addition, a high-definition camera was used to analyze the foam behavior over time. It should be mentioned that each experiment was repeated at least once to ensure the reproducibility of results.

4.2.3 Micromodel Experiments

Micromodel Setup: A special fractured micromodel was designed to imitate the fractured carbonate reservoirs. The wettability of the micromodel was also altered to OW conditions, which

will be explained later. The micromodel is made of a 2D pore structure etched onto the surface of a glass plate that is otherwise completely flat. A second glass plate is then placed over the first, covering the etched pattern and thus creating an enclosed pore space. This cover plate has an inlet hole and an outlet hole drilled at either end, allowing fluids to be displaced through the network of pores. The micromodel was designed such that it has a high-permeability contrast between the matrix and fracture to imitate the highly fractured carbonate formation. The micromodel is placed in a holder consisting of inlet and outlet ports, which communicate with the micromodel at the drilled holes. The holder is capable of handling high pressure during fluid injection.

For each experiment, heavy crude oil was used to saturate the micromodel. Heavy oil was injected with a liquid syringe pump at low flow rate (0.016 cc/h) and room temperature. High-pressure polyetherethoxyketone tubing, with mechanical and chemical resistance, was used for heavy-oil injection. The solvent was injected through chemical-resistance polytetraflour-ethylene tubing. This tube was also used for foam injection because foam bubbles can be visualized. An image of the heavy-oil-saturated micromodel (1×7 cm with fracture thickness of 1 mm) is shown in Figure 4.1. After oil saturation, the micromodel was flooded with different fluids (water, solvent, CO_2, foam, and PEF). A syringe pump (Isco Model 500D) was used for liquid injection. A gas-mass-flow controller (provided by Hoskin Scientific Limited) was used for the accurate injection of CO_2 gas at a constant volumetric flow rate. The pressure was also measured and recorded by a pressure transducer (Omegadyne Model PX409) connected to a computer. No backpressure was used in this study. An inline foam generator was designed before the micromodel inlet. It consists of porous screens with a mesh size of 80 (0.5 cm in length). Foaming solution and gas were injected through this foam generator at a constant flow rate. A transparent injection line (after the foam generator) allowed us to monitor the quality of foam visually. A high-speed digital camera was

used for imaging the flooding processes, and then the captured images/movies were processed by use of Matlab (2013) to assess the oil recovery.

Waterflooding was performed to verify the wettability alteration procedure and the imbibition process, which will be explained later. Therefore, water was injected at a low flow rate (0.0016 cc/min) to monitor the imbibition process. The detailed information of each experiment is represented in Table 4.2. CO_2 gas, foam, and PEF injections were performed after solvent (pentane) flooding to imitate the tertiary recovery process. The quality of CO_2 foam and CO_2 PEF was kept constant at 92%. Foam quality is defined as the ratio of gas volume to total volume of foam.

Wettability Alteration: To change the wettability of the micromodel, which was originally water-wet (WW), a siliconizing fluid (SurfaSil; the chemical composition is primarily dichloro-octamethyl tetrasiloxane) was used to coat the glass surface (Naderi and Babadagli 2008; Shabani Afrapoli et al. 2009, 2010). SurfaSil works by reacting directly with polar groups (silanols) on the glass surface. The silanol bonds formed by this reagent are able to withstand the autoclaving conditions. Furthermore, the change seems to resist repeated cleaning with methanol and toluene (Shabani Afrapoli et al. 2010). SurfaSil (10 vol%) was mixed with pentane (90 vol%) and then injected into the clean and dry micromodel before oil and/or water saturation. Thereafter, pentane followed by methanol was injected to remove any excess chemical from the pore structure. The micro-model was dried in an oven for at least 1 hour (at 100 C) and then in ambient conditions for 24 hours. To verify this process, the same procedure was performed on a glass surface (same glass material as the micromodel). The spreading of an oil droplet on the OW glass surface immersed in water was compared with that of the untreated WW glass surface. The results are shown in Figure 4.2. According to Figure 4.2, the contact angle of the oil droplet with a glass surface changed from

130 to 36 after altering the wettability of the surface. In addition, waterflooding was performed on both WW and OW micromodels to further verify the wettability alteration of the micromodel, which will be discussed later in this part.

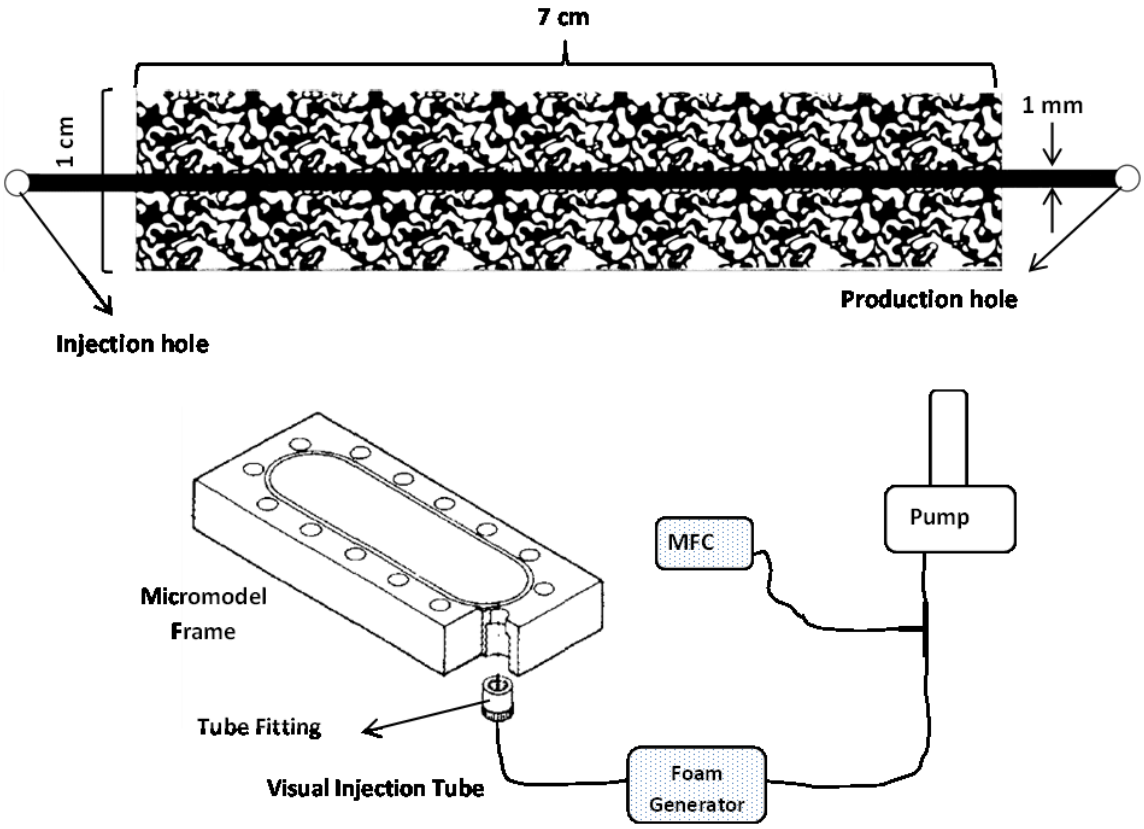

Figure 4.1: Image of the fractured micromodel (1 mm fracture width) and its frame. The black area shows the void space saturated with heavy oil.

Table 4.2: Experimental parameters including injection flow rate. CO_2 foam and PEF were injected after solvent flooding.

EOR Method	TPV*	Wettability	Flow rate (cc/min)		
			Solvent	*CO_2 gas*	*Foam/PEF solution*
Solvent	145	OW	0.08	NA	NA
CO_2	145+122	OW	0.08	0.1	NA
DDBS-Foam	145+128	OW	0.08	0.1	0.008
DDBS-PEF	145+128	OW	0.08	0.1	0.008
CTAB-Foam	145+128	OW	0.08	0.1	0.008

*TPV: Total Pore Volume; 145 is PV of solvent injection which is constant in all tests

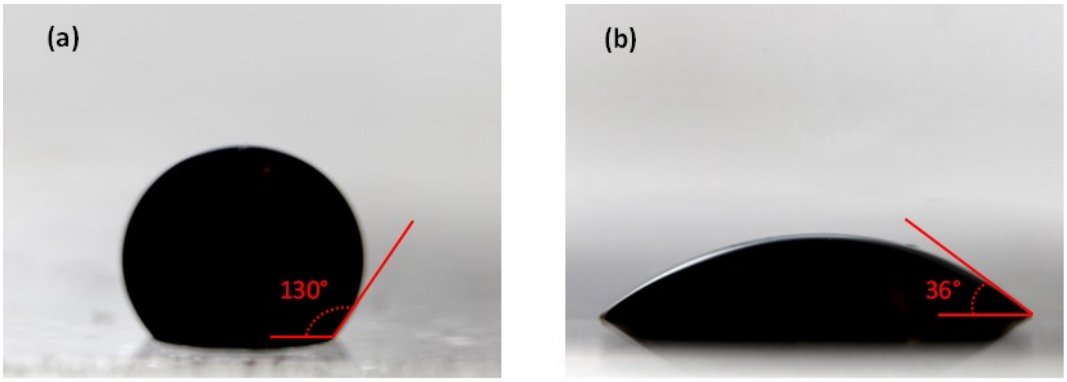

Figure 4.2: Oil droplet on the glass surface immersed in water representing wettability alteration (a) WW glass and (b) OW glass.

4.3 Results and Discussions

4.3.1 Static Analysis of CO_2 Foam and CO_2 PEF in the Presence of Heavy Oil

Analyses of the static stability of CO_2 foam and CO_2 PEF in the presence and absence of heavy oil were performed, and the results are shown in Figure 4.3. Anionic surfactants showed good performance in terms of foamability (Flick 1993; Urban 2003; Rosen and Kunjappu 2012). The static stabilization in anionic surfactants is achieved by electrostatic repulsive forces between the surfactant monolayers. The presence of anionic surfactants at the interface in the foam film will stabilize the film and induce a repulsive force that opposes the film-thinning process. This is called electric-double-layer repulsion (Israelachvili 1991; Schramm and Wassmuth 1994), which depends on the charge density and film thickness.

The major advantage of polymer addition in foaming solutions is viscosity enhancement. Increasing the viscosity of foaming solutions may reduce the liquid drainage rate within the foam lamella. Figure 4.3 shows the foamability and half-life values for CO_2 foam (generated with Na-DDBS and CTAB surfactants) and CO_2 PEF (generated with Na-DDBS surfactant) in the presence and absence of heavy oil. Typically, oils have a detrimental effect on foam stability. Heavy oil, as

seen in Figure 4.3, slightly decreased the foamability and stability of CO_2 foam and CO_2 PEF. However, this effect is less significant in CO_2 PEF, which has a much higher stability than regular foam. Although polymer addition increased the half-life value, it dramatically decreased the foamability of the surfactant. The low foamability of CO_2 PEF can be explained by higher micellar stability (Dhara and Shah 2001). The higher foam stability is also caused by the formation of a dense surfactant/ polymer layer on the solution surface (Petkova et al. 2012). In other words, the addition of polymer results in modifications in the surface and bulk properties of the polymer/surfactant system.

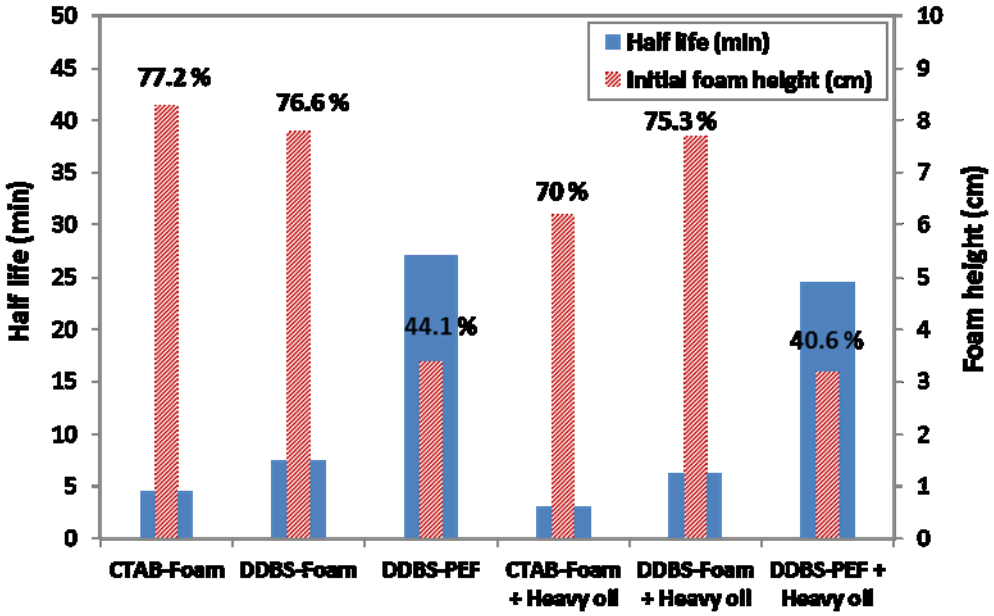

Figure 4.3: Foamability and half-life values of CTAB and DDBS foams and DDBS-PEF in the absence and presence of heavy oil. The numbers represent foam quality (gas percentage).

Polymer addition increased the viscosity of the liquid solution within the foam lamella, reducing the rate of liquid drainage. As a result, more time is required for bubble coalescence and bubble collapse (because of the thinning of the foam lamella). Therefore, PEF lasts much longer than

conventional foam even in the presence of heavy oil. The change in the foam and PEF bubbles' structure (in the presence of heavy oil) over time is shown in Figure 4.4. Liquid drainage and bubble coarsening occurred much slower in PEF compared with that of foam, supporting the fact that polymer addition increases the stability of conventional foam bubbles even in the presence of heavy oil.

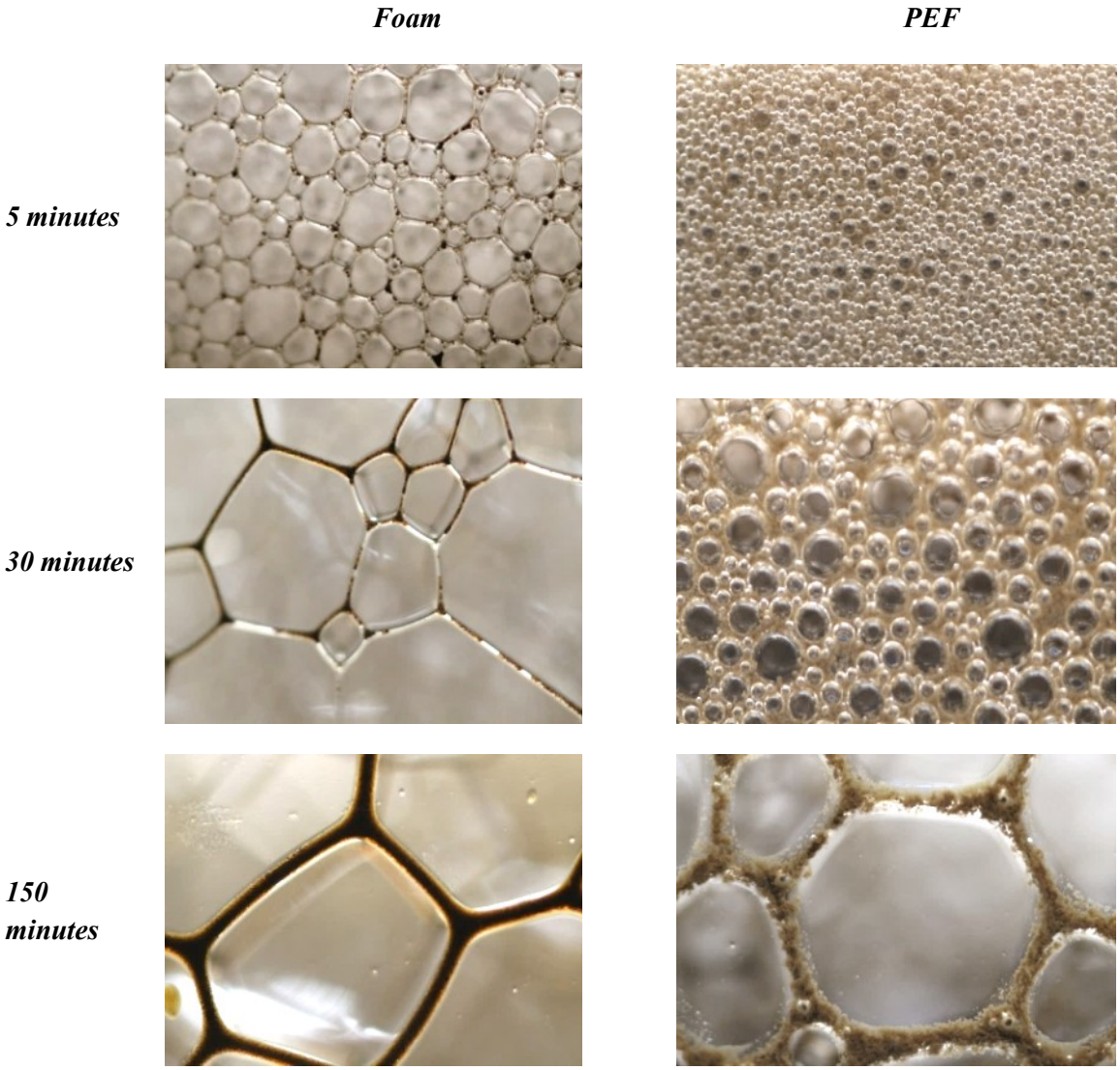

Figure 4.4: Liquid drainage and bubble coarsening phenomena during the static stability of DDBS foam and PEF in the presence of heavy oil (images were taken at 5X magnification).

4.3.2 Effect of Wettability on Heavy Oil Recovery During Waterflooding

According to the procedure explained previously, the micromodel wettability was altered to OW conditions. Before wettability alteration, waterflooding was performed in the WW micromodel for comparison with its performance in the OW micromodel. Unlike the WW micromodel, the OW matrix limited the water imbibition process, which is an important recovery mechanism in fractured reservoirs. At equivalent saturations, the matrix capillary pressure is much higher than the fracture capillary pressure. This difference is the driving force for imbibition, the primary recovery mechanism in fractured carbonates (Mollaei and Maini 2010). Depending on the strength of the capillary forces, oil expulsion from capillary imbibition varies, with low-temperature recoveries ranging from a few percent to as high as 70% (Kyte et al., 1961; Mattax and Kyte, 1962; Kyte, 1970; deSwaan, 1978).

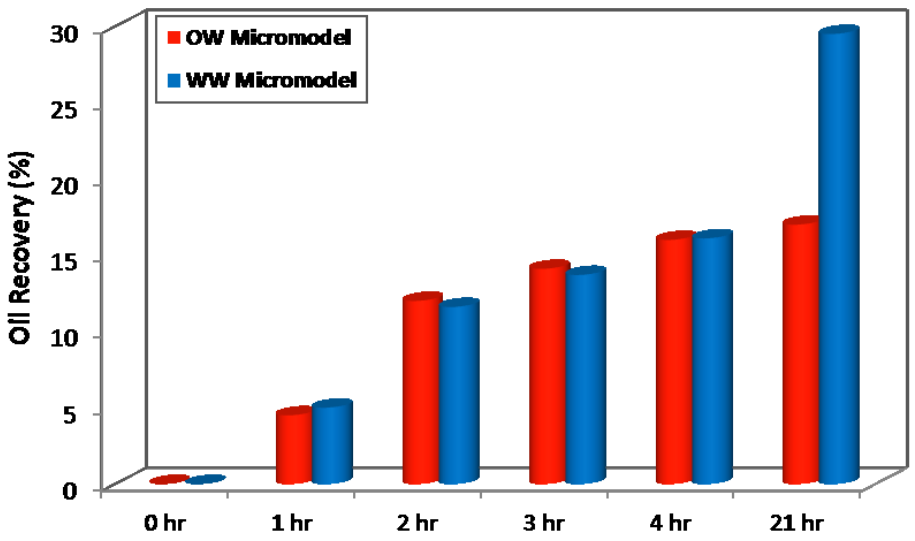

Figure 4.5: Oil recovery during water injection in the WW and OW micromodels over time. The ultimate oil recovery of the WW and OW micromodel after 21 hours was 29.5 % and 17 %, respectively.

Figure 4.6: Micromodel images (1X magnification) during water flooding in the WW and OW micromodels. (a) OW micromodel after 2 hours, (b) WW micromodel after 2 hours, (c) OW micromodel after 21 hours, and (d) WW micromodel after 21 hours.

The heavy oil recovery profile during waterflooding in the WW and OW micromodels is plotted in Figure 4.5. The profile of oil recovery in the WW micromodel was almost similar to that of the OW micromodel during the first 4 hours. The water injection in both models continued overnight to observe further production. Almost no additional production occurred in the OW micromodel. However, in the WW micromodel, the final heavy oil recovery factor (RF) reached approximately 29.5% after 21 hours of water injection. The main phenomenon in charge of the higher oil RF is the capillary imbibition process, as shown in Figures 4.6b and 4.6d. The water swept the fracture by viscous force, but later the capillary effect was dominant. Water in the fracture network

spontaneously imbibed into the matrix block through the small pores, increasing the internal pressure of the matrix block and expelling oil throughout the larger pores. In other words, at the later stage, water mainly imbibes into the matrix, and the flow in the fracture significantly decreased. Water mainly imbibed into those parts with favorable pore structures with higher capillary pressure (i.e., preferred zone for imbibition). On the other hand, during water-flooding in the OW micromodel, water flowed mainly within the fracture and almost no imbibition occurred after 21 hours of water injection (Figures 4.6a and 4.6c).

4.3.3 Hydrocarbon Solvent Flooding

Injecting a light hydrocarbon solvent into the heavy oil reservoir has established an opportunity to recover a higher amount of oil with better quality oil than conventional and thermal recovery processes. Solvent injection into the reservoir was proposed by Butler and Mokrys (1989, 1991). In a fractured carbonate reservoir, the solvent dilutes the oil and then drains down from the matrix, improving heavy oil recovery. However, it is a complex process because of the asphaltene destabilization that occurs and is caused by the changes in temperature, pressure, and solvent type dissolved in oil. Asphaltene flocculation and agglomeration can occur as a result of this destabilization and eventually plugs the pores because of the formation of asphaltene clusters. For solvent injection, light molecular weight hydrocarbon solvents are preferred because of their high diffusion coefficient; however, as the carbon number of *n*-alkane solvents decreases, asphaltene precipitation increases (Fuhr et al. 1991; Buenrostro-Gonzalez et al. 2004; Moreno-Arciniegas and Babadagli 2014).

A solvent (normal pentane in this study) was injected into a heavy oil saturated micromodel before gas, foam, or PEF injections. In each experiment, the solvent was injected at a constant flow rate for a certain period (3 hours) to have the same initial conditions for the tertiary recovery process.

Asphaltene precipitation was inevitable during solvent injection. Figure 4.7 represents the main phenomena happening during solvent injection in the fractured model. Unlike waterflooding, solvent injection is a miscible process, and the main mechanism during solvent oil recovery is diffusion-dispersion rather than viscous force (Da Silva and Belery 1989; Das and Butler 1998; Trivedi and Babadagli 2008). At the early stage of injection, the solvent mixed and diluted the heavy oil, whereas solvent fingering occurred as shown in Figure 4.7a. Thereafter, solvent began to push the oil in the fracture by diffusing into the heavy oil, reducing the viscosity and eventually sweeping the oil in the fracture (Figure 4.7b). At this stage, asphaltene started to precipitate as the oil diluted behind the solvent front. At a later stage of the solvent flooding, asphaltene precipitation increased and flocculation and agglomeration occurred, as seen in Figure 4.7c. The solvent mixed readily with the light fraction of the heavy oil, leaving behind some asphaltenes as an immobile precipitate adhering to the grain, forming parallel ribbons. Several researchers visualized the asphaltene precipitation during solvent injection in heavy oil saturated porous media (Das and Butler 1998; Dehghan et al. 2010; Farzaneh et al. 2010; Pathak et al. 2012). Asphaltene agglomeration and clustering can block the pore throat and result in severe formation damage. Furthermore, it can reduce the efficiency of solvent to diffuse into the matrix and dilute the matrix oil. Further injection of the solvent resulted in more asphaltene precipitation and severe formation damage, as shown in Figure 4.8. The solvent was injected for a longer time (5 hours) to observe the sweep efficiency as well as an asphaltene precipitation. Although further solvent injection increased the ultimate oil recovery value, it drastically damaged the formation and reduced the permeability. At a later stage of solvent flooding, the agglomeration and clustering block the fracture and significantly reduce the injectivity (Figure 4.8).

In this study, asphaltene mainly precipitated at the matrix/fracture interface where the solvent diffused into the matrix. Farzaneh et al. (2010) also showed that most of the asphaltene was precipitated on the fracture's walls. This could be because of the sharp change in the solvent concentration gradient. Pathak et al. (2012) showed that asphaltene precipitation depends on the concentration difference of the solvent on the two sides of the interface. The higher the concentration gradient, the higher the asphaltene precipitation will be. At the early stage of solvent flooding, the solvent gradually diffused into the matrix oil and diluted the oil. Thereafter, oil started to move toward the fracture. When the oil reached the matrix/fracture interface, sharp changes in the concentration of the solvent resulted in severe asphaltene precipitation because the solvent concentration in the fracture is much higher than that of the matrix. In addition, because of the higher rate of mixing during continuous solvent injection, more asphaltene would be precipitated in the flow area (i.e., the fracture). These precipitated asphaltenes initially caused the solvent to be spread better in the media, but after some time the solvent propagation would be prevented by an asphaltene plugging effect in the flow direction, as seen in Figure 4.8. Dehghan et al. (2010) showed that, generally, the asphaltene precipitation problem in the continuous solvent injection process can be partially solved using water-alternating-solvent injection.

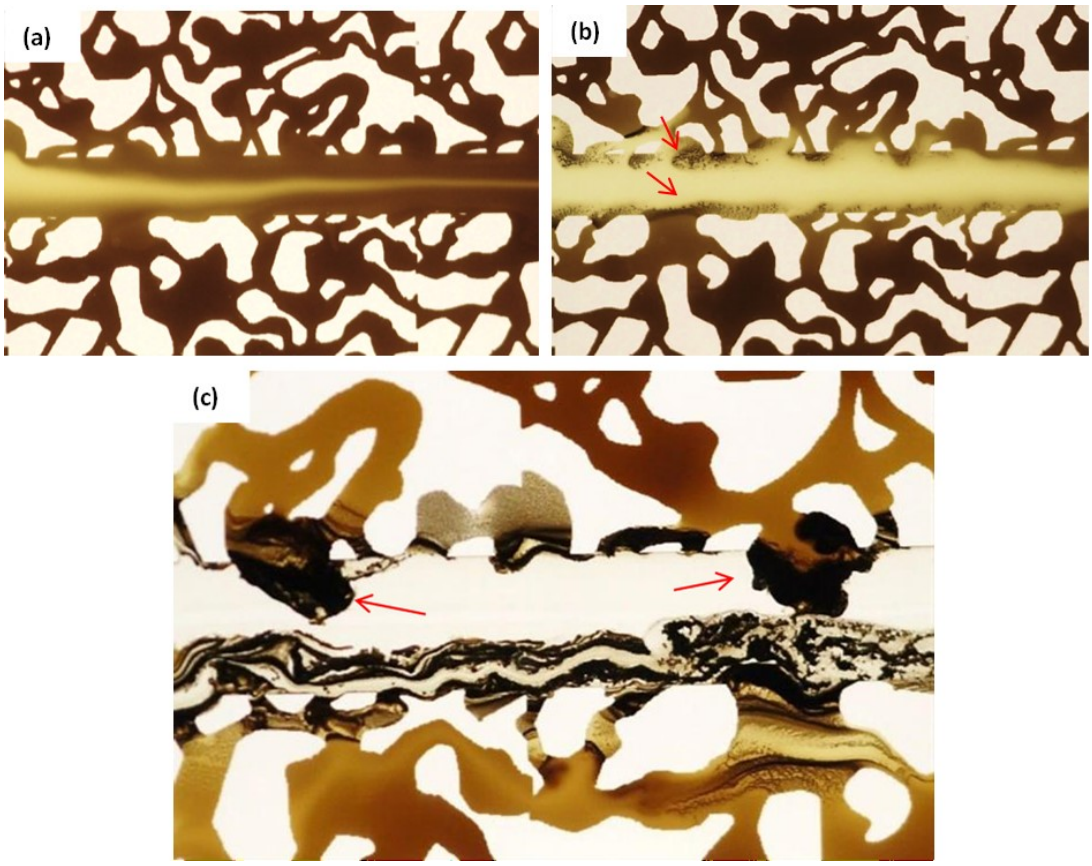

Figure 4.7: Solvent injection in the heavy oil saturated micromodel. (a) Initial stage (2X magnification), (b) during sweeping of the fracture (2X magnification), arrows show the early stage of asphaltene precipitation, and (c) Asphaltene precipitation, agglomeration, and clustering at the later stage (4X magnification).

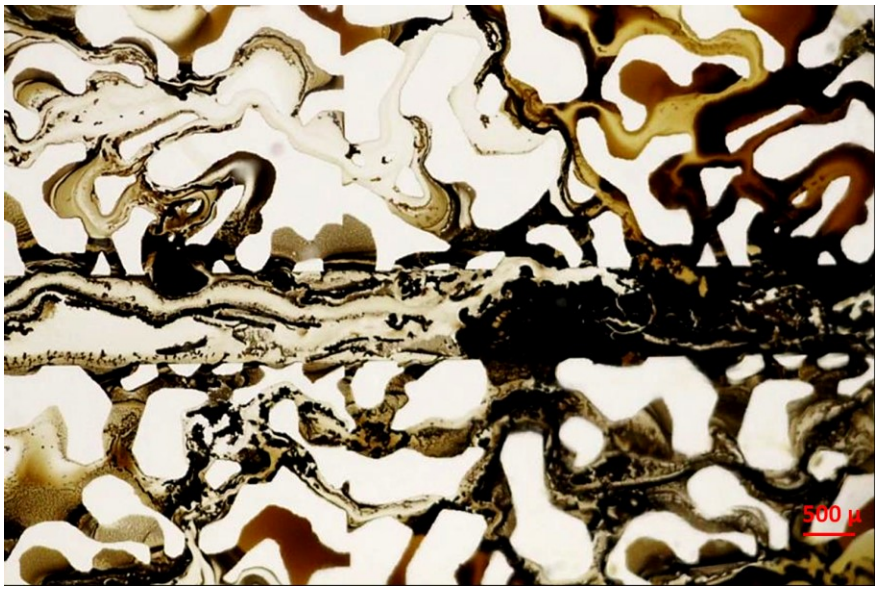

Figure 4.8: Severe formation damage due to asphaltene precipitation after 5 hours of solvent injection.

4.3.4 Performance of CO_2 Gas, Foam, and PEF Flooding After Solvent Injection

The diffusion of solvent into oil is a critical issue: the heavier the oil, the slower the diffusion and the longer the process. The solvent should be given enough time to effectively dissolve into the heavy oil, and this time can be reduced by high pressures, which usually does not exist in shallow heavy oil deposits. Hydrocarbon solvents are more expensive than the oil itself because they are the products of oil through costly processes. Hence, they need to be reclaimed and reused. Therefore, an alternative method should be considered for improving heavy oil recovery in carbonate reservoirs. In a fractured reservoir, oil recovery depends on matrix/fracture interaction, and this is achieved primarily by diffusive mass transfer. CO_2 foam and PEF bubbles can improve further diffusion of fluid into the matrix, despite the high heterogeneity of carbonate reservoirs. Here, the performance of CO_2 foam and PEF was compared with that of CO_2 gas after solvent injection in the fractured micromodel.

As mentioned previously, the solvent swept the fracture similar to the waterflood process. In addition, the solvent could successfully diffuse into the matrix oil and dilute it. Therefore, there are always some zones with diluted oil in the matrix after solvent injection. These are favorable zones for CO_2 gas diffusion as oil viscosity is reduced. Figure 4.9 demonstrates this process. The circle in Figure 4.9a shows that the zones in the matrix with diluted oil were swept by CO_2 gas later, as shown in Figure 4.9b. However, CO_2 gas was not able to sweep all the oil in the matrix (even all the diluted oil zones).

Foam within the porous medium does not behave as a homogeneous fluid, but as multiple films in the porous medium. Therefore, some areas may be completely blocked and motionless. Then, the inlet pressure increases until a coalescence of a number of films restart the flow (Robin et al. 2012). CO_2 foam injection significantly improved the performance of gas injection after solvent flooding.

Foam bubbles reduced gas mobility, resulting in better sweep efficiency. However, improving sweep efficiency in such a fractured formation is not a simple process. Several mechanisms are involved in improving the heavy oil sweep efficiency by foam. The heavy oil sweeping process can be divided into two main stages on the basis of dominant mechanisms. It should be noted that in both stages all mechanisms occurred, but only some of them are dominant, representing characteristics of that stage. These mechanisms include blocking of the fracture by a network of bubbles; diversion of injected fluid into the matrix by increasing displacement pressure; emulsification of the matrix oil; and oil production by ablation. The first two mechanisms are dominant during the early stage of foam flooding, whereas the others are characteristics of the second stage.

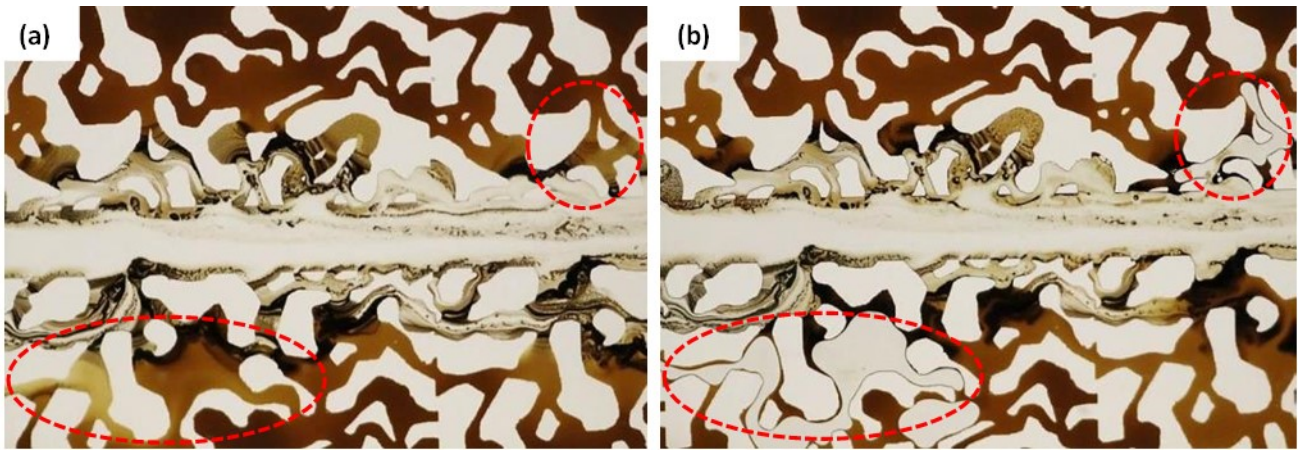

Figure 4.9: CO_2 gas after solvent injection (a) at the end of the solvent flood and (b) during CO_2 gas injection. The highlighted area represents the diluted matrix oil swept by CO_2 injection.

During solvent injection, pressure started to build up; however, after sweeping the fracture, the pressure dropped significantly. The swept fracture created an easy flow path, but the CO_2 foam and CO_2 PEF (unlike gas injection) could build up the pressure, forcing the injected fluid into the matrix. Bubbles blocked the fracture and built up the pressure, which pushed the fluid into the matrix. Sometimes, foam collapsed and resulted in a sudden pressure drop. At that time, a

favorable Δp between the matrix and fracture occurred and caused the movement of low-IFT oil (surfactant, which is already in the matrix, reduced the IFT) from the matrix. An example of pressure fluctuation during foam flooding is shown in Figure 4.10. The blocking of the fracture (highly permeable zone) with CO_2 foam/PEF bubbles and the diversion of injected fluid into the matrix are the main early mechanisms occurring during foam injection in such fractured porous media. When the strong foam is generated within the fracture, it pushes fluid into the matrix even in areas where the solvent could not diffuse. Thereafter, the diverted fluid will push the heavy oil with the help of IFT reduction and emulsification. This early mechanism of foam-sweep efficiency can be seen in Figure 4.11.

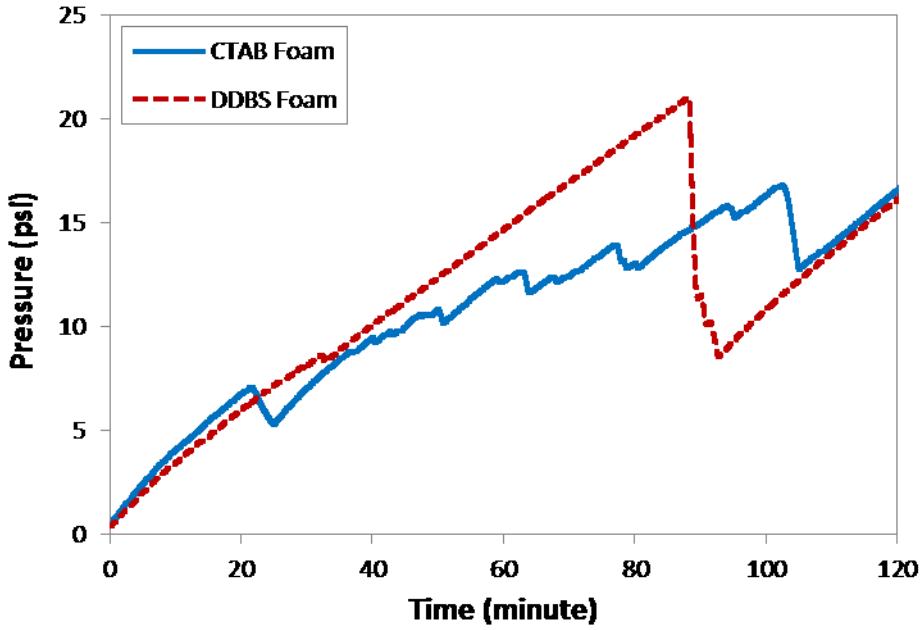

Figure 4.10: Pressure profile of foam generated with CTAB and DDBS surfactants during heavy oil recovery in micromodel after solvent injection; fluctuation in pressure profile representing local instability (collapse) of foam bubbles.

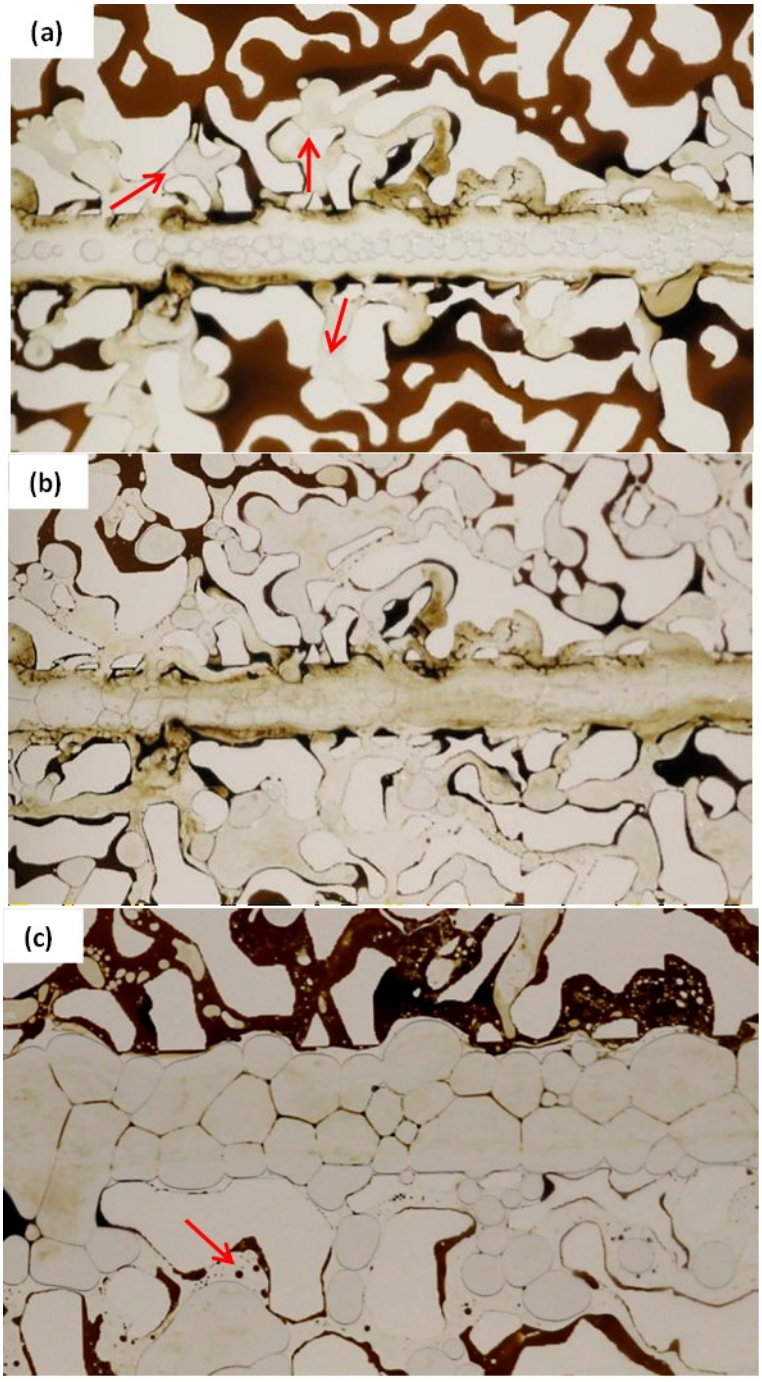

Figure 4.11: Images of the micromodel during CO_2 foam injection; images in (a) and (b) were taken after 10 minutes and 1 hour of foam flooding, respectively (same frame, 2X magnification), representing fluid diversion into the matrix by blocking the fracture path (arrows representing direction of fluid diversion), and (c) a later stage of foam flooding (3.5X magnification), demonstrating the emulsification (arrow) and fluid diversion phenomena. A thin layer of oil remained on the glass surface, maintaining OW conditions.

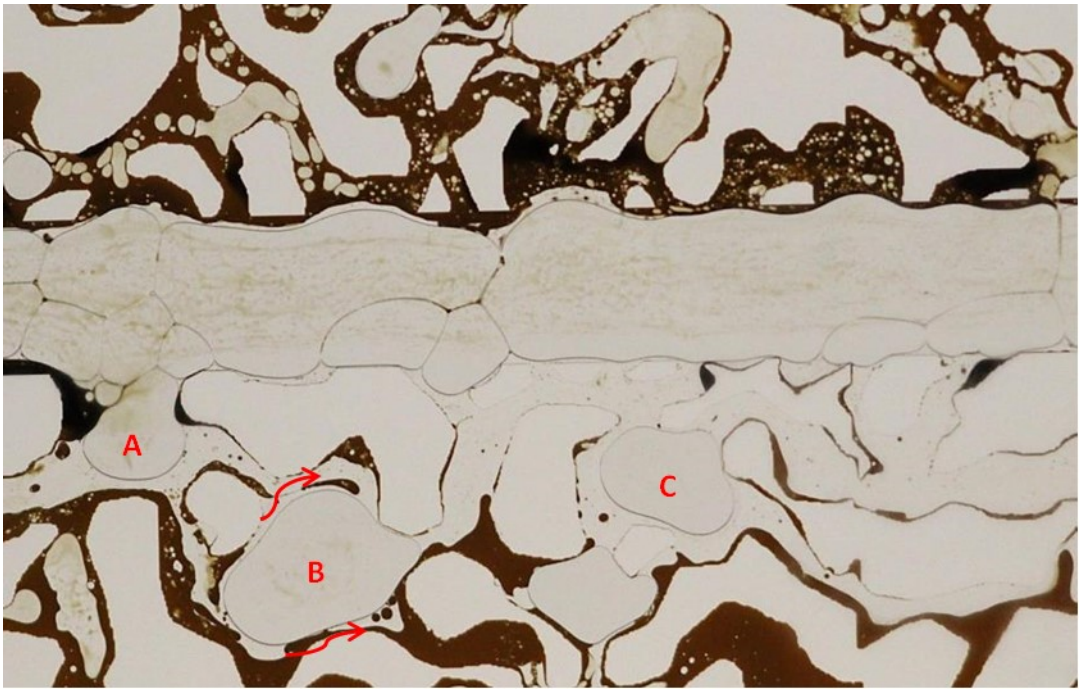

Figure 4.12: Micromodel image (3.5X magnification) representing the ablation/emulsification process at the late stage of foam flooding. Bubble "A" is trying to invade the matrix opening area, while bubble "B" is already in the matrix pore body, helping the ablation process. The arrow represents the flow direction of detached oil from the glass surface. Bubble "C" represents the late ablation process where most of the oil moved from the glass surface around the bubble, leaving a very thin layer of oil on the grain surface.

These mechanisms swept significant amounts of oil from the matrix, which was more efficient in the case of PEF flooding (Figures 4.12 through 4.14). The diverted fluid was more viscous than a conventional foaming solution (in the case of PEF) and significantly improved matrix' oil production. However, at the later stage, other mechanisms are more dominant in the sweeping of the remaining matrix oil. Although the nature of the porous media remained OW during the flooding (as seen in Figures 4.11b and 4.11c), CO_2 foam and CO_2 PEF could significantly improve the sweep efficiency of the oils around the OW grain surface. At a later stage, most of the oil in the matrix was around the grain surface. At this time, unlike the early stage, smaller bubbles began to move into the matrix blocks. Because most of the oil was swept from the matrix, it was now easier for bubbles to invade the matrix. Bubbles entered the matrix and pushed the oil, which could

not be produced by the foaming solution, by further increasing the displacement pressure. This process is shown in Figure 4.11c.

Foam formation is related to the geometry of the porous medium that determines the size of the bubbles. In the case of using a foam generator before injection, once injected, the adaptation to the new porous medium will be automatic, primarily on the basis of the geometric characteristics of the porous medium (Robin et al. 2012). When they reach a larger opening area, bubbles release their energy (on the basis of the Laplace formula) and block those areas. As a result, the liquid is pushed to move in a narrow zone between the bubble and grain surface, where most of the oil is located. Thereafter, the foaming solutions sweep the oil by emulsification and ablation in the area around the grain. The ablation process in the matrix blocks, which can also be performed by CO_2 foam/PEF bubbles, is shown in Figure 4.12.

As explained by Schramm and Novosad (1990), the foam lamella, when contacted with oil attached to the rock surface, can move the oil from the surface and carry it within the foam lamella (also seen in this study). According to the location of oil in the foam lamella and the stability of the lamella (Figures 4.11c and 4.13), the Na-DDBS foam can be classified as a moderate stability foam [Type B, as explained by Schramm and Novosad (1990)]. This type of foam has moderate stability in the presence of oil, and upon contact, the oil spontaneously emulsified into droplets in the plateau borders. However, the collapse of foam caused by oil effect is inevitable and sometimes foam lamella collapsed because of the oil effect, representing Type C of foam/oil interaction (Schramm and Novosad 1990). The oil imbibes into the foam lamella, and it would carry oil droplets some distance before rupturing. It is noteworthy that although values of entering (E) and spreading (S) coefficients may give insight as to the possibility of oil destroying foam, they do not determine the rate of foam destabilization (Manlowe and Radke 1990; Hadjiiski et al. 2003).

Spreading and entering coefficients values are presented in Table 4.3. Oil is predicted to spread as a lens over foam when the spreading coefficient *S* is positive (Ross and Suzin 1985). Similarly, an oil droplet is predicted to be drawn up into and bridge the lamellar region between two adjacent bubbles, breaching the aqueous/gas interface, when the entering coefficient, *E*, is positive. If the oil breaches the interface, this usually causes the interfacial film to lose its foam-stabilizing capability and thin to the rupture point, although "entering" does not always destabilize foam. The *S* and *E* coefficients can be calculated by surface tension and interfacial measurement by

$$S = \sigma_{wg} - \sigma_{wo} - \sigma_{og}$$

$$E = \sigma_{wg} + \sigma_{wo} - \sigma_{og}$$

where σ_{wg}, σ_{og}, and σ_{wo} are surface tension of foaming solution, the surface tension of oil, and IFT of water/oil interface, respectively.

Both surfactants recorded a positive entry coefficient, indicating that oil entry is feasible in all systems. CTAB recorded higher spreading and entering coefficients than Na-DDBS, which is consistent with its low stability observed in Figure 4.3. Although both surfactants had positive *S* and *E* coefficients, they showed decent stability in the presence of oil during oil recovery. This analysis shows that the overall foam stability is not dictated solely by these thermodynamic coefficients and it is also related to the interfacial and bulk properties of the surfactant and the strength of the entry barrier at the gas/liquid interface (Hadjiiski et al. 2003).

Here the stability of foam in the presence of crude oil plays a key role in enhancing heavy oil recovery. The presence of pentane in the fracture (after solvent injection) might affect the injected foam stability in the fracture. However, most of the solvent will be removed from the fracture at an early stage of foam flooding, and foam/PEF stability is mainly affected by the presence of heavy oil.

Table 4.3: Spreading and entering coefficients of oil for studied surfactant solutions based on surface tension and interfacial tension measurements.

Foaming solution	Surface tension (mN/m)	Spreading Coefficient (S)	Entering Coefficient (E)
DDBS	30	2.35	3.05
CTAB	36.5	8.92	9.48

The mechanisms of heavy oil sweeping by CO_2 foam and CO_2 PEF are very similar. However, besides a higher viscosity of the liquid solution, CO_2 PEF bubbles have higher stability in the presence of oil compared with conventional foam. Figure 4.13 shows the collapse of the foam bubbles in the presence of oil, showing that PEF bubbles were more stable than conventional foam bubbles in the presence of heavy oil both in static and dynamic conditions. This is in accordance with the results of Chapter 5 on CO_2 foam/PEF flooding in heavy oil saturated sand-pack, where CO_2 PEF showed higher dynamic stability in the presence of heavy oil. It should be mentioned that the behavior of foam in bulk and porous media is different and all the static tests results are not directly representative of foam in core or reservoir scale. However, stable foam bubbles in bulk test (in the presence of oil) have a higher chance to be stable in porous media. The stability of bubbles is important because they are the main reason for improving sweep efficiency. They block the fracture (highly permeable) path to access the untouched parts of the reservoir. They also directly help oil production by carrying oil within their lamella (as shown in Figures 4.11c and 4.13). Therefore, besides the higher viscosity of a PEF solution, the higher stability of PEF bubbles is responsible for further improving heavy oil sweep efficiency compared with conventional foam. Considering the enhanced characteristics of CO_2 PEF over foam, it could recover the oil layers around the grain surface that could not be recovered during conventional foam flooding, as seen in Figure 4.14. In addition, the cationic CTAB surfactant was also used for CO_2 foam injection. As mentioned earlier, cationic surfactants are able to change the wettability of OW media.

However, the rate of this process is rather slow. The results of foam flooding with an anionic surfactant showed that foam bubbles can force the surfactant solution into the matrix. Therefore, foam generated with a cationic surfactant will help to produce matrix oil faster and more efficiently because of wettability alteration. CTAB foam could remove the oil layer around the matrix grain much better than that of anionic Na-DDBS foam (Figure 4.14). However, the sweep efficiency is still lower than PEF, as seen in Figures 4.14 and 4.15. CO_2 PEF had a higher fluid viscosity and pushed the injected fluid into the matrix more efficiently compared with conventional foams, resulting in higher sweep efficiency. It is worth mentioning that in the case of carbonate rock with extremely low matrix permeability, foam/PEF bubbles would still be able to enter the matrix with relatively higher pressure drop. In a work performed by Conn et al. (2014) in a 2D model of heterogeneous porous media, they also showed that foam effectively displaced trapped oil in the low-permeability region by bubble resistances in the fracture and high-permeability zones, increasing local pressure gradients into the matrix sufficiently to overcome the low permeability capillary entry pressure.

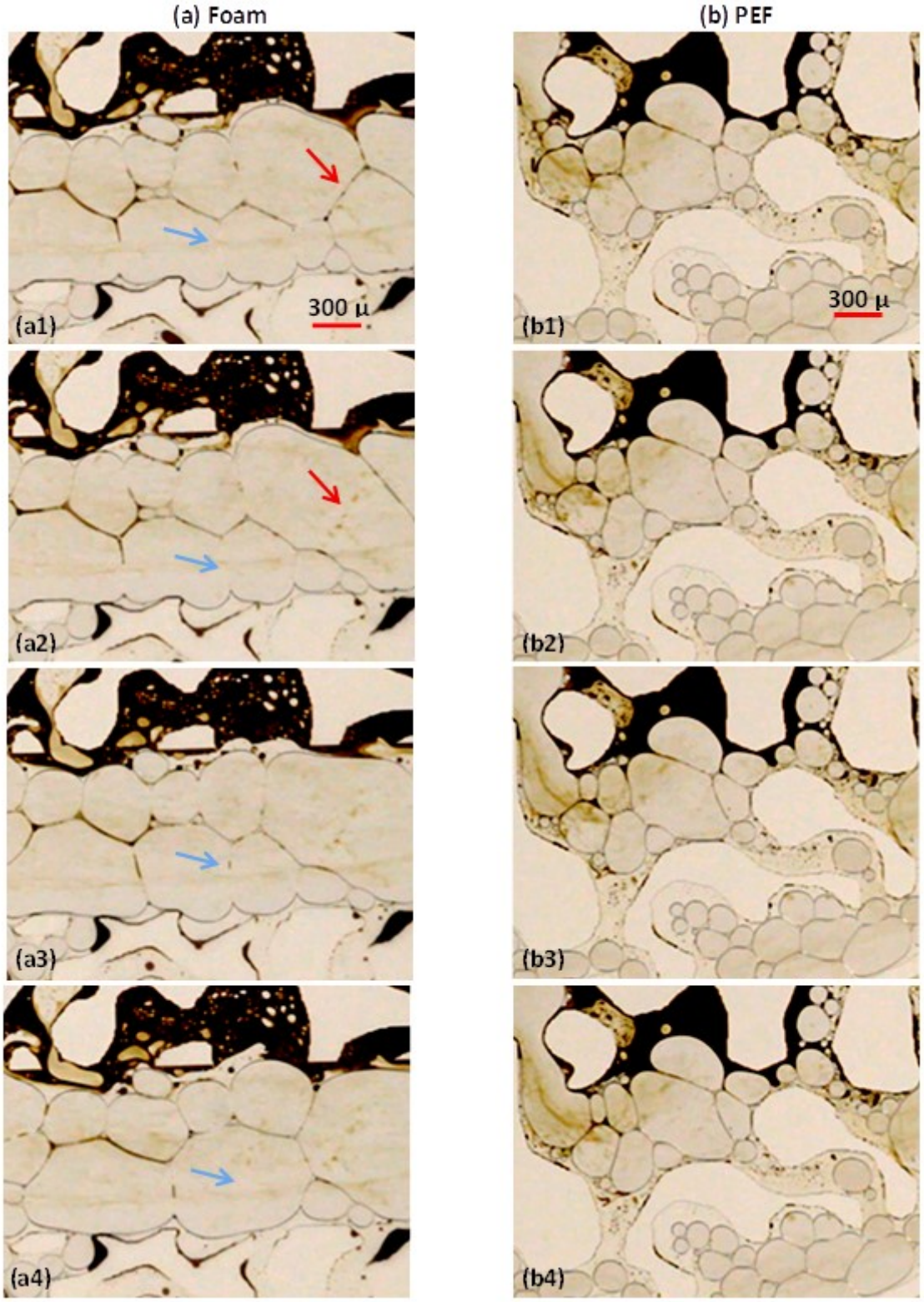

Figure 4.13: Stability of foam and PEF lamella in the dynamic condition in the presence of heavy oil. Foam lamella collapsed more frequent than that of PEF. The arrow shows the collapse of the foam lamella, leaving oil droplets behind. Images (a1) to (a4) and (b1) to (b4) were captured with one second interval at the late stage of foam and PEF flooding, respectively.

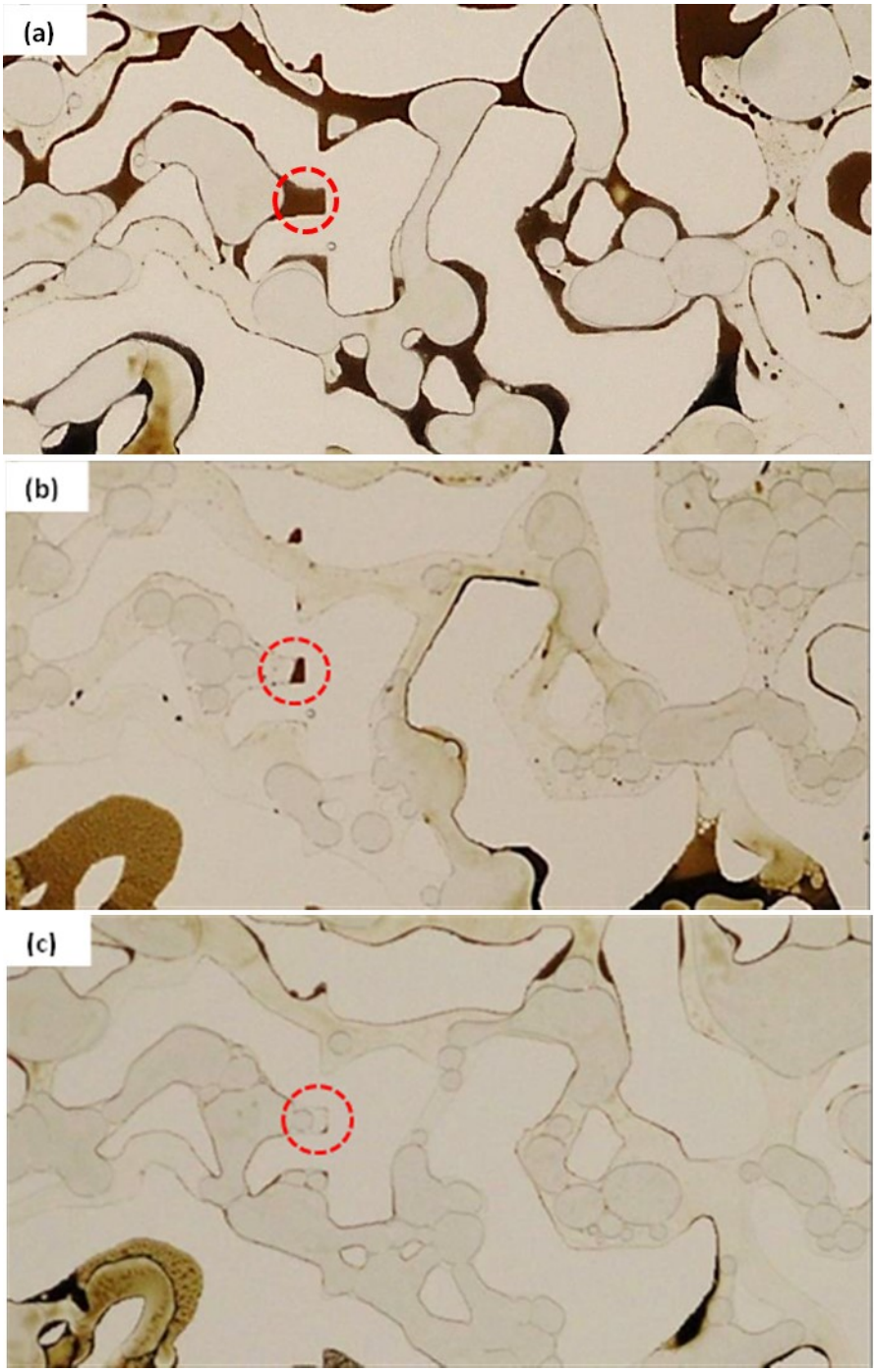

Figure 4.14: Images (4X magnification) taken after two hours of (a) DDBS foam, (b) CTAB foam, and (c) DDBS PEF flooding comparing the efficiency of various foaming solutions for the removal of the oil layer around the grain. PEF swept the matrix oil more efficiently and even removed the oil in a dead-end pore (circled area).

The ultimate oil RF results are shown in Figure 4.15. The ultimate recovery values correspond to 2 hours of injection after 3 hours of solvent flooding. CO_2 flooding could only increase oil recovery by 5%, whereas this value was 49% for the Na-DDBS foam flooding. PEF increased the matrix oil recovery even higher and produced 70% of the residual oil. The CTAB foam improved the ultimate oil recovery (63%) compared with anionic foam; however, it is still lower than PEF (70%). It should be mentioned that the ratio of matrix pore volume to fracture pore volume is higher in the studied micromodel compared with that of real fractured reservoirs. Therefore, the recovery numbers are not directly applicable to the reservoirs. However, the observations are critical to understanding the foam/PEF mechanistic performance and interaction with heavy oil in a fractured carbonate reservoir. Figure 4.16 presents the micromodel images comparing heavy-oil-sweep efficiency during CO_2, foam, and PEF injections after solvent flooding. As explained previously, the higher stability of CO_2 PEF along with the higher liquid viscosity resulted in higher sweep efficiency than foam and CO_2 flooding. CO_2 PEF recovered most of the oil from the fractured micromodel except those parts with asphaltene precipitation. Liquid viscosity and improving displacement pressure are the main reasons for the higher recovery from PEF than from foam. The foam performance also showed outstanding improvement over gas injection. The higher efficiency of the CTAB foaming agent (compared with Na-DDBS foam) in removing the oil layers around the matrix grain can be also seen in Figure 4.14c. The presence of foam bubbles, which increases gas apparent viscosity, is the main reason for the improvement in heavy oil sweep efficiency in heterogeneous porous media.

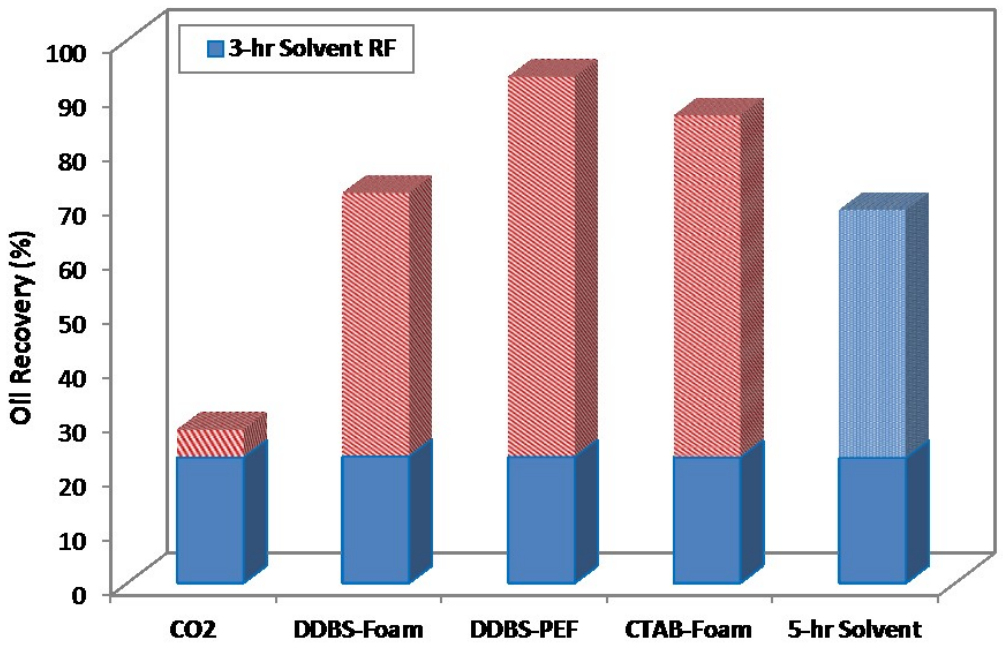

Figure 4.15: Tertiary CO_2 foam and PEF recovery factors (RF) after 3 hours of solvent injection.

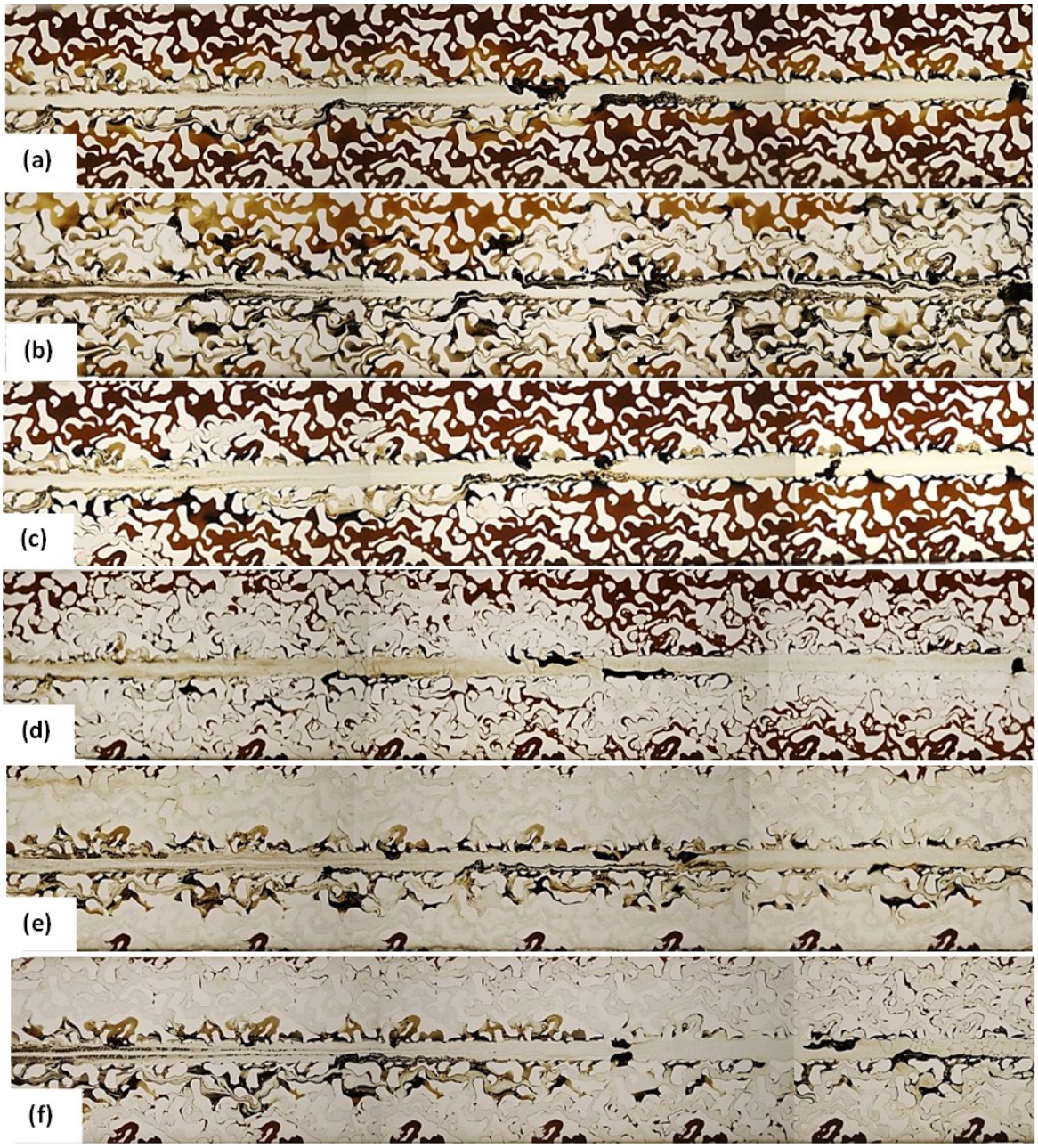

Figure 4.16: Performance of CO_2 gas, foam, and PEF heavy oil sweep efficiency after solvent flooding. Images correspond to the end of (a) 3-hour solvent flooding, (b) 5-hour solvent flooding (c) CO_2 flooding, (d) DDBS foam flooding, (e) DDBS PEF flooding, and (f) CTAB foam flooding after 3 hours of solvent injection.

Part 2: Pore-Scale Mechanisms of Foam Generated with the Hydrocarbon Solvent: Solvent Based Foam (SBF)

4.4 Introduction

In heavy oil reservoirs, due to the high viscosity of the oil, the application of any EOR process including foam EOR is challenging. Moreover, oil-wet nature of carbonate reservoirs makes it difficult for aqueous based foam to efficiently remove the heavy oil. On the other hand, hydrocarbon solvents have been used to decrease heavy oil viscosity and increasing its recovery by diffusion and mixing mechanisms (Butler and Mokrys, 1991; Mokrys and Butler, 1993). It could be expected that, applying solvent based foam (SBF) can significantly improve the performance of oil recovery in those reservoirs with an oil-wet matrix and viscous oil. However, compared to the aqueous foams, it is difficult to generate stable foam from liquid hydrocarbon solvent, because, unlike in water, most of the surfactants are less surface-active in non-polar oils and there is a little or no Gibbs-Marangoni foam stabilization mechanism in nonpolar organic solvents (Shrestha et al., 2006).

Several studies had been done to analyze the potential of foam for oil recovery (Schramm and Novosad, 1990; Rossen, 1996; Farajzadeh et al., 2010; Andrianov et al., 2012; Simjoo et al., 2013; Namdar Zanganeh and Rossen, 2013; Telmadarreie and Trivedi, 2015, 2016; Ferno et al., 2016), mainly dealing with the static and dynamic performance of foam for conventional oil recovery. However, due to the high viscosity of the oil, the effectiveness of foam for heavy oil recovery will significantly reduce (Telmadarreie and Trivedi, 2015, 2016). On the other hand, hydrocarbon solvents have been used for oil recovery for high viscosity oil (Butler and Mokrys, 1991; Mokrys and Butler, 1993; Das and Butler, 1998; Pathak et al., 2010; Moreno-Arciniegas and Babadagli, 2014). The main challenge during the solvent flooding is the slow rate of diffusion and formation

damage mainly due to the asphaltene precipitation. In this chapter, SBF was used for heavy oil recovery to overcome the disadvantages of solvent injection in a fractured heterogeneous porous media. By applying solvent based foam, the solvent can diffuse into the heavy oil and reduce the viscosity while the presence of foam bubbles can help to increase the sweep efficiency by diverting the solvent toward the untouched parts of the reservoir.

Part 1 of this chapter showed the potential of aqueous based foam for heavy oil recovery in carbonate reservoirs after solvent injection. Applying foam after solvent injection could decrease the formation damage while increasing heavy oil sweep efficiency compared to that of solvent injection. The main objective of this part is evaluating the performance of SBF injection for heavy oil recovery from a fractured porous media using visualization and understand the governing mechanisms. It is important to note cost analysis and screening study for selection of surfactant types and concentrations are not the focus of the study.

4.5 Material and Methods

Materials: Two different surfactants were applied for foam generation in this study (Dow Corning 1250 and FluorN™ 1740G). The hydrocarbon solvent for generating SBF was Dodecane. Heavy crude oil with the viscosity of about 30,000 cp (at 22 °C) was used in dynamic experiments.

Static Experiments: to prepare the foaming solution, surfactant was mixed in Dodecane by magnetic stirring (400 rpm for 20 minutes) to prevent the foam generation. The foam was generated with shaking in a glass container. The container was shaken consistently in 30 seconds for each test to have comparable results. Each test was repeated to ensure the reproducibility of the results. The initial foam height value was measured as the foamability of foaming solutions, which is the ability of a solution to generate the foam. The objective of this section was to observe

the relative performance of each foaming solution (at different concentrations) for generating foam.

Surface Tension Measurement: The surface tension of the surfactant solutions was measured by the Du Noüy tensiometer (provided by KRÜSS) using a platinum-iridium ring. The ring method directly measures the maximum pull on the interface to find surface tension value. Surface tension value was taken when a stable reading was obtained, as indicated by at least three consecutive measurements having nearly the same value. After each measurement, the ring was carefully rinsed with deionized water and then a solvent to remove impurities. Thereafter the ring was cleaned with flame.

Dynamic Experiments: Figure 4.17 represents the set up used for pore-scale dynamic experiments. Foaming solution and gas (CO_2) were injected through this foam generator at a constant flow rate. Foam quality was kept content at about 85%. For each experiment, heavy crude oil was used to saturate the micromodel after water saturation. After oil saturation (aged for 24 hours), the micromodel was flooded with water for about 200 minutes. Thereafter, the pre-generated CO_2 foam was injected into the micromodel for almost 3 hours. The main objective of the micromodel study was to visualize the pore scale behavior; therefore, the performance of injected fluid was compare based on images captured at different time intervals rather than injected volume. Extra-heavy oil with a viscosity of about 30,000 cp has been used in all experiments. Chemical resistance tubing was used for injecting viscous oil and a hydrocarbon solvent into the micromodel. Hydrocarbon solvent and SBF were injected after water flood to increase the heavy oil recovery. The dynamic flow experiments with the help of the fractured micromodel are able to visualize the mechanisms involved in both solvent and SBF flooding for extra-heavy oil recovery.

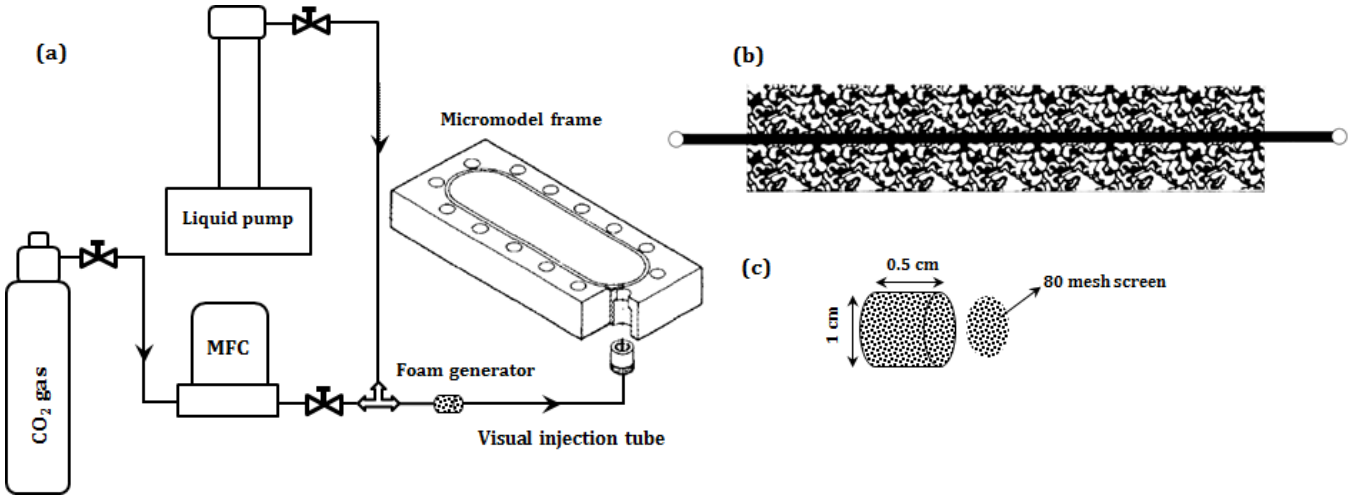

Figure 4.17: A schematic of the dynamic experiment: (a) experimental setup, (b) micromodel, black area shows the porous zone (fracture width is 1000 microns, (c) foam generator. MFC: Mass Flow Controller.

4.6 Results

4.6.1 Static Performance of Solvent Based Foam

Aqueous foam has been extensively studied over the decades. The stable foam could be achieved by controlling the thinning behavior of the foam lamellae. The surfactant or polymer molecules cover the air/liquid interfaces to prevent the collapse of the foam. They are generally effective in increasing foam stability. However, compared to the aqueous foams, it is difficult to stabilize non-aqueous foam (Ivanov, 1970; Mannheimer and Schechter, 1970). Unlike in water, the surfactants are less surface-active in non-polar oils and there is a little or no Gibbs-Marangoni foam stabilization mechanism in non-polar organic solvents (Shrestha et al., 2006). The mechanisms involved in the stability of aqueous (water-based) and non-aqueous (oil-based) foams are basically the same; however, as the surfactants are less surface-active in non-aqueous solvents, it is difficult to get stable non-aqueous foams (Ivanov, 1970; Mannheimer and Schechter, 1970). The surface

tension of oils is usually low, so there is only a little adsorption of hydrocarbon surfactants to the surface. This could be the reason why non-aqueous foams have been sparsely studied.

Figure 4.18 shows the foam decay profiles of two studied surfactants over time. For 1740G surfactant, (Figure 4.18a) the foamability and stability increased with increasing surfactant concentration while this effect is not significant in the case of 1250 surfactant (Figure 4.18b). According to Figure 4.18b, foam generated with 1250 surfactant is less stable than that of 1740G surfactant. There is also no significant increase in foam life by increasing concentration of 1250 surfactant. At 3 wt%, the foam life is only about 50 minutes for 1250 surfactant while this value is more than 200 minutes for 1740 G surfactant at the same concentration.

From the foam decay profile of 1740G surfactant, it was seen that foamability increased when surfactant concentration increased up to a certain value. For example, foam decay profile is not changed with the increase in surfactant concentration from 3 wt% to 5 wt%. This trend is the same for surfactant concentrations increasing from 0.5 wt% to 1 wt% and 10 wt% to 15 wt % as well. Surface tension measurement has been performed to analyze this trend much further.

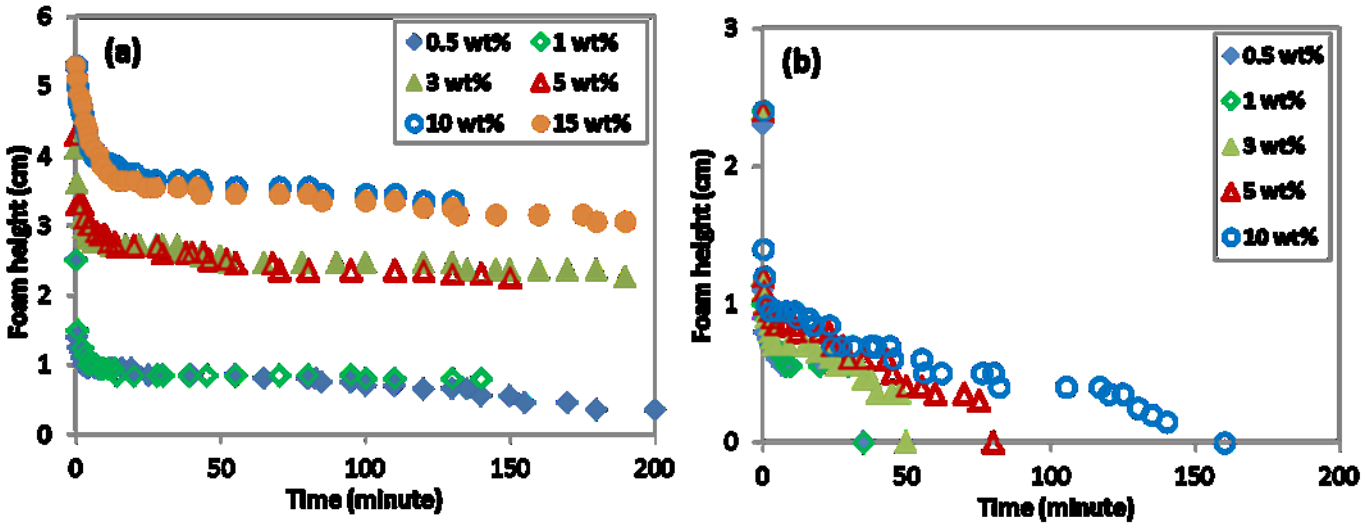

Figure 4.18: Foam height versus time (foam decay profile) of studied solvent based foams generated with (a) FluorN™ 1740G and (b) Dow Corning 1250 surfactants.

For detail study of the static performance of SBF, foamability and surface tension values of studied surfactants are presented in Figure 4.19. There is no significant change in foamability of 1250 surfactants by increasing concentration from 0.5 wt% to 10 wt%. The same trend can be seen in the surface tension value of this surfactant suggesting that by increasing surfactant concentration, suggesting there is no significant increase in surfactant adsorption into the interface and therefore, the foamability is not improved. Considering foam generated with the 1740G surfactant, the initial foam height increases with surfactant concentration (Figure 4.19a). Figure 4.19a shows that at certain intervals, a significant increase in surfactant concentration does not significantly change the foamability (e.g. from 0.5 wt% to 1 wt% and from 3 wt% to 5 wt%). In aqueous based foams, the foamability of a foaming solution usually has an indirect relationship with surface tension ($W=\sigma\times\Delta A$) where "W" is the work required for foam generation, "σ" is the surface tension of foaming solution and "ΔA" is the change in surface area representing the foamability (Stevenson and Li, 2012). However, reduction in the surface tension is not directly comparable to the increase

in the surfactant concentration and the foamability (comparing Figure 4.19a and Figure 4.19b). This suggests other factors are involved in the foamability of the non-aqueous based foams and generating stable non-aqueous based foam is possible yet challenging (Friberg and Ahmad, 1971; Friberg et al., 1984, 1986, 1989; Shrestha and Aramaki, 2012).

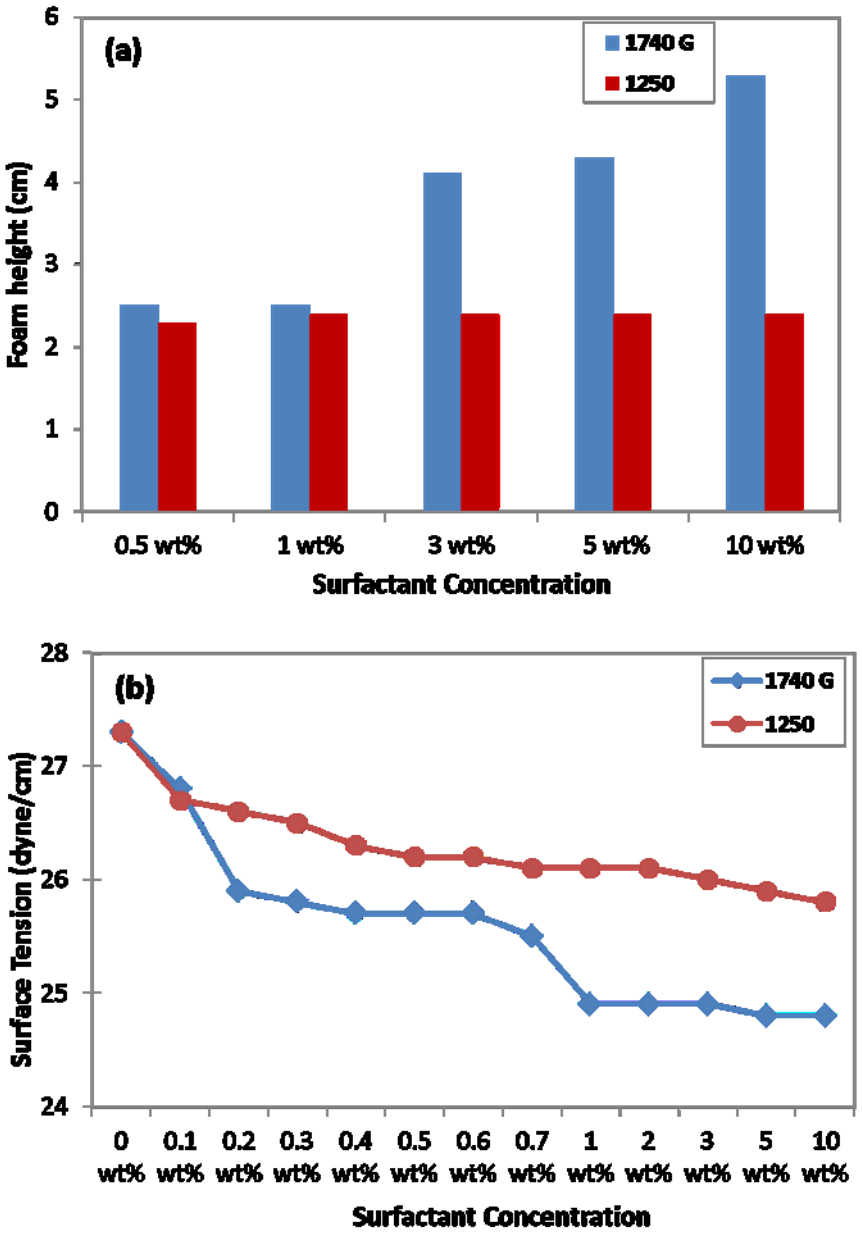

Figure 4.19: Changes in initial foam height (a) and surface tension (b) versus surfactant concentration for studied surfactants.

Immediately after foam generation, the foam film was very thick, because of the presence of an excess amount of liquid in the lamellae, and film breakup was hindered temporarily. As the drainage continued with time, the film thickness decreased and random foam breakage was observed. Therefore, the decrease in the foam volume at the beginning (see Figure 4.19) is mainly caused by the liquid drainage. Increasing surfactant concentration resulted in slightly lower liquid drainage rate. This indicates that the liquid holding capacity of the foams increases with increasing surfactant concentration and due to the higher volume fraction of liquid in the foams; the wet foams persist for a long period.

From visual observation in the course of time, better quality of generated foam (monodispersed spherical bubbles) was observed at higher concentrations of surfactant (especially 1740G surfactant). At lower concentration, foam bubble size was bigger and polydispersed (Figure 4.20).

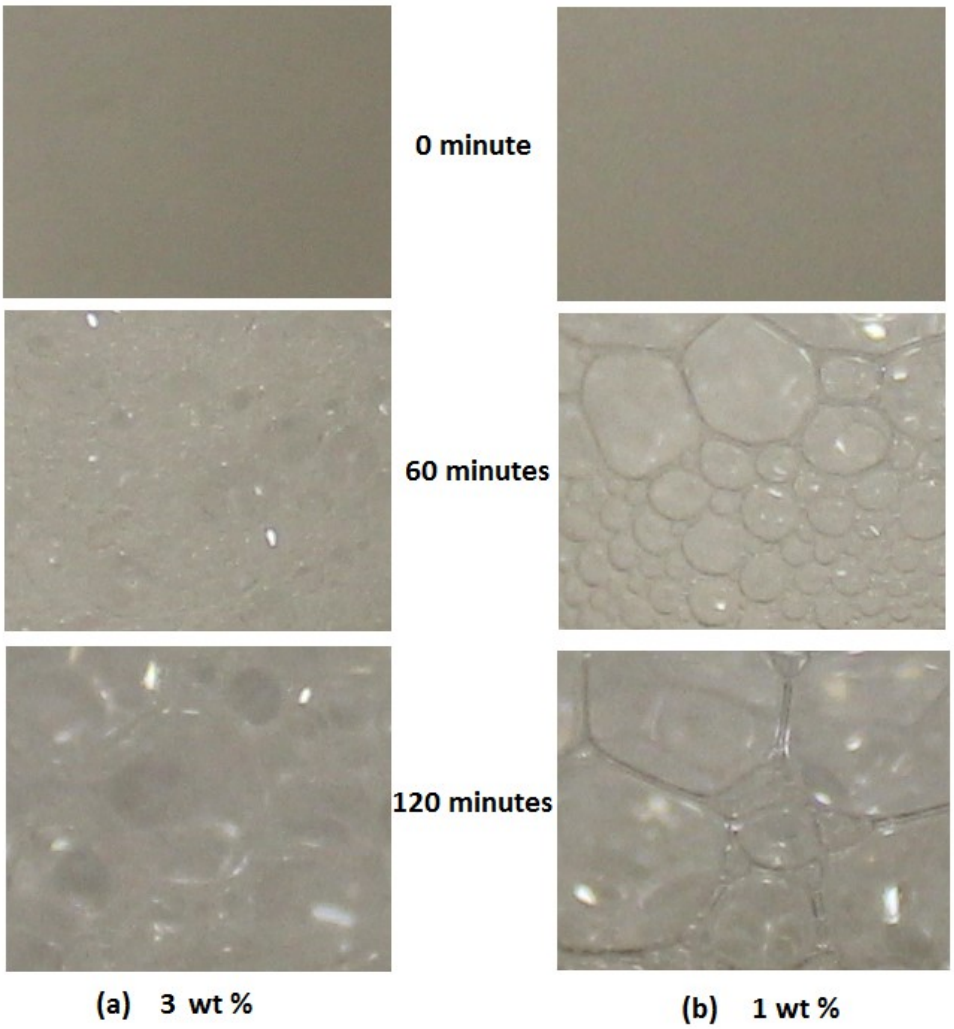

Figure 4.20: Visual observation of SBF bubbles generated with 1740G surfactant at two concentrations; (a) 3 wt% and (b) 1 wt%.

4.6.2 Dynamic Performance of Solvent Based Foam: Micromodel Study

In the solvent flooding, the solvent dilutes the oil and then drains down from the matrix, improving heavy oil recovery in fractured carbonate reservoirs (Butler and Mokrys, 1991). However, the process is complex because of the asphaltene destabilization that occurs due to the changes in temperature, pressure, and solvent type. Asphaltene flocculation and agglomeration eventually plugs the pores because of the formation of asphaltene clusters. For solvent injection, light

molecular weight hydrocarbon solvents are preferred because of their higher diffusion coefficient; however, as the carbon number of n-alkane solvents decreases, asphaltene precipitation increases (Fuhr et al., 1991; Buenrostro-Gonzalez et al., 2004; Moreno-Arciniegas and Babadagli, 2014).

In part 1 of this chapter, solvent injection reduced the oil viscosity and following foam flood increased the sweep efficiency in fractured micromodel. In this part, the foam was generated with the solvent rather than water. Therefore, it was hoped there would be a synergic effect with reducing viscosity due to the presence of a solvent and increasing sweep efficiency by foam bubbles at the same time.

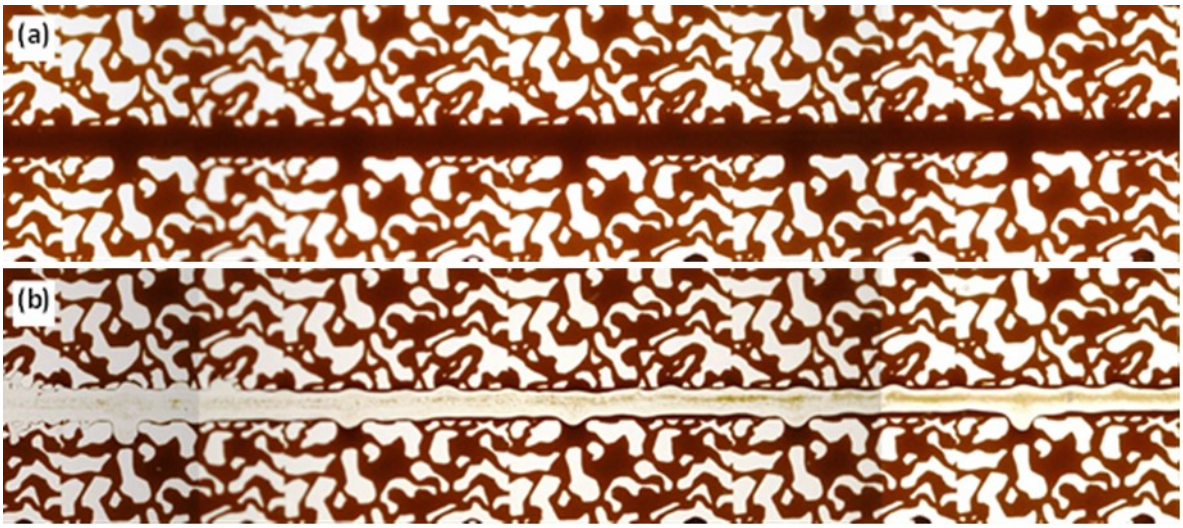

Figure 4.21: Images of oil saturated micromodel (a) and micromodel at the end of water flooding (b). Note: fracture width is about 1000 microns.

Figure 4.21 shows the images of micromodel after oil saturation (a) and at the end of water flooding (b). According to Figure 4.21, water could only sweep the oil within the fracture with no significant effect on the oil saturation in the matrix. In two separate experiments, solvent and SBF were injected after water flood to increase the heavy oil recovery and to visualize the mechanisms involved in the heavy oil recovery process. Figure 4.22 and Figure 4.23 represent images micromodel (after water flooding) at different stages of solvent and SBF flooding, respectively. In

the case of solvent flooding, the solvent could diffuse into the matrix and increase the ultimate oil recovery. However, the ultimate oil recovery was higher for SBF injection, which also benefits from increased sweep efficiency as seen in Figure 4.23. At the end of solvent flooding (Figure 4.22b), the amount of heavy oil remained within the pore structure was higher than that of SBF (Figure 4.23b). The asphaltene precipitation was also severe in the case of the solvent flooding which may prevent further solvent diffusion into the matrix.

Figure 4.22: Images of solvent flooding after initial water flooding (a) 1 hour, and (b) 3 hours.

Figure 4.23: Images of SBF flooding after initial water flooding at (a) 1 hour, and (b) 3 hours.

4.7 Discussions

The residual oil recovery profiles after water flooding for SBF and solvent injections are shown in Figure 4.24. The ultimate recovery of heavy oil by SBF injection (~ 82%) is much higher than that of a hydrocarbon solvent (~ 34%). Figure 4.22b and Figure 4.23b shows images of residual oil saturated micromodel after three hours' solvent and SBF injections, respectively. SBF effectively swept most of the heavy oil from the fractured micromodel. Although the ultimate oil recovery of SBF is higher than that of solvent injection, the initial rate of oil recovery trends is contrasting. During the early phase of injection (up to 75 minutes), solvent flooding resulted in higher oil recovery compared to SBF injection. This can be seen from the oil recovery profile in Figure 4.24 and residual oil saturation images of micromodel after 60 minutes of injection (Figure 4.22a and Figure 4.22b).

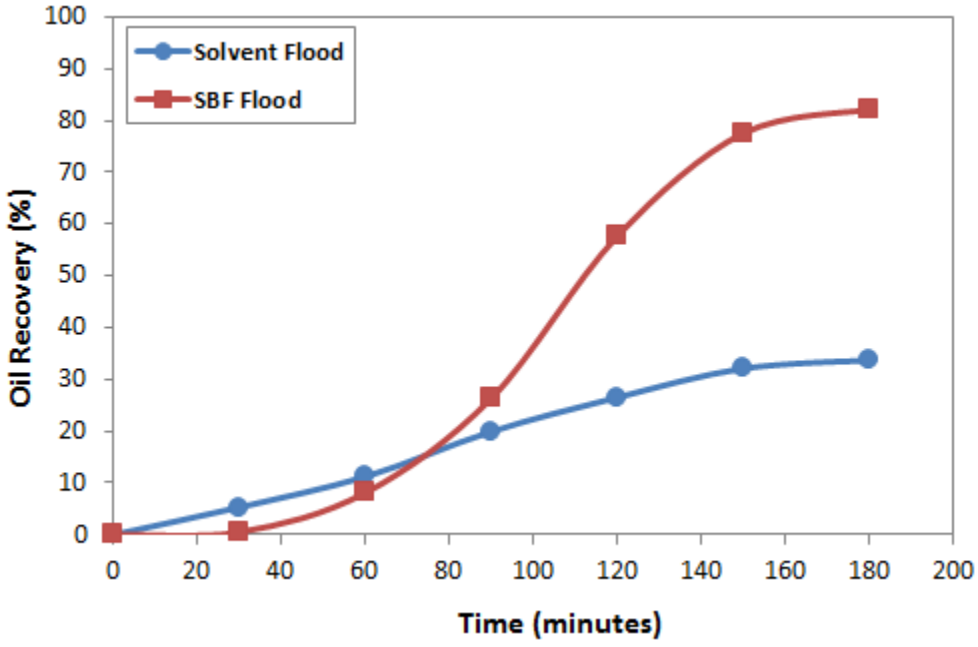

Figure 4.24: Heavy oil recovery profile during solvent and solvent based foam (SBF) injections (residual oil recovery after water flooding).

For a detailed analysis and mechanisms involved in heavy oil recovery behavior from fractured porous media using solvent and SBF injections, visual observation of micromodel at different time intervals are presented in Figure 4.25 and Figure 4.26. Heavy oil recovery and asphaltene precipitation during solvent flooding process are shown in Figure 4.25. At the early stages of solvent injection, the solvent mixed and diluted the heavy oil mainly around the fracture-matrix interface, as shown in Figure 4.25a. Thereafter, solvent diffused into the matrix, reducing the heavy viscosity, and eventually sweeping the oil from the matrix (Figure 4.25b). At this stage, asphaltene started to precipitate as the oil was diluted behind the solvent front. As the solvent injection continued, asphaltene precipitation increased and flocculation and agglomeration occurred (Figure 4.25c). The solvent mixed readily with the light fraction of the heavy oil, leaving behind asphaltene as an immobile precipitate adhering to the grain, forming ribbons like structures parallel to the flow line (dotted rectangle in Figure 4.25). Several researchers have visualized the asphaltene precipitation during solvent injection in heavy oil saturated porous media (Das and Butler, 1998; Dehghan et al., 2010; Farzaneh et al., 2010; Pathak et al., 2012, Moreno-Arciniegas and Babadagli, 2014; Telmadarreie and Trivedi, 2016). Farzaneh et al. (2010) observed the asphaltene precipitation during solvent injection in a fractured porous media. They observed that asphaltene precipitation occurred on the fracture wall resulting in blocked flow pathways. Asphaltene agglomeration and clustering can block the pore throat and result into severe formation damage. Moreover, it can reduce the diffusion of the solvent into the matrix. Further injection of the solvent will result in more asphaltene precipitation and severe formation damage as seen in Chapter 3 and part 1 of this chapter. It was evident from Figure 4.25c that asphaltene mainly precipitated at the matrix-fracture interface where the solvent diffused into the matrix. The higher concentration

gradient of solvent and higher mixing rate are responsible for asphaltene precipitation at this location.

Overall mechanisms involved in SBF flooding are shown in Figure 4.26. At an early stage of SBF flooding, because of high oil saturation around the fracture, most of the solvent diffused into the oil destabilizing the foam bubbles. The low stability of foam resulted in the separation of CO_2 gas and liquid phase (Figure 4.26a). The liquid solvent phase helped to reduce the oil viscosity by diffusing into the viscous oil. At the later stage, foam bubbles were more stable due to lower oil saturation in swept area. The foam bubbles created a resistance to flow in the swept area (i.e. fracture path) and the liquid solvent was diverted toward the untouched part of micromodel (Figure 4.26b). The liquid solvent diffused into the matrix, reduce heavy oil viscosity, and mobilize it. The force provided by foam bubbles pushed the solvent towards the untouched part of the porous media much faster and significantly improves the ultimate heavy oil recovery (Figure 4.24 and Figure 4.26c). The oil recovery in case of SBF injection was less affected by reduced solvent content compared to solvent injection rather sweep efficiency was significantly improved. The presence of foam bubbles effectively improved the solvent/oil contact area especially in the matrix zones away from the matrix-fracture intersection. While foam is injected, more bubbles invade into the matrix (Figure 4.27) and increase the contact between solvent and heavy oil in unswept regions. Therefore, overall sweep efficiency of heavy oil is greatly improved.

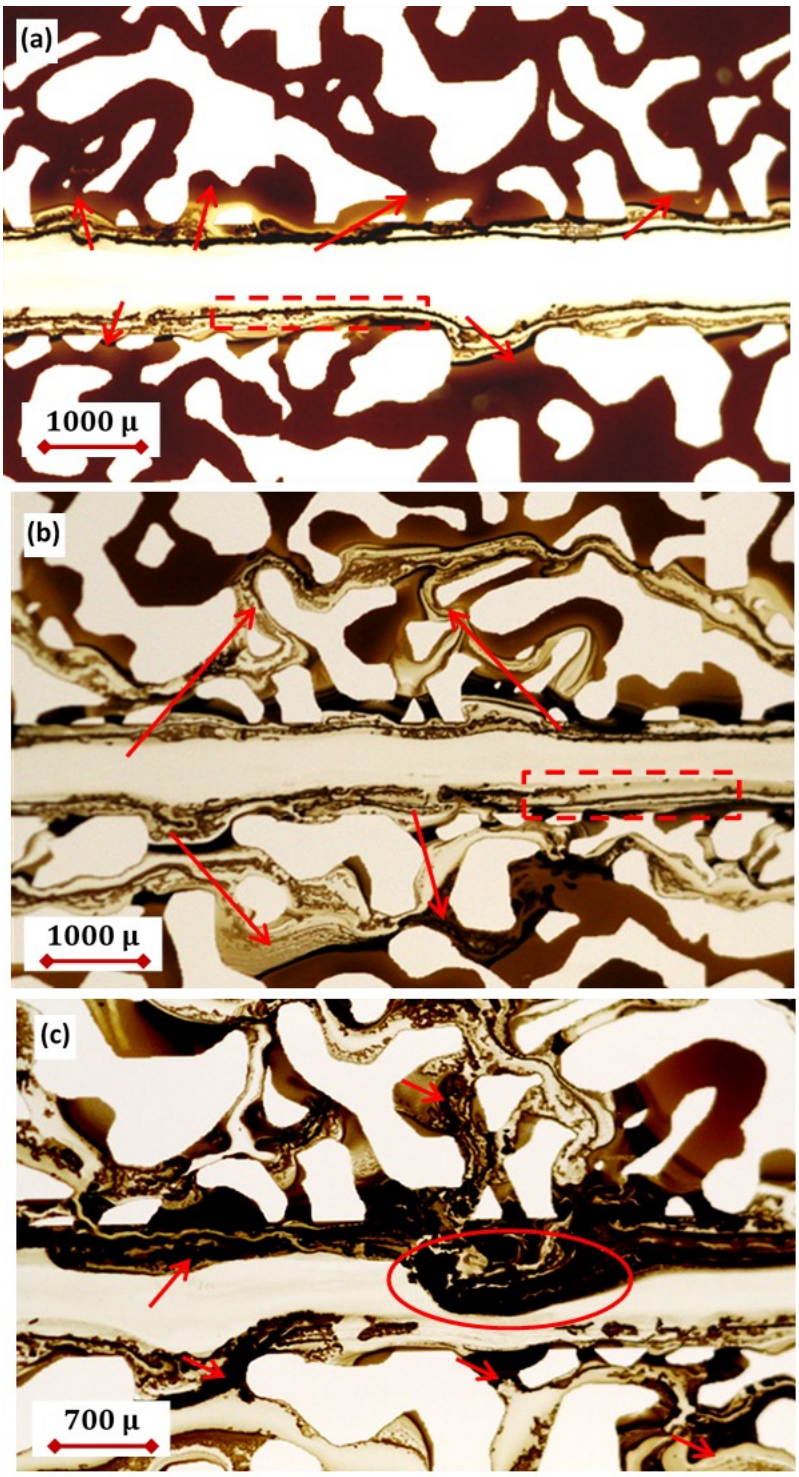

Figure 4.25: (a) early stage (1 hour) of solvent flooding: arrows represent slight solvent diffusion around the fracture, (b) next stage (2 hours) of solvent flooding; arrows show the direction of solvent diffusion further into the matrix, and (c) late stage (3 hours) of solvent flooding representing asphaltene precipitation and clustering resulting in formation damage. Dotted rectangle shows the precipitation of asphaltene as a parallel ribbon on the grain surface.

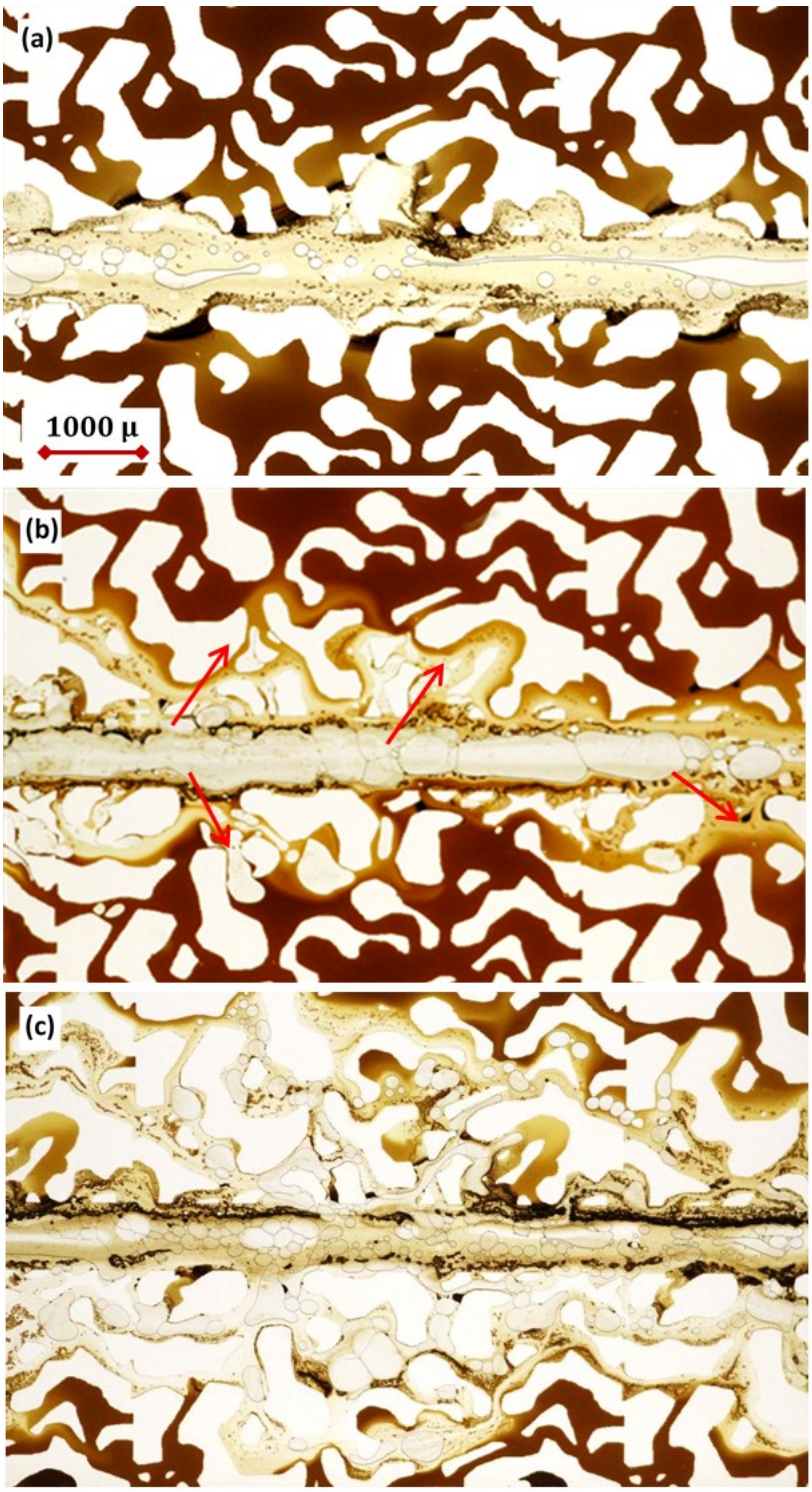

Figure 4.26: (a) early stage (1 hour) of SBF flooding: low stability of foam bubbles, (b) next stage (2 hours) of solvent flooding; arrows show the direction of solvent diffusion further into the matrix, and (c) late stage (3 hours) of SBF flooding.

Besides increasing heavy oil recovery, SBF injection also resulted in the minimum amount of formation damage at the matrix-fracture interface in contrast to solvent flood. Comparing Figure 4.26c and Figure 4.25c, almost no asphaltene precipitation was observed in the matrix during SBF injection whereas solvent injection resulted in significant precipitations. Depending on the quality of foam, usually, less than 20% of SBF is liquid solvent. It is important to note that the foam quality in this study was 85% and corresponding liquid content in SBF was 15%. Therefore, the amount of asphaltene precipitation was much less compared to that of 100% liquid hydrocarbon solvent injection.

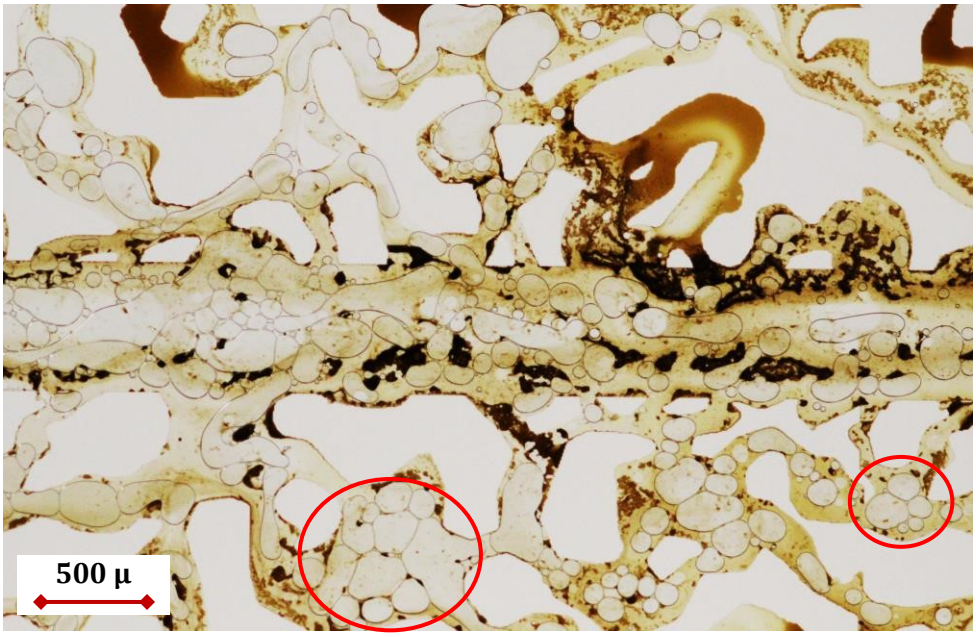

Figure 4.27: Late stage (when the most of the oil swept from the matrix areas around the fracture) of SBF flooding showing invasion of bubbles into the opening area in the matrix and increasing sweep efficiency.

4.8 Summary

The first part of this chapter investigated the pore-scale phenomena during CO_2 foam and PEF heavy oil recovery after solvent injection in fractured carbonate reservoirs. Foam can be used to improve matrix' oil production after solvent injection. Following are the summary of the first part of this chapter:

- Asphaltene precipitation was observed when oil and hydrocarbon solvents were in contact. Asphaltene mainly precipitated in the fracture/matrix interface where the solvent diffused into the matrix. Agglomeration and clustering of asphaltene can block the pore throats and result in severe formation damage while reducing the injectivity and efficiency of solvent diffusion into the matrix.
- Visualization of the foam and PEF EOR process showed that once strong foam is generated, there was almost no flow within the fracture. Because bubbles jammed and blocked the fracture path, the injected fluid was forced to flow into the matrix and swept the oil.
- Several mechanisms are involved in improving heavy oil recovery from fractured carbonate reservoirs. The early mechanisms of production include "blocking of the fracture by a network of bubbles" and "diversion of injected fluid into the matrix," whereas at a later stage "emulsification" and the "ablation" process are the main mechanisms in charge of the further matrix oil recovery.
- Observations through this study showed that the fluctuation in pressure of foam flooding behaved as a "huff 'and' puff" process and increased the matrix' oil recovery. First, the foam blocks the fracture and increases the pressure in both the matrix and the fracture. When foam temporarily collapses, the pressure suddenly drops. However, the rate of the

pressure drop in the matrix is lower than in the fracture, resulting in a temporary pressure difference between the matrix and fracture. This pressure difference improves the oil recovery from the matrix.

- CO_2 gas, foam, and PEF were injected after solvent flooding to improve the heavy-oil recovery. CO_2 increased oil recovery by only 5%, whereas this value was 49 and 70% for Na-DDBS foam and PEF, respectively. Enhancing liquid viscosity (improving both static and dynamic stability of PEF bubbles) and providing adequate injection pressure are the main reasons for the higher recovery from PEF than from foam. Foam also showed outstanding improvement in performance over gas injection. The presence of foam bubbles is the main reason for the improvement in heavy oil sweep efficiency in heterogeneous porous media.
- Applying foam generated with a cationic surfactant (as a wettability alteration agent) resulted in higher matrix' oil recovery compared with foam generated with an anionic surfactant. CTAB could remove oil layers around the matrix grain more efficiently (i.e., the ultimate oil recovery after solvent injection was 63%).

The second part of this chapter visualized the performance of SBF for heavy oil recovery in a fracture oil-wet micromodel representing the fractured reservoirs. Its performance was also compared with that of liquid hydrocarbon solvent injection. Following are the summary based on the observations:

- Static tests revealed that increasing surfactant concentration increased foamability of SBF. However, after a certain point, a significant increase in surfactant concentration does not change the foamability suggesting the influence of other factors involved in the foamability of the non-aqueous based foams.

- Although solvent could diffuse into the heavy oil saturated matrix, the formation damage caused due to asphaltene precipitation was significant that made the solvent injection process for heavy oil recovery in a fractured porous media inefficient.
- At the early stages of SBF flooding, foam bubbles had low stability resulting in two-phase separation. Liquid phase reduced the oil viscosity by diffusion mechanisms. At the later stage of flooding, foam bubbles created resistance to the flow in swept part (i.e. fracture) and the solvent was diverted toward untouched part in the matrix.
- The main mechanism observed through this study during SBF flooding was viscosity reduction by solvent diffusion and fluid diversion with the help of foam bubbles. The diversion mechanism created by the foam bubbles increased the contact of solvent and heavy oil compared to that of pure solvent injection, improving sweep efficiency. SBF flooding resulted in higher ultimate heavy oil recovery from heterogeneous media compared to that of pure solvent injection.
- In addition, foam bubbles created higher driving force compared to that of pure solvent injection resulting from the higher resistance to flow in SBF than that of pure solvent (due to the presence of foam bubbles). Consequently, heavy oil (with reduced viscosity due to solvent diffusion) will be displaced toward the production well much more effectively than that of solvent injection.

Chapter 5: CO_2 Foam and Polymer Enhanced Foam for Heavy Oil Recovery: Bulk and Porous Media (Sand-pack) Studies[5]

5.1 Introduction

Inadequate sweep efficiencies resulting from unfavorable mobility ratios are the main challenges during enhanced oil recovery (EOR) methods, especially in heavy oil recovery. Foam and Polymer Enhanced Foam (PEF) flooding can control the mobility ratio and improve the sweep efficiency, especially in heterogeneous reservoirs. Foam can provide better control of the fluids injected and uniformity of the contact as stronger foams can block the flow channels in high permeability media and divert it toward the low permeable parts (Hirasaki, 1989; Zhou, and Rossen, 1995).

Besides improving sweep efficiency in gas flooding, foam/PEF can be used for mobility control in chemical EOR where the foam is considered an alternative to polymer mobility control in micellar flooding. Zhang et al. (2000) reported laboratory and field studies of foam in Daqing oilfield in China, where the foam was successfully applied in a heterogeneous porous media and compared with the performance of chemical flooding.

There are several challenges for widespread application of foam in porous media such as in situ generation and propagation of foam. Although the principal mechanisms for foam generation have been identified, the precise condition when the strong foam can be generated in the reservoir remained unknown. In a homogeneous porous medium, with steady co-injection of gas and liquid, a minimum pressure gradient is required to create foam (Ransohoff and Radke, 1988; Rossen and

[5] A version of this chapter has been published:
Telmadarreie and Trivedi, 2015. Paper WHOC15-243 Presented at the World Heavy Oil Congress, Edmonton, Alberta.

Gauglitz, 1990; Tanzil *et al*., 2002; Gauglitz *et al*., 2002). One of the proposed ways to enhance foam generation is using small, alternating slugs of liquid and gas (SAG injection) (Rossen and Gauglitz, 1990). SAG injection has several advantages over co-injection of gas and surfactant as it reduces the contact between water and gas in the surface facilities (Mattews, 1989; Heller, 1994) and besides improving injectivity, it can possibly improve foam generation in the near-wellbore region (Rossen and Gauglitz, 1990).

Another important challenge during foam EOR is the detrimental effect of crude oil. There are several studies on the static and dynamic performance of foam-oil systems (Vikingsad et al., 2005; Andrianov et al., 2012; Scharamm and Novosad, 1992; Koczo et al., 1992; Farajzadeh et al., 2010; Simjoo et al., 2013). These studies are mainly focused on performing foam stability experiments (bulk tests) in the presence of different types of light oils and measuring the foam half-life. Some of these researchers also measured the spreading, entering, and, birding coefficients in the foam-oil system and tried to explain the behavior of the foam-oil system. However, the relation between spreading phenomena and foam stability has been inconclusive for general applications. For instance, Andrianov et al. (2012) concluded that there exists a strong correlation between spreading (S) and entering (E) coefficients, and foam stability while Vikingsad et al. (2005) did not find any direct correlation between spreading coefficient and foam stability. Nikolov et al. (1986) mentioned that as the oil drop approaches the liquid-gas interface, the thin liquid film forms between the oil drop and the gas phase called *"pseudoemulsion film"*. According to this study, oil drop cannot enter the interface when the pseudoemulsion film is stable, even if the value of E or S coefficients showing differently.

Chemical methods are among the most common non-thermal EOR process for heavy oil recovery after water flooding. One of the issues with the chemical method for heavy oil reservoirs is the low

injectivity and inadequate sweep efficiency, especially in heterogeneous reservoirs. Foam and Polymer Enhanced Foam (PEF) can improve sweep efficiency over gas and chemical injections. Shallow heavy oil reservoirs in Western Canadian Sedimentary Basin (WCSB), which can be also recovered by non-thermal processes, can be the potential target for foam/PEF EOR application. The high viscosity of the oil and high heterogeneity of these reservoirs can result in inadequate sweep efficiency of conventional non-thermal methods.

Most of the previous studies mentioned above have been performed on light crude oils. In this chapter, the effect of heavy crude oil is studied on the static and dynamic performance of foam. Moreover, PEF is also introduced for improving the performance of conventional foam in heavy oil reservoirs. For this aim, firstly static experiments, including bulk foam stability, and surface tension studies were designed to study the behavior of bulk foam in the presence and absence of heavy oil, as well as the effect of polymer addition on its behavior. In the second part, dynamic experiments of foam/PEF propagation through visual sand-pack were performed to investigate the dynamic stability with and without the presence of heavy oil.

5.2 Materials and Methods

5.2.1 Materials

Various types of surfactant (nonionic, anionic, and cationic) as a foaming agent and one polymer (as a foam stabilizer) were selected for foam/PEF studies as follows:

Nonionic surfactant: Surfonic N85 (Huntsman Corporation) which is a Nonylphenol-ethoxylated nonionic surfactant with a chemical formula of $C_{15}H_{23}$ (OCH_2CH_2)n OH (Mw= 594 g/mol).

Anionic Surfactant: Two anionic surfactants, Sodium dodecylbenzene sulfonate ($C_{12}H_{25}C_6H_4SO_3Na$, Mw=348.5 g/mol)) and C_{14}–C_{16} Alpha olefin sulfonate ($R\text{-}SO_3^-Na^+$, Mw=348.5 g/mol) were used for static foam analysis.

Cationic Surfactant: Cetyltrimethylammonium bromide (CTAB) (Sigma–Aldrich, 99% purity) was also used as a cationic foaming agent ($C_{19}H_{42}BrN$, Mw=364.5 g/mol).

Polymer: Polymer is used to increase the viscosity of the liquid phase. The anionic polyacrylamide polymer FLOPAAM 3330S (supplied by SNF SAS) was used in the preparation of polymer solutions. It has hydrolysis degree of 25-30 % and average molecular weight of 8×10^6.

Hydrocarbons: For both static and dynamic experiments, heavy crude oil (sampled from one of the Canadian oilfields) with dead oil viscosity of 1320 cp (at 22 °C) was used. In addition, a mineral oil was also used for only static analysis of the foam-oil system.

5.2.2 Foam Bulk (Static) Experiments

Foam and PEF generation: For the preparation of the foaming solution, surfactant (0.29 wt%) and in some tests polymer (0.15 wt%) were mixed in water. A magnetic stirrer (400 rpm for 20 minutes) was used for mixing to avoid the foam generation. Thereafter, foam or PEF was generated using a digital Homogenizer (provided by Kinematica Inc.). It should be mentioned that all four surfactants were used for foam static analysis and among them, N85 and DDBS were selected for the static study of PEF.

For foam generation, 100 cc of foaming solution was mixed in a glass cylinder (1000 cc) at high speed for two minutes. The shearing speed and shearing time were kept constant for uniformity of foam created throughout the experiments. In some experiments, 5 cc of oil was added to the foaming solution before the high-speed mixing to study the effect of oil on foam/PEF stability. A schematic of static foam setup is shown in Figure 5.1.

Static stability: The glass cylinder was closed with a plastic seal after foam generation to avoid evaporation. In each experiment, immediately after mixing, the total height, as well as the height of liquid, was measured as a function of time. Foam stability (foam half-life) was recorded based

on the time required to drain half of the liquid from the foam. Moreover, the initial foam height value was also recorded as the foamability of foaming solutions. A high-definition camera was used to analyze the foam behavior with and without the presence of oil. For some detailed analysis of foam-oil interaction, a Leica DM 6000M microscope was used to capture high-quality images. All the experiments were repeated to assure the reproducibility of results.

Surface tension and interfacial tension: The surface tension of the surfactant solutions and their mixtures with polymer was measured by the Du Noüy tensiometer (provided by KRÜSS) using a platinum-iridium ring. The ring method directly measures the maximum pull on the interface to find surface tension value. After each measurement, the ring was carefully rinsed with deionized water and then a solvent (usually acetone) to remove impurities. Thereafter, the ring was cleaned with a flame to remove any impurities. The Interfacial Tension (IFT) measurements were performed using spinning drop method (SITE100, provided by KRÜSS). The lowest measurement range for this instrument is as low as 10^{-6} mN/m with rotational speed up to 15000 rpm (with a capillary diameter of 2.5 mm).

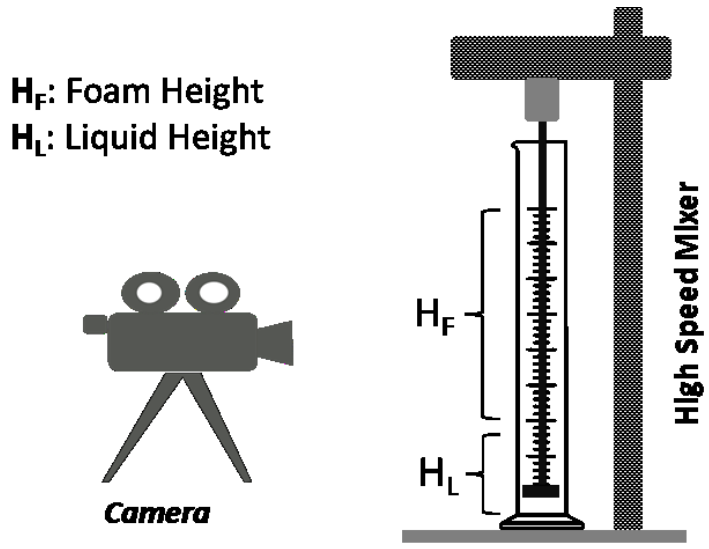

Figure 5.1: A schematic set-up for foam static analysis.

5.2.3 Foam Dynamic Experiments

To analyze the dynamic performance of foam and PEF in porous media, a linear visual sand-pack was used (1-ft in length with an inner diameter of 1-inch). The visual cell was a, packed with glass beads (40-70 meshes) and a special expandable rubber was used to seal the both ends. A metal screen (80 meshes) was used to avoid sand production. After vacuuming the sand-pack (at least 3 hours), water saturation and permeability measurements were conducted. The measured porosity and permeability of the sand-pack were 37±0.5% and 38±0.5 Darcy, respectively. The porous medium was then saturated with heavy crude oil (1320 cp) until no water was produced. A syringe pump (ISCO Model 500D) and a pressure transducer (OMEGADYNE Model PX409) was used for liquid injection and pressure record, respectively. A schematic of dynamic experiments set up is shown in Figure 5.2.

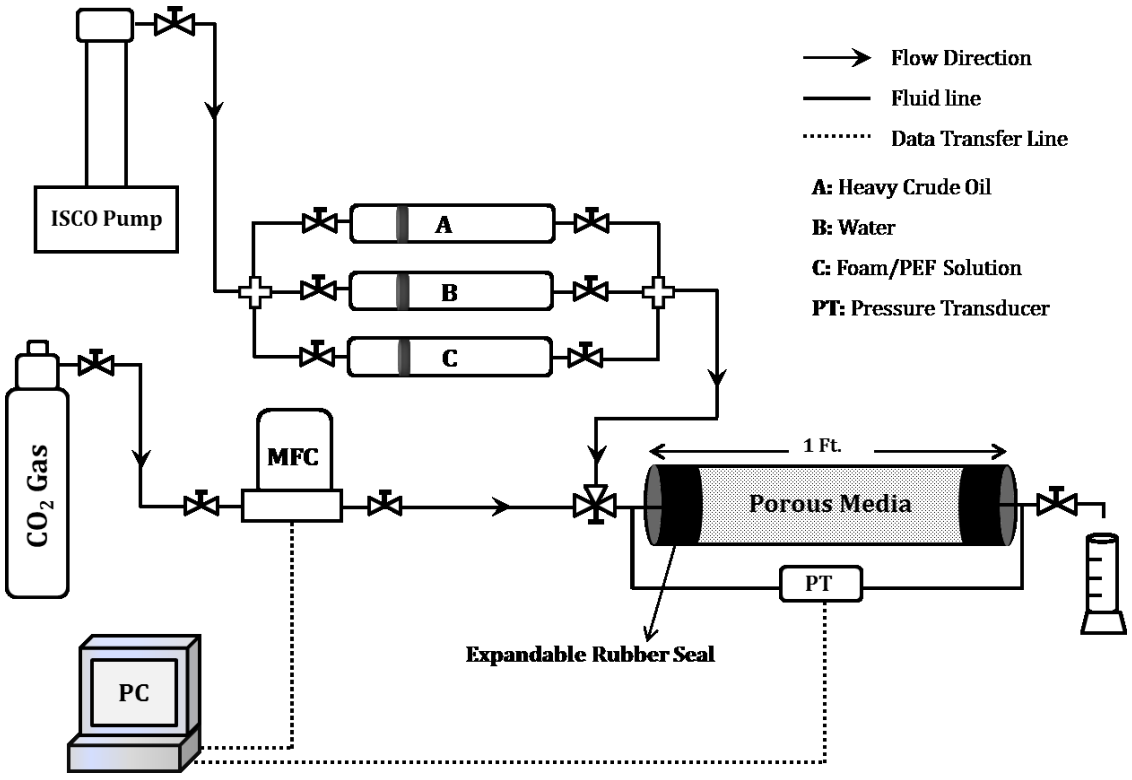

Figure 5.2: Schematic of CO_2 foam/PEF flooding system.

In this study, the foam was generated in-situ with the help of Surfactant Alternating Gas (SAG) injection. During all the experiments, both liquid and gas rates were kept equal (20 ft/D). The injection rate was selected based on the high permeability of the sand-pack and the shear rate of fluid within the porous media (between 1 to 100 s^{-1}). In addition, the high rate ensured that the critical pressure gradient to generate strong foam was exceeded. A gas mass flow controller (provided by Hoskin Scientific Ltd) was used for the accurate injection of CO_2 gas at the constant volumetric flow rate. The slug volume of both liquid and gas was selected as 0.1 fractions of the total pore volume (0.1 PV). Pressure profile and oil recovery were measured as well as sand-pack images were captured during all the experiments to compare the performance of different foaming solutions in heavy oil recovery. It should be mentioned that all flooding was performed in tertiary recovery mode after reaching a constant water cut of 98% during water flooding. Table 5.1 summarized the detail of dynamic experiments on visual sand-pack. Among the studied surfactants non-ionic surfactant N85 (weakest foaming agent) and DDBS (best foaming agent) were selected for dynamic foam and PEF studies. All experiments were performed at ambient condition (room temperature) without using any backpressure.

Table 5.1: Summary of dynamic experiments performed on visual sand-pack: with and without the presence of heavy oil.

Experiment	Porous Media Length (cm)	Ø (%)	K (D)	Soi (%)	WF-RF (%)	Total RF (%)
DDBS-SAG	24.5	36.26	37.69	NA	NA	NA
	24.2	36.86	37.26	93.3	33.5	94
DDBS-PEF	24.4	36.41	37.53	NA	NA	NA
	24.5	37.07	37.87	92.4	33.7	99
N85-SAG	24.5	36.67	37.88	NA	NA	NA
	24.4	37.22	37.72	93.4	33.1	57
N85-PEF	24.4	37.22	38.19	NA	NA	NA
	24.4	36.82	37.91	92.3	33	98

5.3 Results and Discussions

5.3.1 Static Performance of Foam and PEF in the Absence of Heavy Oil

Effect of surfactant type: The changes of normalized foam height (H/H_0) versus time, foamability, and foam stability (half-life) for all studied surfactants are shown in Figure 5.3. The foam decay profiles of all ionic surfactants are almost the same. Among all studied surfactants, DDBS showed better stability (half-life) while CTAB had highest foamability. Foamability is the ability of the surfactant to generate foam. Several references reported the good foamability of anionic surfactants (Flick, 1993; Urban, 2003; Rosen and Kunjappu, 2012) whereas the nonionic surfactants generally produce less foam. The stability of foams generated with ionic or nonionic surfactants is achieved by repulsive forces between the surfactant monolayers (Verwey and Overbeek. 1948). Therefore, the ionic surfactants (DDBS, AOS, and CTAB) generated more foam with relatively higher stability compared to that of nonionic N85 surfactant. According to Figure 5.3b, initial foam height (foamability) and half-life (foam stability) of anionic surfactants are higher than that of the nonionic surfactant. In fact, if the nonionic surfactants do not create a well adsorption monolayer on the water/air interface, it will not stabilize the foam films by steric repulsion. In this case, the foaming is very low due to the instability of the foam films (Marinova et al., 2012). Furthermore, the presence of ionic surfactants at the interface in the foam film will stabilize the film and induce a repulsive force that opposes the film thinning process. This is called the Electric double-layer repulsion (Israelachvili, 1991, Schramm and Wassmuth, 1994) which depends on the charge density and the film thickness.

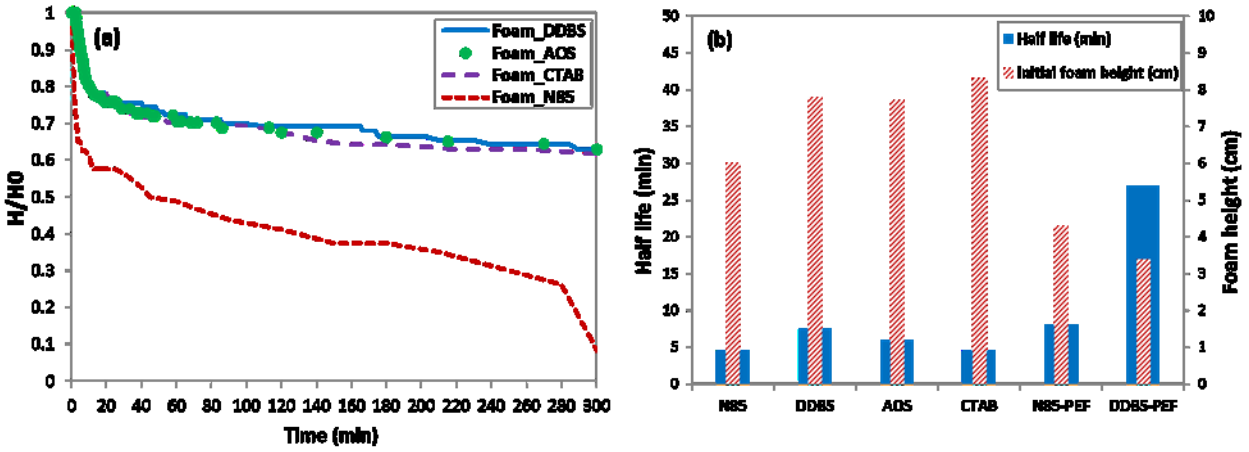

Figure 5.3: (a) Foam decay profiles and (b) foamability and half-life values for studied surfactants: anionic DDBS and AOS, nonionic N85 and cationic CTAB. Polymer increased foam stability while decreases the foamability of surfactants.

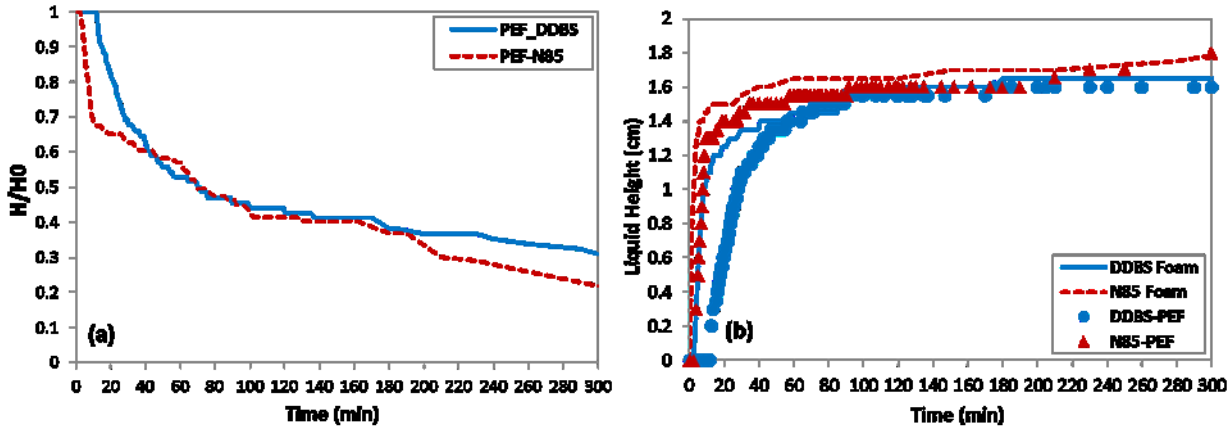

Figure 5.4: (a) PEF decay profile, and (b) liquid drainage profiles of the studied foams and PEFs.

Effect of polymer addition: The major advantage of polymer addition in foaming solution is viscosity enhancement which may improve the foam stability by lowering the liquid drainage rate in the foam. The foamability and half-life values for polymer enhanced foams are shown in Figure 5.3b. The CTAB surfactant was not compatible with the anionic polymer. Anionic AOS surfactant had similar performance to anionic DDBS surfactants with, and without polymer (results are not presented here). Therefore, anionic DDBS and nonionic N85 surfactants were selected for PEF

studies. Although polymer increased the half-life value, it drastically decreased the foamability of surfactant. For the PEF generated with the nonionic surfactant N85 and anionic polyacrylamide polymer, the only slight improvement was seen on the half-life value while the polymer significantly reduced the foamability. The anionic polyacrylamide polymer significantly increased the stability of foams generated with anionic DDBS surfactant. Figure 5.4 shows the PEF decay profile (part a) and liquid drainage rate (part b) of foam and PEF. The N85-PEF decayed faster than DDBS-PEF. Polymer increased the viscosity of liquid solution within the foam lamella, reduced the rate of liquid drainage, and consequently increased the stability of foam as seen in Figures 5.3b and 5.4b. However, this enhancement was less for N85 surfactant which is the relatively poor foaming agent. Therefore, proper selection of surfactant and polymer is essential to have optimum stability for PEF.

Surface tension measurement: Viscosity enhancement by the addition of polymer is not the only criteria for a significant increase in foam stability and therefore polymer-surfactant interaction should be considered. Comparing foam/PEF generated with each surfactant; the addition of polymer slightly increased the surface tension as seen in Figure 5.5, therefore the foamability decreased. The numbers in this Figure represent quality (gas content, foamability) of foam/PEF. This can be explained by the work done for generation of foam or PEF using following equation:

$$W=\Delta A \times \sigma \quad (1)$$

where W is the work done for foam generation, ΔA is a change in area or foamability, and σ is surface tension.

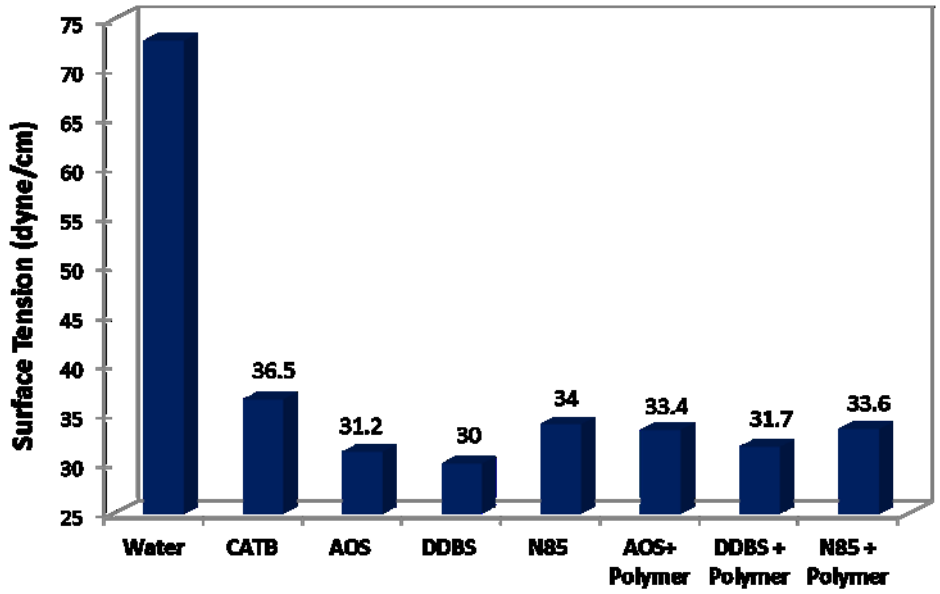

Figure 5.5: Surface tension values for the different foaming solutions; the numbers in x-axis represent quality (or gas percentage) of corresponding foam/PEF.

5.3.2 Static Performance of Foam and PEF in the Presence of Heavy Oil

Oils generally destabilize and can also stabilize a foam system (Koczo et al., 1992). In this chapter effect of heavy crude oil and mineral oil was examined on foam stability. The results are shown in Figure 5.6. The presence of heavy oil decreased the foamability and stability of foams and PEFs generated with all surfactants, especially N85. On the other hand, mineral oil both stabilized and destabilized the studied foams. In terms of foamability, the addition of mineral oil had no drastic effect on foamability and foam stability of foams compared to that of heavy oil. Considering foam stability, in some cases, the addition of mineral oil resulted in increasing the foam stability (N85, AOS, and CTAB foams).

The addition of polymer in DDBS solution has a significant effect on the stability of foam-oil system such that the oil has no significant drastic effect on DDBS-PEF (Figure 5.6b). However, N85 foam stability in the presence of oils did not increase with the addition of polymer.

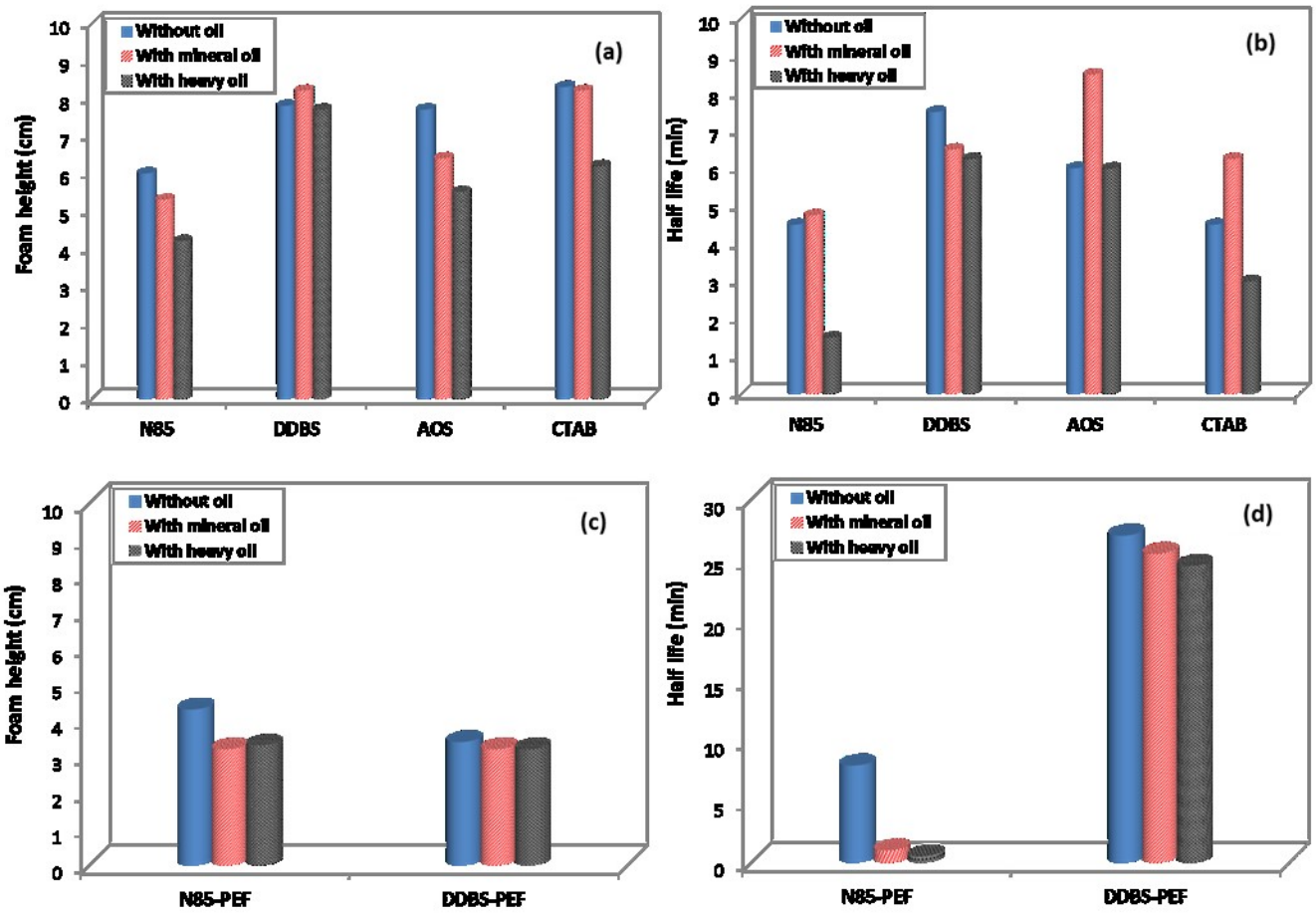

Figure 5.6: Effect of heavy oil and mineral oil on (a) foamability and (b) foam stability of studied foams, (c) foamability and (d) foam stability of studied PEFs.

The decay profiles of DDBS and N85 surfactants were selected for detailed discussion of foam-oil interaction. The foam decay profile was divided into four stages (according to Denkov, 2004) as shown in Figure 5.7 where the normalized foam height is plotted versus time for different foam-oil systems. Both types of oils increased the foam destruction rate; however, mineral oil had relatively less drastic influence in both foam systems. This is more evident in the N85-foam

system. On the other hand, mineral oil interestingly reduced the liquid drainage rate (stage I) and also had no drastic effect on foam decay life. The behavior of each foam-oil system at each stage can be explained as follows:

Stage I: During Stage I the main process affecting the foam decay profile is liquid drainage. It should be mentioned that some minor bubble coarsening may have occurred during this stage, but the dominant phenomenon was the liquid drainage. Images of the foam bubble texture at the foam top and liquid-foam interface during this stage are shown in Figure 5.7.

Stage II: There was no significant liquid drainage in Stage II; however, the optical observation of foam column demonstrated a significant change in bubbles structure during this period. The small bubbles disappeared, and bubble coarsening occurred, because of gas diffusion through the films (Figure 5.8). Stage II is too short in case of N85 surfactant foam system. This is due to the less potential of N85 (nonionic) surfactant to generate stable foam and almost immediately after drainage stage, the foam started to collapse. Beside surfactant weakness, the anti-foaming effect of oil increased the rate of foam collapse. Stage II is about 40 minutes for the DDBS foam system showing the better stability of DDBS surfactant (anionic) to generate the most stable foam. A similar trend was seen in foam-mineral oil system; however, the length of stage II in DDBS-mineral oil system increased to more than 50 minutes as seen in Figure 5.7b.

Stage III: The onset of stage III is identified by rupture of bubbles in the upper layer of foam column. According to Denkov (2004), when a certain critical value of the compressing capillary pressure (which is higher at the foam top) is reached, the foam starts to collapse. Stage III is called "anti-foaming" stage because the shape of profile strongly depends on the anti-foaming behavior of the oil. In a foam-oil system, after foam generation, oil droplet is immediately drained from the foam film and rests in foam lamella and Plateau Borders (PBs) because the droplets are smaller

than the foam film thickness. During this stage, by thinning the foam film/lamella and increasing oil droplet size (due to flocculation/coalescence of droplets) the lamella eventually will break. Figure 5.9 shows the collapse of foam lamella at the antifoaming stage, which is most probably due to the drastic effect of oil.

Comparing N85 and DDBS foams in the presence of heavy oil, the N85 foam starts to collapse immediately after liquid drainage (stage I) and foam column collapsed in less than 2 hours. Heavy oil also significantly reduced the length of stage III (increased rate of foam destruction) in DDBS foam. In mineral oil system, the rate of DDBS-foam destruction (slope of the curve at stage III) was less than that of heavy oil, representing the less detrimental effect of mineral oil on foam stability.

Stage IV: Over time in Stage III, the rate of foam destruction gradually decreased in magnitude and stage IV is reached when the foam volume remained almost constant (residual foam height) before the foam dies. Unlike N85-foam-heavy oil system, stage IV interval is evident in the DDBS foam system. In N85 foam- heavy oil system, foam collapsed right after liquid drainage stage and died without any residual foam height; i.e. the height of the foam at stage IV. As noticed earlier, mineral oil showed less drastic effect such that unlike heavy oil system, stage IV can be seen in "N85 foam-mineral oil" system.

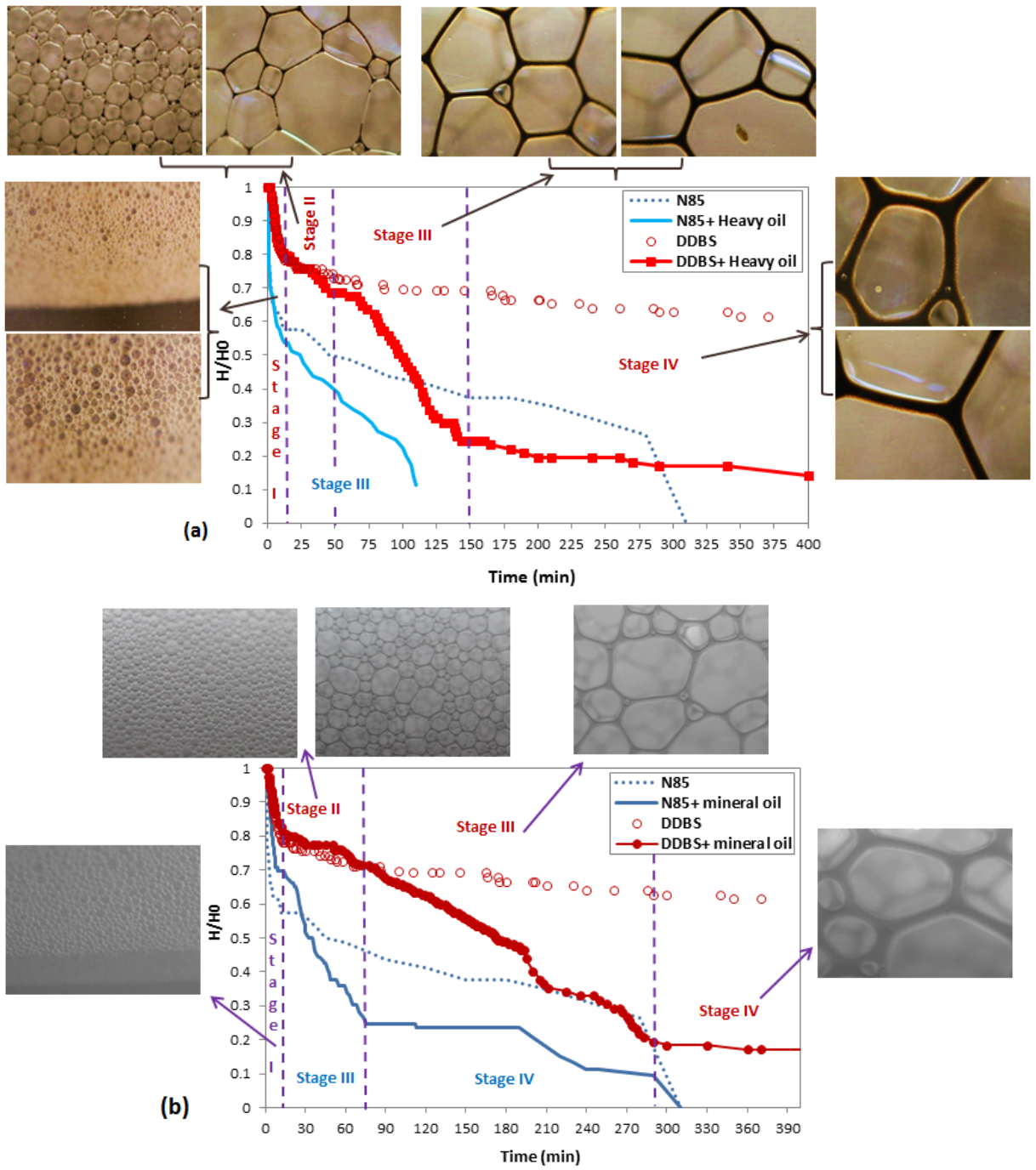

Figure 5.7: Foam decay profile for N85 (nonionic) and DDBS (anionic) surfactants; considering the effect of (a) heavy and (b) mineral oil; images correspond to DDBS foam (5X magnification).

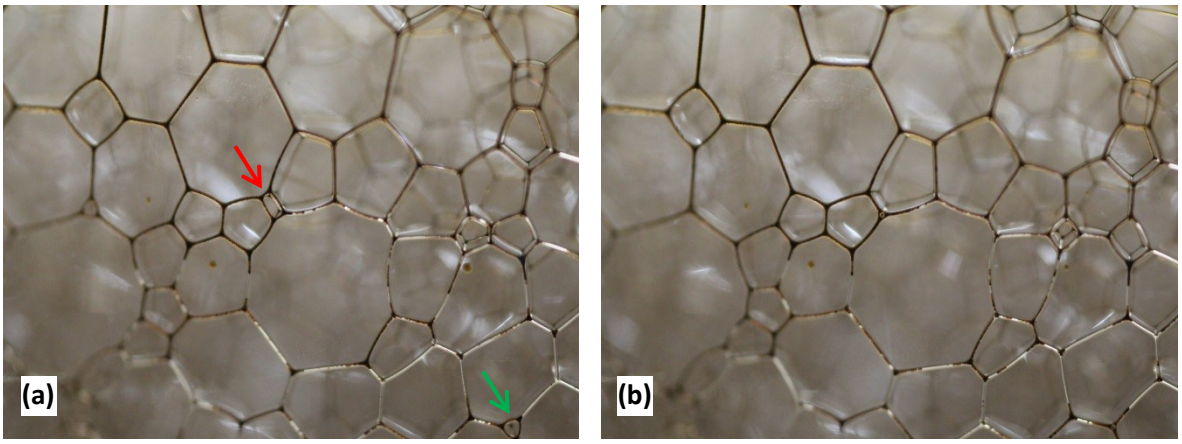

Figure 5.8: Air diffusion from the small bubbles toward the larger ones leads to the disappearance of the small bubbles and to the gradual accumulation of oil drops in the nodes and the Plateau borders during stage II (DDBS foam with heavy oil). Images (b) were captured seconds after images (a).

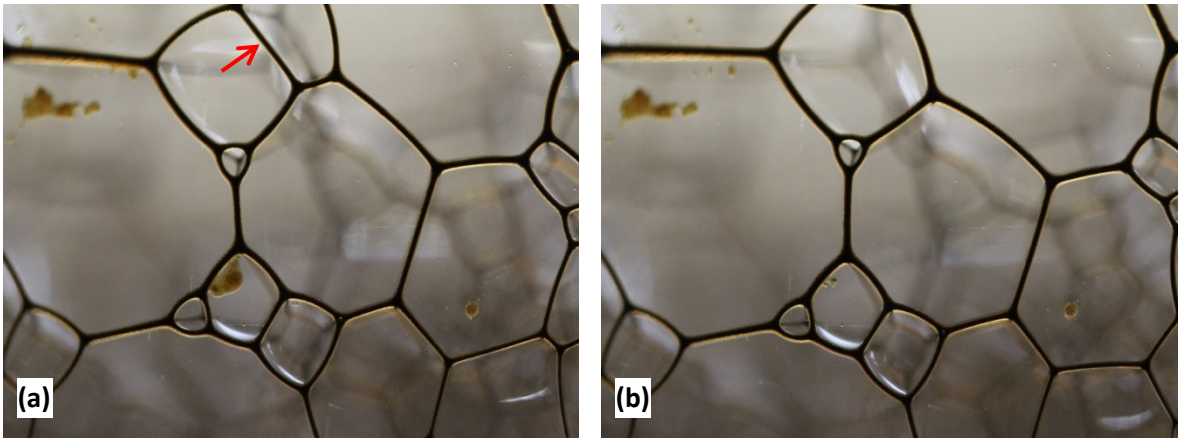

Figure 5.9: Oil droplets overcome the electrostatic interactions and break a foam lamella during stage III; DDBS foam with heavy oil (2X magnification).

Like foam decay profile, we can define different stages in PEF decay profile in the presence of heavy oil as antifoam. The behavior of PEF generated with both surfactants in the presence of heavy oil is shown in Figure 5.10. Three stages can be defined in PEF-oil profile for detail analysis. Let's first consider the PEF generated with DDBS surfactant (Figure 5.10a). The characteristics of each stage are as follows;

Stage I: in the PEF-oil system, this stage is different from that of the foam decay profile. The PEF decay profile is quite constant without any change. No liquid drainage or foam collapse occurred. This stage can be characteristic of polymer effectiveness in increasing the stability of the conventional foam. We can call this stage as "stability improvement stage" because the main outcome of this stage is the stability of PEF. So, the larger stage I represent the more improvement of stability by the addition of polymer. However, PEF image studies revealed some minor changes happening to the PEF structure during this stage. Gas diffusion from smaller bubble to a larger one (based on the Laplace formula) and bubble coalescence is evident. However, this change is minor and the rate of bubble coalescence is very low compared to conventional foam. The images taken at the beginning and end of this stage (top of PEF column) prove this claim.

Stage II: this stage is similar to Stage III of the foam-oil system, the only difference is that liquid drainage and antifoaming (foam collapse) phenomena happening almost together at this stage. As seen the difference between with oil and without oil curves appear first at this stage, representing the antifoaming effect of the oil. Images taken during this stage show the dominant phenomena happening in the course of time during stage II.

Stage III: this stage is also can be correlated to Stage IV of the foam-oil system. Almost no liquid drainage and foam collapse was seen at this stage. Only large bubbles remained, and the process of bubble rearrangement was very slow. PEF remained at the residual foam stage much more than conventional foam, demonstrating the higher stability of PEF compared to foam in the presence of heavy oil.

Considering N85-PEF (Figure 5.10b), its decay profile is almost similar to N85 foam profile. Although polymer slightly increased the lifetime of conventional N85 foam in the presence of heavy oil (from 120 minutes to around 260 minutes), still stability is low such that stage I

(representing the ability of the polymer to postpone the liquid drainage rate) is missing. This result also suggests that to get the maximum effect of polymer in enhancing the stability of foam, proper selection of foaming agents and its combination with the polymer is essential.

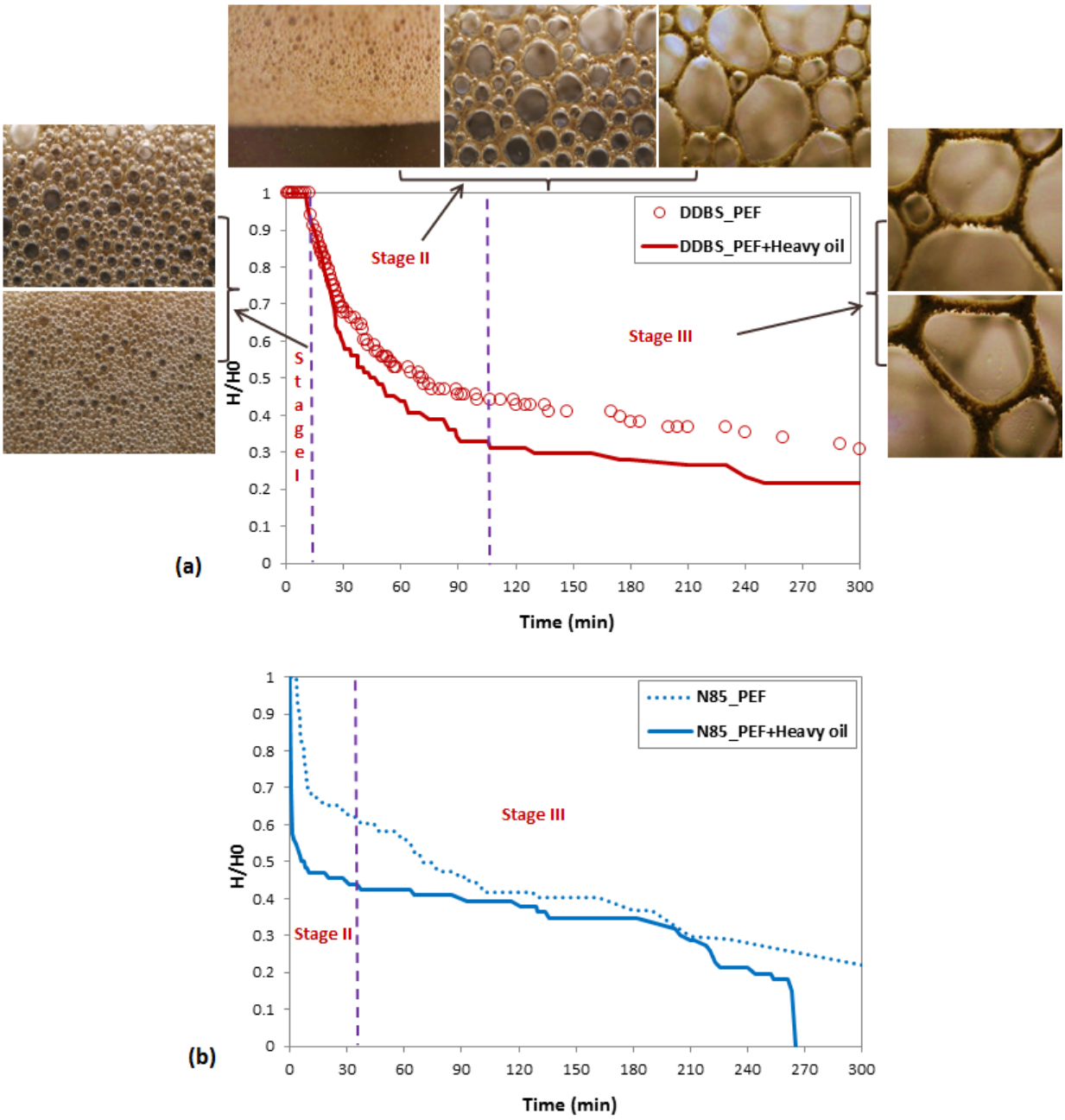

Figure 5.10: PEF decay profile in the presence of heavy oil; (a) DDBS (anionic) surfactant and (b) N85 (nonionic) surfactant; images correspond to DDBS-PEF (5X magnification).

5.3.3 More Insight into Impact of Oil on the Foam Stability

A mixture of gas bubbles and oil droplets are called foamulsions or foamed emulsions Koczo et al., 1992). When emulsion droplets are trapped and jammed between the bubbles may result in stable foamulsions (Rio et al., 2014). The presence of emulsion droplets within the foam structure can slow down the drainage and coalescence (Salonen et al., 2012). During liquid drainage, the aqueous phase and emulsion drops flow together through the foam structure (foam film and plateau borders). However, oil drops drain slower than that of the aqueous phase. This is the reason for increasing the concentration of oil within the lamella in course of time as seen in Figure 5.11. In this study, most of the oil stayed in the foam structure even after the collapse of the majority of foam lamellas. Oil droplet moves within foam lamella in the form of an emulsion (Figures 5.12 and 5.13) and destabilizes a foam system by entering and spreading in the water-gas interface. Oil drop must first overcome the repulsive forces (electrostatic or steric interactions) in the aqueous pseudoemulsion film to destabilize a foam lamella (Nikolov et al. 1986; Manlowe and Radke 1990). Koczo et al. (1992) studied the effect of emulsion on foam stability. Their study on solubilized oil as well as emulsified oil systems showed that later one may improve the stability of foam system while solubilized oil will decrease the foam stability. The packed emulsion droplets (in emulsified oil systems) prevent the liquid drainage through the foam structure due to the increased hydrodynamic resistance.

It is noteworthy that though values of entering (E) and spreading (S) coefficients may give insight into the potential of the oil to destabilize a foam system; however, these coefficients cannot explain the rate of foam destabilization (Manlowe and Radke, 1990; Hadjiiski et al., 2003). Spreading and entering coefficients values are presented in Table 5.2. Oil can spread as a lens over gas/liquid interface when the spreading coefficient S is positive (Ross and Suzin 1985). Similarly, an oil

droplet is predicted to enter the aqueous–gas interface, when the entering coefficient, E, is positive. The S and E coefficients can be calculated by surface tension and interfacial measurement by the following formula (Schramm and Novosad, 1992):

$S = \sigma_{wg} - \sigma_{wo} - \sigma_{og}$

$E = \sigma_{wg} + \sigma_{wo} - \sigma_{og}$

Where σ_{wg}, σ_{og}, and σ_{ow} are surface tension of the foaming solution, the surface tension of oil, and interfacial tension of water/oil interface, respectively.

As shown in Table 5.2, all the surfactants studied here showed a positive entry coefficient, which indicates that oil entry is feasible in all systems. DDBS recorded the lowest spreading and entering coefficients, which is consistent with its highest stability in the presence of oil (Figure 5.6b). Although all surfactants had positive S and E coefficients, they showed decent stability (except N85) in the presence of oil in the static test. Despite positive values of E and S for DDBS surfactant, it showed acceptable dynamic stability during heavy oil recovery. Therefore, the overall foam stability cannot be solely explained by these coefficients, and it may relate to the interfacial and bulk properties of the surfactant as well (Hadjiiski et al., 2003). As long as the pseudoemulsion film is stable, oil droplet can't destabilize the foam by entering the water-gas interface (Nikolov et al. 1986). If the surfactants in the aqueous phase can stabilize foam films then it can be expected that the same surfactants could, but not necessarily will stabilize the pseudoemulsion film as well (Nikolov et al. 1986).

As seen in Figure 5.11, emulsion droplets within the foam lamella destabilize and create a bigger droplet; however, as long as the pseudoemulsion is stable the oil cannot enter into the interface, create a lens, and destabilize the foam lamella.

In addition, the presence of emulsion droplets within the foam lamella affects the stability of the foam. Figure 5.13 shows the emulsion within the foam lamella created by mineral and heavy oil. These images can possibly show the reason for more stable foaming solutions in the presence of mineral oil than that of heavy oil. The presence of the dense assembly of droplets trapped and jammed in between the bubbles increases the local viscosity and reduces the rate of both films thinning and Plateau borders shrinking (Salonen et al., 2012), resulting in a slowing down of the coarsening phenomena (Martinez, et al, 2008). Note that in a higher fraction of oil, there should be enough free surfactant present in water to improve the foam stability (Salonen et al., 2012). However, this is not the case for foam system with the presence of heavy oil. The microscopic images of heavy oil emulsion within the foam lamella demonstrate flocculation of several oil droplets within the lamella. The flocculation eventually results in droplet coalescence and form bigger oil droplet or oil lens, which is detrimental to foam stability. As shown in Figure 5.7b, mineral oil slightly reduced the liquid drainage rate (stage I) and had no drastic effect on foam total life; i.e. N85 foam died after about 5 hours with/without mineral oil.

The polymer can increase the foam stability even in the presence of heavy oil. Studied polymer did not have any significant effect on surface properties of surfactant solutions (Figure 5.5). Therefore, the main reason for increasing the stability of PEF compare to that of conventional foam is an improvement in the stability of liquid films, resulting in stronger oil-resistance ability. Polymer increases the liquid viscosity within the foam lamella and significantly decreases the rate of liquid drainage. As a result, a longer time is required for bubble coalescence and eventually bubble collapse due to the thin foam lamella. Consequently, the polymer enhanced foam last much longer than conventional foam even in the presence of heavy oil. It should be mentioned that the mechanisms involved in oil-foam interaction in bulk could not be extended to porous media.

Table 5.2: IFT value (at 25 °C), entering, and spreading coefficients of studied surfactants in the presence of oils.

Surfactant Solution (0.29 wt.%)	Mineral Oil			Heavy Oil		
	IFT (mN/m)	E	S	IFT (mN/m)	E	S
N85	0.51	7.21	6.19	0.58	10.08	8.92
DDBS	0.33	3.03	2.37	0.54	6.04	4.96
AOS	0.50	4.7	3.7	1.10	7.7	5.7
CTAB	0.16	9.56	9.24	0.90	12.9	11.1

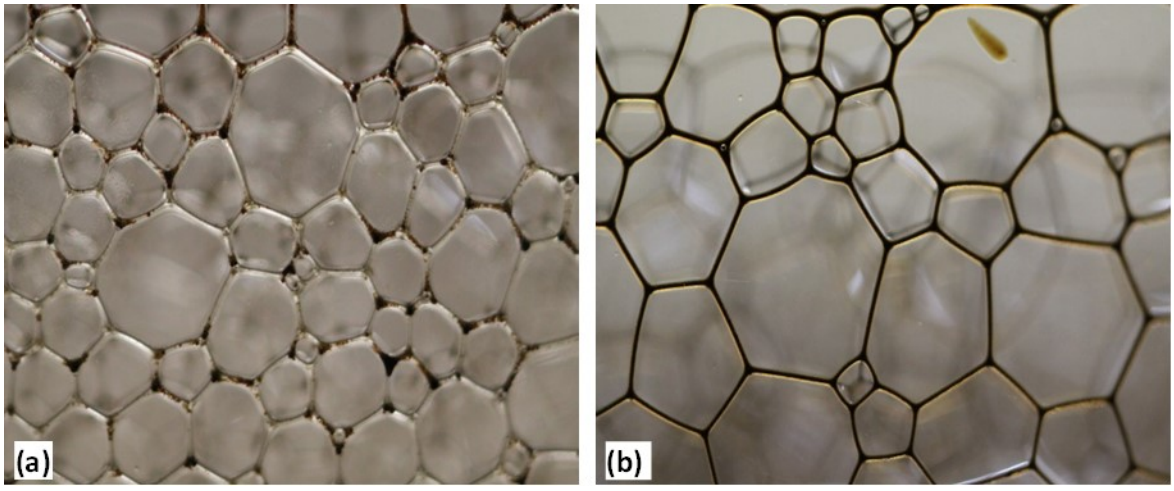

Figure 5.11: Images of foam generated with DDBS surfactant and heavy oil after 3 minutes (a) and one hour (b); oil saturation increased within the lamella over time (foam top, 2X magnification).

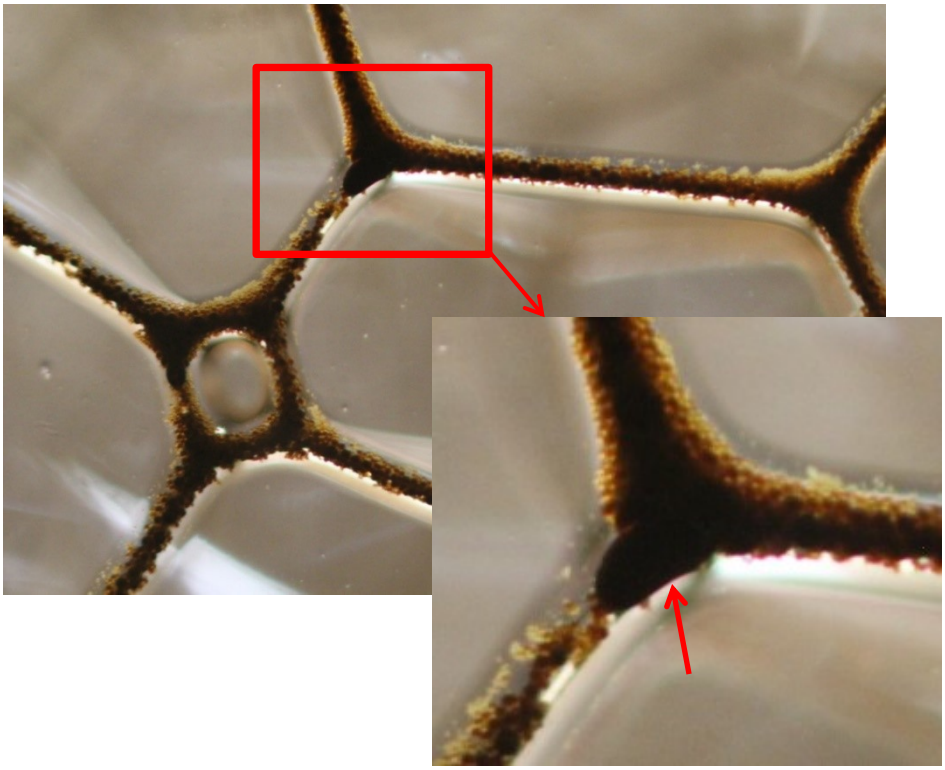

Figure 5.12: Flocculation and coalescence of oil droplets within the foam lamella resulting the generation of oil lenses that eventually destabilize the foam (5X magnification).

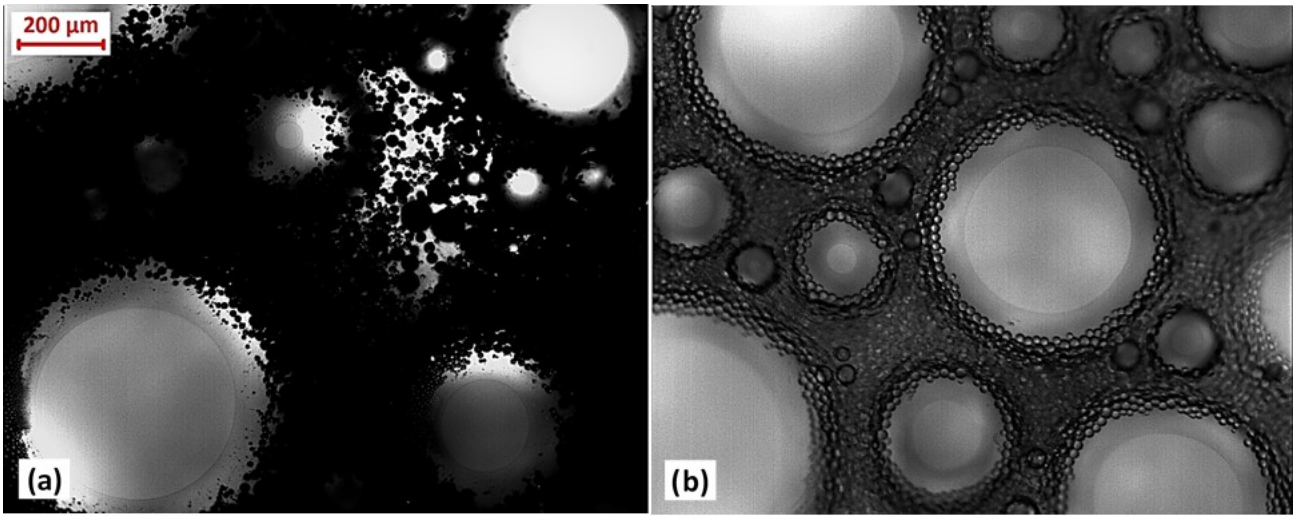

Figure 5.13: Microscopic image of foam-oil systems showing oil emulsion within the lamella (10 X magnification); (a) heavy oil + N85 foam, (b) mineral oil + N85 foam,

5.3.4 Dynamic Performance of Foam and PEF in the Absence of Heavy Oil

The pressure profile during SAG injection in water-saturated sand-pack can be divided into three distinct stages as shown in Figure 5.14. The images of sand-pack at each of the stages are also shown. Because the porous media is not pre-saturated with surfactant and injection method is alternative, relatively long time is required for the foam generation. During this time, surfactant and gas act as separate slugs, (two phases) and foam is not generated. This is characteristic of Stage I. It can be said that the shorter length of Stage I demonstrate the better performance of the solution in terms of generating the foam faster within the porous media. The onset of foam generation coincides with the beginning of Stage II. An abrupt increase in pressure profile during SAG injection represent the generation of foam (Li et al., 2010). During Stage II, the foam is generated and propagated trough porous media and results in an increase in the pressure drop. The slope of this stage shows how fast the foam can propagate within the porous media and it can be used as criteria for comparing the performance of the foaming solutions. At the end of Stage II, foam occupied the whole length of sand-pack and the pressure drop will remain constant; this is the onset of Stage III. This stage can be termed as steady state foam injection. Pressure drop remains constant during Stage III; however, there might be some fluctuations in pressure drop. Small pressure drop fluctuations during this stage demonstrate the temporary channeling or collapse of foam which will be recovered at the end of same slug or the next successive slug injection. The sand-pack images (Figure 5.14) show the foam-channeling phenomenon during stage III. Less channeling with lower pressure drop fluctuation can be used as criteria to compare the dynamic stability of the generated foam within the porous media.

The onset of foam generation, Stage II of an abrupt increase in pressure profile, is different for all studied foaming solutions studied here (Figure 5.15). N85-foam had the weakest performance

during flow through water-saturated sand-pack. Stage III was not observed for N85-foam even after the injection of 9 PV of SAG. In addition, the large local pressure drop can be seen during its propagation demonstrating the low stability of the foam. Although the addition of polymer could not accelerate the N85 foam generation/propagation, it increased its dynamic stability during N85-PEF injection. Pressure drop fluctuations were very low during N85-PEF propagation. Stage III was observed after ~ 7 PV of injection (Figure 5.15). These features of N85-PEF compared to that of N85-foam represent its high dynamic stability within the water-saturated porous media. Moreover, polymer accelerated the foam generation and propagation for DDBS surfactant solution flow through water-saturated porous media. It increased the stability of foam by decreasing pressure fluctuations (Figure 5.15).

Mobility reduction factor (MRF) of foam and PEF has a direct relationship to its pressure drop in porous media. Higher values of the MRF (or pressure drop) indicate the foam is more finely textured and stronger. If the foam is very strong, the MRF is higher and for weak foams, the MRF values are smaller (Kovscek, 1998). Both foam and PEF showed much higher MRF/pressure drop than that for DDBS-surfactant-polymer (SP) injection. The large pressure difference between SP solution and the corresponding PEF represents the excellent mobility control potential (by increasing apparent viscosity) of PEF for heavy oil recovery, especially in heterogeneous reservoirs by diverting the fluid toward low permeability zones or unswept zones due to unfavorable mobility contrast (Telmadarreie and Trivedi, 2015 and 2016).

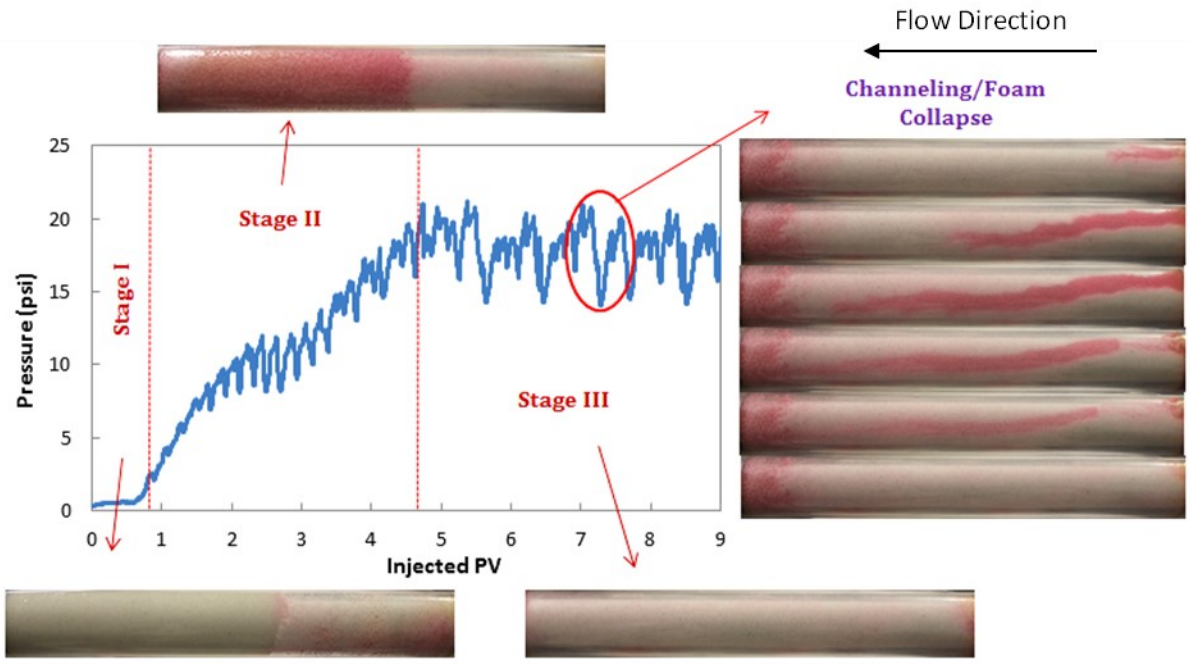

Figure 5.14: Typical profile of pressure during SAG injection in water-saturated porous media. Red and white colors show the existence of liquid and foam, respectively.

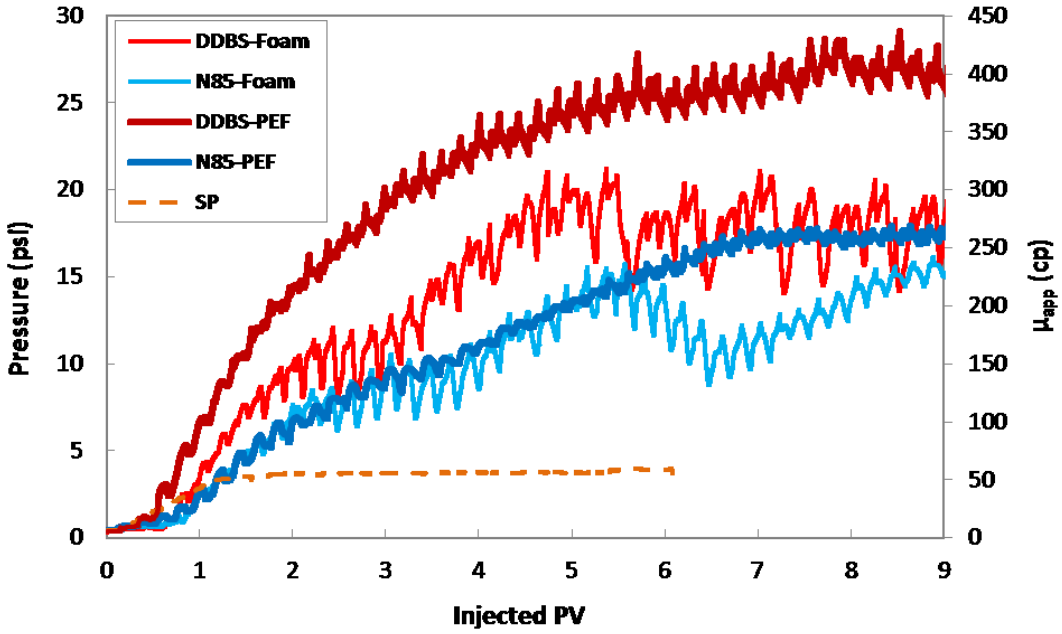

Figure 5.15: Foam, PEF, and SP pressure/apparent viscosity profiles during flow through water-saturated sand-pack.

Figure 5.16 shows the sand-pack images during N85-foam and N85-PEF injection in water-saturated media. Red color represents the liquid while the white color is for CO_2 foam or gas. Higher saturation of red color during N85-PEF injection represents higher liquid content (i.e. lower foam quality) of PEF compared to that of N85-foam. During dynamic condition, PEF channeling, if happened, was smaller and recovered fast. Nevertheless, during N85-foam injection, larger channeling representing the collapse of foam was evident and abundant, representing the lesser dynamic stability of foam compared to that of PEF. Similar behavior was observed during DDBS foam and PEF injection (results are not presented here). It is worth mentioning that, according to the injection rates of liquid and gas in this study, the generated foam in the porous media are wet foam with relatively high liquid content. Therefore, the behavior presented here is representative of wet foam performance in porous media.

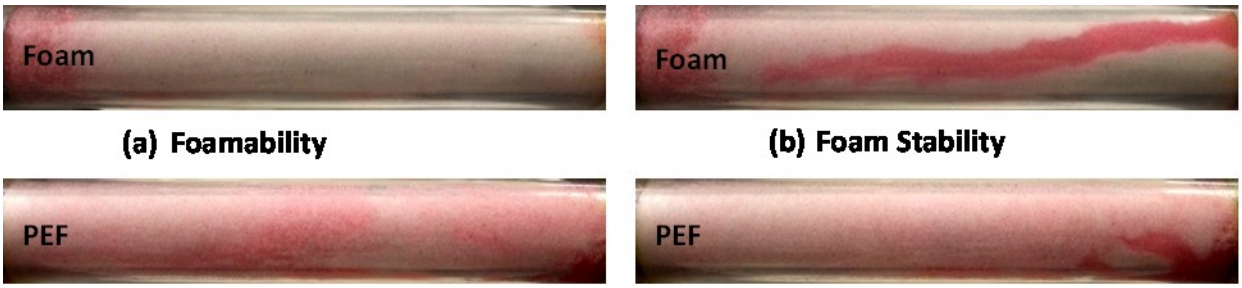

Figure 5.16: (a) Foamability and (b) foam stability of N85 foaming solution in a dynamic condition; PEF showed lower foamability, but higher stability (less channeling) than that of foam.

5.3.5 Dynamic Performance of Foam and PEF in the Presence of Heavy Oil

In this section, foam and PEF flooding were conducted by alternate injection of foaming solution and CO_2 gas in the heavy oil saturated porous media. Anionic DDBS and nonionic N85 surfactants were selected for foam and PEF injection in dynamic experiments in the presence of heavy oil. All the flooding experiments were performed after reaching water cut of ~98% during water flooding

(residual oil saturation was 66 ±1 %) i.e. residual oil saturation condition to imitate the tertiary recovery process.

Figure 5.17 shows the pressure and apparent viscosity profiles of foam and PEF propagation in heavy oil saturated sand-pack for different foaming solutions. It is worth mentioning that the trend in pressure profile seen in this study is valid for the similar experimental condition (i.e. injection mode and foam quality).

The first peak in pressure profile is due to the development of the oil bank through porous media and then its production. The corresponding oil-cut is in its highest value at this time. Heins et al. (2014) also made similar observations. At the same experimental condition of permeability, core dimension, flow rate, and viscosities of oil and foaming solution, the observed pressure drop could have a direct relationship with the quality of the generated foam or PEF at this stage. Higher pressure drop represents higher apparent viscosity of foam or PEF within porous media. At the initial stage of foam injection, bubbles first entered larger pore channels with lower entrance capillary pressure and the foam texture is coarse. Then, the local pressure gradient increased because of the increased foam flow resistance, and therefore foam bubbles entered relatively small pore channels (Farshbaf Zinati et al., 2007). The foam flow repeated this process until the steady state was reached. The pressure drop increased, and the foam texture became finer as foam entered smaller pore channels because the porous media shaped the foam (Ettinger and Radke, 1992).

Per Figure 5.17, strong PEF was generated and started to propagate in the case of DDBS-PEF case. This can be explained by high-pressure drop at the early time of injection. However, this is not the case for N85-PEF.

For detailed analysis, foam/PEF pressure drop, change of residual oil saturation, oil-cut, and images of porous media at different injected pore volume are plotted in Figure 5.18. Comparing

DDBS foam with N85-PEF, although the later one could produce a significant amount of residual heavy oil at oil bank production (about 55% at 1.5-2 PV, Figure 5.18a), the strong PEF propagation did not start immediately. On the other hand, DDBS foam produced much less oil at the same time (about 23%) while the strong foam propagation started much faster than that of N85-PEF. Therefore, the higher oil recovery/lower oil saturation after oil bank production cannot guarantee the rapid propagation of strong foam/PEF. The average oil saturation in the porous media when strong foam/PEF started to propagate is also shown in Figure 5.18 (dashed lines).

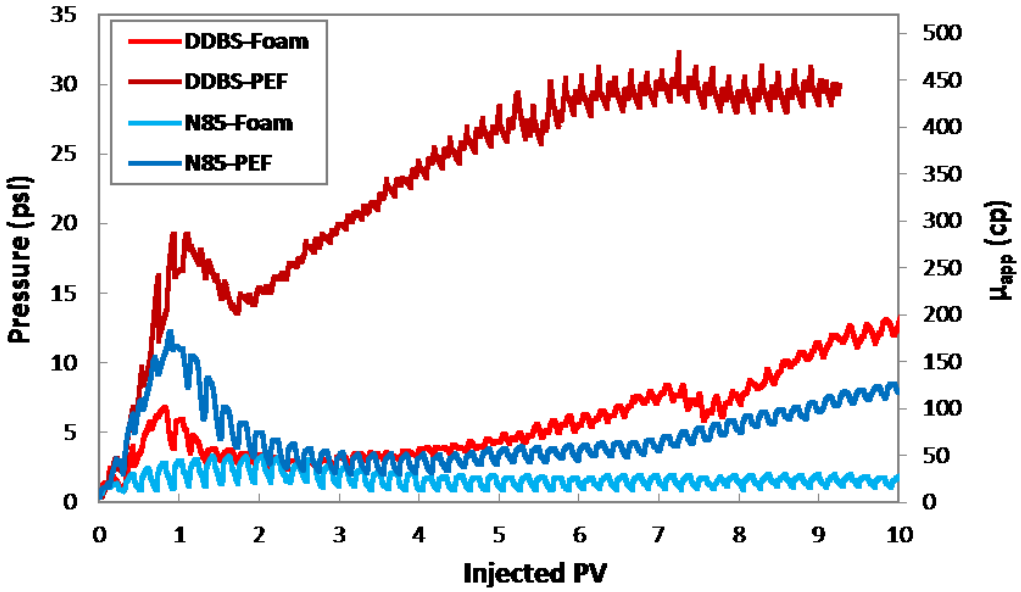

Figure 5.17: Pressure profiles and apparent viscosity during foam and PEF flow through heavy oil saturated sand-pack.

Change in oil saturation is represented as percent of original oil in place. After water flooding, the remaining oil saturation in the sand-pack was around 66%. Since the water saturation also affects the performance of the foam/PEF, all the tertiary recovery (foam/PEF) were performed around similar water saturation (Zanganeh et al., 2011). The weak foaming solutions resulted in a lower apparent viscosity of foam within porous media. For N85 surfactant solution, foam generation was unsuccessful up to 10 PV of SAG injections. After oil bank production, the rate of foam collapse

may have been much higher than that of foam generation that resulted in no pressure build up and therefore stable foam did not propagate through porous media. The addition of polymer into N85 surfactant solution slightly increased the apparent viscosity and resulted in N85-PEF propagation. On the other hand, in the case of DDBS foaming solution, foam could generate and propagate through porous media faster than N85-PEF. This again shows the importance of selecting a proper foaming agent. In addition to a strong foaming agent, polymer significantly improved the foam propagation through heavy oil saturated porous media. Considering DDBS-PEF curve, PEF started to propagate right after oil bank production. It reached to steady state foam injection where almost entire sand-pack was occupied by PEF. At this point, the pressure drop value should be almost similar to that of water-saturated sand-pack at steady state (stage III) (Figures 5.15 and 5.17). The pressure fluctuation at this time is less for DDBS-PEF demonstrating the higher stability of PEF in the presence of heavy oil.

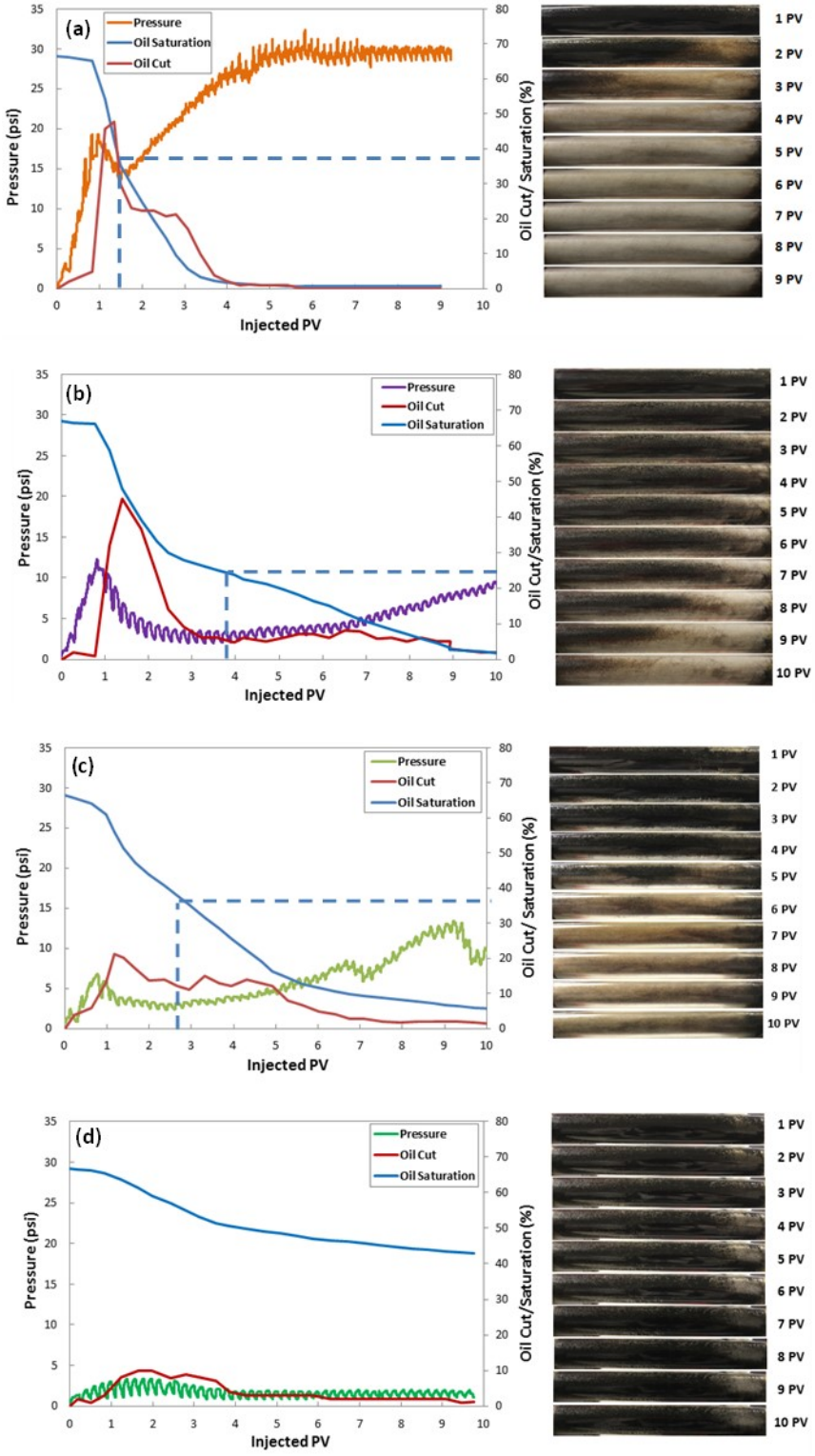

Figure 5.18: Pressure, oil saturation, and oil-cut profiles during heavy oil recovery by foam/PEF; (a) DDBS-PEF, (b) N85-PEF, (c) DDBS-foam and (d) N85-foam. Dotted lines show the oil saturation in which strong foam/PEF begins to propagate.

Visual observation of the sand-pack (Figure 5.18) showed that oil appeared to move with the passage of gas bubbles while it had very little movement during liquid injection. These observations are in accordance with results of Li et al. (2010).

It is worth mentioning that foam generation in the heavy oil saturated porous media with residual oil saturation is not similar to that of water saturated. The foam is generated in the areas with lower oil saturation, and then it propagates to the other area and eventually sweeps the porous media. For a comparative view on the value of average oil saturation when the foam or PEF starts to propagate, the end of oil bank production can be considered as a time for foam or PEF propagation in the presence of residual heavy oil. At this point, the pressure decreases due to the oil bank production and again build up because of the strong foam propagation. The saturation of oil at this point can be called the average oil saturation where a strong foam or PEF can start to propagate through porous media. This saturation for DDBS foam is ~ 37%, whereas for N85-PEF is ~ 25 %. DDBS-PEF started to propagate at ~38% oil saturation; however, no decrease in pressure profile was observed after oil bank production, suggesting that DDBS-PEF could also be stable and propagate at higher oil saturations. As a result, overall sweep efficiency is improved. Visual images of sand-pack confirm this finding. During DDBS-PEF injection most of the oil was displaced after 3.5 PV and piston-like displacement was observed (Figure 5.18a).

The total heavy oil recovery profiles during water, foam, and PEF flooding are shown in Figure 5.19. Initial waterflood recovery was 33±1 % for all experiments at 98% water-cut. The DDBS-PEF had the best performance during heavy oil recovery (total recovery factor of ~ 98 %,) while N85-foam had the lowest recovery among all cases (~ 57 %). The ultimate oil recovery of DDBS foam (~ 98 %) was slightly higher than N85-PEF (94 %). DDBS foam swept almost equal amount of heavy oil as N85-PEF without the addition of any polymer.

Images of typically produced oil samples from foam or PEF flooding are also shown in Figure 5.19. Emulsified oil was observed from the effluent. The early produced samples mainly contain water and some oil droplets. The produced oil at this stage is emulsified oil droplet. At end of stage I when the developed oil bank is produced, the samples consisted of a water-in-oil emulsion and free CO_2 gas. After that, the oil was produced in form of oil-in-water emulsion with gas bubbles. The produced foam during PEF injection demonstrated much higher stability compared to that of foam. In addition, produced foam was denser and cleaner during PEF flooding.

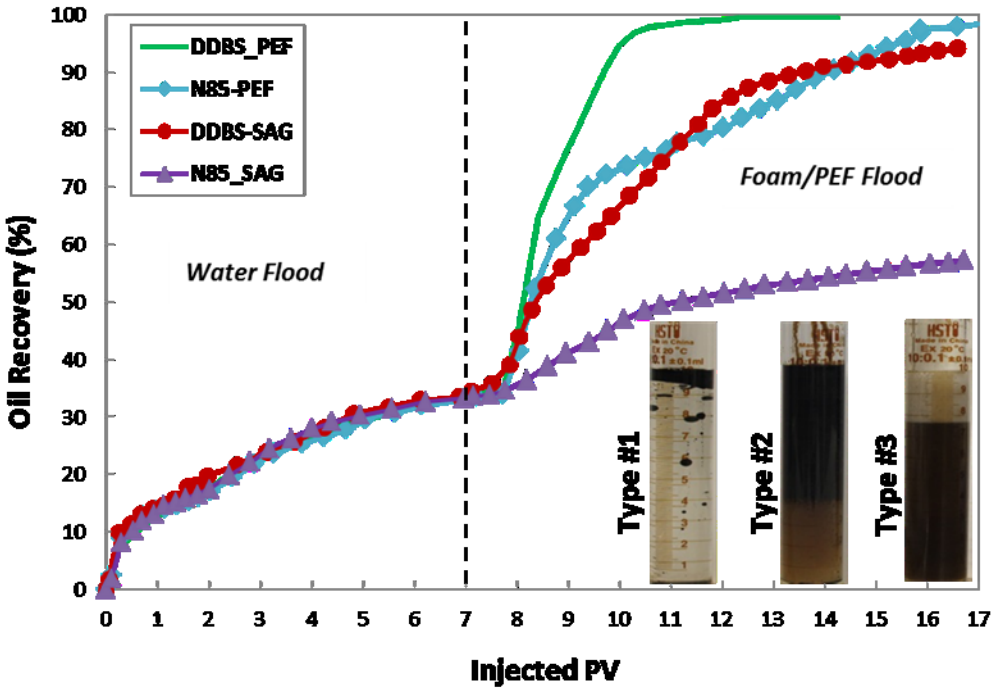

Figure 5.19: Total heavy oil recovery profiles during water and foam/PEF flooding with different foaming solutions. The images show the typical of foam/PEF flooding effluent samples after the water flood; Type #1: oil-in-water emulsion, Type #2: water-in-oil emulsion and free gas, and Type #3: water-in-oil emulsion and foam.

Overall, DDBS-PEF showed the best performance in both static and dynamic experiments in the presence of heavy oil. DDBS-PEF was also injected with the co-injection mode to see any further

improvement in dynamic performance for heavy oil recovery. Injection pressure and oil recovery profiles of DDBS-PEF injected with alternate and co-injection methods are plotted in Figure 5.20. Oil bank development and production are similar for both injection modes; however, the rate of PEF propagation was lower in the case of co-injection as shown by the slope of the curve. As shown before, the rate of foam propagation has a direct relationship to the rate of oil production. This can be seen comparing oil recovery profiles in Figure 5.20. The separation in pressure curves in Figure 5.20 firstly appeared after about 2 PV injections. The similar trend can be seen in oil recovery profile, demonstrating a strong relationship between foam propagation and oil production rates. Although ultimate oil recovery was the same for both injection modes, alternate injection generates PEF and produced oil faster than the co-injection mode. Furthermore, alternate injection could generate stronger foam with a higher apparent viscosity (pressure profile) compared to that of co-injection mode, resulting in better mobility control and sweep efficiency.

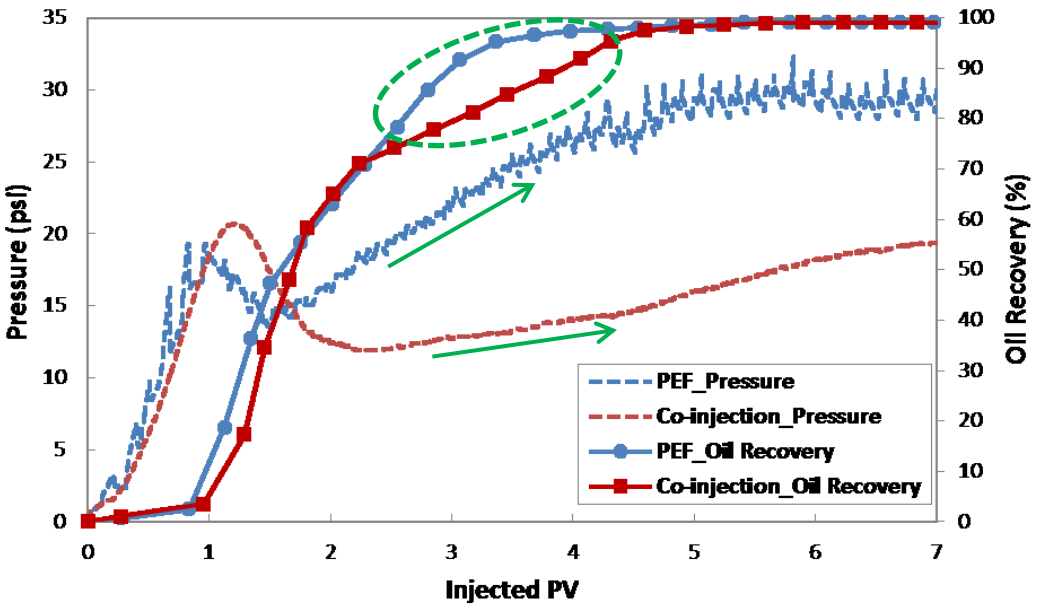

Figure 5.20: Heavy oil recovery and pressure profiles during DDBS-PEF flooding: alternate and co-injection modes. Highlighted areas represent the effect of PEF propagation rate (arrows) on oil production profile.

5.4 Summary

This chapter investigated the potential of foam and PEF for increasing heavy oil recovery. Static and dynamic experiments were designed and conducted to obtain new insight into the performance of foam and PEF for heavy oil recovery. Although the physics of foam in bulk and porous media are rather different, the results from the detailed static analysis are essential to predict the performance of foaming solution for the heavy oil recovery.

- The selection of foaming agent plays a key role in the performance of PEF for heavy oil recovery. However, the addition of polymer to a weak foaming agent (e.g. N85 surfactant in this study) may enhance the performance of foam in the presence of oil in dynamic experiments.
- Entering and spreading coefficient values are required for oil-foam interaction discussion but may not be enough. Pseudoemulsion film stability should be considered to support the results of foam stability.
- The porous media experiments showed better performance of PEF in the presence of heavy oil compared to that of foam. The addition of polymer to the good foaming solution accelerated the foam generation and increased its stability in heavy oil saturated porous media. DDBS-PEF produced ~ 98% of residual oil saturation while this value was ~ 78% for DDBS-foam after 3.5 PV injections.
- PEF showed higher resistance to heavy oil compared to that of conventional foam. It can be generated in higher oil saturation and could be a good option for EOR method after water flooding in heavy oil reservoirs, where the residual oil is relatively high.

- The rate of strong foam propagation after oil bank production has a direct relationship with the rate of oil production. Alternate injection of foaming solution and gas showed better performance for sweeping heavy oil compared to that of co-injection mode.
- Overall, both static and dynamic performances of foam and especially PEF showed their potential as a displacing fluid for enhanced heavy oil recovery.

Chapter 6: CO_2 Foam and Polymer Enhanced Foam for Heavy Oil Recovery and CO_2 Sequestration: Homogenous and Fractured Core Samples

6.1 Introduction

With growing concerns about climate change and CO_2 emission, sequestration of CO_2 in EOR operations has been recognized as one of the most practical means of reducing CO_2 emissions into the atmosphere. CO_2 EOR and sequestration lower the cost of CO_2 sequestration by recovering incremental oil, which is more attractive in mature oilfields. Western Canadian Sedimentary Basin (WCSB) where many oil pools are near depletion can be one of the favorable CO_2 sequestration targets where the most of the required infrastructure is already in place (Moritis, 2000 & 2002; Shaw and Bachu, 2002). It is worth mentioning that because of several technical and economic reasons, not all oil reservoirs are suitable for CO_2 EOR and sequestration. Besides screening for EOR suitability, oil recovery, and CO_2 sequestration capacity, other economic criteria should be considered for a successful CO_2 EOR and sequestration project (Shaw and Bachu, 2002). Per basin and regional-scale suitability study performed by Bachu and Steward (2002), WCSB is generally suitable for geological sequestration of CO_2 including EOR. However, determining the oil recovery and capacity for CO_2 sequestration should be performed individually for each reservoir. Since 1990's CO_2 sequestration has been performed on a large scale in Norway and more than 35 million tons of CO_2 has bee injected into the hydrocarbon reservoirs during the CO_2 EOR process (Moritis, 2002). Weyburn CO_2 project (located in Saskatchewan, Canada) is also one of the successful projects in both CO_2 EOR and sequestration (Malik and Islam, 2000).

Although CO_2 EOR has proven to be an effective method for some reservoirs, the low viscosity and therefore high mobility of the injected CO_2 leads the poor sweep efficiency, especially in heterogeneous and/or heavy oil reservoirs. Foam injection can improve the sweep efficiency compared to conventional gas injection (Rossen, 1996). The foam EOR application is particularly suited for heterogeneous reservoirs as foam selectively reduces the mobility of high permeable zones more effectively (Lake, 1989; Alkan et al., 1991; Rossen, 1996; Haugen et al., 2012), and it is a field scale proven technique at immiscible and miscible conditions (Henry et al., 1996; Holm and Garrison, 1988; Stevens et al., 1992; Sanders et al., 2012).

Haugen et al. (2012) studied foam flow in fractured limestone core samples for EOR purpose. They found that in-situ generation of foam in such fractured core sample was not feasible. On the other hand, the pre-generated foam could increase the oil recovery significantly but only after the significant amount of injection. Farajzadeh et al. (2010) studied a foam model in a fractured reservoir to increase matrix oil recovery. They found that very strong foam is required to create enough pressure drop which can result in oil recovery from the matrix. Haugen et al., (2014) investigated the foam performance on mobility control and EOR in fractured oil-wet carbonate rocks. Per their experimental results, the miscible injection of CO_2 foam had significantly increased the oil sweep efficiency than that of immiscible injection of N_2 foam. Also, with the help of CT-scan, they observed that a limited amount of gas could invade into the matrix during immiscible foam injection, and matrix oil mainly displaced by the invasion of the surfactant.

Several studies performed to investigate the potential of foam for EOR (Nikolov et al., 1986; Farajzadeh et al., 2010; Li et al., 2010; Ashoori et al., 2012; Simjoo et al., 2012; Haugen et al., 2012 & 2014; Telmadarreie and Trivedi, 2016). Although CO_2 EOR and sequestration process have been studied before (Malik and Islam, 2000, Ghomian et al., 2008; Dai et al., 2014), but no

study has been performed on the potential of CO_2 foam and especially CO_2 polymer enhanced foam (PEF) for both EOR and CO_2 sequestration. Therefore, this chapter presents the experimental results on the potential of CO_2 foam and CO_2 PEF for relatively viscous oil recovery from homogeneous sandstone, fractured sandstone, and fracture carbonate core samples focusing on the effect of heterogeneity and polymer addition. Furthermore, the potential of the CO_2 sequestration is also investigated in the core samples representing both homogeneous and heterogeneous (fractured) reservoirs.

6.2 Experimental

In this section, the material and experimental procedure used in this study are explained. This experimental study follows three main goals: (1) compare the oil recovery efficiency of foam and PEF in both homogenous and fractured cores (2) investigate the potential of CO_2 foam and CO_2 PEF for CO_2 sequestration (3) analyze the effect of polymer addition and heterogeneity on the performance of foam for both EOR and CO_2 sequestration.

6.2.1 Fluid Properties

A relatively heavy oil, sampled from a Canadian oil reservoir, with the viscosity of 670 cp (at 22 ˚C) was used for core flooding experiments. Water saturation and water flooding were performed with 1000 ppm brine solution (NaCl). Surfactant and polymer used in this study were Na-DDBS (1500 ppm) and Flopaam 3330S (1000 ppm), respectively. Both foam and PEF solutions were generated with 1000 ppm brine solution. It should be mentioned the stability of foam generated with the surfactant and the polymer used in this chapter was analyzed in Chapter 5.

6.2.2 Rock Samples

Rock samples (sandstone and carbonate) were outcrop sampled from the same block to avoid any significant change in rock properties (e.g. porosity and permeability). Both sandstone core (Buffed

Brea) and carbonate core (Indiana limestone) were 6 inches and 2 inches in length and width, respectively. The fractured core sample was prepared from the same cores and cut in length with 3 mm saw blade. Figure 6.1 shows the images of homogenous and fractured core samples. In the case of fractured carbonate core, the matrix is also heterogeneous as seen in Figure 6.1b.

(a) Sandstone rock sample (b) Carbonate rock sample

Figure 6.1: Images of core samples (Sandstone and carbonate) used in this study.

6.2.3 Foam Generation

A foam generator was designed and used for foam injection in this study. The foam generator was made of glass beads with 40-70 mesh sizes (210-400 microns) packed inside a metal tube (4 inches and 3/8 inches in length and width, respectively). Both sides of the tube were sealed with 120 mesh size (125 microns) screens. The schematic of foam generator is shown in Figure 6.2. The foaming solution was first injected into the foam generator to minimized chemical absorption. Thereafter, foam/PEF solution and CO_2 gas were co-injected and generated foam/PEF was visualized after the foam generator to inspect the quality of foam before entering to the core samples.

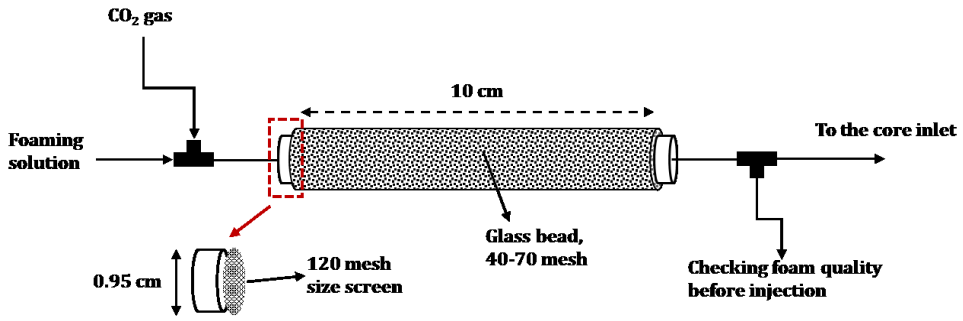

Figure 6.2: Schematic of foam generator used for pre-generated foam/PEF injection.

6.2.4 Experimental Procedure

The dried core plugs were vacuumed overnight and porosity was determined by brine saturation and material balance calculation. Matrix permeability of core samples was also calculated by Darcy's law during injection of brine at constant flow rates (at least 5 different flow rates). Thereafter, heavy oil was injected into the core overnight to reach residual brine saturation condition (at least 5 pore volume of heavy oil was injected in each experiment). Next, water flooding (1000 ppm brine solution) was performed for about 2.5 PV corresponding to water cut of 98%. CO_2 foam/PEF was injected after waterflood as a tertiary EOR method for heavy oil recovery. A mass flow controller was used for accurate CO_2 gas injection in the experimental condition. Pre-generated foam/PEF was injected into the core with the help of a foam generator explained before in this chapter. The quality of generated foam/PEF was kept constant during all experiments (80 %). Each experiment was also followed with 1-1.5 PV of chase waterflood to observe any further liquid/gas production.

Figure 6.3 shows the detailed schematic of core flood system used in this study. A custom designed glass phase separator was used to separate the produced liquids from CO_2 gas. CO_2 gas, water, and

oil samples were measured continuously at effluent samples for further analysis. Produced CO_2 gas was measured continuously with the help of mass flow meter connected to the data acquisition system. The pressure was also measured at different sections of the core as seen in Figure 6.3 (inlet, 2" and 4" from the inlet, and outlet). The inlet/outlet sections of the core holder have networks of flow paths (Figure 6.3a) for effective injection of fluid into the core sample which is more important in the case of the fractured core to ensure the injected fluid is in contact with both matrix and the fracture. It should be mentioned that the back pressure was set to 150 psig during all steps of each experiment. Also, confining pressure was always 150 psig above the injection pressure and the experiments were performed at room temperature (about 22 ˚C). A total of five core flood experiments (three fractured and two homogenous core samples) was performed and the experimental parameters are represented in Table 6.1.

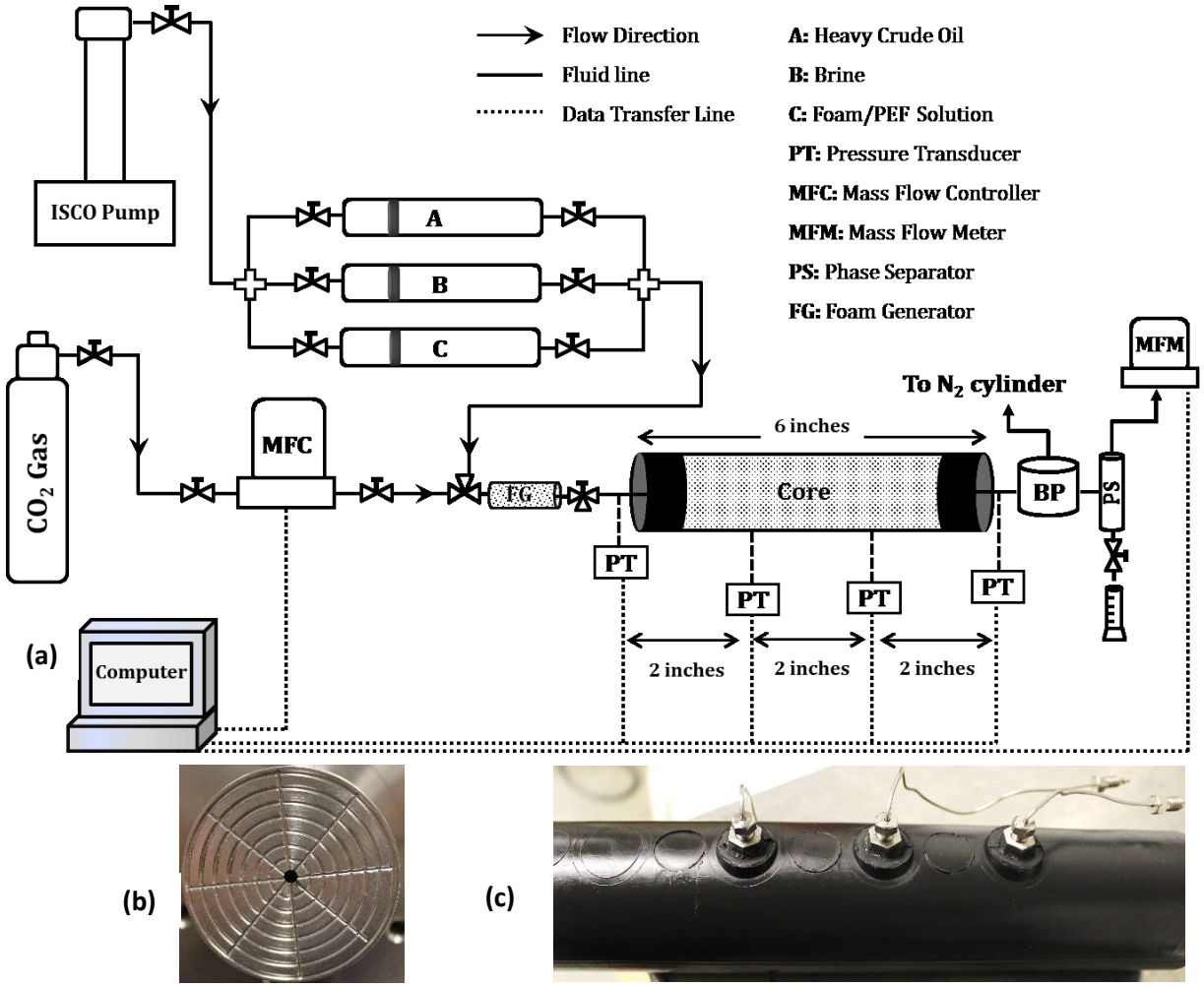

Figure 6.3: (a) Schematic of core flood system used in this study, (b) image of the injection port, and (c) rubber sleeves with three pressure taps for pressure measurement along the core length.

Table 6.1: Summary of core properties and injection parameters.

EOR method	Core type	Fractured?	Matrix Ø (%)	Matrix K (D)	Flow rates (cc/min)			µoil (cp)	Soi
					qw	ql	qg		
CO_2 Foam	Sandstone	No	24.3	0.27	0.25	0.25	1	670	82.7
CO_2 PEF	Sandstone	No	23.6	0.22	0.25	0.25	1	670	82.2
CO_2 Foam	Sandstone	Yes	24.4	0.25*	0.25	0.25	1	670	76.7
CO_2 PEF	Sandstone	Yes	24.1	0.25*	0.25	0.25	1	670	70.8
CO_2 PEF	Carbonate	Yes	20	0.2*	0.25	0.25	1	670	70

*Average matrix permeability

6.3 Results

This section describes the experimental results in detail focusing on the performance of the injected fluids within the porous media. Pressure along the length of the core sample, liquid production, and CO_2 gas production were recorded for further analysis to investigate the potential of CO_2 foam for heavy oil recovery and CO_2 sequestration which will be analyzed in the discussion section. It should be mention that in all experiments flooding was performed in the following sequence: 1) waterflood, 2) CO_2 foam/PEF flood, 3) extended waterflood (EWF).

6.3.1 Homogenous Sandstone Core

6.3.1.1 Waterflood

Two tests were performed on homogeneous sandstone core samples. Typical pressure and water cut profiles during water flooding in homogenous core sample are shown in Figure 6.4. During water flooding, at first, pressure increased to push the heavy oil in the pores towards the production. Then pressure started to drop when the oil produced and the pressure dropped drastically when the water breakthrough occurred. In this case, the breakthrough happened around 0.2 PV. When the pressure reaches a plateau (in this case after about 0.8-1 PV) the water cut will be at its maximum value and there will be no significant oil production afterward.

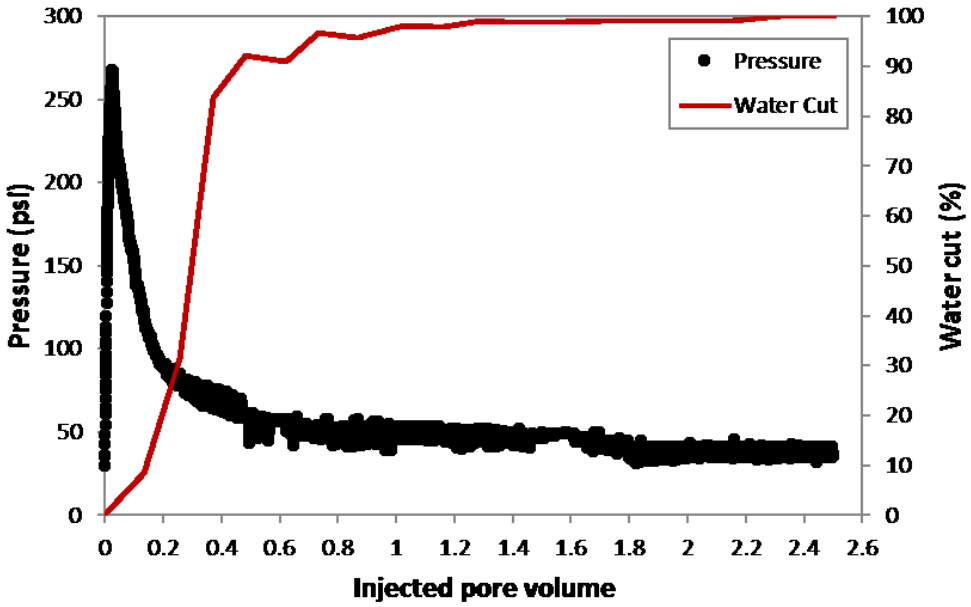

Figure 6.4: Pressure profile and water cut during water flooding in a homogeneous core sample.

6.3.1.2 CO_2 foam/PEF flood

CO_2 foam and CO_2 PEF were injected into the homogeneous sandstone core saturated with heavy oil as a tertiary recovery method (after waterflood). However, their performances were quite different in terms of pressure profile as shown in Figure 6.5. Let's first consider the profile of pressure in foam injection. At early time of foam injection, the overall pressure drop increased rapidly (0-0.2 PV) as the injected fluid contacted the heavy oil in porous media. Then the pressure slightly and gradually increased between 2-8 PV interval. This interval is foam propagation stage where the foam is moving within the porous media as seen in Chapter 5. The slope of the pressure curve represents how fast foam can propagate which can be hindered due to the negative effect of oil. After about 8 PV, the foam propagated in much slower rate. Oil started to produce after about 3.5 PV of foam injection (early time of foam propagation) resulted in pushing some untouched oil (during waterflood) to move toward the core outlet. At about 10.5 PV, the pressure at first section of the core (2 inches from the inlet) started to increase showing that a strong foam front was

reached at this section. Oil production increases with foam propagation and up to 12 PV of injection, strong foam front could not reach to the end section of the core per the pressure drop. However, the foam was produced at the outlet along with oil as showing in the Figure 6.5a.

In the case of CO_2 PEF flooding, the pressure profile is different (Figure 6.5b). On the contrary to the foam pressure profile, PEF injection pressure increased rapidly up to 1-2 pore volumes and then it started to decrease slightly and reached a platform after about 7-8 pore volumes. The increase in pressure at early injection of PEF was due to the oil bank movement as can be inferred from the oil recovery profile. Moreover, foam front moved much faster in the case of PEF at it reached to the second section of the core after about 2 PV of injection per pressure profile. PEF is more stable than conventional foam in the presence of heavy oil (see Chapter 5). Therefore, it is more efficient in sweeping the oil. It should be mentioned that the performance of foam and PEF in a homogenous rock sample agrees with the previous results obtained in the homogeneous sand-pack study during foam and PEF injection for heavy oil recovery (see Chapter 5). Moreover, per visual observation of effluents, the amount and stability of PEF bubbles produced at the outlet were higher than that of foam showing the higher stability of PEF in the presence of oil than that of conventional foam. In the case of foam, most of the gas was produced as a free gas rather than bubbles.

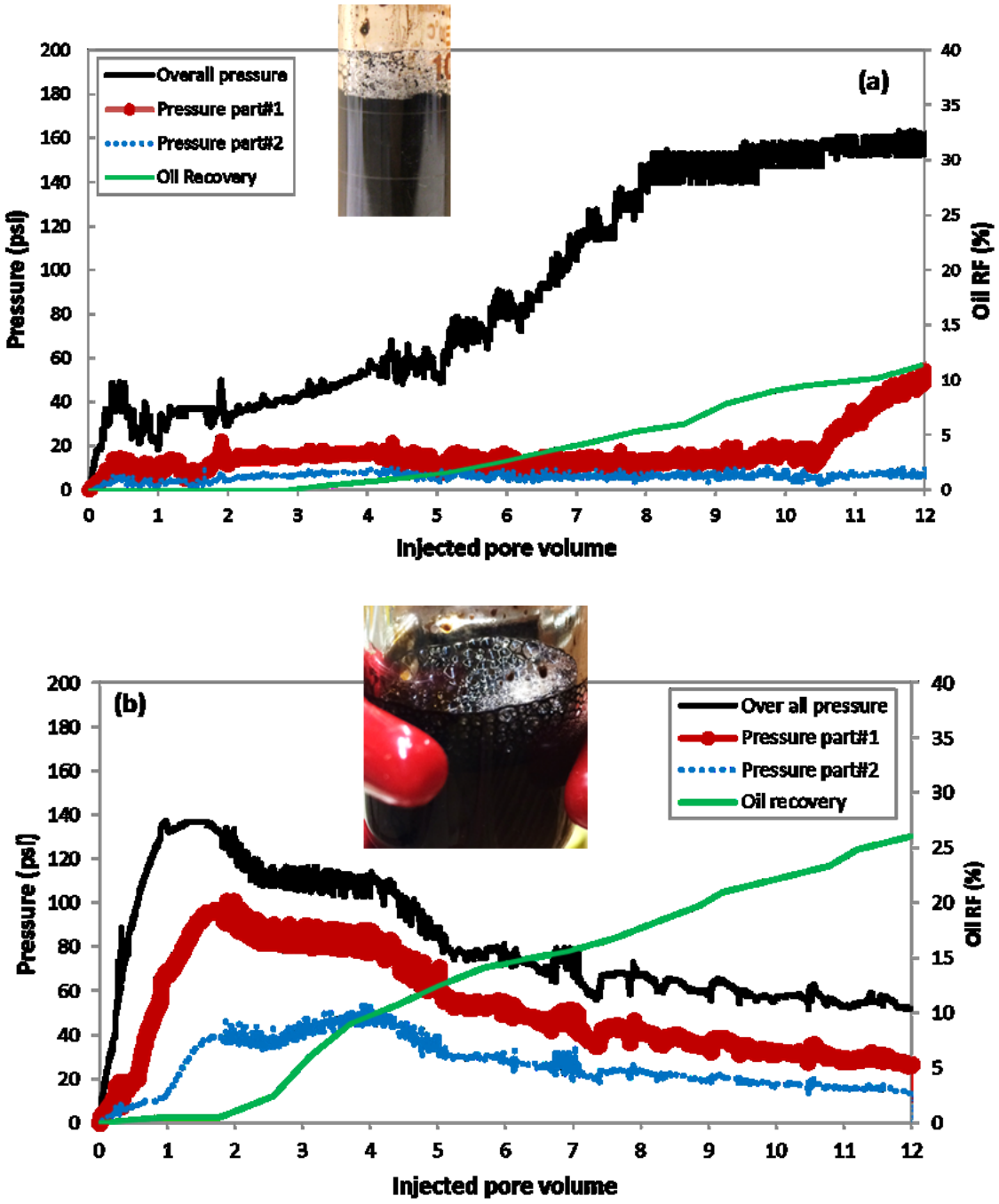

Figure 6.5: Differential pressure profile and oil recovery during injection of Foam(a) and PEF (b) for heavy oil recovery in homogeneous sandstone core. Part#1 and part#2 are 2 inches and 4 inches away from the inlet section, respectively.

6.3.2 Fractured Cores: Sandstone and Carbonate

The performance of both waterflood and CO_2 foam/PEF flood is quite different in the fractured core samples compared to that of homogeneous samples. It should be mentioned that the pressure transducers were located at maximum distance from the fracture and deep into the matrix. So, any change in pressure in the core section can be detected if it is high enough to reach deep into the matrix.

6.3.2.1 Waterflood

There was no increase in overall pressure drop along the fractured core sample during water flooding (Figure 6.6) as water mainly flowed through the fracture. Per water cut profile, the injected water push and produced the oil in the fracture up to about 0.3 PV. After that, the water cut was always more than 90% and no significant oil recovery was observed.

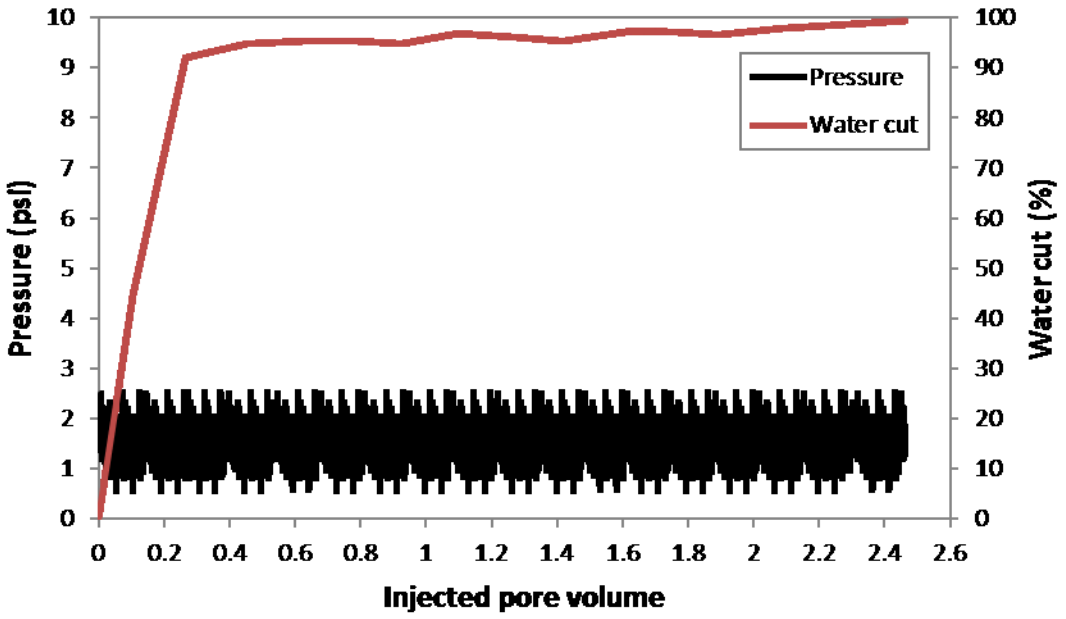

FF:

Figure 6.6: Pressure profile and water cut during water flooding in a fractured core sample.

6.3.2.2 CO_2 foam/PEF flood

Both CO_2 foam and PEF injections could not increase the pressure drop in a fractured core sample. However, they resulted in additional oil recovery after waterflood (Figure 6.7). It should be mentioned that after about 10 PV of injection, PEF pressure profile started to increase which was not the case during foam flooding. The oil cut profiles also show that PEF could produce slightly more oil than that of foam injection. The additional oil recovery can be due to the fluid diversion into the matrix which will be discussed later in this chapter.

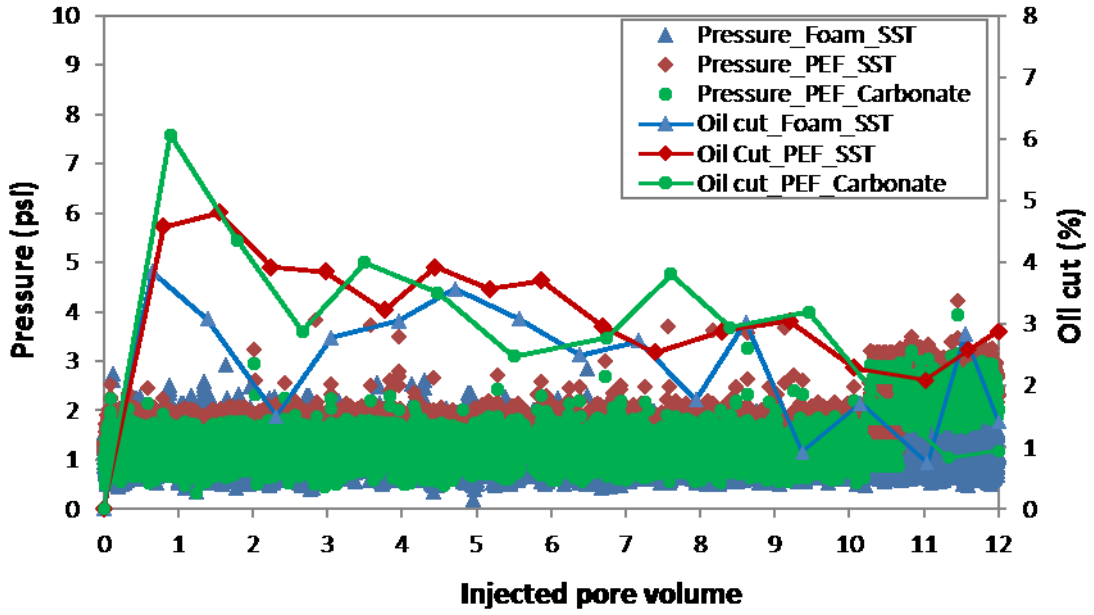

Figure 6.7: Overall pressure drop and oil cut profiles during CO_2 foam and CO_2 PEF injection in fractured sandstone and carbonate core samples.

6.4 Discussions

This study aimed to analyze the performance of CO_2 foam and CO_2 PEF in terms of (1) heavy oil recovery and (2) CO_2 sequestration which is discussed in this section. Moreover, the effect of

polymer addition and heterogeneity (fracture) are also investigated in the performance of CO_2 foam/PEF during heavy oil recovery.

6.4.1 Enhanced Heavy Oil Recovery

The CO_2 foam was used as a tertiary heavy oil recovery process after water flooding. The performance of foam flooding in terms of heavy oil recovery is discussed in this section in two conditions: (1) addition of polymer to conventional foam (PEF) and (2) effect of fracture on foam flooding performances.

Effect of heterogeneity: High permeability contrast between fracture and matrix creates an easy flow path for any injected fluid for EOR purpose and results in inadequate oil recovery. During waterflood process (Figure 6.8) heavy oil recovery significantly reduced in fractured core compared to that of the homogenous core sample. In homogenous core after water breakthrough (about 0.3-0.4 PV), where an easy path was created by channeling, oil production is insignificant. Relatively constant pressure profile after about 0.6 PV of water injection shows the effect of channels created by water injection resulting in a path of least resistance for injected water. On the other hand, in the fractured core sample water at first sweep the oil inside the fracture (up to about 0.2 PV). However, after sweeping the fracture, the oil is still producing but the oil production is low. At this time, there is a significant contact area between the water in the fracture and oil in the matrix resulting in additional oil recovery by imbibition process which is a slow process.

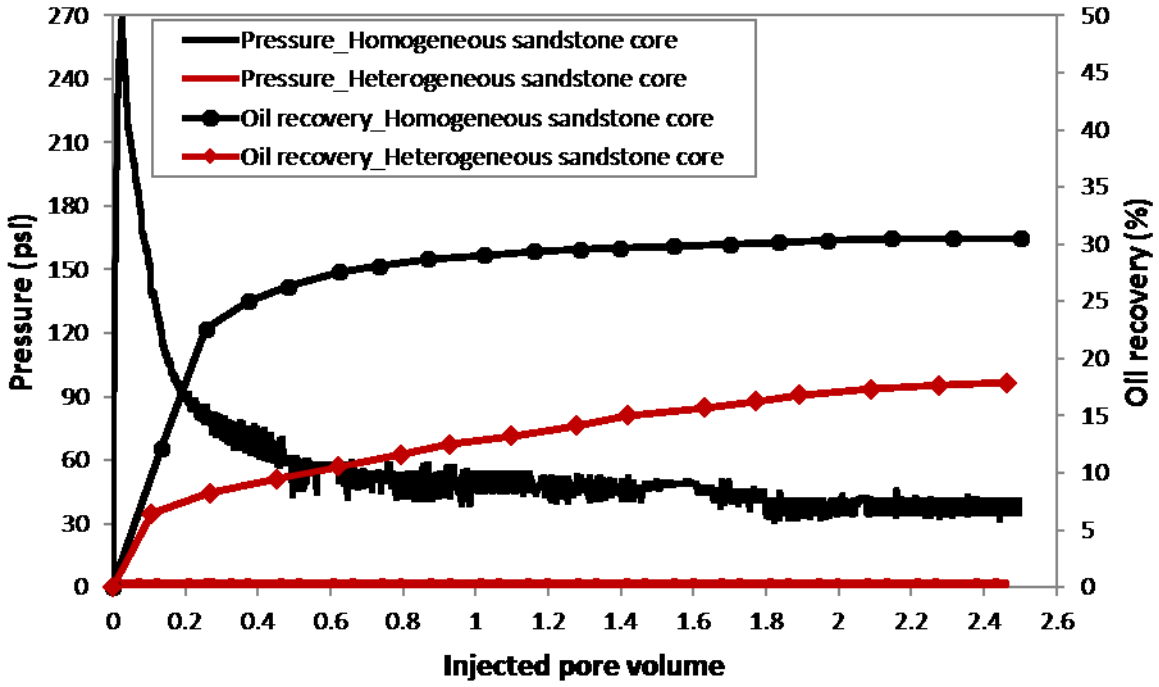

Figure 6.8: Effect of heterogeneity (fracture) on pressure and oil recovery profiles during waterflood.

CO_2 foam/PEF were injected into the core samples after water flooding where an easy path of flow was created by water channels (in homogeneous core sample) or fractured filled with water (fractured core sample). Unlike water flooding process, the ultimate heavy oil recovery by foam from homogenous and fractured core samples are almost similar. However, the pressure profiles are different as seen in Figure 6.9. The oil was produced in homogeneous core much later than that of the fractured core. This different can be due to the water flooding performance on heavy oil recovery. In homogenous core, water produced more than 30 % of original oil in place (OOIP) however this value was only about 17% in the fractured sample. During foam flood in the fractured core, the oil started to produced after about 1 PV of injection. At this time foam already occupied the fracture and interacted with matrix by fluid diversion and oil began to produce from the matrix.

Injected surfactant diverted into the matrix more easily as foam create a resistance to flow in the fracture and improve the oil recovery from the matrix.

However, in the case of the homogeneous core, foam at first should block the easy path created by water (which is much more than fracture volume in case of the fractured core). Then the resistance to flow will result in the diversion of injected foam toward the untouched part of the core and eventually oil started to produce after about 2.5 PV of foam injection. The rate of oil production in the homogeneous core is higher than that of fractured one suggesting that further injection of foam may result in higher oil recovery in homogenous core compared to that of fractured one.

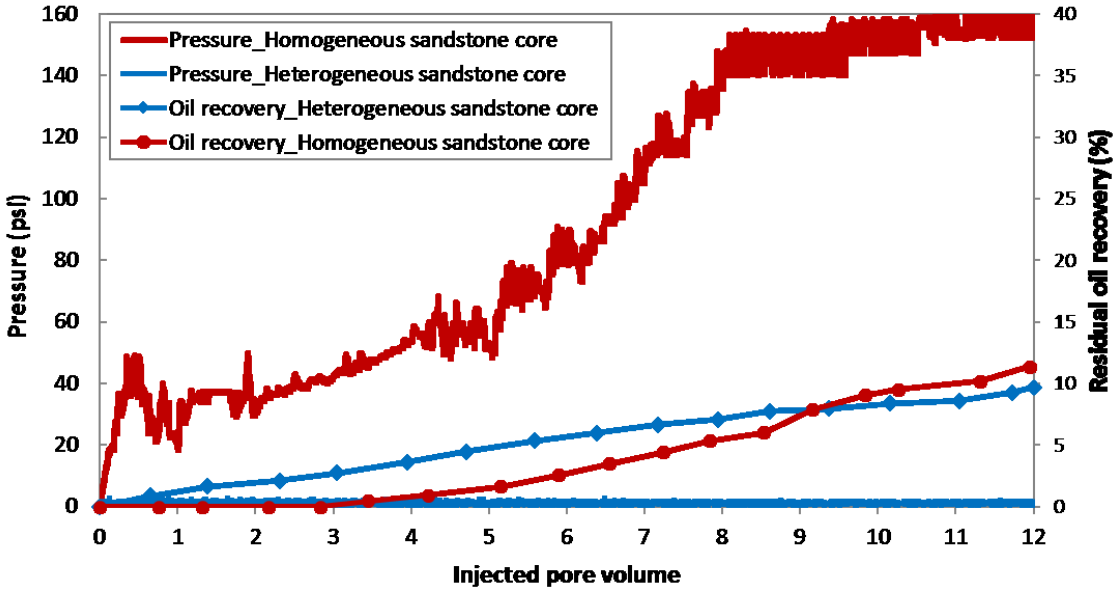

Figure 6.9: Effect of heterogeneity (fracture) on pressure and oil recovery profiles during CO_2 foam flooding process.

Effect of polymer addition (PEF): The addition of polymer to the conventional foam increases its stability in the presence and the absence of oil. When the oil is viscous, polymer addition plays an important role in oil recovery by stabilizing the foam in the presence of oil and reducing the mobility.

Figure 6.10 shows the performance of CO_2 foam and CO_2 PEF on homogenous rock sample in terms of pressure and oil recovery profiles. The addition of polymer to the foam significantly improved the heavy oil recovery and could produce more than 26% of the residual oil. This value was only about 11% in case of conventional foam injection. PEF also propagate much faster than foam as seen in the slope of the pressure profile. The rate of foam propagation is a battle between stability/regeneration of foam bubbles and foam collapse due to the oil effect. Faster propagation (which can be due to the higher stability of PEF in the presence of oil) also resulted in faster oil production such that oil started to produce after about 1.5 PV which was about 1 PV earlier than foam injection.

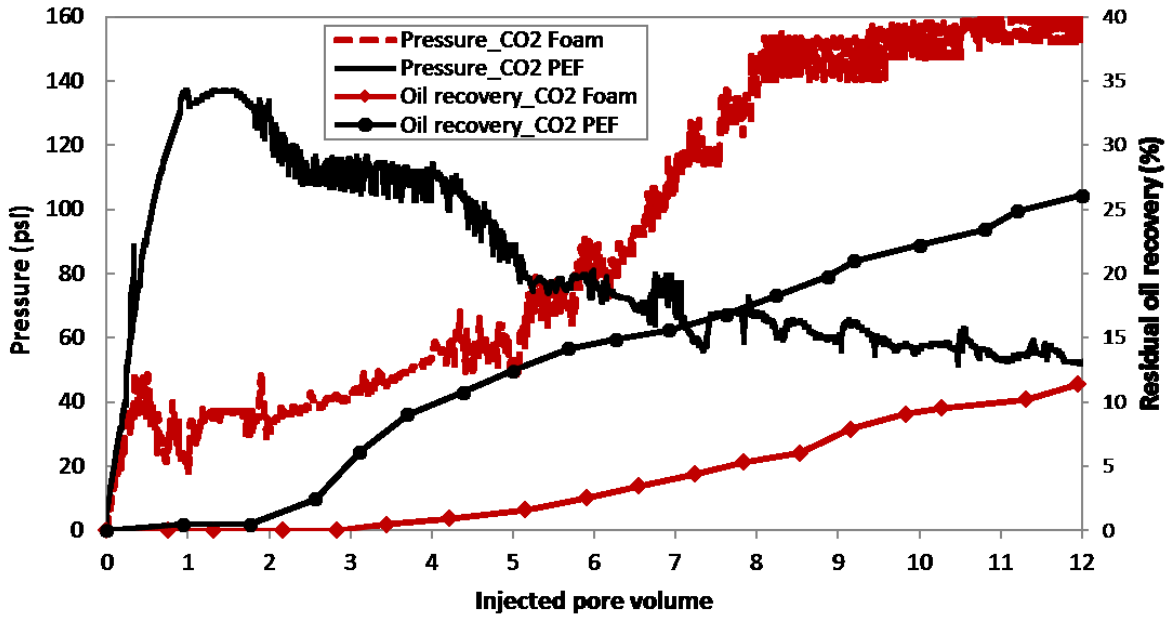

Figure 6.10: Effect of polymer addition (PEF) on pressure and oil recovery profiles during CO_2 foam flooding in the homogeneous core sample.

In the fractured core sample (Figure 6.11), unlike homogeneous one, PEF only slightly increased the oil recovery after injection of 12 PV. However, at this time pressure started to slightly increase showing the potential of more oil recovery in the longer injection. This behavior in fractured

porous media is also observed by Haugen et al. (2014). They also observed that in some fractured core samples, there was no significant increase in the pressure drop even after 40 PV of foam injection. The additional oil recovery can be explained by liquid diversion toward the matrix. Foam bubbles reduced the fluid mobility in the fracture zone and divert the liquid into the matrix resulting further oil recovery. This process was slightly more efficient in case of PEF. It should be mentioned there was no significant gas invasion into the matrix which is shown in next section.

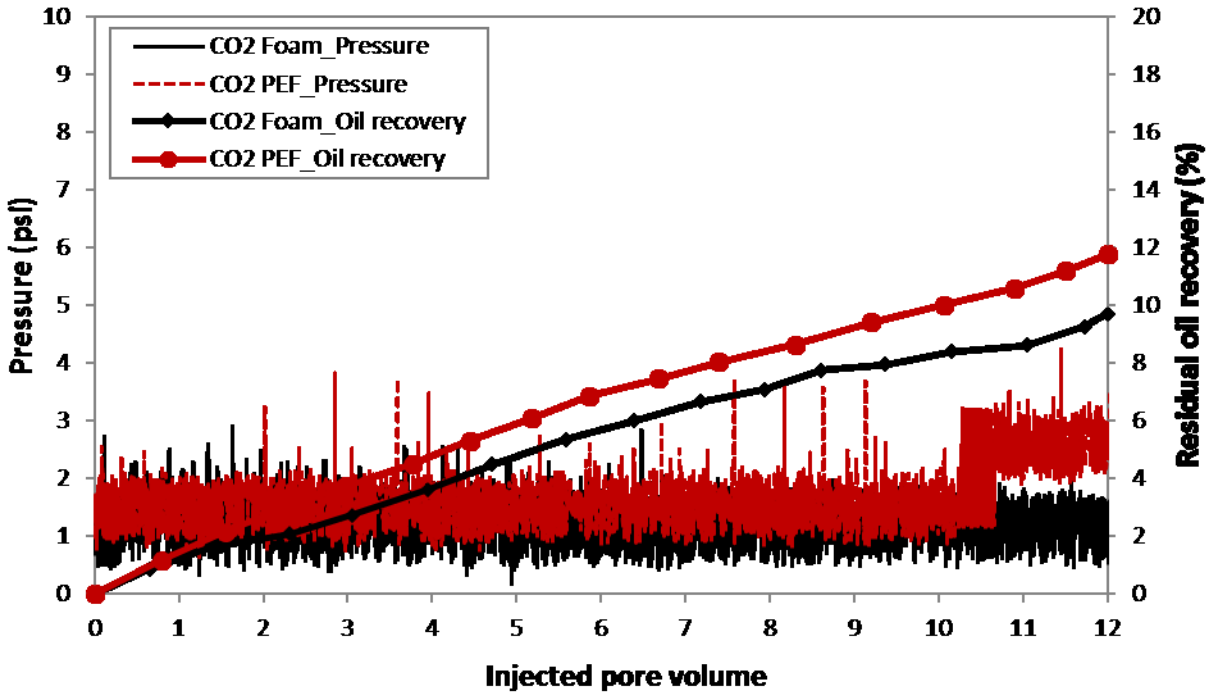

Figure 6.11: Effect of polymer addition (PEF) on pressure and oil recovery profiles during CO_2 foam flooding in the fractured core sample.

Figure 6.12 compares the ultimate oil recovery values in all experiments. PEF had better performance both in homogeneous and heterogeneous core samples compared to that of foam injection. The heavy oil recovery (OOIP) by CO_2 PEF were 17.8% and 11.7% for homogenous and fracture core sample, respectively. This value was 8% and 7.9% for CO_2 foam flooding. In the

case of foam injection, oil recovery value was almost the same in homogenous and the fractured core showing that the foam may equally perform in both conditions. Moreover, extended waterflood after foam/PEF injection could produce some more oil showing the fact that foam bubbles are relatively effective in fluid diversion in the porous media and injected water could reach untouched parts of the core.

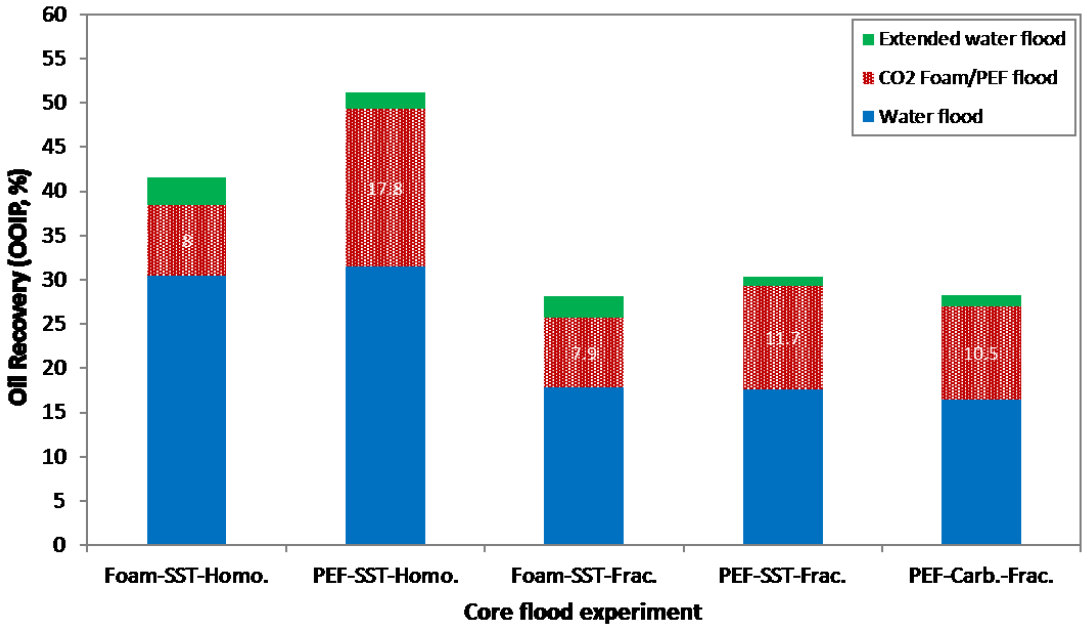

Figure 6.12: Ultimate oil recovery values for all experiments during waterflood, foam/PEF injection, and extended waterflood (EWF).

6.4.2 CO_2 Sequestration

The amount of produced CO_2 gas was continuously monitored and recorded during all experiments to calculated the amount of remained CO_2 gas in the core by simple material balance. The discussion in this section is only based on material balance and the objective is to see how the dynamic stability of foam in the presence of oil will affect the amount of CO_2 stored in the rock sample even after extended waterflood process.

Figure 6.13 shows the profile of injected and produced CO_2 gas. The red colored area shows the amount of CO_2 gas inside the core. As seen, the amount of CO_2 gas inside the core is more significant in homogenous rock sample rather than fractured one. Extended waterflood (EWF) also produced some of the gas inside the core, however, still, some CO_2 gas remained even after EWF. In the case of fracture core, the amount of CO_2 sequestration was not significant showing the fact that most of the gas remained in the fractured area and CO_2 gas could not invade into the matrix zone. This shows that the pressure inside the fracture was not high enough to improve the gas diversion (by overcoming the capillary pressure) which was also observed in another study (Haugen et al., 2014).

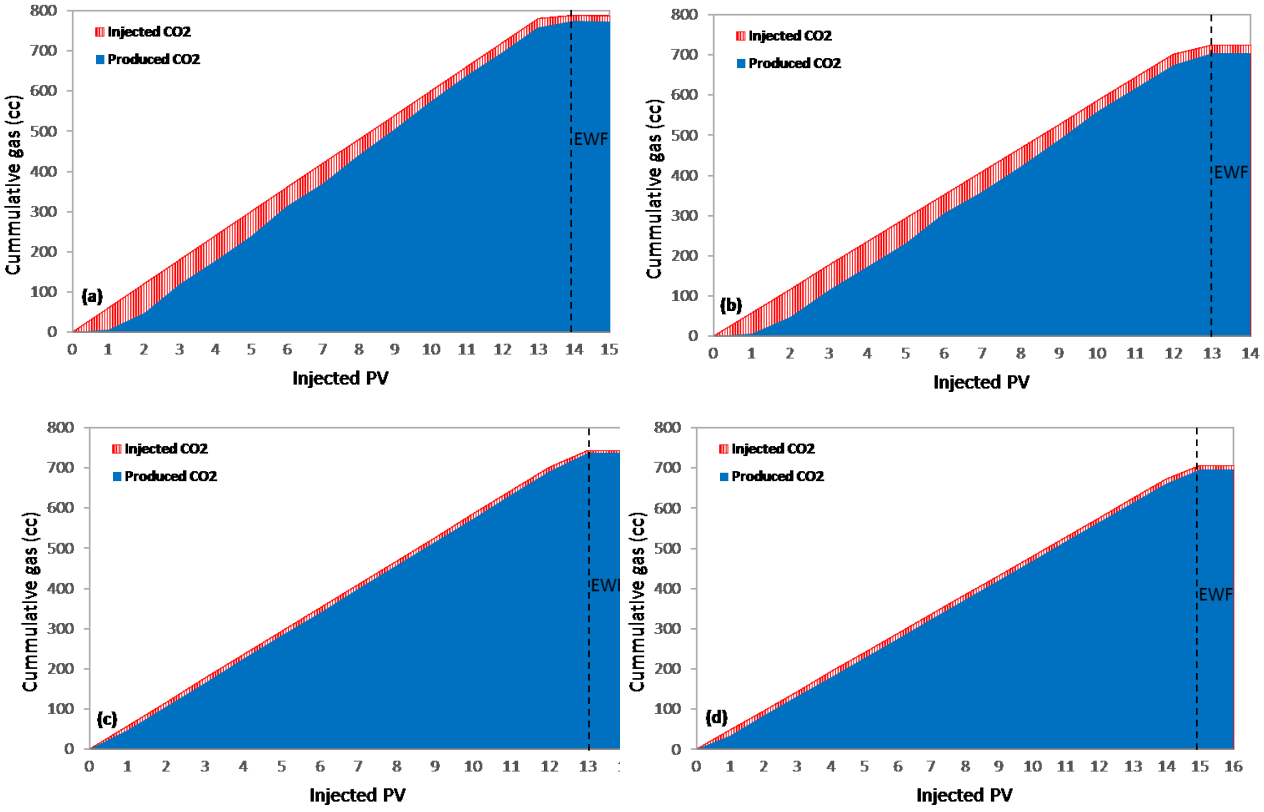

Figure 6.13: Cumulative CO_2 gas injection and production profiles during (a) CO_2 foam injection in the homogeneous core, (b) CO_2 PEF injection in the homogeneous core, (c) CO_2 foam injection in the fractured core, and (d) CO_2 PEF injection in the fractured core.

As seen in Chapter 5, PEF was more stable in the presence of oil compared to that of foam in both static and dynamic conditions. Here the objective is to see how the enhanced dynamic stability and foam collapse rate in porous media will contribute to the CO_2 gas production rate and thus CO_2 sequestration potential. Figure 6.14 is plotted to show the final amount of CO_2 gas remained within the core after CO_2 foam/PEF injection and after extended waterflood. More that 40% of PV in the homogenous core occupied by the CO_2 gas at the end of PEF flooding. This value was about 27% for foam flooding showing the fact that how the addition of polymer can enhance the dynamic stability of foam bubbles and thus reducing the amount of produced CO_2 gas. After EWF process, more CO_2 gas was produced from the core but still significant amount of gas remained in the porous media (more than 15% and 25% in case of CO_2 foam and CO_2 PEF flooding, respectively). In the fractured porous media, foam or PEF could not divert the gas into the matrix area and CO_2 gas only remained inside the fracture and the sequestration process was not significant. However, still, the CO_2 PEF could hold more gas inside the core even after EWF compared to that of foam.

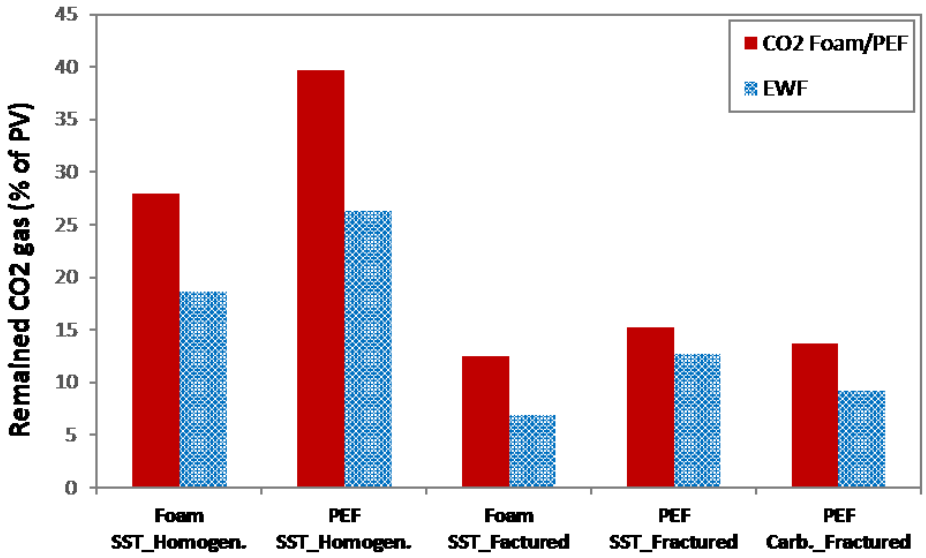

Figure 6.14: Amount of CO_2 gas (% of PV) remained inside the porous media at the end of CO_2 foam/PEF injection and extended waterflood process.

6.5 Summary

The addition of polymer could increase the stability of conventional foam and this chapter aimed to analyze and compare the performance of CO_2 foam and CO_2 PEF for heavy oil recovery and CO_2 sequestration as a tertiary EOR method (i.e. after water flooding). Followings are the summary of this chapter:

- Foam injection improved heavy oil recovery after water flooding in homogenous core sample and could produce more than 10 % of residual oil remained in the core after water flooding. The interesting fact is that the residual oil recovery value was almost the same in the fractured core showing that the foam can also increase residual oil recovery in fractured porous media.
- The addition of polymer to conventional CO_2 foam (CO_2 PEF) could significantly improve its performance for heavy oil recovery, especially in the homogenous core sample. CO_2 PEF recovered about 26% and 12% of residual oil in the core after water flooding process in the homogeneous and fractured core, respectively.
- Pressure profiles during injection of CO_2 foam and CO_2 PEF showed a faster propagation rate for PEF in homogeneous porous media showing that CO_2 PEF had more dynamic stability in the presence of oil compared to that of conventional foam. This also resulted in faster oil production and higher ultimate oil recovery during CO_2 PEF injection.
- Profile of pressure and amount of remained gas at the end of CO_2 foam/PEF in the fractured core samples showed that there was no significant gas diversion into the matrix and most of the gas remained in the fractured area. Additional oil recovery from the fractured core was due to the liquid (surfactant/polymer) diversion into the matrix.

- Besides improving heavy oil recovery, the addition of polymer could increase the dynamic stability of foam bubbles in the presence of oil such that less CO_2 gas production occurred in the case of CO_2 PEF compared to that of CO_2 foam. At the end of CO_2 PEF injection, CO_2 gas occupied about 40% of pore volume improving the CO_2 sequestration potential of CO_2 foam by more than 15% of PV.

Chapter 7: CO_2 Microbubbles – A Potential Fluid for Enhanced Heavy Oil Recovery: Bulk and Porous Media Studies[6]

Previous chapters investigated the performance of CO_2 foam and CO_2 PEF for heavy oil recovery in both pore-scale and core-scale. This chapter aims to investigate the potential of CO_2 microbubbles, as an improved version of CO_2 PEF, for heavy oil recovery. Both bulk and porous media experiments were performed at the different conditions to achieve this goal.

7.1 Introduction

High heterogeneity, as well as the high viscosity of crude oil, reduces the potential of foam EOR. While CO_2 flooding is used in deeper, hotter, and higher pressure reservoirs, shallow heavy oil reservoirs can be the potential target for application of CO_2 microbubbles as reservoir temperature and pressure is lower than oil reservoirs located in higher depth. For high temperature and high-pressure reservoirs (deep reservoirs), microbubbles should be generated with the surfactants and polymers which are screened for such condition. In addition, the detrimental effect of crude oil on foam stability is one of the main challenges during foam EOR process. On the other hands, colloidal gas aphrons (CGA) are very stable microbubbles which combine surfactant, polymer, and gas in their structure. The components to create microbubbles (surfactant, polymer, and gas) are already in abundant use in EOR field operations. Use of appropriate polymer and surfactant along with the CO_2 gas can enhance the stability and mobility reduction characteristic of

[6] A version of this chapter has been published:
Telmadarreie et al., 2016. Journal of Petroleum Science and Engineering, http://dx.doi.org/10.1016/j.petrol.2015.10.035.

microbubbles. Therefore, understanding their stability and flow characteristics are of prime importance in the successful application of CO_2 microbubbles for EOR and sequestration.

Sebba (1987) was first to report that small bubbles with diameters of several tens of micrometers differ from their larger counterparts in many important properties and have been potential for many industrial applications. Some of these applications include separation of metals and other impurities by the colloidal gas aphrons (CGA) floatation process (Ciriello et al., 1982; Cilliers and Bradshaw, 1996), extraction of enzymes (Save et al., 1993), protein recovery (Noble et al., 1998), and removal of contaminants from soil (Roy et al., 1994). Growcock et al. (2005) carried out extensive studies on the physical characteristics and chemical composition of the CGAs to be used as a drilling fluid in the petroleum industry. In terms of their structures and properties, CGAs differ from foams, especially with their enhanced half-life and therefore, CGAs can potentially perform better for sealing high permeable formations. Other important characteristics of CGAs are their gas-blocking ability by reducing its mobility and increased the stability of the surfactant/polymer solution.

Aphrons have been characterized as a core of gas with a shell composed of three layers of surfactant molecules and a viscosified aqueous layer (Figure 7.1). The first phase (inner layer) contains surfactant molecules encapsulating the gas core which provides a barrier against the second phase. The second phase is described as comprised of viscosified water, an optional stabilizer, and surfactant molecules positioned such that the hydrophobic portion of the molecules extends into a third phase. The third phase is described as containing another layer of surfactant molecules aligned with the hydrophilic (polar) portion extending into the bulk fluid. The third phase then contains a bilayer of surfactant molecules, which serves as an effective barrier to coalesce with adjacent aphrons. Since aphrons exhibit little affinity for each other, they may form

agglomerates without coalescence. Agglomerated aphrons (polyaphrons) have been reported to be stable over a period of months, without any significant phase separation (Gupta and Cawiezel, 2013). Not only do such aphrons exhibit little affinity for each other, they also exhibit little affinity for the mineral surfaces of the pore or fracture of the formation. Consequently, the seal formed by aphrons is soft. The lack of adhesion seen with agglomerated aphrons enables aphrons to be easily removed from pores or fractures after pressure is released, preventing formation damage (Gupta and Cawiezel, 2013).

In contrast to microbubbles, a conventional surfactant stabilized bubble or foam is simply a sphere of gas separated from its aqueous environment by a thin surfactant film. The hydrophobic tail of the surfactant is oriented towards the gas core, while the hydrophilic head is oriented towards the bulk water (see Figure 7.1).

According to some studies on CGA characterization, CGAs possess a large interfacial area, separate easily from the bulk liquid phase, has similar flow properties to those of water and exhibit relatively high stability (Sebba, 1987; Save and Pangarkar, 1994; Jauregi et al., 1997; Chaphalkar et al., 1993). Stability is one of the important characteristics of CGA that will be influenced by their structure (Sebba, 1987). Under pressure, the coalescence of CGA is delayed, and hence these dispersions exhibit higher stability as compared to conventional foams. The identification of these properties has led researchers to consider CGA for various applications in the petroleum industry. The CGAs have been used successfully as drilling fluid to prevent drilling fluids from leaking into the formations. They can be used in a subterranean formation containing lost circulation zones or depleted reservoirs. CGAs have also been successfully utilized in pilot field applications. This success has been due to the fact that the CGAs have the unique ability to form a bridge in high permeable part of reservoirs, which mitigates fluid migration (Montilva et al., 2002).

Aphrons can be defined as a method to decrease the density of fluid circulated in the borehole as well as the invasion of fluid into formations already been contacted by fluid (Brookey, 1999). They have a resistance to movement within the formation due to their high Low Shear Rate Viscosity (LSRV) and they can also be used in dense drilling fluid as compressible objects. Since aphrons contain gas into their center core, they are relatively more compressible than that of conventional drilling fluids (Carstensen et al., 2007). Using CGAs allows formulating drilling fluids whose density can be optimized to remove the cuttings effectively with less energy expended (Green and Smith, 2007). Most recently, aphrons and energized foams have been studied for hydraulic fracturing of underground formations (Gupta and Cawiezel, 2013). As the aphron fluid is being pumped into the formation during fracturing, microbubbles/aphrons move faster than the liquid phase and thus move toward the front of the fluid. The bubble barrier and radial flow pattern of the fluid rapidly reduce the shear rate, raise the fluid viscosity, and prevent the fluid invasion into the formation, especially in those formations where high leak-off potential exists (Gupta and Cawiezel, 2013). Thus, CGAs behave as a unique bridging material, forming a microenvironment in a pore network or fracture. Furthermore, safety concerns and cost issues of compressors and high-pressure equipment used in air or foam drilling reduces significantly; as conventional mud equipment can be used for the creation and storage of aphrons (White et al., 2003).

Most of the previous studies on CGAs were limited to analysis of microbubbles stability in different conditions (pressure, temperature, surfactant, and polymer concentrations). For example, Longe (1989) studied the effect of temperature on CGAs and found that CGAs were relatively stable at temperatures below 104 °F, and were fully unstable at temperatures above 149 °F. Amiri and Woodburn (1990) studied the rate of drainage, as well as the CGA bubble size, by recording the images of the CGAs over time. Save et al. (1993) analyzed the half-life of CGAs by measuring

the rate of drainage as a function of various parameters, including the effect of viscosity. They found that increasing viscosity also increased the half-life of the CGA. Moreover, Bjorndalen and Kuru (2008a) studied the change in the size of the microbubbles and apparent viscosity of the CGA-based drilling fluids. They showed that microbubbles become unstable (i.e. the bubbles become larger than their original size) when they are exposed to a depressurization process following pressurization. Their results also showed that between 77 °F and the 122 °F, the increase in bubble size is more drastic than from 122 °F to 167 °F, indicating the CGAs are more sensitive to temperature change at lower temperatures.

Physico-chemical characteristics of CGA have been previously reported by many researchers (Bjorndalen and Kuru, 2008b; Cardoso et al., 2010; Shivhare and Kuru, 2010; Spinelli et al., 2010; Arabloo et al., 2012). In addition, Bjorndalen et al. (2014) and Shivhare and Kuru (2014) analyzed the pore-blocking performance of aphron within the porous media. They showed that CGA fluids exhibit more effective pore blocking ability when flowing through low permeability zones than that of high permeability zones. Furthermore, Ghosh (2013) studied the rheological characteristic of CO_2 microbubbles at elevated pressure (up to 800 psi) and temperature (167 °F) condition. Although there are few studies on air microbubbles behavior under high pressure (compression/decompression) and temperature (Growcock, 2005; Bjorndalen and Kuru, 2008a), to the best knowledge of the authors no work has been reported on the behavior of CO_2 microbubbles (rheology as well as stability) after elevated pressure and temperature conditions (effect of compression/decompression). Analyzing CO_2 microbubbles under such conditions can improve our understanding of performance and potential of this fluid to perform under the reservoir conditions as displacing fluid for EOR, especially in channeled or fractured reservoirs. Therefore, one of the objectives of this study was to characterize rheology and stability of CO_2

microbubbles after they are exposed to elevated pressure and temperature conditions. Initial CO_2 microbubbles, as well as preserved samples, were studied for their rheological and size characteristics. The CO_2 microbubbles were then subjected to a pressure–volume–temperature (PVT) study and the changes in their properties were observed. The CO_2 microbubbles after PVT test were analyzed and compared with the sample preserved for long duration and at the initial conditions, for their rheological and size characteristics. Besides the flow behavior of CO_2 microbubbles in porous media is also presented later in this chapter. Both the core and pore-scale experiments (sand-pack and fractured micromodel) were performed to compare the performances of base fluid and CO_2 microbubbles during heavy oil recovery.

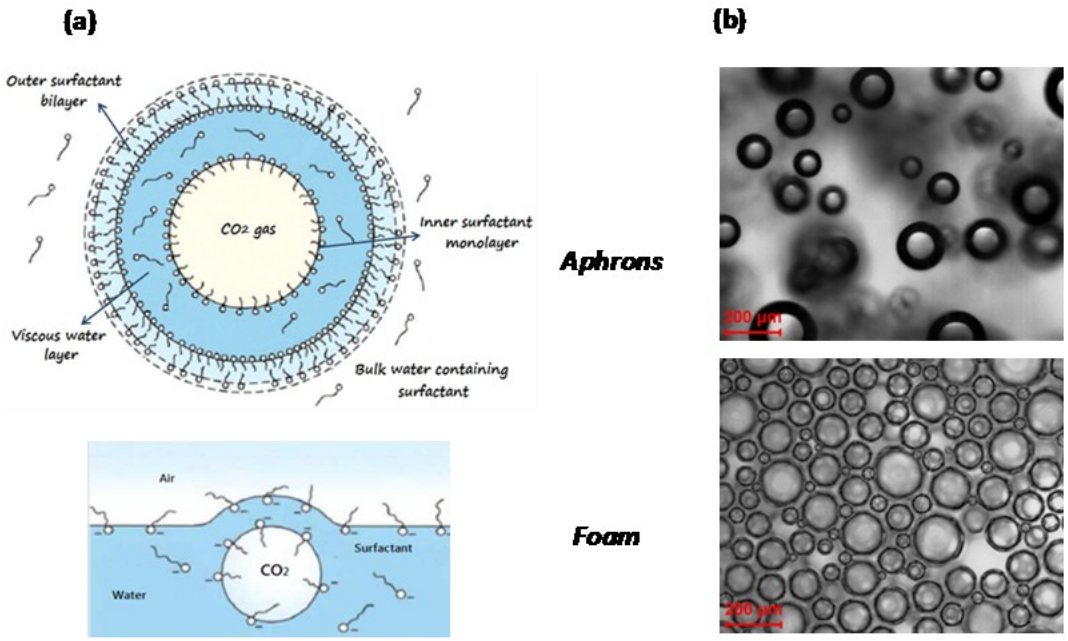

Figure 7.1: (a) Schematic and (b) microscopic images of CO_2 microbubbles and foam, representing their shape and structure (Sebba, 1987).

7.2 Materials and Experimental Procedures

To characterize CO_2 microbubbles, several experiments such as rheological study, microbubble size analysis, and PVT experiments were performed and results are presented in the following sections. Experiments were performed using samples collected under three different conditions; initial or fresh CO_2 microbubbles, preserved samples in a cylinder and CO_2 microbubbles after PVT test. In addition, oil recovery performance of CO_2 microbubbles was compared to that of base fluid in porous media saturated with heavy oil. A schematic of the experimental procedure is shown in Figure 7.2.

7.2.1 Materials

Surfactant: Surfactants are the major chemical constituent in CO_2 microbubbles. Surfactants are classified according to the nature of the charged group present on the surfactant head. Their main function is to lower the surface tension. In this study, a non-ionic surfactant (Surfonic N85, Huntsman Corporation) was used for generation of CO_2 microbubbles. The surfactant is nonylphenol-ethoxylated nonionic surfactant with a chemical formula of $C_{15}H_{23}$ $(OCH_2CH_2)_n$ OH (n is the number of ethylene oxide units ≈ 8–9).

Polymer: Polymers are an essential component of microbubbles that enhances the stability of the aphrons by increasing the viscosity of the water lamellae in the aphron shell. The shear thinning polymer will allow the microbubbles to be stable under cyclic compression and expansion while keeping the morphology same (Brookey, 1998). In this study, Xanthan Gum (anionic biopolymer) was used for stabilization of CO_2 microbubbles. Xanthan gum is a natural polysaccharide, which is known as a strong viscosifying agent (supplied by Baroid Industrial Drilling Products Co.). The based fluid for the preparation of microbubbles contains the N85 surfactant (0.29 wt%) and Xanthan Gum polymer (0.55 wt%) mixed in water.

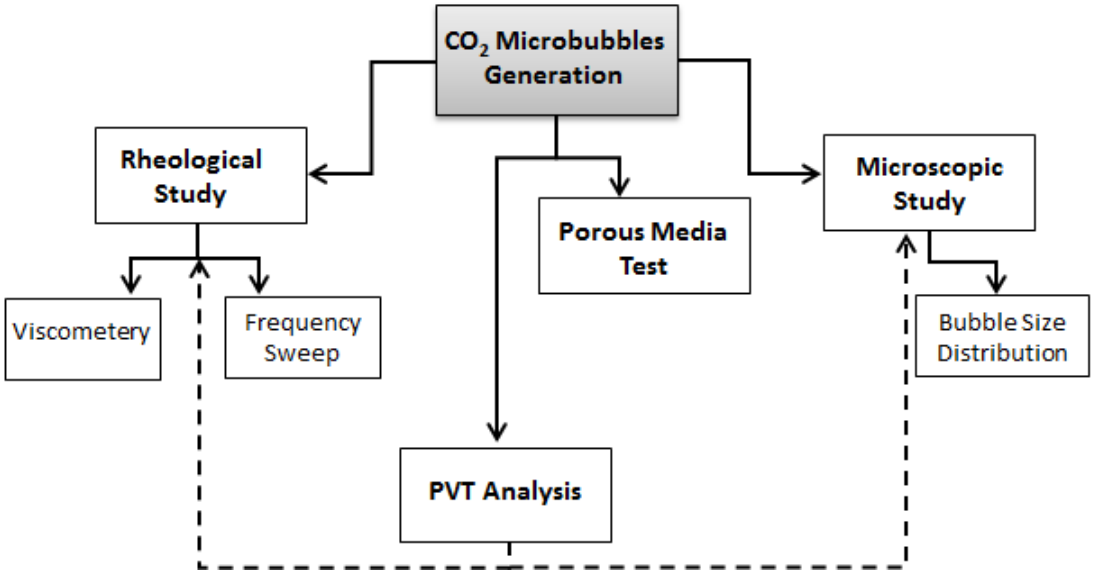

Figure 7.2: Schematic of experimental procedures for CO_2 microbubbles study.

7.2.2 CO_2 microbubbles Generation and Preparation

For the preparation of base fluid, an optimum condition that gives the highest yield of aphrons was determined as 0.55 wt% of the polymer, 0.29 wt% of surfactant in water. The surfactant is dispersed in the polymer solution by magnetic stirring (400 rpm for 20 min) to prevent the generation of foam. Thereafter, CO_2 aphrons was generated using a Polytrons DT6100 digital homogenizer (provided by Kinematica Inc.). The solution was put into the homogenizer with high-speed blender and CO_2 gas was injected into the homogenizer and mixed with the speed of 8000 rpm for 5 min. The shearing speed and shearing time were kept constant for uniformity of microbubbles created throughout the experiments. Before passing CO_2, the system was vacuumed to prevent mixing of air during the generation of CO_2 microbubbles. The concentration range of surfactants used is above their critical micelle concentration.

7.2.3 PVT Analysis

The experimental apparatus consists of a Schlumberger DBR PVT Cell (100 cc, 15 kpsi) housed in an oven and connected to a GT6K pump (500 cc, 20 kpsi). The maximum and minimum flow rates of the pump are 1000 cc/h and 0.01 cc/h (±0.02%), respectively. The temperature range of oven is from -99 °F to +374 °F with an accuracy of ±33 °F. The maximum working pressure and temperature of visual glass cell PVT (10 in. diameter, 16.25 in. height) are 15 kpsi and 392 °F, respectively. The apparatus allows visual observation of the content and interface location through a glass window with a camera focused on the cell, and the image of the fluid transmitted to a computer.

Following microbubbles generation, they were collected in a confined cylinder (normally under 35±5 psi pressure) with a differential pressure of normally 5 psi. About 60 ml of sample was injected into the PVT cell. Before filling with the sample, the PVT cell was first vacuumed for about 15 min. After reaching stable operating conditions in the PVT cell, the sample was injected and the pressure, volume, and temperature were controlled using the control system. For unloading the sample after PVT test, the system pressure was gradually ramped down at a constant rate, and the sample collected on the cylinder for further analyses. Finally, after each experiment, the PVT cell was cleaned using deionized water. Water was injected into the glass cell and used to clean the cell with high-speed stirring. This process repeated three times to ensure the complete cleaning of the cell.

Several PVT experiments were performed on CO_2 microbubbles samples. In all experiments, samples were pressurized up to 2000 psi; however, compression rate and temperature were different in each experiment. Samples were analyzed in a PVT cell at temperatures of 77 °F, 122 °F, and 167 °F (25 °C, 50 °C, and 75 °C, respectively) and two compression rates; 1.4 psi/min and

0.7 psi/ min. In order to investigate the impact of pressure and temperature on samples, before and after each PVT test CO_2 microbubbles were analyzed for rheological characterization as well as bubble size. A schematic of the experimental setup for PVT test is shown in Figure 7.3.

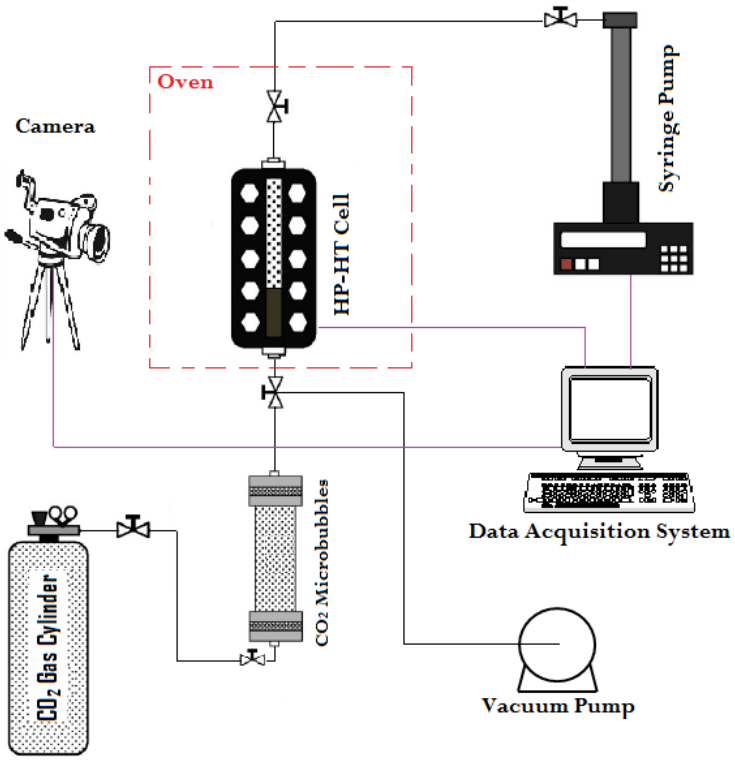

Figure 7.3: Schematic of PVT experimental setup.

7.2.4 Microbubble Size Analysis

The Leica DM 6000M microscope was used to analyze the microbubbles. Immediately after microbubbles generation, the sample was poured into a microscopic slide for bubble size study. Similarly, after each PVT experiment, samples were analyzed for bubble size distribution. The prepared images were analyzed for measuring bubble diameters with the Leica MW software. For each sample, the bubble size distribution was measured based on micrographs of microbubbles

observed under the microscope and sampled from the container less than 1 minute after it was generated. Around 200 individual bubbles were analyzed to find the bubble size distributions and average bubble diameter (D50). Microbubbles were classified based on their size on 7 bins (bin size of 50 μm) and plotted versus their frequency for size distribution analysis.

7.2.5 Rheological Study

The BOHLIN CVOR rheometer was used in this study (supplied by Malvern Instruments) for rheological characterization of CO_2 microbubbles. The CVOR150 Peltier cell attached to the BOHLIN rheometer was used to rheologically characterize the fluids at ambient pressure in a cone and plate measuring system. Studied samples were placed in a 150 μm gap between a rotating upper cone with a 4° angle and a diameter of 40 mm, and a fixed lower plate with a diameter of 60 mm.

Viscometry tests were carried out at shear rates varying from 0.01 to 100 s^{-1}. Frequency tests were carried out on CO_2 microbubbles samples at a frequency range of 0.01–1 Hz, keeping the stress value constant at 0.04775 Pa. These tests provide elastic and viscous modulus (G′ and G″) data as a function of angular frequency.

7.2.6 Porous Media Experiments

A linear visual sand-pack was used to study the performance of CO_2 microbubbles in porous media. The 1D system was a 1-ft long glass column with 1-in. inner diameter, packed with glass beads (40–70 meshes). The visual cell was dry packed by continuously shaking the cell during packing to induce mixing and settling. A special expandable rubber sealed each end tightly, and a metal screen (80 meshes) was put between the rubber and the glass beads. The visual cell was vacuumed for at least 3 h to remove any air. Thereafter, the cell was saturated with water to measure porosity (37±0.5%) and permeability (38±0.5 Darcy). Then, the visual cell was saturated

with heavy crude oil (1300 cp). The initial oil saturation was 92% (±0.5%). A syringe pump (ISCO Model 500D) was used for fluid injection. The pressure was also continuously measured and recorded by a pressure transducer (OMEGADYNE Model PX409) connected to a computer. CO_2 microbubbles and base fluid were injected at a constant flow rate of 0.25 cc/min and pressure profile and oil recovery were measured to compare their performance in heavy oil recovery.

7.2.7 Fractured Micromodel Experiments

In order to visualize the performance of microbubbles during heavy oil recovery, the fracture micromodel was used in this study. The micromodel is made of a two-dimensional pore structure, which is etched onto the surface of a glass plate, which is otherwise completely flat. A second glass plate is then placed over the first, covering the etched pattern, and thus creating an enclosed pore space. This cover plate has an inlet hole and an outlet hole drilled at either end, allowing fluids to be displaced through the network of pores. The micromodel was designed such that it has a high permeability contrast between the matrix and fracture (1 mm thickness) to imitate the heterogeneous formation. The micromodel is placed in a holder with inlet and outlet ports, which communicate with the micromodel at the drilled holes. The holder is capable of handling high pressure during the fluid injection. Figure 7.4 shows the image of heavy oil saturated micromodel and experimental setup.

Micromodel was first saturated with water and then drained with heavy oil to reach the irreducible water saturation. CO_2 microbubbles and base fluid were injected at the flow rate of 0.083 cc/min. A high-quality camera was used to capture quality images. Both sand-pack and micromodel experiments were performed at ambient condition. The maximum injection pressure during microbubbles injection was around 20 psi.

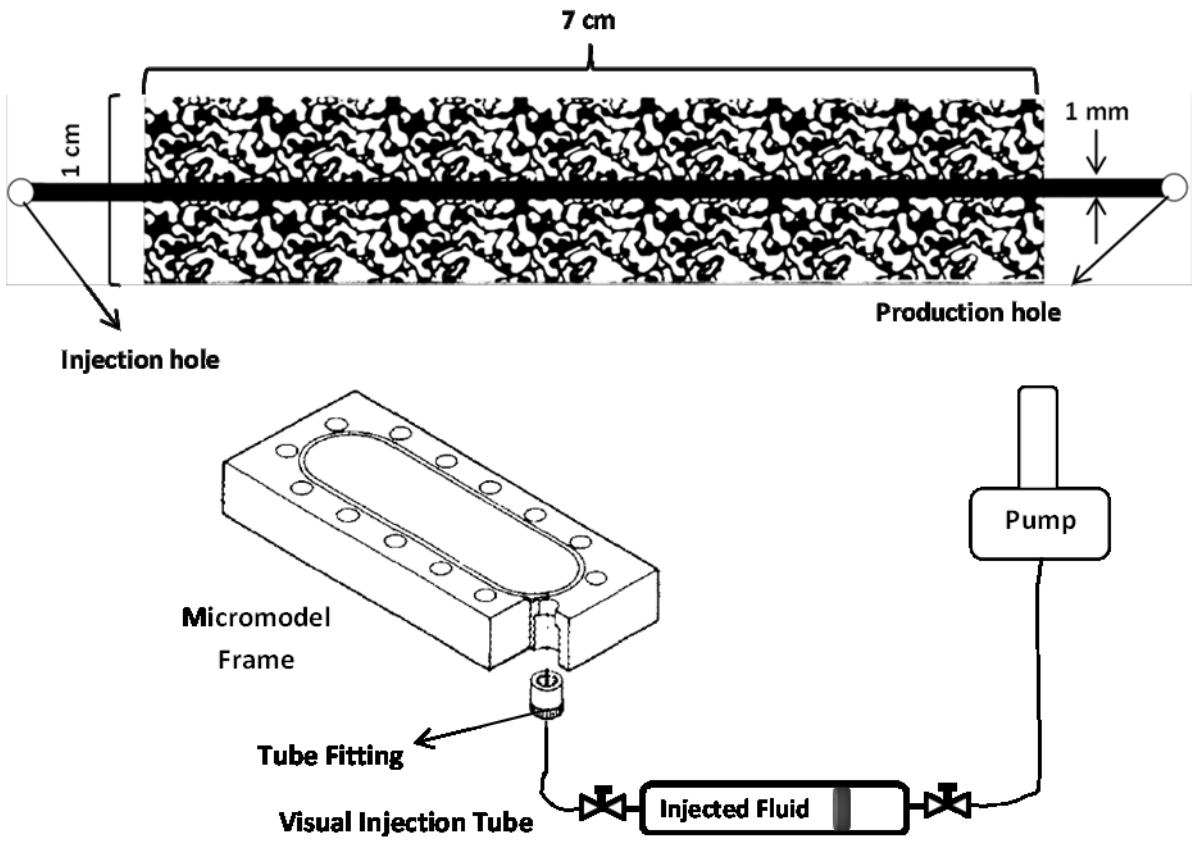

Figure 7.4: Schematic of fractured micromodel (1 mm fracture width) and its frame. The black area shows void space saturated with heavy oil.

7.3 Results and Discussion

7.3.1 CO_2 Microbubbles at Elevated Pressure and Temperature (PVT Test)

Due to the presence of gas in the form of microbubbles in the bulk of the base fluid, the pressure–volume–temperature (PVT) relationship of CO_2 gas microbubbles is of particular interest. During the PVT tests, the volume of the sample was measured while pressure was increased. The PVT tests were conducted at constant temperature conditions (77 °F, 122 °F, and 167 °F).

The variation of CO_2 microbubbles volume with pressure is shown in Figure 7.5. By increasing the pressure, the microbubbles shrink to rearrange based on pressure change; however, they are

still present in the solution. Simulation studies by White et al. (2003) showed that microbubbles could survive up to 3000 psi. Visualization tests by Ivan et al. (2002) indicated that CGAs could be maintained at a pressure of at least 1500 psi. Growcock et al. (2005) also demonstrated that even at near 2000 psi pressure the air core in CGA will not diffuse into the liquid phase. Bjorndalen and Kuru (2008a, 2008b) visually studied the effect of pressure on the microbubbles size up to 500 psi. According to their study, at a pressure of 50 psi microbubbles reached around 60% of their original size. Thereafter, the shrinkage rate reduced such that at the pressure of 500 psi, microbubbles shrunk to around 30% of their original size.

The volume of CO_2 microbubbles reduced rapidly at lower pressure (<100 psi) when pressurized in PVT cell (Figure 7.5). Further increasing the pressure, microbubbles shrunk at a constant rate. Moreover, the effect of volume shrinkage was more drastic at higher temperatures as shown in Figure 7.5. At temperatures, higher than 50 °C (122 °F), bubble sizes changed at a faster rate; therefore, volume change is more drastic.

In addition, the rate of pressurization also affects the P–V behavior of CO_2 microbubbles as shown in Figure 7.5(b). The observed volume reduction was higher in low pressurizing rate test (i.e. 48-h PVT test) and temperature enhanced this reduction. As it will be discussed later, this could be due to the fact that at the lower pressurization rate, microbubbles have more time to rearrange

based on applied pressure. Moreover, higher temperatures can significantly decrease the viscosity of aphron fluid and result in drastic changes of volume while pressurizing at PVT cell.

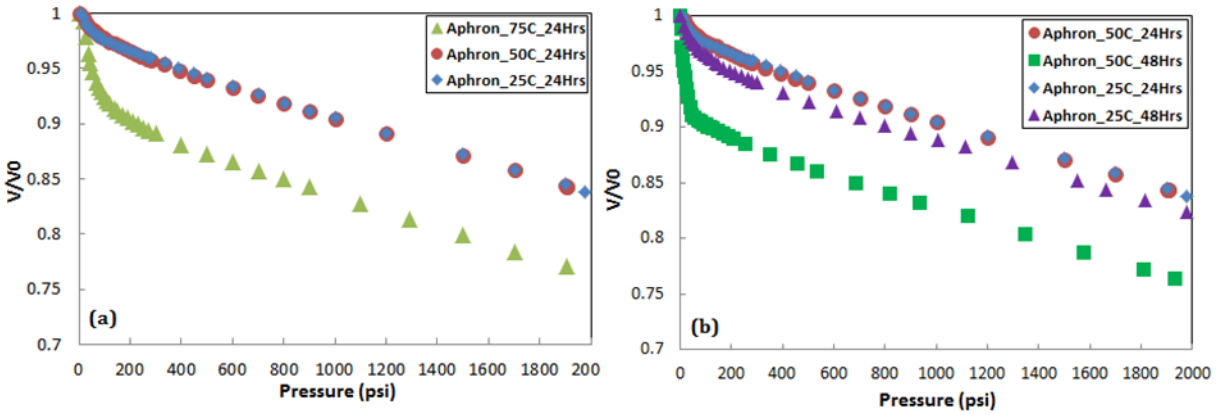

Figure 7.5: Pressure versus normalized volume of CO_2 microbubbles at constant temperatures; (a) 24 hours and (b) 48 hours PVT tests.

7.3.2 Microbubble Size Analysis of CO_2 Microbubbles

The measurement and analysis of the microbubbles diameter after compression/decompression is important as the bubble size is one of the principal factors involving in pore blockage to divert the flow and enhance the oil recovery. The CO_2 microbubbles were analyzed in various conditions such as under pressure, different temperatures and during the time to find the behavior of this fluid, particularly at near reservoir condition.

7.3.3 CO_2 Microbubbles Stability

The microbubbles when generated contain a wide range of size distribution up to 200 µm in diameter. Under the atmospheric condition, the microbubbles of very small diameter diminish very rapidly leaving microbubbles in the 25 µm to about 200 µm size ranges. This is due to the excess pressure within the microbubbles that increases as the diameter decreases. Thus, the smaller microbubbles will tend to diminish in size by transferring their gas to the larger ones with lower extra pressure.

The aqueous bi-layer in the aphron structure will remain stable as long as the water film meets certain criteria for film thickness and viscosity (Sebba, 1987). The film must have a certain minimum thickness below that the film will break. Furthermore, the film must have a minimum viscosity. Water molecules tend to diffuse out of the film and into the bulk liquid (Sebba, 1987). This also serves to thin and destabilize the film. However, the rate of transfer of film water is inversely proportional to viscosity. In Figure 7.1, if the viscosity is too low, the aqueous layer between the inner surfactant layer and the outer surfactant bilayer of aphron becomes too thin and the bi-layer cannot be maintained. If the aqueous layer becomes very thin, polar head groups from the inner surfactant layer will face polar head groups from the outer surfactant bilayer. Due to repulsion between polar groups, this situation cannot exist for long. The viscosity of the aqueous layer is a direct function of the bulk viscosity of the base fluid. Therefore, if an aphron system is diluted sufficiently, the viscosity will decrease, and eventually, the aphrons will be converted into the conventional foam bubbles. Consequently, in designing aphron, a viscosifier such as a biopolymer is generally added.

The increase of the microbubbles size with time is an important factor for determining the ability of the bubble to block the rock pores. The frequency distribution of bubble diameters in CO_2 microbubbles after 0, 3, 6, 24, and 48 hours is shown in Figure 7.6. As shown in the figure, the maximum frequency of bubble diameters shifted to higher values over time (from 100 μm at the initial sample to >300 μm after 24 hours), showing a decrease in quality of microbubbles. After two days in the ambient condition, the number of bubbles significantly decreased. However, more than 60% of microbubbles had a diameter less than 300 μm. Microscopic images of microbubbles during exposure to the air are shown in Figure 7.7.

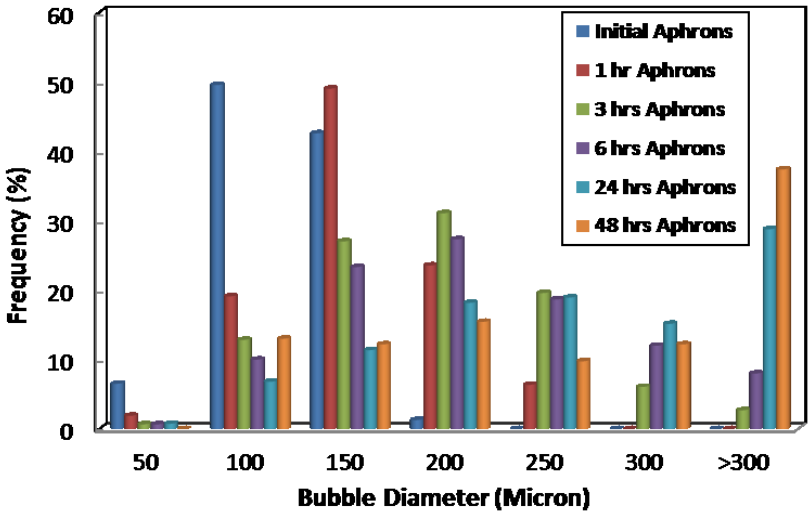

Figure 7.6: Size distributions of CO_2 microbubbles with time.

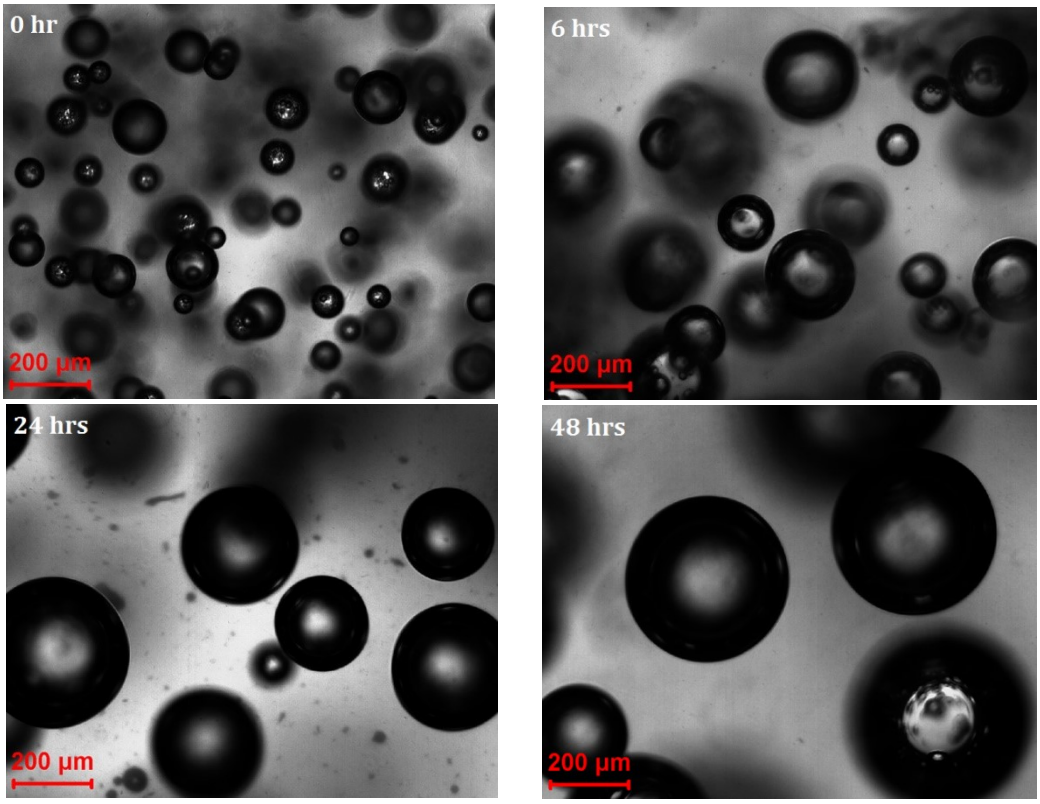

Figure 7.7: CO_2 microbubbles during exposure to the air at room condition.

7.3.4 CO_2 Microbubbles after PVT Tests

Several PVT experiments were performed to analyze the effect of compression/decompression and temperature on microbubbles. Bubble size was measured before each PVT test and compared with the bubble size distribution of sample after the PVT test where microbubbles compressed and decompressed at different temperatures. In general, the measured diameter of the microbubbles shifted towards higher values after PVT tests (Figure 7.8a), but still, more than 90% of microbubbles have diameters less than 300 μm.

The bubble size distribution was measured based on micrographs of microbubbles observed under the microscope. The bubble size distribution was measured from 200 individual bubbles using the image analysis software. The mean bubble diameter, D50, for initial microbubbles was between 100 and 120 mm for all samples. The microbubbles slightly increased in size after PVT test (Figure 7.8b). The microbubbles sample preserved after their generation for a similar period of time as the PVT test had a comparable D50 with that undergone compression and decompression during PVT test, showing a good stability of microbubbles at high pressure and temperature conditions. After PVT test, CO_2 microbubbles increased in size by 25% (±5%); whereas preserved sample enlarged by 33% (±5%). The higher temperature increased the number of large bubbles (>300 μm) (Figure 8a). Based on previous studies, the CGAs were relatively stable at temperatures below 40 °C (104 °F) and were fully unstable at temperatures above 65 °C (149 °F) (Longe, 1989).

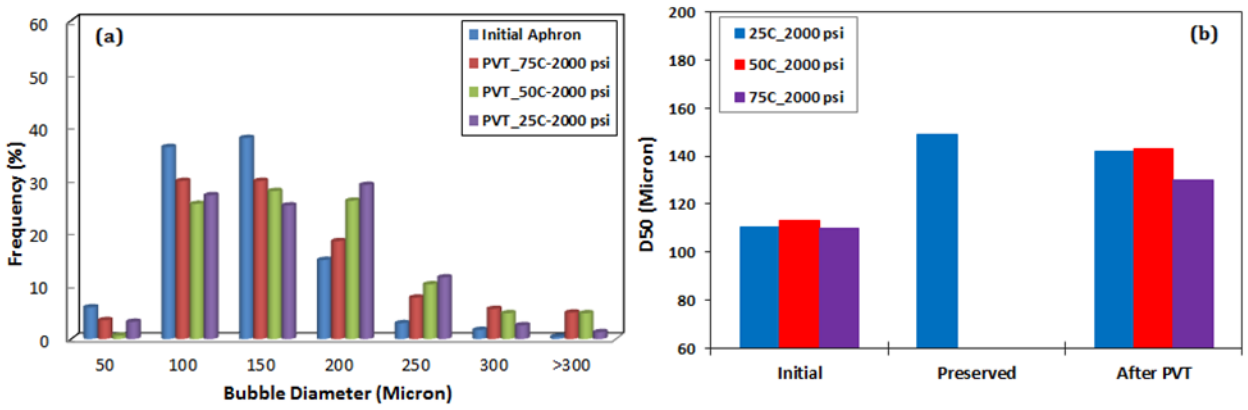

Figure 7.8: (a) Distribution of CO_2 microbubbles size and (b) D50 of CO_2 microbubbles diameter; initially, preserved and after 24 hours PVT tests.

The change in CO_2 microbubbles size during 24 and 48 h PVT analysis (showing the effect of pressurization rate on microbubbles stability) is shown in Figure 7.9. In both tests, the final compression pressure was 2000 psi, whereas the rate of pressurization was different, i.e. in 48-h PVT test, pressurization rate was half of the 24-h test. The microbubbles are affected by the rate of pressurization and/or depressurization. The D50 of CO_2 microbubbles increased in size by 25% (±5%) and 31% (±5%) after compression for 24 and 48 h (up to 2000 psi at the temperature of 25 °C or 77 °F), respectively. The D50 of the preserved sample enlarged by 33% (±5%) at ambient condition. As discussed earlier, the microbubbles enlargement effect was more drastic at a higher temperature and this effect is more evident at the lower pressurization rate. As seen in Figure 7.9(a) and (b), the maximum frequency of initial microbubbles diameter lies between 100 and 150 µm; however, this maximum value is 150–200 µm and >300 µm after 24-h and 48-h PVT test, respectively.

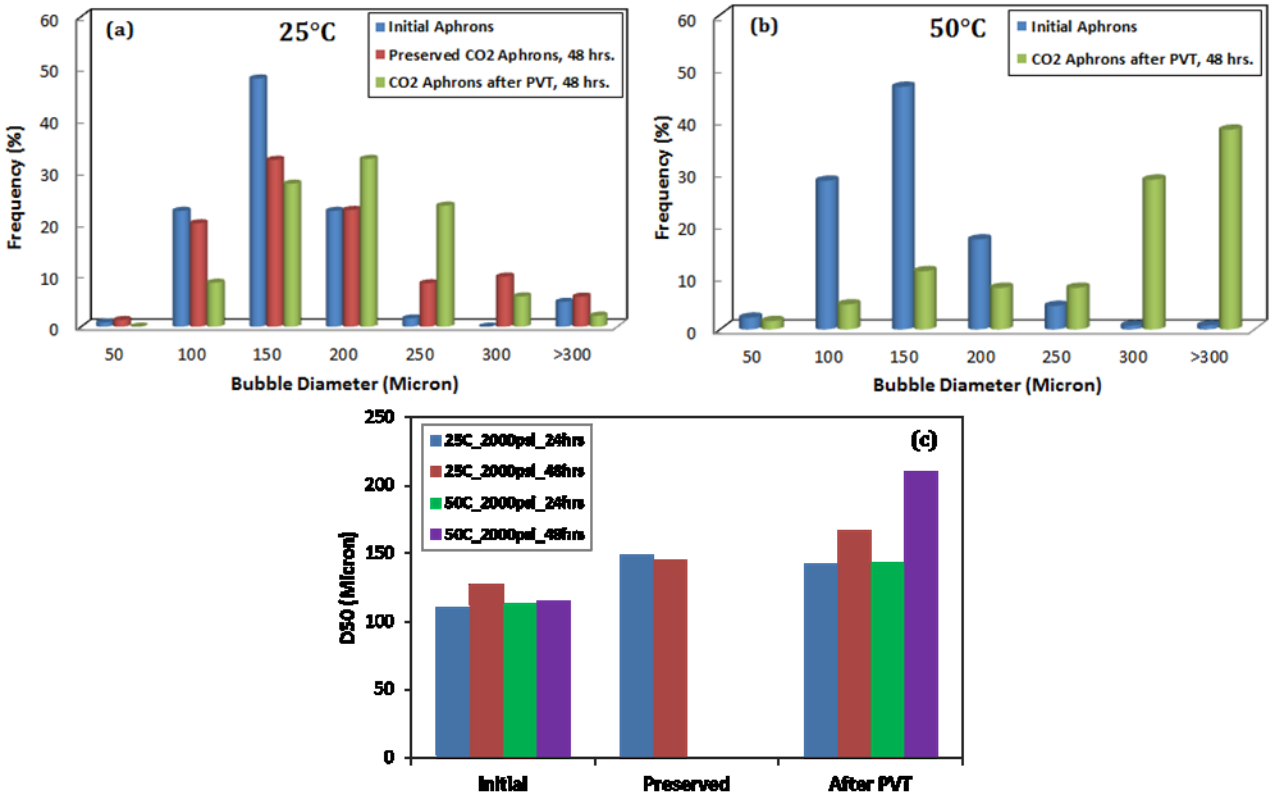

Figure 7.9: CO_2 microbubbles size distribution after 48 hours PV tests: (a) 25°C and (b) 50°C, and (c) D50 of CO_2 microbubbles diameter; initially, preserved and after PVT tests.

Figure 7.10 shows the ability of aphrons to survive during compression and recover or regenerate during decompression after PVT tests. Rapid changes in pressure appear to affect the stability of CO_2 microbubbles much less than slow changes in pressure. These observations agree with Belkin et al. (2005). The slow changes would permit the surfactants and polymers in the aphron shell to rearrange more completely when the pressure (so as the microbubbles size) is changed. During the initial stages of pressurization, the aphron shell compacts and contains an excess of surfactants and polymer, which is expected to decrease its permeability. Therefore, the higher pressurization/depressurization rate gives the less time for surfactants and polymer re-arrangement and resulting in higher stability of microbubbles. At higher temperature, many smaller aphrons

disappeared during compression; on decompressing, the number of bubbles was significantly reduced and the survivors were larger.

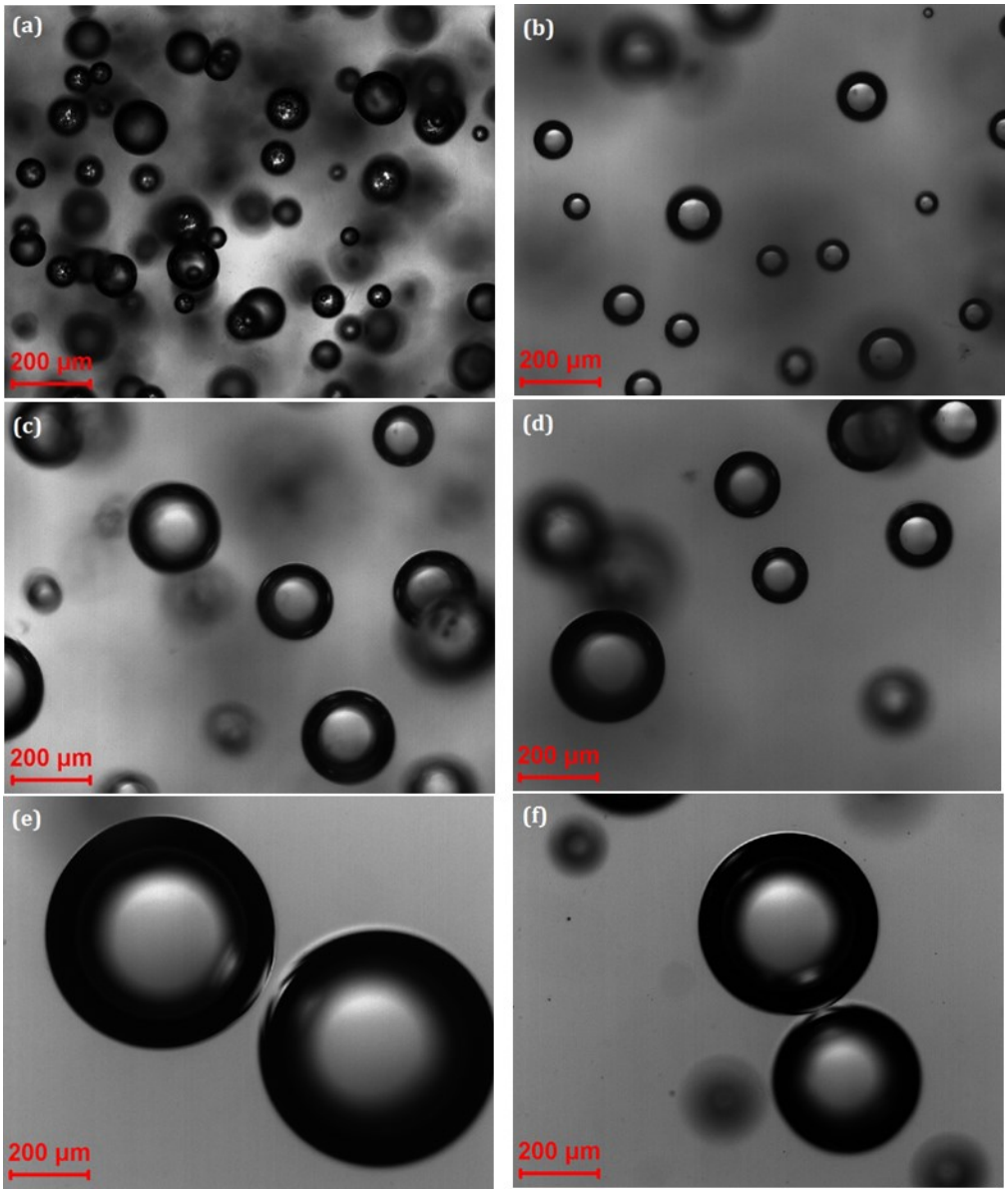

Figure 7.10: Microscopic images of CO_2 microbubbles; (a) Initial, (b) after PVT 25°C, 24 hrs, (c) after PVT 25°C, 48 hrs, (d) after PVT 50°C, 24hrs, (e) after PVT 50°C 48 hrs and (f) after PVT 75°C 24 hrs.

7.3.5 Rheological Study of CO_2 Microbubbles

The viscosity profiles of initial CO_2 microbubbles and base fluid samples (prepared at the same conditions) are almost similar at all shear rates and the shear thinning behavior is evident (Figure 7.11a). As seen, the addition of CO_2 gas to the base fluid solution slightly increased the viscosity at low shear rate region; i.e. at a shear rate of 0.01593 s^{-1} the viscosity of the base fluid and microbubbles is 240 and 284.4 Pa s, respectively. This is due to the structure of CO_2 microbubbles that has a viscous layer surrounded the CO_2 gas. The loss (G″, viscous component) and storage (G′, elastic component) modules of both initial CO_2 microbubbles and base fluid samples slightly increase with respect to frequency (Figure 7.11b). The storage modulus G′ is larger than the loss modulus G″ in all ranges of angular frequency for both samples, under which the elastic component dominates the viscoelastic properties of CO_2 microbubbles and base fluid solution.

The complex modulus (G*) in Figure 7.11c remains constant with increasing stress (s) until the critical stress value is reached, and then G* begins to decrease. The region where G* is independent of the applied stress amplitude is referred as the linear viscoelastic region. All the rheological analyses have been performed in the linear viscoelastic region. The existence of the linear viscoelastic region implies that physical entanglements of the polymer chains in the solutions have not been altered as a result of varied stress amplitudes. Moreover, the moduli are slightly flat and fairly insensitive to frequency (Figure 7.11c), which is typical of highly elastic materials. The storage modulus in all cases was larger than the loss modulus by a factor of 2.

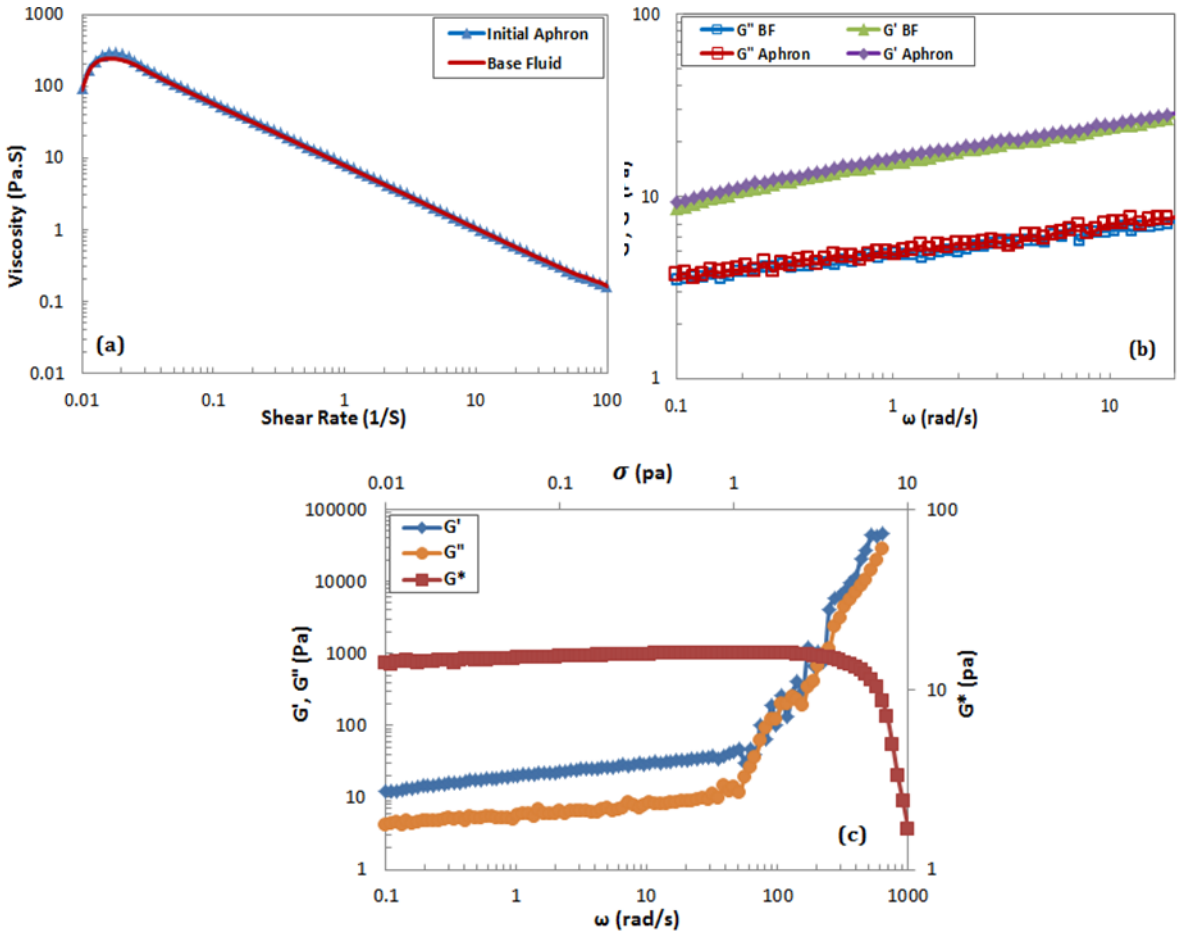

Figure 7.11: (a) Viscosity profile versus shear rate, (b) storage (G') and loss (G") modules versus angular frequency for initial CO_2 microbubbles and the base fluid, and (c) G′ and G″ versus frequency and G* versus stress for initial CO_2 microbubbles.

7.3.6 Rheology of CO_2 Aphrons before and after PVT Tests

After each PVT test, a sample of CO_2 microbubbles was analyzed for rheological characterization and compared with the initial sample. The results are represented in Figures 7.12 and 7.13.

Figure 7.12 shows the viscosity profiles, viscous and elastic moduli of CO_2 microbubbles after PVT tests. After PVT tests at the temperature of 25 °C (77 °F) and 50 °C (122 °F), no major change was seen in viscosity profiles of CO_2 microbubbles compared with the initial sample (Figure 7.12a). However, at the temperature higher than 50 °C (122 °F), a significant decrease in viscosity was evident, particularly at lower shear rates. Similar trends were observed in elastic and viscous

moduli of microbubbles after PVT tests (Figure 7.12b). The moduli profiles of microbubbles significantly decreased at 75 °C (167 °F). One reason can be due to the existence of a critical temperature for the polymer involved in generating CO_2 microbubbles. The polymer loses its structure at a certain temperature and the microbubbles are not able to keep the viscous layer intact.

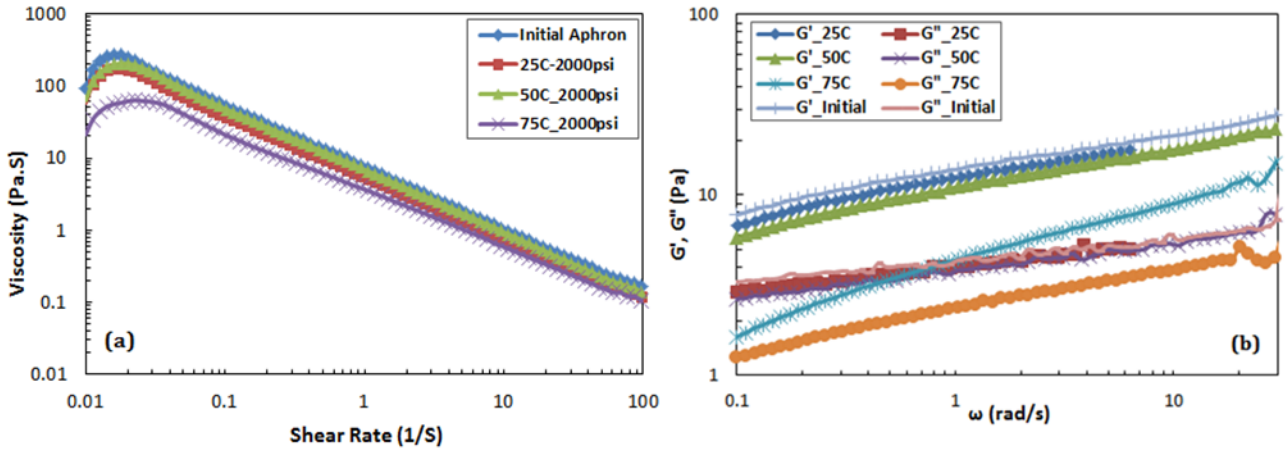

Figure 7.12: Rheological comparison of CO_2 microbubbles after HP-HT PVT tests; viscosity profiles (a) and moduli profiles (b) after 24-hr PVT tests.

The rheological properties of the CO_2 microbubbles after PVT experiments (25 °C and 50 °C) are compared with the initial microbubbles in Figure 7.13. At 25 °C (77 °F), there was no significant difference in rheological properties of CO_2 microbubbles after 24-h and 48-h PVT tests. On the other hand, the moduli and viscosity of CO_2 microbubbles significantly decreased at 50 °C (122 °F) (Figure 7.13c and Figure 7.13d). These results suggest that the effect of the pressurization/depressurization rate on microbubbles stability will be more drastic at higher temperatures. Another explanation is that, if the microbubble is shrinking (due to pressure increases in PVT cell), some of the surfactants is forced to leave the microbubbles surface toward the bulk solution. At lower pressurization rate, the surfactant has more time to leave the microbubbles and rearrange. On the way back (assuming that the microbubbles have kept their

form and properties) the microbubbles will expand. However, there is not enough surfactant now to keep the water and gas together (Growcock et al., 2007). Most likely, the microbubbles will break into its constituent parts resulting drastic change in rheological behavior. These results are also in accordance with the bubble size analysis of the microbubbles. After 48-h PVT test, there have been fewer amounts of the microbubbles and from which most of them were unstable (bigger) compared to 24-h test.

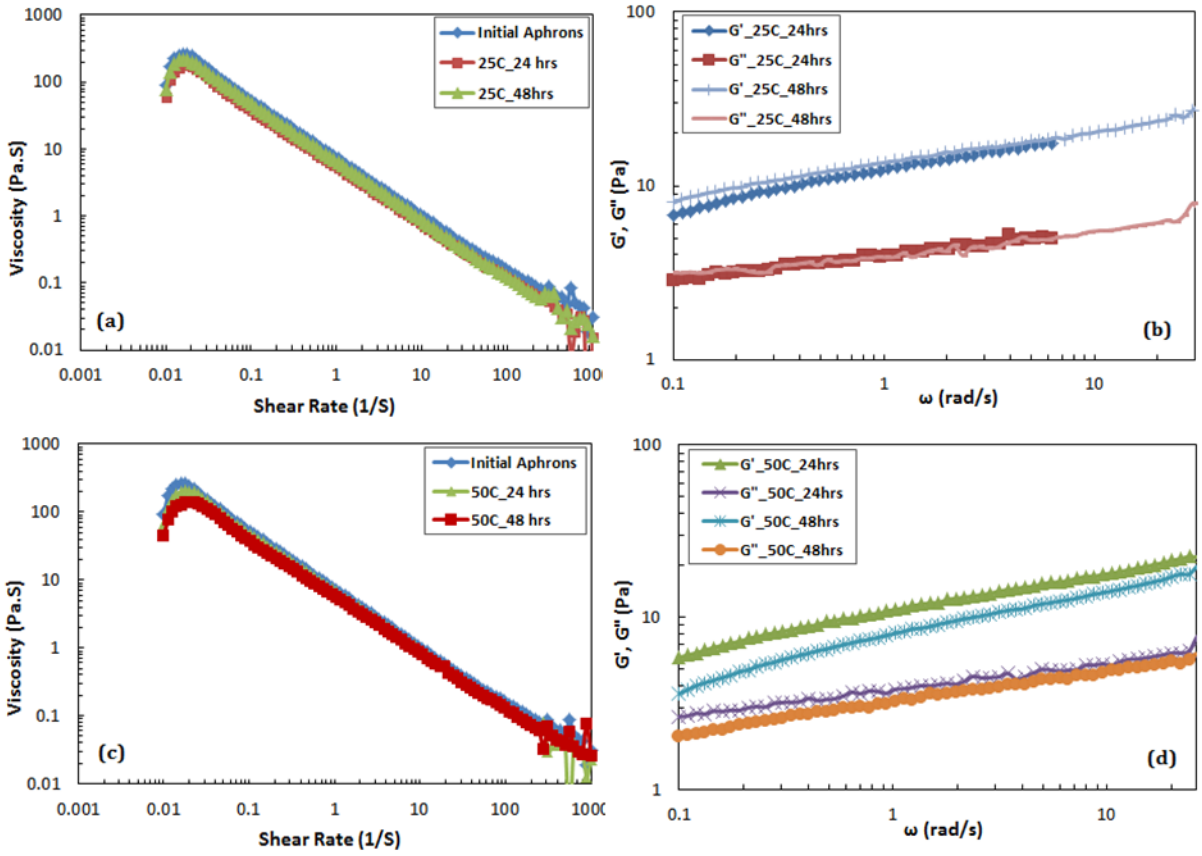

Figure 7.13: Rheological comparison of CO_2 microbubbles after 24-hr and 48-hr PVT tests; (a) viscometry and (b) moduli profiles at 25 °C, (c) viscometry and (d) moduli profiles at 50 °C.

7.3.7 Potential Use of CO_2 Microbubbles for EOR

The problems associated with current enhanced oil recovery process for heterogeneous reservoirs are based on inadequate sweep efficiencies and unfavorable mobility ratios during CO_2 gas injection, which leave much of the recoverable oil upswept in the reservoir (i.e. after water flooding). Therefore, using a blocking agent is essential to divert injected fluid to the unswept part of the reservoir. Microbubbles performance in EOR should be different from foams. The gas content of aphron is less than 30%, whereas foam used for EOR has much higher gas content (50–99%). The main objective of using foams for EOR is increasing gas apparent viscosity, whereas microbubbles contain mainly liquid base fluid with the sparse dispersion of gas bubbles. When compressed, microbubbles stability is much higher than conventional foam bubbles. However, they deform under pressure and shear like conventional bubbles. Laboratory experiments have shown that with only a small pressure differential, “bubbly flow” of the aphrons occurs, by which the low-density microbubbles rush to the fluid front and form a soft seal ahead of the liquid phase (Growcock et al., 2007).

Furthermore, the polymer is usually added to the injected water to increase the viscosity and, therefore, reduce the mobility ratio. Consequently, the addition of the polymer should lead to higher sweep efficiency and increase the oil recovery. However, in the highly heterogeneous reservoirs, the polymer sweep efficiency may be inadequate. On the other hand, aphron fluid follows the “bubbly flow theory” (Popov and Growcock, 2005); therefore, microbubbles move faster than the liquid base fluid. Thus, microbubbles will block the high permeable/transmissible zones, especially those loss zones (with the help of Laplace pressure and Jamin effect) and divert the injected fluid to those areas with lower sweep efficiency. Overall, the microbubbles can be

applied as displacing fluid in those heavy oil reservoirs with a high degree of heterogeneity where the sweep efficiency and then oil recovery is not satisfactory.

Microbubble size analysis, rheological analysis as well as the PVT study of microbubbles under elevated pressure and temperature reveals the capability of this fluid to survive under reservoir condition. It is worth mentioning that static stability of microbubbles is not directly representative of their stability in porous media; however, they should be stable at static conditions for further consideration in porous media, therefore, the static stability results can be used for comparing the stability of microbubbles with its base fluid. As microbubbles are compressed (as also seen during the PVT test), they become highly energized. This energy is available for bubble expansion and pressure sealing within the reservoir (Laplace pressure and Jamin effect). The Jamin effect is defined as the resistance to liquid flow through capillaries, which is due to the presence of bubbles that can be explained by the Laplace formula; $\Delta p=2\sigma/r$. Furthermore, polymer-solution injectivity is an important consideration. For example, routine injection well cleanup jobs may be required if the polymer solution damages injectivity. These cleanup jobs can detract from the polymer flood's economics and effectiveness. Polymer solution injectivity is more favorable when a polymer solution such as aphron exhibits shear-thinning viscosity behavior. Due to the presence of gas bubbles, aphron has the higher compressibility than base fluid. This characteristic of microbubbles results in better injectivity of this fluid into the reservoir. Shivana et al. (2012) studied various combinations to determine the optimum concentration to yield stable microbubbles for smooth and undisturbed flooding operation. They reported lower injection pressure and a stable displacement front for CGAs during core flood experiments.

In order to study the behavior of CO_2 microbubbles during the oil recovery process, sand-pack experiments were performed and the results were compared to the base fluid flooding. For this

aim, a linear visual sand-pack model was used to conduct the tests at ambient pressure and temperature conditions. As seen in Figure 7.14, CO_2 microbubbles showed higher injectivity compared to the base fluid while ultimate oil recoveries of both fluids are the same. The small amount of CO_2 gas in the form of microbubbles increased the compressibility and significantly improved the injectivity. Despite slightly earlier oil production during base fluid injection, both CO_2 microbubbles and the base fluid almost reached their ultimate oil recovery (around 98%) after about 1.5 PV injections. At that time (1.5 PV), an injection pressure of base fluid was 5 times higher than that of CO_2 microbubbles. This result shows that how CO_2 microbubbles significantly improved the injectivity of base fluid without any change in ultimate oil recovery. Another interesting fact is that CO_2 microbubbles were observed in the produced liquid after flooding in heavy oil saturated porous media, demonstrating their high stability during EOR process. Figure 7.14(b) shows the picture of produced microbubbles sample after heavy oil EOR. During the early stage of flooding, effluent samples only contained water and heavy oil. After the breakthrough, emulsified oil was produced with the microbubbles; however, most of the oil was produced before breakthrough due to piston like displacement. It is worth mentioning that the resistance factor of injected fluid is directly proportional to the pressure drop in porous media. Since the injection of CO_2 microbubbles increases the pressure drop compared to that of water or gas injections, it has comparatively higher resistance factor. It is worth mentioning that too high resistance factor results in low injectivity as seen during base fluid flooding in both sand-pack and micromodel.

The effectiveness of CO_2 microbubbles and base fluid during heavy oil recovery in a fracture-dominated system was also studied. Figure 7.15 shows the performance of microbubbles and base fluid in the fractured micromodel during heavy oil recovery. Images of micromodel during the CO_2 microbubbles and base fluid injections at different time intervals are shown in Figure 7.15(a)–

(d). After about 24 hours of injection, CO_2 microbubbles could sweep almost all oil from both matrix and fracture. However, base fluid could only sweep the oil in fracture and had little effect on matrix oil near the fracture. During base fluid flooding, injected fluid first created a channel within the fracture and then expanded until sweeping the oil only within the fracture.

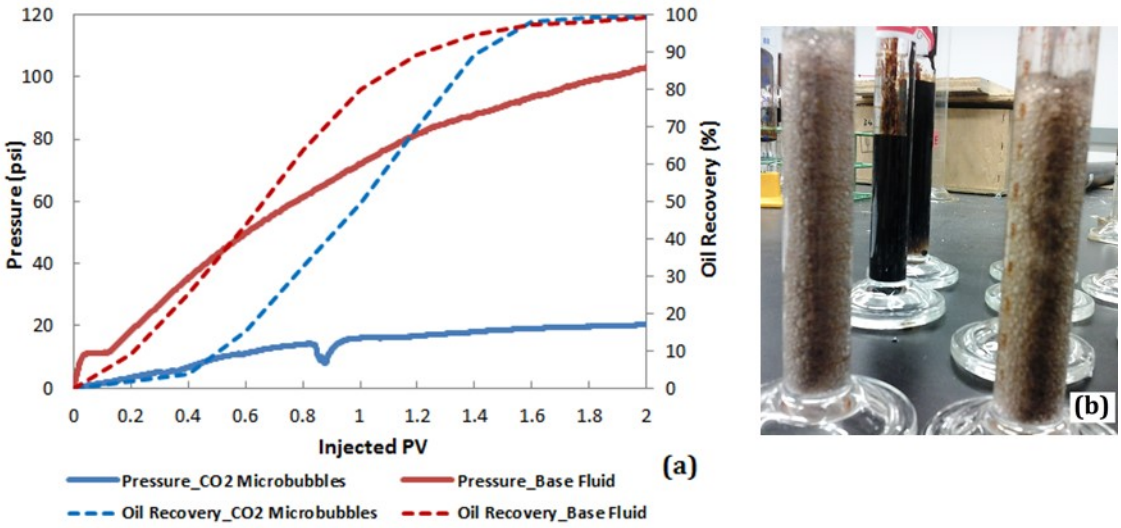

Figure 7.14: (a) Injection pressure and oil recovery for CO_2 microbubbles and base fluid during flow through 1D sand-pack experiment, and (b) CO_2 microbubbles effluent samples.

Figure 7.16 clearly illustrates the mechanisms of oil displacement by microbubbles from the matrix in pore-scale experiments. At the early stage, microbubbles only swept the fracture as expected. As flooding continued, the gas phase distributed as discrete aphron bubbles in a continuous liquid phase (bubbly flow) resulted in resistance to flow within the fracture. A single aphron bubble may easily move within the fracture path while a network of bubbles increases the capillary force resulting resistance to flow within the fracture. The hydrophobic nature of the aphron shell enables aphrons to clump together, yet resist coalescence. As shown by Growcock et al. (2004), aphrons can form large aggregates in the pore throats or fracture tip. This structure possesses the same hydrophobic character of the individual aphrons (Sebba, 1987). The resistance to flow within the

fracture caused the diversion of injected fluid toward the matrix. The invasion of fluid into the matrix can be seen in Figure 7.16. This process is responsible for the high sweep efficiency of microbubbles in heavy oil saturated matrix. As seen in Figures 7.15 and 7.16, stable microbubbles accumulate and create a bridging mechanism, which further increases the resistance to flow within the fracture. Thereafter, the base liquid fluid containing the polymer and surfactant invaded into the matrix. Within the matrix, the surfactant emulsified the heavy oil, reduced the interfacial tension, and recovered the oil droplets from the matrix. The presence of polymer enhanced the viscosity and improved the oil recovery process. These oil droplets then were moved towards the fracture and were transported with the help of microbubbles to the producer. This process continued until most of the oil was swept from the matrix.

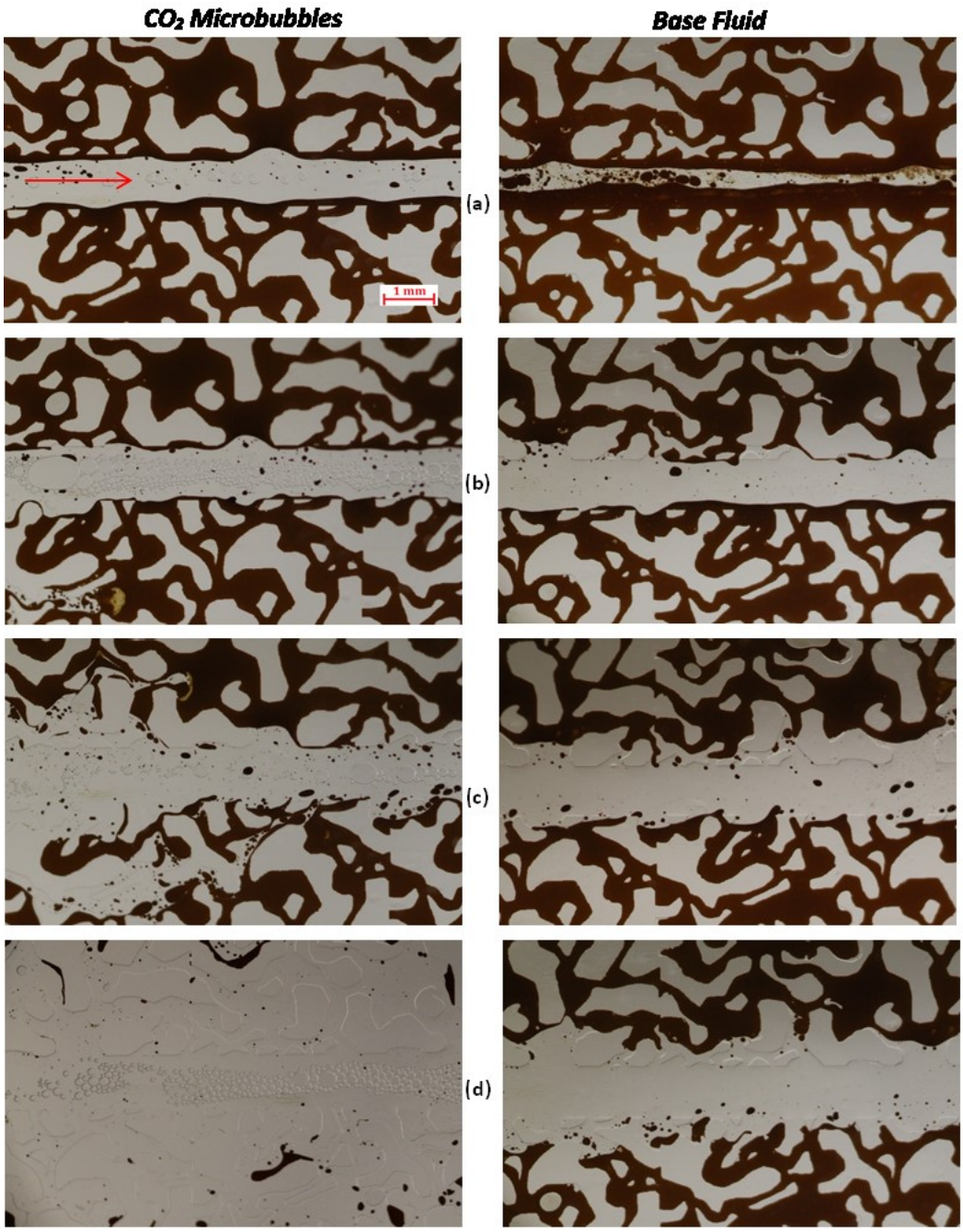

Figure 7.15: Images of the fractured micromodel during microbubble and base fluid flooding for heavy oil recovery (arrow representing flow direction, from left to right); after (a) 10 min, (b) 30 min, (c) 14 h, and (d) 24 h of flooding.

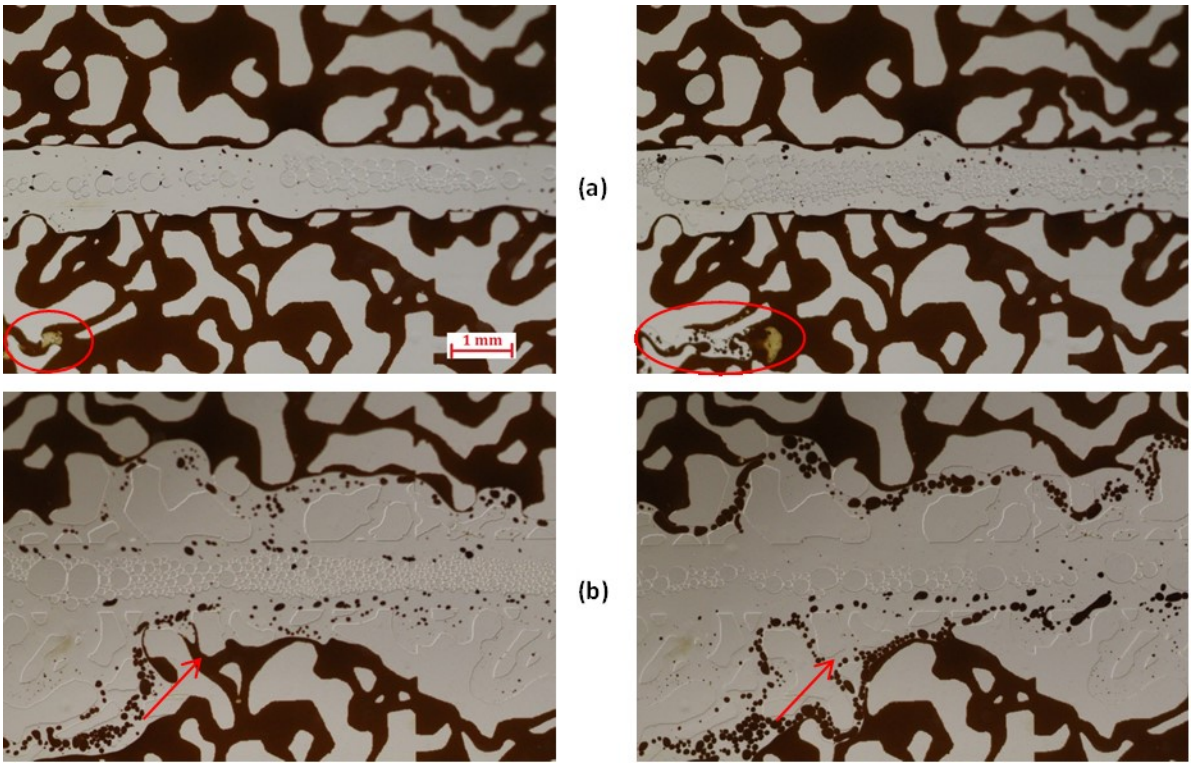

Figure 7.16: Heavy oil recovery by CO_2 microbubbles; (a) and (b) images were taken during the early stage (15 and 20 min, respectively); representing fluid invasion into the matrix and emulsification of oil, (b) and (c) images show the later stage of flooding (60 and 65 min, respectively); arrows representing flow direction of emulsified oil from matrix toward the fracture.

7.4 Summary

Microbubbles have a unique structure compared to conventional foam bubbles and because of the characteristics of this structure; they offer many benefits to petroleum industry applications. The sealing feature of aphrons drives a micro-environment seal in larger openings; indicating high potential of this fluid for enhanced oil recovery, especially in heterogeneous reservoirs. This chapter aimed to characterize the properties of CO_2 microbubbles by rheological, microbubble size, PVT as well as flow behavior studies. The summary of this chapter is as follows:

- CO_2 microbubbles show a long time rheological stability, even after being exposed to ambient conditions for 48 h.

- The size of CO_2 microbubbles (D50) increased only by 25±5% after 24 h PVT tests (without any major loss in the number of bubbles), whereas for the samples under ambient conditions (for 24 h) D50 of microbubbles increased by 33±5% of their original size, demonstrating good stability of microbubbles under elevated pressure and temperature condition.
- The lower rate of pressurization/depressurization has a drastic effect on the size of microbubbles, enhanced by increasing temperature. Low pressurization/depressurization rate, provides enough time for surfactant rearrangement. Consequently, microbubbles became more unstable (bigger in size).
- PVT tests indicated that microbubbles can survive at least up to a pressure of 2000 psig and temperature of 50 °C (122 °F). However, above this temperature, the stability of microbubbles was decreased; the bubbles have grown and appear to be larger than their initial size.
- This study showed that temperature above 50 °C (122 °F) can be critical for rheological properties and the P-V relation of CO_2 microbubbles.
- CO_2 microbubbles showed outstanding performance and stability, as well as the better injectivity compared to the liquid base fluid during heavy oil recovery in porous media.
- Furthermore, detailed micromodel studies showed that in a heterogeneous porous media, the resistance to flow in fracture (due to the presence of microbubbles) resulted in high sweep efficiency and indicated the potential of CO_2 microbubbles for enhanced heavy oil recovery, particularly in heterogeneous reservoirs with low sweep efficiency.

Chapter 8: Conclusions and Recommendations

8.1 Conclusions and Contributions

The focus of this thesis was to conduct laboratory experiments which would help in understanding mechanisms and performance of CO_2 foam/PEF for enhanced heavy oil recovery in various scenarios such as heterogeneity, effects of crude oil, wettability, etc. Also, the objective was to analyze how foam can be applied as an EOR method for heavy oil reservoirs in combination with current heavy oil recovery methods to improve the overall efficiency of the process. Following are the main conclusions of this thesis.

8.1.1 CO_2 Foam and CO_2 PEF for Improving Chemical EOR Methods

8.1.1.1 Static Analysis of Foam/PEF

- In the static (bulk foam) analysis in the presence and the absence of heavy crude oil, PEF showed higher stability than that of conventional foam. However, per the results of this thesis, selecting the proper type of surfactant is important to have a stable PEF in the presence of oil. PEF generated with a weak foaming agent could not significantly increase the stability of the conventional foam.

8.1.1.2 Pore-scale

- Pore-scale observation through this thesis proved that stable foam/PEF bubbles can significantly push the injected fluid toward untouched parts of the porous media and increase the oil recovery compared to that of surfactant flooding. Due to the liquid viscosity enhancement and bubble stability improvement, the effectiveness of PEF in heavy oil sweep efficiency was much higher than that of conventional foams. PEF bubbles generated

an additional force to divert surfactant/polymer into the matrix of the fractured porous media and resulted in additional oil recovery.

- EOR performance of each foaming solution in oil wet fractured porous media depends on its ability to generate stable foam rather than its wettability alteration potential. Because viscous flow is dominant in foam EOR and produces the oil faster and more effective than that of imbibition flow. For example, the ability of studied surfactants to imbibe into the matrix was in the order of CTAB >> N85 > DDBS, while their ability of matrix oil recovery during foam flooding after surfactant flooding was in the order of DDBS > CTAB > N85. Foaming potential is more important than wettability alteration when selecting a surfactant for foam EOR. However, a surfactant with good performance in both foaming and wettability alteration can have a synergic effect on heavy oil recovery.

8.1.1.3 Core-scale

- The porous media experiments (sand-pack) showed better performance of PEF in the presence of heavy oil compared to that of foam. The addition of polymer to the strong foaming solution accelerated the foam generation and increased its stability in heavy oil saturated porous media. PEF produced ~ 98% of residual oil saturation while this value was ~ 78% for foam after 3.5 PV injections.
- In actual rock samples, the addition of polymer to conventional CO_2 foam could significantly improve its performance for heavy oil recovery. CO_2 PEF recovered about 26% and 12% of residual oil (after water flooding process) in the homogeneous and fractured core, respectively.
- Per the injection pressure profiles, the addition of polymer to the conventional CO_2 foam resulted in faster propagation of PEF in homogeneous porous media showing that CO_2 PEF

had more dynamic stability in the presence of oil compared to that of conventional foam. This also resulted in faster oil production and higher ultimate oil recovery during CO_2 PEF injection.

8.1.2 CO_2 Foam/PEF to Improve EOR by Hydrocarbon Solvent Injection

- One of the main issues during hydrocarbon solvent injection is asphaltene deposition and formation damage. Observation through this study revealed the relation between dominant flow mechanism and shape of deposited asphaltene. Parallel depositions (usually in viscous dominant flow) are less destructive than that of perpendicular depositions (usually in diffusion dominant flow).
- The combination of foam and hydrocarbon solvent, either as an SBF or post-solvent foam flooding could significantly reduce the formation damage and improve the heavy oil recovery. Since by applying foam, the dominant flow mechanism is no longer diffusion and viscous flow plays more important role in the recovery process. Therefore, asphaltene deposition is less and formation damage is not severe.

8.2 Contributions

- On of the main contribution of this study was visualizing and analyzing the mechanisms involved in different EOR methods (especially CO_2 foam/PEF) in a fractured porous media containing heavy oil. Different mechanism and behavior were introduced throughout the thesis which can improve our understanding of the EOR process by foam/PEF in such reservoirs.
- For the first time, this study analyzed different shapes of asphaltene deposition and potential of formation damage based on dominant flow mechanism. This can significantly

contribute to designing and conducting an efficient EOR method in reservoirs where the asphaltene deposition and formation damage is a significant issue.

- Introducing the potential of new hybrid-solvent EOR by combining with foam/PEF which resulted in improving the heavy oil recovery and reducing the formation damage caused by asphaltene deposition.

8.3 Possible Applications

The findings can be applied to improve heavy oil recovery from homogenous and fractured reservoirs. CO_2 foam and especially CO_2 PEF have the potential to be used in the reservoirs where the polymer is using as a mobility control agent.

Moreover, CO_2 foam/PEF can be used in combination with hydrocarbon solvent injection to reduce the formation damage resulting from asphaltene deposition during the solvent injection process.

8.4 Recommendations for Future Work

- In the future, it would be helpful to understand further about the performance of CO_2 foam/PEF in core scale with the help of CT scan analysis. It can be a helpful method to accurately measure and study the amount and the distribution of CO_2 remained in the rock at the end of foam EOR process.
- This study did not consider the effect of temperature on foam/PEF performance. Foaming solutions need to be also evaluated at the elevated temperatures and high salinity, especially for carbonate formations.
- CO_2 microbubbles, as an enhanced version of CO_2 PEF, could increase the heavy oil recovery and CO_2 sequestration much further due to its higher stability. However, more

research is required to analyze its field application potential (e.g. preparation and generation in field scale, cost analysis for EOR, screening the target reservoirs, etc.).

- Dynamic behavior of asphaltene deposition in fractured media revealed interesting results in terms of the shape of deposited asphaltene and pore blocking ability. This can be studied further in both pore-scale and core-scale.
- In this thesis, various mechanisms were observed in pore-scale during foam/PEF EOR. Pore-scale modeling can be performed to analyze these mechanisms much further.

References

Aarra, M.G., Ormehaug, P.A., Skauge, A., and Masalmeh, S.K. 2011. Experimental Study of CO_2- and Methane- Foam Using Carbonate Core Material at Reservoir Conditions. Paper SPE 141614 presented at the SPE Middle East Oil and Gas Show and Conference, 25-28 September, Manama, Bahrain.

Adibhatla, B., and Mohanty, K.K. 2006. Oil Recovery from Fractured Carbonates by Surfactant-Aided Gravity Drainage: Laboratory Experiments and Mechanistic Simulations. Paper SPE 99773 presented at SPE/DOE Symposium on Improved Oil Recovery, Tulsa, Oklahoma, 22-26 April.

Alargova, R.G., Warhadpande, D.S., Paunov, V.N., and Velev, O.D. 2004. Foam Superstabilization by Polymer Microrods. Langmuir 20 (24): 10371-10374.

Amiri, M.C., and Woodburn, E.T., 1990. A Method for the Cfharacterization of Colloidal Gas Aphron Dispersions. Chemical Engineering Research and Design, 68 (2), 154-160.

Andrianov, A., Farajzadeh, R., Mahmoodi Nick, M., Talanana, M., and Zitha, P.L.J. 2012. Immiscible foam for enhancing oil recovery: bulk and porous media experiments. Ind. Eng. Chem. Res. 51 (5): 2214-2226.

Arabloo, M., Shahri, M.P., Zamani, M., 2012. Characterization of Colloidal Gas Aphron-Fluids Produced from a New Plant-Based Surfactant. Journal of Dispersion Science and Technology, 34(5), 669-678.

Austad, T., and Milter, J. 1997. Spontaneous Imbibition of Water into Low Permeable Chalk at Different Wettabilities Using Surfactants. Paper SPE 37236 presented at the SPE International Symposium on Oilfield Chemistry, Houston, 18–21 February.

Austad, T., Matre, B., Milter, J., Sævareid, A., and Øyno, L. 1998. Chemical flooding of oil reservoirs 8. Spontaneous oil expulsion from oil- and water-wet low permeable chalk material by imbibition of aqueous surfactant solutions, Colloids Surf., A 137 (1-3): 117-129.

Aveyard, R., Binks, B.P., Fletcher, P.D.I., Peck, T.G., Rutherford, C.E. 1994. Aspects of aqueous foam stability in the presence of hydrocarbon oils and solid particles. Advanced Colloid Interface Science, 48 (5 April 1994): 93-120.

Baghdikian, S., and Handy, L.L. 1991. Transient Behavior of Simultaneous Flow of Gas and Surfactant in Consolidated Porous Media. DOE report DOE/BC/14600-10.

Basheva, E.S., Ganchev, D., Denkov, N.D., Kasuga, K., Satoh, N., and Tsujii, K. 2000. Role of Betaine as Foam Booster in the Presence of Silicone Oil Drops. Langmuir 16 (3): 1000-1013.

Belkin, A., Irving, M., O'Connor, B., Fosdick, M., Hoff, T., and Growcock, F. B., 2005. How Aphron Drilling Fluids Work. SPE Annual Technical Conference and Exhibition, Dallas.

Bernard, G.G. and Jacobs, W.L. 1965. Effect of Foam on Trapped Gas Saturation and on Permeability of Porous Media to Water. SPEJ. 5 (4): 295-300.

Bickerman, J. J. Foams, Springer Verlag, New York, 1973.

Binks, B.P., and Horozov, T.S. 2005. Aqueous foams stabilized solely by silica nanoparticles. Angew. Chem., Int. Ed., 44 (24): 3722-3725.

Binks, B.P., Kirkland, M., and Rodrigues, J.A. 2008. Origin of stabilisation of aqueous foams in nanoparticle-surfactant mixtures. Soft Matter, 4 (12): 2373-2382.

Bjorndalen, N, Jossy, W.E., Alvarez, J.M., Kuru, E., 2014. A laboratory investigation of the factors controlling the filtration loss when drilling with colloidal gas aphron (CGA) fluids. Journal of Petroleum Science and Engineering, 117 (2014): 1-7.

Bjorndalen, N., and kuru, E., 2008a. Stability of Microbubble-Based Drilling Fluids under Downhole Conditions. Journal of Canadian Petroleum Technology, 47(6), 40-47.

Bjorndalen, N., and kuru, E., 2008b. Physico-Chemical Characterization of Aphron-Based Drilling Fluids. Journal of Canadian Petroleum Technology, 47(11), 15-21.

Bond, D.C. and Holbrook, O.C., 1958. Gas Drive Oil Recovery Process. US Patent No. 2,866,507.

Bourbiaux, B.J., 2009. Understanding the Oil Recovery Challenge of water drive fractured reservoirs. International Petroleum Technology Conference (IPTC), Doha, Qatar, 7-9 December.

Brookey T., 1998. Microbubbles: New Aphron Drill-In Fluid Technique Reduces Formation Damage in Horizontal Wells. SPE International Symposium on Formation Damage Control, Lafayette, Louisiana.

Brookey, T.F., 1999. Aphron-Containing Well Drilling and Servicing Fluids. United State Patent US 5881826.

Buenrostro-Gonzalez, E., Lira-Galeana, C., Gil-Villegas, A., and Wu, J., 2004. Asphaltene precipitation in crude oils: Theory and experiments. AIChE J. 50 (10): 2552-2570

Butler, R., and Mokrys, I.J., 1989. Solvent Analog Model of Steam-Assisted Gravity Drainage. AOSTRA J. Res. 5 (1): 17–32.

Butler, R., and Mokrys, I.J., 1991. A New Process (VAPEX) for Recovering Heavy Oils using Hot Water and Hydrocarbon Vapor. J Can Pet Technol 30 (1): 97-106.

Calvert, J.R.: "Foam in Motion." in Foams: Physics, Chemistry and Structure, A. J. Wilson, Springer Verlag, Berlin, 1989.

Cardoso, J., Spinelli, L., Monteiro, V., Lomba, R., Lucas, E., 2010. Influence of Polymer and Surfactant on the Aphrons Characteristics: Evaluation of Fluid Invasion Controlling. eXPRESS Polymer Letters, 4(8), 474-479.

Carstensen, B., Gupta, R., Luton, M.J., Peiffer, D.J., Pokutylowicz, N.M., Polizzotti, R.S., Spiecker, P.M., 2007. Method for fabricating compressible objects for a variable density drilling mud. Patent Publication number WO2007145735 A2; 2007.

Cervantes-Martinez, A., and Maldonado, A., 2007. Foaming behaviour of polymer–surfactant solutions. J. Phys. Condens. Matter, 19 (24): 7 pp.

Chambers, K.T., Radke, C.J., 1991. Capillary phenomena in foam flow through porous media. In: Morrow, N.R. (Ed.), Interfacial Phenomena in Petroleum Recovery. Marcel Dekker, New York, NY, pp. 191_255. (Chapter 6).

Chaphalkar, P.G. Valsaraj, K.T. and Roy, D., 1993. A Study of the Size Distribution and Stability of Colloidal Gas Aphrons Using a Particle Size Analyzer. Separation Science and Technology, 26(6), 1287-1302.

Chen, Q., Gerritsen, M.G., and Kovscek, A.R., 2010a. Improving Steam-Assisted Gravity Drainage Using Mobility Control Foams: Foam Assisted-SAGD (FA-SAGD). Paper SPE 129847 presented at the SPE Improved Oil Recovery Symposium, 24-28 April, Tulsa, Oklahoma, USA.

Chen, Q., Gerritsen, M.G., and Kovscek, A.R., 2010b. Modeling Foam Displacement with the Local Equilibrium Approximation: Theory and Experiment Verification. SPEJ 15 (1): 171-183.

Chen, Y., Elhag, A.S., Poon, B.M., Cui, L., Ma, K., Liao, S.Y., Omar, A., Worthen, A., Hirasaki, G.J., Nguyen, P.Q., and Johnston, K.P., 2012. Ethoxylated Cationic Surfactants for CO_2 EOR in High Temperature, High Salinity Reservoirs. Paper SPE 154222 presented at the SPE Improved Oil Recovery Symposium, 14-18 April, Tulsa, Oklahoma, USA.

Chillenger, G.V., and Yen, T.F., 1983. Some Notes on Wettability and Relative Permeability of Carbonate Rocks, II. Energy and Sources 7 (1): 67-75.

Chou, S.I., 1991. Conditions for generating foam in porous media. Paper SPE 22628 presented at the SPE Annual Technical Conference and Exhibition, 6-9 October, Dallas, TX.

Cilliers, J.J., Bradshaw, D.J., 1996. The Flotation of Fine Pyrite Using Colloidal Gas Aphrons. Minerals Engineering, 9(2), 235-241.

Ciriello, S., Barnett, S.M., Deluise F. J., 1982. Removal of Heavy Metals from Aqueous Solutions Using Microgas Dispersions. Separation Science Technology, 17(4), 521-534.

Conn, C.A., and Ma, K., and Hirasaki, G.J., and Biswal, S.L., 2014. Visualizing oil displacement with foam in a microfluidic device with permeability contrast. Lab Chip, 14 (20): 3968-3977.

Cuenca, A., Lacombe, E., Morvan, M., Le Drogo, V., Giordanengo, R., Chabert, M., and Delamaide, E., 2014. Design of Thermally Stable Surfactants Formulations for Steam Foam Injection. Paper SPE 170129 presented at the SPE Heavy Oil Conference-Canada, 10-12 June, Calgary, Alberta, Canada.

Cui, Z.G., Cui, Y.Z., Cui, C.F., Chen, Z., and Binks, B.P., 2010. Aqueous Foams Stabilized by In-Situ Surface Activation of CaCO3 Nanoparticles via Adsorption of Anionic Surfactant. Langmuir 26 (15): 12567-12574.

Da Silva, F.L., and Belery, P., 1989. Molecular diffusion in naturally fractured reservoirs: a decisive recovery mechanism. SPE 19672, paper presented at the 64th SPE Fall Meeting, San Antonio, TX, 8-11 October.

Das, S.K., and Butler, R.M., 1998. Mechanism of the vapor extraction process for heavy oil and bitumen. J. Pet. Sci. Eng. 21(1-2):43-59

de Haas, T.W., Fadaei, H. Guerrero, U., and Sinton, D., 2013. Steam-on-a-chip for oil recovery: the role of alkaline additives in steam assisted gravity drainage. Lab Chip, 13 (19): 3832-3839.

Dehghan, A.A., Farzaneh, S.A., Kharrat, R. Ghazanfari, M. H., and Rashtchian. D., 2010. Pore-Level Investigation of Heavy Oil Recovery during Water Alternating Solvent Injection Process. Transp. Porous Med. 83 (3): 653–666.

Denkov, N.D., 2004. Mechanisms of Foam Destruction by Oil-Based Antifoams. Langmuir 20 (22), 9463-9505.

deSwaan, A., 1978. Theory of Waterflooding in Fractured Reservoirs. SPEJ. 18 (02): 117-122.

Dhara, D., and Shah, D.O., 2001. Effect of Poly (ethylene glycol)s on Micellar Stability of Sodium Dodecyl Sulfate. Langmuir 17 (23): 7233-7236.

Dilgren, R.E., Deemer, A.R., and Owens, K.B., 1982. The Laboratory Development and Field Testing of Steam/Noncondensible Gas Foams for Mobility Control in Heavy Oil Recovery. paper SPE 10774 presented at the SPE California Regional Meeting, 24-26 March, San Francisco, California.

Edmunds, N.R., 1998. Investigation of SAGD steam trap control in two and three dimensions. Paper SPE 50413 presented at the SPE International Conference on Horizontal Well Technology, 1-4 November, Calgary, Alberta, Canada.

Espinoza, D.A., Caldelas, F.M., Johnston, K.P., Bryant, S.L., and Huh, C., 2010. Nanoparticle-stabilized supercritical CO_2 foams for potential mobility control applications. Paper SPE 129925 presented at the SPE Improved Oil Recovery Symposium, 24-28 April, Tulsa, Oklahoma, USA.

Ettinger, R. A., and Radke, C. J., 1992. Influence of Texture on Steady Foam Flow in Berea Sandstone. SPERE 7 (01): 83-90.

Farajzadeh, R., Andrianov, A., and Zitha, P.L.J., 2010. Investigation of Immiscible and Miscible Foam for Enhancing Oil Recovery. Ind. Eng. Chem. Res. 49 (4): 1910-1919

Farshbaf Zinati, F., Farajzadeh, R., and Zitha, P. L. J., 2007. Modeling and CT scan Study of the Effect of Core Heterogeneity on Foam Flow for Acid Diversion. Paper SPE 107790 presented at the European Formation Damage Conference, 30 May-1 June, Scheveningen, the Netherlands.

Farzaneh, S.A., Kharrat, R., and Ghazanfari, M.H., 2010. Experimental Study of Solvent Flooding to Heavy Oil in Fractured Five-Spot Micro-Models: The Role of Fracture Geometrical Characteristics. JCPT 49 (03): 36-43.

Ferno, M. A., Gauteplass, J., Pancharoen, M., Haugen, Å., Graue, A., Kovscek, A. R., and Hirasaki, G., 2016. Experimental Study of Foam Generation, Sweep Efficiency, and Flow in a Fracture Network. SPEJ. doi:10.2118/170840-PA.

Fjelde, I., Zuta, J., and Duyilemi, O.V., 2008. Oil Recovery from Matrix during CO2-Foam Flooding of Fractured Carbonate Oil Reservoirs. Paper SPE 113880 presented at the Europec/EAGE Conference and Exhibition, 9-12 June 2008, Rome, Italy.

Flick, E. W., 1993. Industrial surfactants; Noyes Publications: Park Ridge, NJ; 2nd ed.

Friberg, S.E., and Ahmad, S.I., 1971. Liquid crystals and the foaming capacity of an amine dissolved in water and p-xylene. J. Coll. Interface Sci., 35 (1): 175-175.

Friberg, S.E., Blute, I., and Stenius, P., 1989. Foam stability in a glycerol system. J. Coll. Interface Sci., 127 (2): 573-82.

Friberg, S.E., Blute, I., Kunieda, H., and Stenius, P., 1986. Stability of hydrophobic foams. Langmuir, 2 (5): 659-64.

Friberg, S.E., Chang, S., Greene, W.B., and Gilder, R.V., 1984. A nonaqueous foam with excellent stability. J. Coll. Interface Sci., 101 (2): 593-595.

Fuhr, B.J., Cathrea, C., Coates, L., Kalra, H., and Majeed, A.I., 1991. Properties of asphaltenes from a waxy crude. Fuel 70 (11): 1293–1297.

Fujii,S., Ryan, A.J., and Armes, S.P., 2006. Long-Range Structural Order, Moiré Patterns, and Iridescence in Latex-Stabilized Foams. J. Am. Chem. Soc. 128 (24): 7882-7886.

Galas, C., Clements, A., Jaafar, E., Jeje, O., Holst, D., and Holst, R., 2012. Identification of Enhanced Oil Recovery Potential in Alberta, Final Report. Prepared for Energy Resources Conservation Board, Sproule Associates Limited, 629 p.

Garrett, P.R., 1993. The Mode of Action of Antifoams, in Defoaming: Theory and Industrial Applications, edited by P.R. Garrett, Marcel Dekker, New York, p. 14.

Gauglitz, P.A., Friedmann, F., Kam, S.I., and Rossen, W.R., 2002. Foam generation in homogeneous porous media. J. Chem. Eng. Sci. 57 (19): 4037–4052.

Gonzenbach, U.T., Studart, A.R., Tervoort, E., and Gauckler, L.J., 2006. Ultrastable Particle-Stabilized Foams. Angew. Chem., Int. Ed. 45 (21): 3526-3530.

Green, D.W., and Willhite, G.P., 1998. Enhanced Oil Recovery, SPE textbook seires vol.6, pp.166,

Green, T.C. and Smith, K.W., 2007. Drilling Fluids Containing Microbubbles. Patent Publication number WO2009070317 A1.

Grigg, R.B. and Mikhalin, A.A., 2007. Effects of Flow Conditions and Surfactant Availability on Adsorption. Paper SPE 106205 presented at the International Symposium on Oilfield Chemistry, 28 February-2 March, Houston, Texas, USA.

Growcock F., 2005. Enhanced Wellbore Stabilization and Reservoir Productivity with Aphron Drilling Fluid Technology. Technical Report, MASI Technologies LLC, DOE Award Number DE-FC26-03NT42000.

Growcock, F. B., Belkin, A., Fosdick, M., Irving, M., O'Connor, B., and Brookey, T., 2007. Recent Advances in Aphron Drilling Fluid Technology. SPE Drilling & Completion, 22(2), 74-80.

Growcock, F. B., Simon, G. A., Rea, A. B., Leonard, R. S., Noello, E., and Castellan, R., 2004. Alternative Aphron-Based Drilling Fluid. IADC/SPE Drilling Conference, Dallas, Texas.

Gunda, N.S.K., Bera, B., Karadimitriou, N. K., Mitra, S.K., and Hassanizadeh, S.M., 2011. Reservoir-on-a-chip (ROC): a new paradigm in reservoir engineering. Lab Chip, 11 (22): 3785–3792.

Gupta, R., and Mohanty, K.K., 2010. Temperature Effects on Surfactant-Aided Imbibition into Fractured Carbonates. SPEJ 15 (03): 588-597.

Gupta, R., and Mohanty, K.K., 2007. Temperature Effects on Surfactant-Aided Imbibition into Fractured Carbonates. Paper SPE 110204 presented at the SPE Annual Technical Conference and Exhibition, Anaheim, 11-14 November.

Gupta, R., and Mohanty, K.K., 2008. Wettability Alteration of Fractured Carbonate Reservoirs. Paper SPE 113407 presented at the SPE Symposium on Improved Oil Recovery, Tulsa, Oklahoma, 20-23 April.

Gupta, S., and Cawiezel, K.E., 2013. Method of Fracturing with Aphron Containing Fluids. Patent Publication number US 2013/0126163 A1.

Hadjiiski, A., Denkov, N.D., Tcholakova, S., and Ivanov I.B., 2003. Role of entry barriers in the foam destruction by oil drops K.L. Mittal, D.O. Shah (Eds.), Adsorption and Aggregation of Surfactants in Solution, Marcel Dekker, New York, pp. 465-498.

Hamida, F.M., Demiral, B.M.R., Shallcross, D.C., Castanier, L.M., and Brigham, W.E., 1990. Further Characterization of Surfactants as Steamflood Additive. Paper SPE 20065 presented at the SPE California Regional Meeting, 4-6 April, Ventura, California.

Hammond, P.S., and Unsal, E., 2009. Spontaneous and Forced Imbibition of Aqueous Wettability Altering Surfactant Solution into an Initially Oil-Wet Capillary. Langmuir, 25 (21): 12591-12603.

Haugen, Å., Fernø, M.A., Graue, A., and Bertin, H.J., 2012. Experimental Study of Foam Flow in Fractured Oil-Wet Limestone for Enhanced Oil Recovery. SPERE 15 (02): 218-228.

Heidari, P., Alizadeh, N., Kharrat, R., Ghazanfari, M.H., and Laki, A.S., 2013. Experimental Analysis of Secondary Gas Injection Strategies. Petroleum Science and Technology, 31(8), pp. 797-802.

Heins, R., Simjoo, M., Zitha, P. L. J., and Rossen, W. R., 2014. Oil Relative Permeability during Enhanced Oil Recovery by Foam Flooding. Paper SPE 170810 presented at the SPE Annual Technical Conference and Exhibition, 27-29 October, Amsterdam, the Netherlands.

Heller, J.P., 1994. CO_2 Foams in Enhanced Oil Recovery, in Foams: Fundamentals and Applications in the Petroleum Industry, Schramm, L.L. (ed.), ACS advances in Chemistry Series, 3, No. 242, Am. Chemical Soc., Washington, D.C.

Heuer, G.J., Jacocks, C.L., 1968. Control of gas-oil ratio in producing wells, US Patent 3368624.

Hirasaki G.J., 1989. A Review of the Steam Foam Process Mechanisms. Paper SPE 19518, SPE, Richardson, Texas.

Hirasaki, G., and Zhang, D.L., 2004. Surface Chemistry of Oil Recovery from Fractured, Oil-Wet, Carbonate Formation. SPEJ, 9(2): 151-162.

Hirasaki, G.J., 1989. The Steam-Foam Process. J. Petr. Technol. 41 (05): 449-456.

Hirasaki, G.J. and Lawson, J.B., 1985. Mechanisms of Foam Flow in Porous Media: Apparent Viscosity in Smooth Capillaries. SPEJ. 25 (2): 176-190.

Hoefner, M.L., Evans, E.M., Buckles, J.J., Jones, T.A., 1995. CO_2 foam: results from four developmental field trials. SPERE 10 (4), 273-281.

Isaacs, E.E., Ivory, J., and Green, M.K., 1994. Steam-Foams for Heavy Oil and Bitumen Recovery. In Foams: Fundamentals and Applications in the Petroleum Industry, 242, 6, 235-258. Advances in Chemistry, American Chemical Society.

Israelachvili, J. N., 1991. Intermolecular and Surface Forces. 2ed, Academic Press, San Diego, 1991.

Ivanov, I.B., Radoev, B., Manev, E., and Scheludko. A., 1970. Theory of the critical thickness of rupture of thin liquid films. Trans. Faraday Soc., 66: 1262-73.

Jauregi, P., Gilmour, S. and Varley, J., 1997. Characterization of Colloidal Gas Aphrons for Subsequent Use for Protein Recovery. The Chemical Engineering Journal, 65(1), 1 - 11.

Jian, G., Hou, Q., and Zhu, Y., 2015. Stability of Polymer and Surfactant Mixture Enhanced Foams in the Presence of Oil under Static and Dynamic Conditions Journal of Dispersion Science and Technology 36 (4): 477-488

Khalil, F. and Asghari, K., 2006. Application of CO_2-foam as a Means of Reducing CO_2 Mobility. J Can Pet Tech 45 (1): 37-42.

Kiani, M., Kazemi, H., Ozkan, E., and Wu, Y.S., 2011. Pilot Testing Issues of Chemical EOR in Large Fractured Carbonate Reservoirs. Paper SPE 146840 Presented at the SPE Annual Technical Conference and Exhibition, Denver, Colorado, USA, 30 October-2 November.

Kibodeaux, K.R. and Rossen, W.R., 1997. Coreflood Study of Surfactant- Alternating-Gas Foam Processes: Implications for Field Design. Paper SPE 38318 presented at the SPE Western Regional Meeting, 25-27 June, Long Beach, California, USA.

Koczo K., Lobo L., and Wasan D.T., 1992. Effect of oil on foam stability: aqueous film stabilized by emulsions. J. Colloid and Interface Science 150 (2): 492-506.

Kovscek, A.R., 1998. Reservoir Simulation of Foam Displacement Processes. The 7th UNITAR International Conference on Heavy Crude and Tar Sands, October 27–31, in Beijing, China.

Kovscek, A.R., Patzek, T.W., and Radke, C.J., 1994. Mechanistic Prediction of Foam Displacement in Multidimensions: A Population Balance Approach. Paper SPE 27789 presented at the SPE Improved Oil Recovery Symposium, 17–20 April, Tulsa, Oklahoma, USA.

Kovscek, A.R., Radke, C.J., 1994. Fundamentals of foam transport in porous media. In: Schramm, L.L. (Ed.), Foams in the Petroleum Industry. American Chemical Society, Washington, DC, pp. 115-163.

Kristiansen, T.S., and Holt, T., 1992. Properties of Flowing Foam in Porous Media Containing Oil. SPE/DOE Enhanced Oil Recovery Symposium, 22-24 April, Tulsa, Oklahoma.

Kyte J. R., 1970. A Centrifuge Method to Predict Matrix-Block Recovery in Fractured Reservoirs. SPEJ 10 (02): 164–170.

Kyte J.R., Naumann, V.O., and Matiax, C.C., 1961. Effect of Reservoir Environment on Water-Oil Displacements. J. Petr. Technol. 13 (06): 579-582.

Lake, L., W., 1989. Enhanced oil recovery, Englewood Cliffs, N.J., Prentice Hall, 550 p.

Lau, H.C., 2012. Alkaline Steam Foam: Concepts and Experimental Results. SPERE 15 (04): 445-452.

Lau, H.C. and O'Brien, S.M., 1988. Effects of spreading and nonspreading oils on foam propagation through porous media. SPE Res. Eng., 3: 893-896.

Lee, H., Lee, S.G., and Doyle, P.S., 2015. Photopatterned oil-reservoir micromodels with tailored wetting properties. Lab Chip, 2015, DOI: 10.1039/C5LC00277J.

Li, R.F., Yan, W., Liu, S., Hirasaki, G., and Miller, C.A., 2010. Foam Mobility Control for Surfactant Enhanced Oil Recovery. SPEJ 15 (04):934-948.

Liu, Y., Grigg, R., and Svec, R.K., 2006. Foam Mobility and Adsorption in Carbonate Core. Paper SPE 99756 presented at the SPE/DOE Symposium on Improved Oil Recovery, 22-26 April, Tulsa, Oklahoma, USA.

Longe, T.A., 1989. Colloidal Gas Aphrons: Generation, Flow Characterization and Application in Soil and Groundwater Decontamination; Ph.D. dissertation, Virginia Polytechnic Institute and State University.

Lyford, P.A., Pratt, H.R.C., Shallcross, D.C., and Grieser, F., 1998. The Marangoni Effect and Enhanced Oil Recovery Part I. Porous Media Studies. Can. J. Chem. Eng. 76 (02): 167-174.

Maestro, A., Guzman, E., Santini, E., Ravera, F., Liggieri, L., Ortega, F., and Rubio, R.G., 2012. Adsorption Isotherms and Wettability of Silica Nanoparticle- Surfactant Nanocomposite Interfacial Layers. Soft Matter 8 (03): 837-843.

Manlowe, D.J., and Radke, C.J., 1990. A Pore-Level Investigation of Foam/Oil Interactions in Porous Media. SPERE 5 (04): 495-502.

Mannheimer, R.J., and Schechter, R.S., 1970. Shear-dependent surface rheological measurements of foam stabilizers in nonaqueous liquids. J. Coll. Interface Sci., 32: 212-24.

Manrique, E. J., Muci, V. E., and Gurfinkel, M. E., 2006. EOR Field Experiences in Carbonate Reservoirs in the United States. Paper SPE 100063 presented at the SPE Symposium on Improved Oil Recovery, Tulsa, 22-26 April.

Marinova, K.G., Dimitrova, L.M., Marinov, R.Y., Denkov, N.D., and Kingma, A., 2012. Impact of the Surfactant Structure on the Foaming/Defoaming Performance of Nonionic Block Copolymers in Na Caseinate Solutions. Bulg. J. Phys. 39, pp. 53-64.

Martinez, A.C., Rio, E., Delon, G., Saint-Jalmes, A., Langevin, D., and Binks, B.P., 2008. On the origin of the remarkable stability of aqueous foams stabilised by nanoparticles: link with microscopic surface properties. Soft Matter 4 (7): 1531-1535.

Mattax C.C., and Kyte, J.R., 1962. Imbibition Oil Recovery from Fractured, Water-Drive Reservoir. SPEJ, 2(02): 177-184.

Mattews, C.S., 1989. Carbon Dioxide Flooding, in Enhanced Oil Recovery II: Processes and Operations, Donaldson, E. C., Chilingarian, G. V., and Yen, T. F. (eds.), Elsevier Science Publ. Co., New York.

Meng, L., Kang, W., Zhou, Y., Wang, Zh., Liu Sh., Bai B., 2008. Viscoelastic Rheological Property of Different Types of Polymer Solutions for Enhanced Oil Recovery. Journal of Central South University of Technology, 15(1), 126-129.

Miller, C.A. and Neogi, P., 1985. Interfacial Phenomena: Equilibrium and Dynamic Effects, Marcel Dekker: New York.

Mokrys, I.J., and Butler, R.M., 1993. In-Situ Upgrading of Heavy Oils and Bitumen by Propane Deasphalting: The Vapex Process. Paper SPE 25452 presented at the Production Operation Symposium, Oklahoma City, 21-23 March.

Mollaei A., and Maini, B., 2010. Steam Flooding of Naturally Fractured Reservoirs: Basic Concepts and Recovery Mechanisms. JCPT 49 (01): 65-70.

Montilva, J., Ivan, C. D., Friedheim, J., and Bayter, R., 2002. Aphron Drilling Fluid: Field Lessons from Successful Application in Drilling Depleted Reservoirs in Lake Maracaibo. Offshore Technology Conference, Houston, Texas.

Moreno-Arciniegas, L., and Babadagli, T., 2014. Optimal Application Conditions of Solvent Injection into Oil Sands to Minimize the Effect of Asphaltene Deposition: An Experimental Investigation. SPERE 17 (04): 530-546.

Naderi, K., and Babadagli, T., 2008. Clarifications on Oil/Heavy Oil Recovery under Ultrasonic Radiation through Core and 2D Visualization Experiments. JCPT 47 (11): 56-62.

Namdar Zanganeh, M., and Rossen, W., 2013. Optimization of Foam Enhanced Oil Recovery: Balancing Sweep and Injectivity. SPERE, 16 (01): 51-59.

Needham, R.B., 1968. Plugging of High Permeability Earth Strata. U.S. Patent No. 3412793.

Nikolov, A.D., Wasan, D.T., Huang, D.W., Edwards, D.A., 1986. The Effect of Oil on Foam Stability: Mechanisms and Implications for Oil Displacement by Foam in Porous Media. Paper SPE 15443 presented at the SPE ATCE, 5-8 October, New Orleans, Louisiana.

Noble, M., Jauregi, P., Kaul, A., Varley, J., 1998. Protein Recovery Using Gas–Liquid Dispersions. Journal of Chromatography B: Biomedical Sciences and Applications, 711(1-2), 31-43.

Pathak, V., Babadagli, T., and Edmunds, N., 2012. Mechanics of Heavy-Oil and Bitumen Recovery by Hot Solvent Injection. SPERE 15 (02): 182-194.

Patzek, T.W., 1996. Field Applications of Steam Foam for Mobility Improvement and Profile Control. SPERE 11 (2): 79–86.

Patzek, T.W., and Koinis, M.T., 1988. Kern River Steam Foam Pilots. Paper SPE 17380 presented at the SPEIDOE Enhanced Oil Recovery Symposium, Tulsa, April 17-20.

Paul, K.T., Satpathy, S., Manna, I., Chakraborty, K., and Nando, G., 2007. Preparation and Characterization of Nano structured Materials from Fly Ash: A Waste from Thermal Power Stations, by High Energy Ball Milling. Nanoscale Research Letters 2(8): 397-404.

Petkova, R., Tcholakova, S., and Denkov, N. D., 2012. Foaming and Foam Stability for Mixed Polymer-Surfactant Solutions: Effects of Surfactant Type and Polymer Charge. Langmuir 28 (11): 4996-5009.

Popov, P., and Growcock, F.B., 2005. R&D Validates Effectiveness of Aphron Drilling Fluids in Depleted Zones. Drilling Contractor, 61(3), 55-58.

Pratt, H.R.C., 1991. Marangoni Flooding with Water Drives: A Novel Method for EOR. Paper SPE 22982 presented at the SPE Asia-Pacific Conference, Perth, Australia, 4-7 November.

Ransohoff, T. C., and Radke, C. J., 1988. Mechanisms of Foam Generation in Glass-Bead Packs. SPERE 3(02): 573-585.

Ravera, F., Santini, E., Loglio, G., Ferrari, M., and Liggieri, L., 2006. Effect of nanoparticles on the interfacial properties of liquid/liquid and liquid/air surface layers. J. Phys. Chem. B 110 (39): 19543-19551.

Reis, J.C., 1990. Oil Recovery Mechanism in Fractured Reservoirs during Steam Injection. Paper SPE 20204 presented at the SPE/DOE Seventh Symposium on Enhanced Oil Recovery, Tulsa, Oklahoma, 22-25 April.

Robin, M., Behot, J., and Sygouni, V., 2012. CO_2 Injection in Porous Media: Observations in Glass Micromodels under Reservoir Conditions. Paper SPE 154165 presented at the SPE Improved Oil Recovery Symposium, Tulsa, Oklahoma, 14-18 April.

Roehl, P.O., and Choquette, P.W., 1985. Carbonate Petroleum Reservoirs. Springer-Verlag, New York.

Romero, C., Alvarez, J.M., and Muller, A.J., 2002. Micromodel Studies of Polymer-Enhanced Foam Flow through Porous Media. Paper SPE 75179 presented at the SPE/DOE Improved Oil Recovery Symposium, Tulsa, OK, April 13-17.

Roostapour, A., and Kam, S., 2013. Anomalous Foam-Fractional-Flow Solutions at High Injection Foam Quality. SPERE 16 (1): 40-50.

Rosen, M.J., and Kunjappu, J.T., 2012. Surfactants and Interfacial Phenomena. Fourth Edition, John Wiley & Sons, Inc., Hoboken, NJ, USA.

Ross, S., and Suzin, Y., 1985. Measurement of dynamic foam stability. Langmuir 1(01): 145–149.

Rossen, W.R., 1996. Foams in Enhanced Oil Recovery. In Foams: Theory, Measurements, and Applications, ed. Prudhomme R. K. and Khan S., Surfactant Science Series, 413–464. New York: Marcel Dekker.

Rossen, W.R., and Gauglitz, P.A., 1990. Percolation Theory of Creation and Mobilization of Foam in Porous Media. AICHE J. 36 (08): 1176-1188.

Rossen, W.R., van Duijn, C.J., Nguyen, Q.P., Shen, C., and Vikingstad, A.K., 2010. Injection Strategies to Overcome Gravity Segregation in Simultaneous Gas and Water Injection into Homogeneous Reservoirs. SPEJ 15 (01): 76-90.

Rossen, W.R., Zeilinger, S.C., Shi, J.X., and Lim, M.T., 1999. Simplified Mechanistic Simulation of Foam Processes in Porous Media. SPEJ 4 (03): 279-287.

Roy, D., Valsaraj, K.T., Constant, W.D. and Darji, M., 1994. Removal of Hazardous Oily Waste form a Soil Matrix using Surfactants and Colloidal Gas Aphron Suspensions under Different Flow Conditions. Journal of Hazardous Materials, 38(1), 127-144.

Salonen A, Lhermerout R, Rio E, Langevin D, Saint-Jalmes A., 2012. Dual gas and oil dispersions in water: production and stability of foamulsion. Soft Matter 8 (03): 699-706.

Santini, E., Krägel, J., Ravera, F., Liggieri, L., and Miller R., 2011. Study of the monolayer structure and wettability properties of silica nanoparticles and CTAB using the Langmuir trough technique, Colloids and Surfaces A: Physicochem. Eng. Aspects 382 (1-3): 186-191.

Save, S.V., Pangarkar, V.G., Kumar S.V., 1993. Intensification of Mass Transfer in Aqueous 2-phase Systems. Biotechnology and Bioengineering, 41(1), 72-78.

Schramm, L L. and Wassmuth, F., 1994. Foams: Basic Principles in Foams: Fundamentalsand Application in the Petroleum Industry, Schramm, L. L. (Ed.), American Chemical Society, Washington, DC.

Schramm, L.L., 2005. Emulsions, Foams, and Suspensions: Fundamentals and Applications, Wiley-VCH: Weinheim.

Schramm, L.L., and Novosad, J.J., 1990. Micro-visualization of foam interactions with a crude oil. Colloids and Surfaces 46 (01): 21-43.

Schramm, L.L., and Novosad, J.J., 1992. The destabilization of foams for improved oil recovery by crude oils: effect of the nature of the oil. JPSE 7(1): 77-90.

Sebba, F., 1987. Foams and Biliquid Foams-Aphrons. John Wiley & Sons, Chichester, 236 p.

Seethepalli, A., Adibhatla, B., and Mohanty, K.K., 2004. Physicochemical Interactions during Surfactant Flooding of Fractured Carbonate Reservoirs. SPEJ 9 (4): 411-418.

Shabani Afrapoli M., Crescente C., Alipour S., and Torsaeter, O., 2009. The effect of bacterial solution on the wettability index and residual oil saturation in sandstone. JPSE 69 (3-4): 255-260.

Shabani Afrapoli, M., Alipour, S., and Torsaeter, O., 2010. Effect of Wettability and Interfacial Tension on Microbial Improved Oil Recovery with Rhodococcus sp 094. Paper SPE 129707 presented at the SPE Improved Oil Recovery Symposium, Tulsa, Oklahoma, 24-28 April.

Shivhare, S., and Kuru, E., 2010. Physico-Chemical Characterization of Non-Aqueous Colloidal Gas Aphron- Based Drilling Fluids. Canadian Unconventional Resources and International Petroleum Conference, Calgary, Alberta, Canada.

Shivhare, S., and Kuru, E., 2014. A study of the pore-blocking ability and formation damage characteristics of oil-based colloidal gas aphron drilling fluids. Journal of Petroleum Science and Engineering, 122 (2014): 257-265.

Shrestha, L.K., and Aramaki, K., 2012. Non-Aqueous Foams: Formation and Stability, in Foam Engineering: Fundamentals and Applications (ed P. Stevenson), John Wiley & Sons, Ltd, Chichester, UK.

Shrestha, L.K., Aramaki, K., Kato, H., Takase, Y., and Kunieda, H., 2006. Foaming Properties of Monoglycerol Fatty Acid Esters in Nonpolar Oil Systems. Langmuir, 22 (20): 8337-8345

Simjoo, M., Rezaei, T., Andrianov, A., and Zitha, P.L.J., 2013. Foam stability in the presence of oil: Effect of surfactant concentration and oil type. Colloids Surfaces A: Physiochem. Eng. Aspects 438 (5 December): 148-158.

Singh, G., Hirasaki, G.J., and Miller, C.A., 1997. Dynamics of Foam Films in Constricted Pores", AIChE Journal, Vol. 43, No. 12, 3241-3252.

Singh, R., and Mohanty, K.K., 2016. Foams Stabilized by In-Situ Surface-Activated Nanoparticles in Bulk and Porous Media. SPEJ, 21 (01): 21-130.

Singh, R., and Mohanty, K.K., 2015. Synergy between Nanoparticles and Surfactants in Stabilizing Foams for Oil Recovery. Energy & Fuels 29 (02): 467-479.

Smith DH. (ed.). 1988. Surfactant-Based Mobility Control: Progress in Miscible-Flood Enhanced Oil Recovery. ACS Symp. Ser. No. 373, Am. Chem. Soc., Washington, D.C.

Song, W., and Kovscek, A.R., 2015. Functionalization of Micromodels with Kaolinite for Investigation of Low Salinity Oil-Recovery Processes. Lab Chip, 2015, DOI: 10.1039/C5LC00544B.

Spinelli, L.S., Neto, R.G., Layla, F.A., Monteiro, V., Lomba, R., Michel, R., and Lucas, E. , 2010. Synthetic-based Aphrons: Correlation between Properties and Filtrate Reduction Performance. Colloids and Surfaces A: Physicochemical and Engineering Aspects, 353 (1), 57-63.

Standnes, D.C., and Austad, T., 2000a. Wettability alteration in chalk 1. Preparation of core material and oil properties. JPSE 28 (03), 111–121.

Standnes, D.C., and Austad, T., 2000b. Wettability Alteration in Chalk 2. Mechanism for Wettability Alteration from Oil-Wet to Water-Wet Using Surfactants. JPSE 28 (03): 123-143.

Stevenson, P., and Li, X., 2012. Pneumatic Foam, in Foam Engineering: Fundamentals and Applications (ed P. Stevenson), John Wiley & Sons, Ltd, Chichester, UK.

Stoll, W.M., Hofman, J.P., Lighthelm, D.J., Faber, M.J., and Van den Hoek, P.J., 2008. Toward Field-Scale Wettability Modification—the Limitations of Diffusive Transport. SPERE 11 (03): 633-640.

Su, K., Lia, X., Zhao, X., and Zhang, H., 2013. Coupled CO_2 Enhanced Oil Recovery and Sequestration in China's Demonstration Project: Case study and Parameter Optimization. Energy Fuels, 27, 378-386.

Taber, J.J. and Martin F.D., 1983. Technical Screening Guides for the Enhanced Recovery of Oil. Paper SPE 12069, presented at the 58th SPE Annual Technical Conference and Exhibition, San Francisco, California, USA, October 5-8, 1983.

Taber, J.J., Martin, F.D., and Seright, R.S., 1997. EOR Screening Criteria Revisited -Part 1: Introduction to Screening Criteria and Enhanced Recovery Field Projects. SPERE 12 (03): 189-198.

Tamura, T., Kageyama, M., Kaneko, Y., Kishino, T., Nikaido, M., 1999. Direct observation of foam film rupture by several types of antifoams using a scanning laser microscope. J. Colloid Interface Sci. 213 (01): 179-186.

Tang, S., Tian, L., Lu, J., Wang, Z., Xie, Y., Yang, X., and Lei, X., 2014. A Novel Low Tension Foam Flooding for Improving Post-Chemical-Flood in Shuanghe Oilfield. Paper SPE 169074 presented at the SPE Improved Oil Recovery Symposium, 12-16 April, Tulsa, Oklahoma, USA.

Tanzil, D., 2001. Foam Generation and Propagation in Heterogeneous Porous Media. Ph.D. dissertation, Department of Chemical Engineering, Rice University.

Tanzil, D., Hirasaki, G. J., and Miller, C.A., 2002. Conditions for Foam Generation in Homogeneous Porous Media. Paper SPE 75176 presented at the SPE/DOE Symposium on Improved Oil Recovery, Tulsa, OK, 13-17 April.

Telmadarreie, A., Trivedi, J., 2017. Dynamic Behavior of Asphaltene Precipitation and Distribution Pattern in Carbonate Reservoirs during Solvent Injection: Pore-Scale Observations. Paper SPE 184970 presented at the SPE Canada Heavy Oil Conference, Calgary, Alberta, February 14-15.

Telmadarreie, A., and Trivedi, J.J., 2016. New Insight on Carbonate-Heavy-Oil Recovery: Pore-Scale Mechanisms of Post-Solvent Carbon Dioxide Foam/Polymer-Enhanced-Foam Flooding. SPEJ, 21 (05): 1655-1668.

Telmadarreie, A., Trivedi, J., 2016. Post-Surfactant CO_2 Foam/Polymer-Enhanced Foam Flooding for Heavy Oil Recovery: Pore-Scale Visualization in Fractured Micromodel. Transp. Porous Med., volume 113, Issue 3, pp 717–733.

Telmadarreie, A., Doda, A., Trivedi, J., Kuru, E., Choi, P., 2016. CO_2 Microbubbles - a Potential Fluid for Enhanced Oil Recovery: Bulk and Porous Media Studies. Petroleum Science and Engineering Journal. Vol. 138, 160-173.

Telmadarreie, A., and Trivedi, J.J., 2015. Insight on Foam/Polymer Enhanced Foam Flooding for Improving Heavy Oil Sweep Efficiency. World Heavy Oil Congress, Edmonton, Alberta, Canada, 24-26 March.

Treiber, L.E., Archer, D.L., and Owens, W.W., 1972. A Laboratory Evaluation of the Wettability of Fifty Oil-Producing Reservoirs. SPEJ 12 (6): 531-540.

Trivedi, J., and Babadagli, T., 2009. Oil Recovery and Sequestration Potential of Naturally Fractured Reservoirs during CO_2 Injection. Energy Fuels, 23 (8), 4025-4036.

Trivedi, J.J., and Babadagli, T., 2008. Efficiency of Diffusion-Controlled Miscible Displacement in Fractured Porous Media. Transp. Porous Med. 71 (3): 379-394.

Urban, D. G., 2003. How to Formulate and Compound Industrial Detergents. Book Surge Publishing, United States.

Veerabhadrappa, S.K., Trivedi, J.J. and Kuru, E., 2013. Visual Confirmation of the elasticity dependence of unstable secondary polymer floods. Industrial & Engineering Chemistry Research, 52(18), 6234-6241.

Verwey, E.J.W. and Overbeek, J.Th.G., 1948. Theory of the Stability of Lyophobic Colloids, Elsvier, Amsterdam, 1948.

Vikingstad, A.K., Skauge, A., Hoiland, H., Aarra, M.G., 2005. Foam-oil interactions analyzed by static foam tests. Colloids Surfaces A: Physiochem. Eng. Aspects 260 (1-3): 189-198.

White, C.C., Chesters, A.P., Ivan, C.D., Maikranz, S., and Nouris, R., 2003. Aphron-based Drilling Fluid: Novel Technology for Drilling Depleted Formations in the North Sea. SPE/IADC Drilling Conference, Amsterdam, Netherlands.

Wiebe, R., and Gaddy, V.L., 1940. The Solubility of Carbon Dioxide in Water at Various Temperatures from 12 to 40' and at Pressures to 500 Atmospheres. Critical Phenomena. Journal of the American Chemical Society, 62(4), 815-817.

Worthen, A.J., Bryant, S.L., Huh, C., and Johnston, P.K., 2013. Carbon Dioxide-in-Water Foams Stabilized with Nanoparticles and Surfactant Acting in Synergy. AIChE J. 59 (9): 3490-3501.

Xie, X., Weiss, W.W., Tong, Z., and Morrow, N.R., 2005. Improved Oil Recovery from Carbonate Reservoirs by Chemical Stimulation. SPEJ 10 (03): 276-285.

Yan, W., Miller, C.A., and Hirasaki, G.J., 2006. Foam Sweep in Fractures for Enhanced Oil Recovery. Colloids and Surfaces A: Physicochem. Eng. Aspects. 282–283 (2006): 348-359.

Zhang, H., Miller, C.A., Garrett, P.R., Raney, K.H., 2003. Mechanism for defoaming by oils and calcium soap in aqueous systems. Journal of Colloid and Interface Science, 263 (02): 633-644.

Zhang, J., Nguyen, Q.P., Flaaten, A., and Pope, G.A., 2009. Mechanisms of Enhanced Natural Imbibition with Novel Chemicals. SPERE, 12 (06): 912-920.

Zhang, W., Youn, S. and Doan, Q., 2007. Understanding reservoir architectures and steam-chamber growth at Christina Lake, Alberta, by using 4D seismic and crosswell seismic imaging. SPERE 10 (5): 446-452.

Zhang, Y., Yue, X., Dong, J., and Yu, L., 2000. New and Effective Foam Flooding to Recover Oil in Heterogeneous Reservoir. Paper SPE 59367 presented at the SPE/DOE Improved Oil Recovery Symposium, 3-5 April, Tulsa, Oklahoma.

Zhang, Z.F., Freedman, V.L., and Zhong, L., 2009. Foam Transport in Porous Media - A Review

Zhao, X., and Liao, X., 2012. Evaluation Method of CO_2 Sequestration and Enhanced Oil Recovery in an Oil Reservoir, as Applied to the Changqing Oilfields, China. Energy Fuels, 26(8), 5350-5354.

Zhou, Z.H., and Rossen, W.R., 1995. Applying Fractional-Flow Theory to Foam Processes at the Limiting Capillary Pressure. SPE Adv. Technol. 3 (1): 154-162.

Zuta, J., and Fjelde, I., 2010. Transport of CO_2-Foaming Agents During CO_2-Foam Processes in Fractured Chalk Rock. SPERE 13 (04): 710-719.